Imine Catalyst Stability

Max Leonard Hammond

A thesis submitted in partial fulfilment of the requirements for the degree of Doctor of Philosophy in Chemistry

University of Warwick, Department of Chemistry

May 2006

Table of Contents

List of Figures

List of Schemes

List of Tables

List of Abbreviations

aPP	Atactic Poly(Propene)
CGC	Constrained Geometry Catalyst
DCM	Dichloromethane
DFT	Density Functional Theory
EPR	Electron Paramagnetic Resonance
FFT	Fast Fourier Transform
GPC	Gel Permeation Chromatography
HDPE	High Density Poly(Ethene)
HT	High Throughput
iPP	Isotactic Poly(Propene)
MAO	Methyl Aluminoxane
MI	Migratory Insertion
MM	Molecular Mechanics
M_n	Number-average Molecular Weight
M_w	Weight-average Molecular Weight
MWD	Molecular Weight Distribution
MWt	Molecular Weight
NMR	Nuclear Magnetic Resonance
PC	Personal Computer
PDi	Polydispersity Index
PE	Poly(ethene)
PP	Poly(propene)
RBF	Round-bottomed Flask
RT	Room Temperature
QM	Quantum Mechanical
sPP	Syndiotactic Poly(Propene)
TEA	Triethylamine
THF	Tetrahydrofuran
T_m	Peak melting temperature of a polymer
XRD	X-Ray Diffractometry

Acknowledgements

I am enormously grateful to the many people who have been a part of my life during the time I have worked on this thesis, both professionally and personally. First and foremost must be my supervisor, Prof. Peter Scott, who gave me the opportunity to undertake this work, and whose support and rigorous academic critique enabled me to reach this point.

Thanks are also due to Dr. Stefan Spitzmesser at BP (then Innovene, then Ineos, due to the machinations of a corporate spin-off) for his assistance with DFT and HT, and also for his valuable insights into the chemical industry, and a couple of thoroughly enjoyable trips to Brussels.

Various technical support services have been essential for the work contained herein, notably Adam Clarke (NMR), Peter Brindley (amazing glassware) Guy Clarkson and Paul O'Shaugnessey (XRD), John Bickerton (Mass Spectrometry), the electronic and mechanical workshops (and especially Kirk for all his help with my rig), Warwick Analytical Services and Medac Ltd (elemental analyses), Steve Holding at RAPRA (GPC), and the technical team at Ineos (polymer characterization and large-scale testing).

The guys in the Scott group have provided an enjoyable and occasionally productive working environment; my special thanks go to Geezer for launching me into this, and to Stuart for being my backup brain. My family and friends have always been there for me, especially Caroline, who helped me get going with this endeavour, and Andrea who didn't let me stop.

Declaration

The work reported in this thesis was carried out in The Chemistry Department, University of Warwick, between October 2002 and February 2006. Unless otherwise stated it is the work of the author and has not been submitted in whole or in part for any other degrees at this or any other university.

Publications

The following publication has arisen from the work described in this thesis:

R. K. J. Bott, M. Hammond, P. N. Horton, S. J. Lancaster, M. Bochmann and P. Scott, *Dalton Trans.*, 2005, 3611-13.

Summary

Chapter 1 presents a review of the background and current research regarding Schiff-base olefin polymerization catalysts, with special reference to the salicylaldimine species. An attempt is made to review trends within the current literature.

Chapter 2 describes the synthesis and polymerization properties of tetradentate ligands with a bibenzyl backbone at titanium and zirconium centres, prepared with the intent of sterically hindering a 1,2-Migratory Insertion into the ligand imine functionality. A custom-built polymerization reactor was used to determine the stability of the catalytic systems. Steric protection is moderately successful in enhancing the stability of these systems.

Chapter 3 reports the synthesis and detailed polymerization behaviour of a series of group 4 catalysts based on salicyloxazoline ligands, which should be resistant to 1,2-Migratory Insertion. Comparisons are made between polymerization under different conditions, including using High-Throughput methodology to screen catalysts under a range of differing conditions rapidly. Such systems are extremely active for polymerization of ethene, but demonstrate limited stability at elevated temperature.

Chapter 4 presents our investigations into the polymerization behaviour of salicyloxazoline catalysts containing a *para*-methoxy substituent on the phenoxy donor unit. This substituent significantly enhances the stability of the catalysts at elevated temperature.

Chapter 5 explores the nature of the active species in polymerizations with group 4 salicyloxazoline species. Alkyl cations of such species are generated from metal alkyl species with borate activators, and also from metal chloride species with MAO. We conclude that the primary deactivation mechanism is loss of ligand to aluminium co-catalyst, and that the methoxy substituent prevents this. A computational approach (DFT) is also applied, to examine the catalytic pathways which may be available to various stereoisomers of the catalyst.

Chapter 6 details the experimental procedures used during this work.

1 Introduction

1.1 Single-Site polymerization catalysts

1.1.1 Background

In the fifty years since the discovery of Ziegler-Natta type olefin polymerization catalysts,[1] much work has been devoted to the development of single-site catalysts such as metallocenes[2] and the so-called "Constrained Geometry Catalysts" (CGCs, Figure 1.1).[3] Unlike heterogeneous catalysts such as the Ziegler-Natta systems, single-site catalysts have well-defined active sites, allowing systematic variation of the catalyst to exert a good degree of control over the resultant polymer structures. Until recently, the metallocene/alkylaluminium systems originally investigated by Kaminsky[4] were the most active single-site olefin polymerization catalysts known; even today Cp_2ZrCl_2 is still the standard against which many new systems are compared.

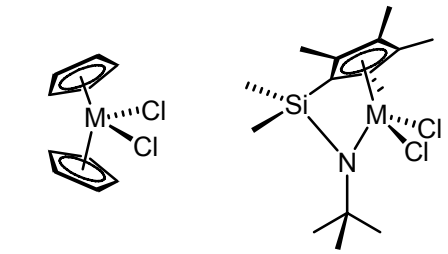

Metallocene **CGC**

Figure 1.1 – Single site catalysts

Of the post-metallocene olefin polymerization catalysts,[5,6] those based on imine (and especially Schiff base) ligands have shown particular promise, and these will be the subject of this review. In particular we will focus on salicylimine-based

systems, and we will attempt where possible to relate catalyst structure to resultant polymerization activity and polymer properties.

Two of the most extensively investigated imine ligands are acen and salen[7] (Figure 1.2) which are tetradentate ligands, and usually co-ordinate in a planar *trans* manner.

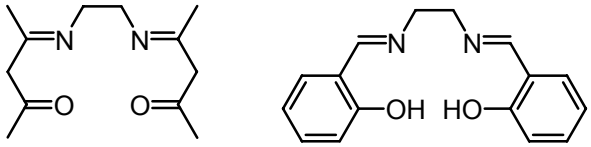

acen **salen**

Figure 1.2 - N_2O_2 Schiff Base Ligands

It is generally acknowledged that active single-site polymerization catalysts must have two *cis*-located sites available for and active towards olefin insertion.[8] Unsurprisingly therefore, the *trans*–complexes of acen and salen have not shown activity towards olefin polymerization.

Some work has shown that salen and acen (or derivatives) can adopt *cis*–β (*i.e. cis,cis,cis, vide infra* §1.2.1) geometry at group 4 metal centres,[9] but the majority of examples are nevertheless of *trans* structures. [Zr(salen)Cl_2(THF)] (in which the chlorides adopt *cis* geometry upon loss of the THF) has been shown to be a moderately active catalyst for ethene polymerization.[10]

Brookhart and co-workers have developed ligand systems for nickel (II) and palladium (II) centres, based on α-diimine[11] (*e.g.* **1**) and imine-phosphine[12] (*e.g.* **2**) donors (Figure 1.3) which are active catalysts for polymerization of ethene.

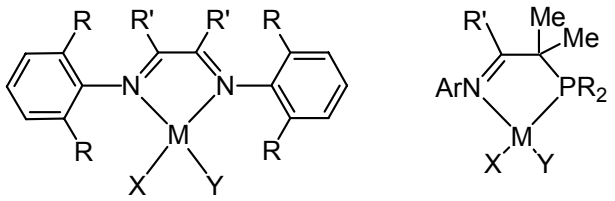

(1) **M = Ni, Pd** **(2)**

Figure 1.3 – Imine-based catalyst systems reported by Brookhart

The α-diimine systems were the first post-metallocene catalysts to show comparable activities and polymer molecular weights to the metallocenes, and have been comprehensively reviewed by Ittel *et al.*[13] Variation of the ligand system and polymerization conditions can produce polyethene (PE) anywhere between oligomers and high molecular weight (MWt) PE, $M_w \approx 1{,}000{,}000$ u, with optimum productivities in the region of 10-1000 $kg_{PE}\ mol_{Ni}^{-1}\ bar^{-1}\ h^{-1}$. These catalysts can produce PE with unusual branching properties, as a result of migration of the active metal centre along the polymer chain.

Gibson and co-workers have also investigated imine based ligand systems.[14] In 1998, Gibson and Brookhart independently discovered[15] a series of iron–centred imine-pyridine catalysts (one of the most active examples being **3**) that are very active for ethene polymerization, producing unbranched high density polyethene (HDPE) of M_w typically ranging from 15,000 – 610,000 u, and with productivities of 450 – 11,000 $kg_{PE}\ mol_{Fe}^{-1}\ bar^{-1}\ h^{-1}$.

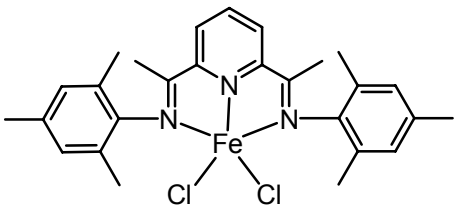

(3)

Figure 1.4 - Brookhart/Gibson imine-pyridine system

1.1.2 Salicylimine Catalysts for Olefin Polymerization

1.1.2.1 Ligand Design

The salicylaldimine (phenoxy-imine, FI) catalyst systems (*e.g.* **4**) discovered independently by Fujita and Coates[16,17] have shown perhaps the greatest promise of the many post-metallocene systems investigated.[18,19] The salicylaldimine unit allows for easy variations of the system on both the phenol and imine functionalities. As we shall see, such variations lead to profound effects on polymerization.

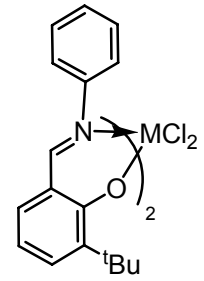

M = Ti, Zr, Hf

(4)

Figure 1.5 - Salicylaldimine precatalysts

1.1.2.2 Metal Centres

The polymerization properties of the group 4 salicylaldimine species will be discussed in detail in §1.3 below, this present section shall serve to briefly introduce the properties of such species.

Titanium

Titanium complexes of salicylaldimine ligands have proven to be active catalysts for ethene polymerization.[20] Some examples using fluorinated aniline substituents on the imine functionality have been shown to be "living" catalysts for the polymerization of ethene and propene, producing high molecular weight polyethene (see §1.3.4).

Zirconium

Complexes of salicylaldimine ligands based on zirconium have shown extremely high activity for ethene polymerization when activated with methylaluminoxane (MAO), including some with productivities two orders of magnitude higher than [Cp_2ZrCl_2].[17,18,21-24] Systems based on zirconium typically produce low molecular weight polyethene, and have been reported to produce multimodal polymer molecular weight distributions.[25]

Hafnium

Although there are fewer reports in the literature of investigations into the hafnium complexes of salicylaldimine ligands than into the titanium and zirconium analogues, those that have been presented[17,21] suggest that the activity and product molecular weight of polymerizations using such species lie between those using titanium and zirconium based systems.

Other Metals

Vanadium complexes of salicylaldimine ligands have been reported to be active for ethene/propene copolymerization, exhibiting behaviour similar to commercial vanadium catalysts.[26] When supported on $MgCl_2/Et_mAl(OR)_n$, such complexes provide highly active, thermally robust catalysts for ethene polymerization.[27]

Gibson *et al.* have explored the properties of the chromium complexes of a range of salicylaldimine ligands, reporting moderate to high activity in the polymerization of ethene.[28] They have reported forming high molecular weight linear PE with broad molecular weight distributions, and have suggested that the active species may retain only one of the initial two salicylaldimine ligands.

Grubbs and co-workers have developed a series of salicylaldimine catalysts based on the later transition metals. The neutral Ni systems (**5**) tolerate heteroatoms and can thus co-polymerize ethene with functional additives.[29]

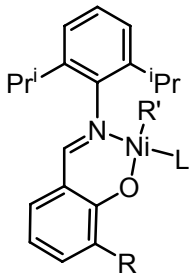

(5)

Figure 1.6 - Grubbs' salicylaldimine systems

1.2 Structures and Stability of Group 4 Complexes

1.2.1 Stereochemistry

There are eight different possible isomeric forms which two A,B-bidentate ligands and two monodentate ligands may adopt around an octahedral metal centre. This is shown in Figure 1.7 for the case of two N,O ligands and two chlorides; the *cis*–Cl species (**a-c)** also have corresponding enantiomers.

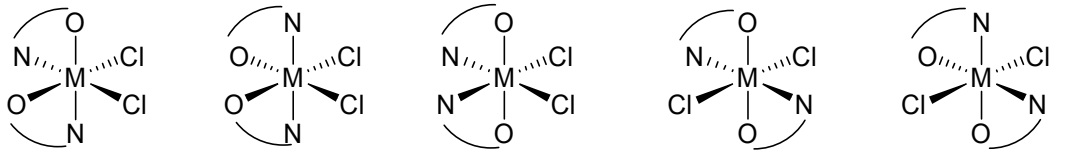

* Λ enantiomer shown, Δ also exists

Figure 1.7 - Isomers of two N,O ligands at an octahedral metal centre

Fujita investigated the relative energies of these isomers for species (**4**) where M = Zr, using Density Functional Theory (DFT).[17] He calculated the *cis,trans,cis*-

species (Figure 1.7c) to have the lowest formation enthalpy, with the other isomers 20-40 kJ mol^{-1} higher in energy. The bulky phenoxy–groups are *trans* to each other in this orientation, the electron donating imine donors are *trans* to the electron withdrawing chloride ligands, and O-Ti π-bonding should occur.[30] Knight has shown however that some such species may exist as a mixture of *cis,trans,cis* and *cis,cis,cis* isomers,[31] with the *cis,cis,cis* isomer representing ~30% of the product. This is not reflected in the data presented by Fujita *et al.*, but in any event the structural nature of the precatalyst may have little or no bearing on the nature of the active species in a polymerization – *q.v.* §1.3.1.

1.2.2 Stability of C=N Bond

The imine functionality in a salicylaldimine species is reactive, specifically toward reduction. This would be expected to significantly affect the nature of the active species in a polymerization, and so is of fundamental interest in the study of these species.

1.2.2.1 1,2-Migratory Insertion

In our laboratory, it has previously been shown that a biaryl-bridged salicylaldimine species may undergo 1,2-Migratory Insertion (MI) reactions with metal-bound alkyl ligands (Figure 1.8).[32]

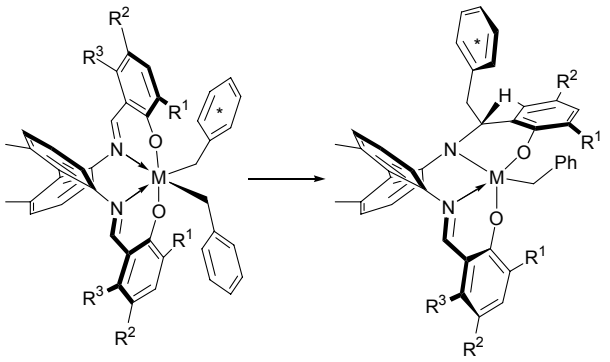

Figure 1.8 - 1,2-MI of alkyl ligand to aldimine functionalty

Modification of the ligand by methyl-substitution of the phenoxy ring in the 3-position effectively blocks the 1,2-MI deactivation pathway, although a slower radical decomposition pathway was demonstrated.[33] The modified biaryl-bridged species are long-lived catalysts for ethene polymerization, albeit with far lower activity than the non-bridged equivalents. This latter observation has been attributed to increased congestion at the active site.[31,34] Unbridged salicylaldimine species do not possess an increased lifetime when modified in the same way; they are believed to be insufficiently rigid to hold the methyl group in a position to block the MI reaction.

1.2.2.2 Intramolecular Reduction

A further possibility for reduction of the imine bond is the reaction with another component in the polymerization reaction. Typically, single-site catalysts are activated with an aluminium alkyl species, most commonly methylaluminoxane (MAO), which is present in large excess. Alternatively, they may be activated stoichiometrically with perfluorinated boron aryl species such as $B(C_6F_5)_3$, $[PhNHMe_2][B(C_6F_5)_4]$, or $[CPh_3][B(C_6F_5)_4]$.[35] When such stoichiometric activators are used, typically an amount of an aluminium species such as $^{i}Bu_3Al$ is added as a scavenger for protic impurities in solvent and monomer feeds.

Fujita has shown[30] that the species **4** (M = Ti) produces* very different forms of PE when activated with $^{i}Bu_3Al/[Ph_3C][B(C_6F_5)_4]$ in comparison to those produced when activated with MAO; activation with MAO (1250 eq.) results in very high activity and poly(ethene) (PE) with low molecular weight (3310 kg mol^{-1} bar^{-1} h^{-1}, M_v = 51 x 10^4 u), whereas activation with $^{i}Bu_3Al/[Ph_3C][B(C_6F_5)_4]$ results in

* Reaction conditions: 25 °C, 5 min polymerization time

moderate activity, but very high molecular weight (190 kg mol^{-1} bar^{-1} h^{-1}, M_v = 481 x 10^4 u).

This behaviour was attributed to the reduction of the imine functionality in the ligand by aluminium hydride species present in $^{i}Bu_3Al$. Indeed, reaction of the titanium complex with $^{i}Bu_3Al$, followed by hydrolysis of the ligand yielded a salicylamine compound, whereas reaction with MAO and subsequent hydrolysis yielded the original salicylaldimine proligand (Figure 1.9).

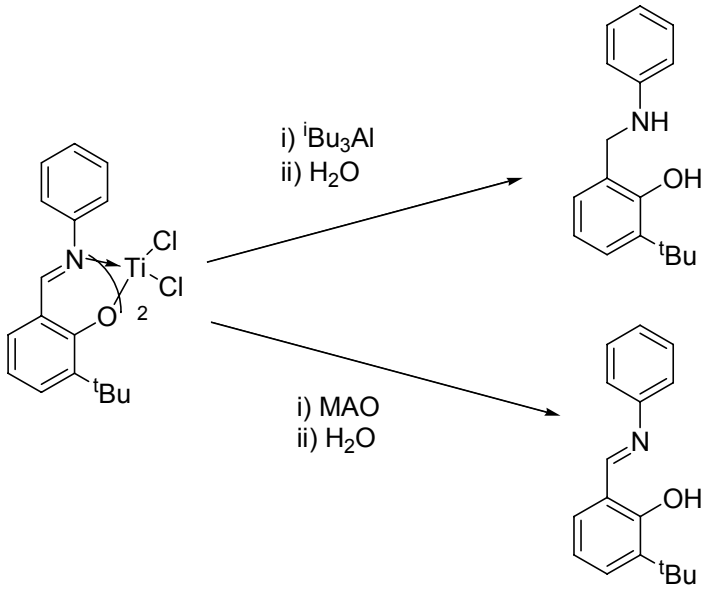

Figure 1.9 - Reduction of salicylaldimine complex by $^{i}Bu_3Al$

1.2.2.3 Reduction-Resistant Ligands

If the aldimine functionality in the ligand is replaced with a more substituted imine bond, reduction should be significantly slowed, or prevented altogether. There have been a number of attempts to produce such species, although as yet none have yielded highly active catalysts.

Ketimines

The synthesis of salicylketimine ligands is considerably more challenging than the synthesis of equivalent salicylaldimine species, and consequently complexes of such

are less frequently reported.[36] Fujita reported forming some salicylketimine complexes, which showed low activity in ethene polymerization.[21]

Coates has recently developed a facile synthesis of salicylketimine compounds, and has found that the titanium complexes of such ligands (**6**) are active as catalysts for living polymerization of ethene when activated with MAO, albeit with low activity.[37] In salicylaldimine species, living behaviour has only been observed in species possessing fluorinated aryl moieties (see §1.3.4).

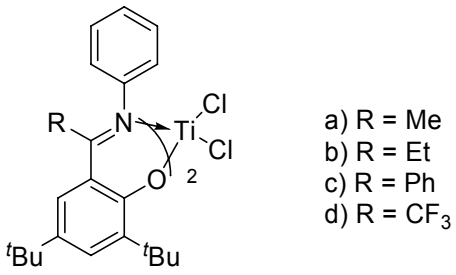

6

Figure 1.10 - Titanium salicylketimine complexes

Pyridyl Systems

The use of pyridyl ligands as donors is widespread within single-site catalysis,[5,6] and some examples of salicyl-pyridyl systems on titanium (**7**) have been reported.[38] However, it is not necessarily constructive to compare directly the salicyl-pyridyl systems with salicylaldimine systems, since there are some fundamental differences between the *cis, cis, trans* (*i.e. cis*-O, *trans*-N) isomer in preference to the *cis, trans, cis* (*i.e. cis*-N, *trans*-O) preferred by salicylaldimines, and unlike the salicylaldimine complexes, a bulky substituent *ortho* to the oxygen donor is not required for high activity (see §1.3.2).

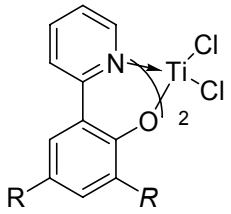

R = Me, ^{t}Bu

7

Figure 1.11 - Salicyl-pyridyl Systems

Salicyloxazoline Systems

Floriani has reported that group 4 metal alkyl complexes of salicyloxazoline ligands (**8)** could form cations when treated with $[HNEt_3][BPh_4]$, but that these cations showed very low activity for ethene polymerization.[39] Nickel complexes of such ligands were listed in a patent by workers at Du Pont,[40] but no characterization or catalytic activity data were presented.

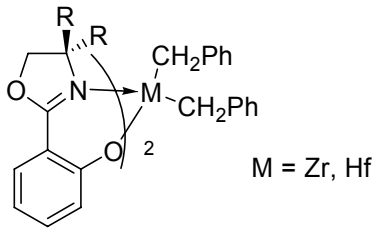

8

Figure 1.12 - Salicyloxazoline Ligands

1.2.3 Metal Alkyl Species

The great majority of reported salicylimine complexes discussed above are based on metal chloride centres; there are fewer reports of metal alkyl compounds. We have previously reported $[L_2Zr(CH_2Ph)_2]$ species,[34] Coates has reported the formation of metal alkyl species with salicylketimine ligands,[41] and Floriani has reported alkyls of salicyloxazoline ligands (*vide supra*). The rarity of reported group 4 metal alkyl

species with salicylaldimine ligands is of interest, since alkyl cations are implicated in the mechanism for polymerization (see §1.3.1), and are frequently observed for other single-site catalysts.[35]

1.3 Polymerization

1.3.1 Cation-Based Polymerization

1.3.1.1 Cation Formation and Stability

The active species in olefin polymerization catalyst mediated by single-site catalysts is generally believed to be a coordinatively unsaturated metal alkyl cation.[6,17,42] There are several possible routes to form such a species (Figure 1.13): abstraction of an alkyl anion, abstraction of an anionic spectator ligand such as chloride, or a combined alkylation/abstraction process such as that provided by MAO.

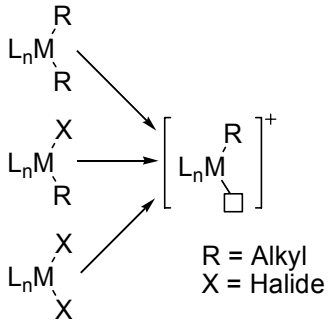

Figure 1.13 - Possible routes to formation of proposed active species

In metallocene catalyst systems, there is good evidence that the counterion remains attached to the metal centre *via* bridging methyl groups, forming complexes of the type $[L_2M(\mu\text{-}Me)_2(AlMe_2)]^+[MeMAO]^-$ or $[L_2M(Me)(\mu\text{-}Me)(MAO)]$.[43]

Previous work in our laboratory has shown that the group 4 benzyl cations of salicylaldimine species formed with $B(C_6F_5)_3$ show very poor stability, even at -78 °C.[31] Recently, group 4 salicylaldimine alkyl cations have been formed by

reaction of the appropriate chloride species with TMA-depleted MAO.[44] The reports by Fujita suggested that the cationic species initially formed decomposes into a second, inactive species (proposed to be $LAlMe_2$), and that this decomposition was slower in the presence of monomer (Figure 1.14).

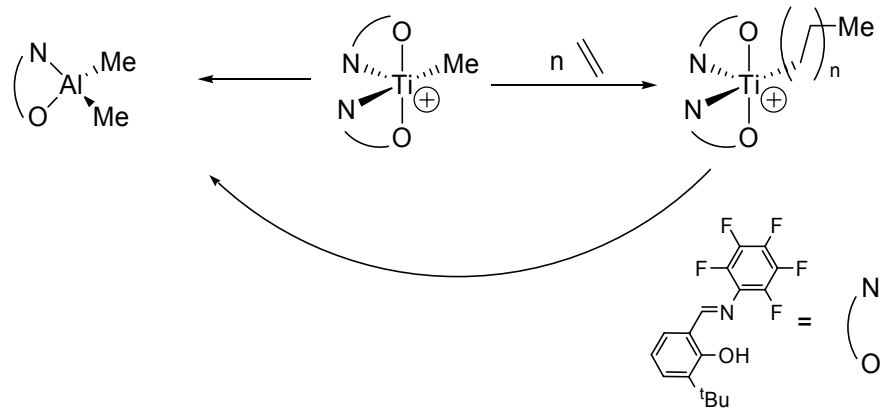

Figure 1.14 - Suggested decomposition pathway for salicylaldimine metal cations formed with MAO[44]

A more comprehensive investigation by Talsi *et al.*[45] confirms that the active species in polymerization is the alkyl cation, but goes further by establishing that a solvent molecule is weakly co-ordinated to the vacant site at the metal centre, and that – in contrast with the metallocene catalysts – the titanium methyl is not bridging to the MAO counterion. In contrast to the previous reports however, it was found that the polymeryl cation $[L_2TiP]^+$ decomposed *more* rapidly than the free cation, to $[LAlMe_2]$ and unidentified Ti^{3+} species (which were detected by EPR spectroscopy).

It seems likely that a rapid decomposition of the species believed to be responsible for polymer chain propagation will adversely affect the lifetime of such catalysts.

1.3.1.2 Cation Structures

Although the stereochemistry of the precatalyst compounds being introduced to the polymerization reaction can be readily determined by NMR and crystallographic techniques, it is somewhat more challenging to directly determine the structural nature of the active species in the polymerization. Few alkyl cations of salicylaldimine catalysts have been reported, and all of those possess perfluorinated aryl substituents on the imine nitrogen.[44,45] No crystal structures of such species have been presented.

Fujita has proposed that a number of differing geometrical isomers of the alkyl cation may be present in the reaction mixture,[25,46] thus explaining the multimodal molecular weight distributions observed in the polymer produced by such systems. The relative formation energy of each of the cations shown in Figure 1.15 was calculated (DFT) for each of the complexes shown in Table 1.1.

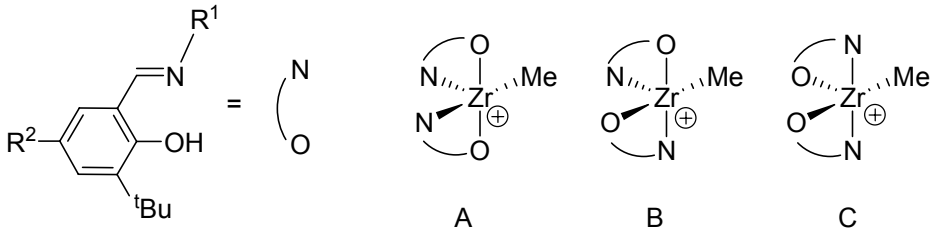

Figure 1.15 - Calculated cationic structures

Complex	R^1	R^2	Relative formation Energy kJ mol^{-1} [relative probability of isomer]			Polymer Modality
			A	**B**	**C**	
1	C_6H_5	H	0 [89%]	6.6 [9%]	11.2 [2%]	1
2	C_6H_5	CH_3	0 [37%]	-1.2 [56%]	4.9 [7%]	2
3	C_6H_5	OCH_3	0 [90%]	6.9 [8%]	11.6 [2%]	2
4	C_6F_5	H	0 [100%]	37.6 [0%]	29.3 [0%]	1
5	C_6F_5	OCH_3	0 [100%]	24.8 [0%]	22.6 [0%]	1

Table 1.1 Formation energy and relative probability of isomers

The resultant polymers generated from species 1, 2, 4 and 5 were found to have modality consistent with the predicted distribution of isomers of the cation (*i.e.* bimodal for complex 2, unimodal for 1, 4 and 5). Complex 3 however showed bimodal molecular weight distribution, but should be expected from the calculated energies to show a unimodal distribution. It seems therefore that such analysis is of only limited benefit. With hindsight, it seems likely that the influence of the counter-ion and co-ordinated polymer can not be so readily ignored.

The stability of the various possible isomers may only be one factor in determining the actual nature of the active species. It has been proposed that a methoxy substituent in the *para* position on the phenoxy ring can have a significant effect on stability of the active species, and therefore on the nature of the catalyst itself (*q.v.* §1.3.3)

1.3.2 Polymerization Activity

One problem that arises when attempting to review the structure/activity relationships in this field is the infrequency with which the reported *productivity* of a particular catalyst system is deconvoluted into its component *activity* and *lifetime*.

1.3.2.1 Steric Bulk

It has been repeatedly observed that for the salicylaldimine catalysts, a large steric bulk *ortho* to the phenoxy donor is critical for high-yielding polymerization.[17,21,23,47] It has been proposed that two factors may explain this effect: the bulk may protect the oxygen atom from co-ordination by Lewis acids (co-catalyst, or another molecule of the active cationic species),[18,23,48] or it may be responsible for enhancing the separation of the ion pair.[48,49]

1.3.2.2 Metal Centre

The activity of salicylaldimine systems towards ethene polymerization varies considerably with the choice of metal. Titanium systems typically show significantly lower productivity than the zirconium homologues, but produce higher molecular weight polymer.[18] During polymerization of ethene with **9**/MAO, the titanium system shows an activity of 3.58 kg_{PE} $mmol^{-1}$ bar^{-1} h^{-1} and produces polymer with M_v = 32.6 x 10^4 u whereas the zirconium system shows activity of 519 kg_{PE} $mmol^{-1}$ bar^{-1} h^{-1} with M_v = 1 x 10^4 u.

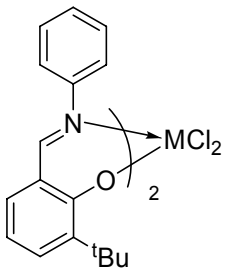

9

Figure 1.16 – Basic salicylaldimine complex structure

Titanium–based catalysts have been noted to give disproportionately high activity in *n*-hexane compared to toluene.[30] This has been attributed to the elimination of competition between toluene and ethene for co-ordination at the active site, which is not unprecedented.[50]

The hafnium complexes have been less frequently reported than the titanium or zirconium species, but seem to show intermediate behaviour – moderate molecular weight and moderate activity.[17,21]

1.3.3 Catalyst Deactivation

When attempting to understand the nature of polymerization catalysts, it is of fundamental importance to differentiate between *activity* and *lifetime*. Much of the published work regarding salicylaldimine catalysts makes no distinction between the two components. Reported experiments typically utilize very short reaction times, and operate at approximately room temperature, where deactivation is likely to be slow.[21-24] It has been the experience of our laboratory that salicylaldimine systems show limited lifetimes, especially at industrially favoured temperatures (≥ 50 °C).[31]

There are several possible routes to deactivation of the active species in polymerization: the most frequently proposed are reduction of the imine bond,

which may itself yield a catalytically active species (*q.v.* §1.2.2.2), or loss of ligand to aluminium (*q.v.* §1.3.1), which probably will not.

In an attempt to investigate the importance of ligand loss toward catalyst activity and lifetime, Fujita and co-workers synthesized a series of zirconium salicylaldimine catalysts possessing methoxy–substituents on the phenoxy ring, *para* to the oxygen donor, with the intention of strengthening the Zr–O bonds.[51] They determined that the species including the methoxy functionality were substantially more "active" at high temperature than those without. It is impossible to determine using the data presented whether this modification has improved activity *per se* or has in fact improved lifetime, but the net result is an observed increase in productivity.

It was proposed that this enhancement in "activity" was caused by increasing the electron-donating ability of the ligand, but results obtained when the N-substituent was varied are inconsistent with this, with cyclohexyl and *n*-hexyl substituents enhancing "activity" at high temperature, compared to a phenyl substituent.

1.3.4 Living Polymerization

There have been several examples of salicylimine catalysts which are believed to show "living" polymerization behaviour (*i.e.* the rates of chain transfer and termination reactions are zero).

1.3.4.1 Fluoroaryl Species

The first class of salicylimine group 4 catalysts reported as demonstrating living polymerization behaviour (for both ethene and propene) contained fluorine substituted aryl groups attached to the imine nitrogen.

It has been proposed that an unprecedented attractive interaction between the fluorine *ortho* to the imine nitrogen and the *β*-hydrogen on the growing polymer chain (Figure 1.17) prevents chain-transfers, and this appears to be backed by theoretical and structural studies,[52,53] including a recent neutron-diffraction study demonstrating [C–H···F–C] in titanium benzyl complexes.[54]

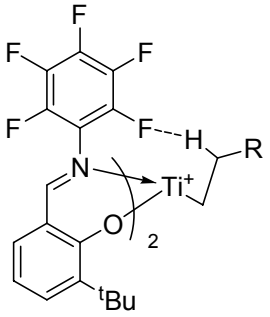

Figure 1.17 – "Living" catalysts

However, studies utilizing QM and QM/MM techniques have suggested that the effect of the fluorine substituents is actually a *steric* effect.[55-57] Chain propagation occurs *via* a compact four-centre transition state, whereas for *β*-hydride transfer to monomer a larger six-centre transition state is required. The presence of fluorine atoms in the *ortho* positions destabilizes the more sterically demanding transition to *β*-hydride transfer.[56] This is conceptually similar to the way in which 2,2′-substituted *rac*-bis(1-indenyl) *ansa*-metallocenes[57] and square-planar Brookhart–type systems[13] are believed to operate.

1.3.4.2 Ketimine Species

The salicylketimine systems developed by Coates[37] (**7**, see §1.2.2.3) also show living behaviour for polymerization of ethene, albeit at a low activity. This is of particular note since they do not have the fluorine substituents on the imine substituent necessary for living polymerization with salicylaldimine species (*vide supra*).

1.3.5 Polymer Properties

Salicylaldimine catalyst systems can produce a number of novel polyolefinic materials, and a recent review has comprehensively discussed the nature of these materials and the use of salicylaldimine catalysts in their production.[59] The following section of this introduction will briefly reiterate the classes of material available, and will attempt to relate the structure of the catalyst system to the materials produced.

1.3.5.1 Poly(ethene)

Molecular Weight Control

Salicylaldimine catalysts produce high-density PE (HDPE), *i.e.* there is virtually no branching of the polymer chains. Variation of the ligand in the catalyst system produces substantial variation in the polymer produced, with molecular weight being variable between 10^3 and 10^7 u.

There does not appear to be a clear relationship between ligand structure and polymer molecular weight, but several factors play a role. Increased bulk on the substituent on the imine nitrogen usually results in a higher molecular weight.[17,24] *Ortho*-fluorination of an aryl substituent also increases the molecular weight of the polymer produced (*q.v.* §1.3.4.1). It seems likely that both effects are due to hindrance of β-hydride transfer from the growing polymer chain.

As previously discussed, it is believed that differing isomers of the active species present in the reaction mixture are responsible for multimodal polymer molecular weight distributions observed with some of these systems (*q.v.* §1.3.1.2).

Activation of some precatalysts with $^{i}Bu_3Al$ has been shown to reduce the imine functionality to amine, resulting in a less active system, but one which produces much higher molecular weight PE[22,30] (*q.v.* §1.2.2.2).

The choice of metal centre also plays a role in determining the molecular weight of the PE produced, varying in the order Ti > Hf > Zr.[17,21]

Vinyl Terminated Polymers

Some salicylaldimine catalyst systems, in particular those with cycloalkyl substituents on the imine nitrogen, give low molecular weight PE (M_w = 2000–4000 u) with a high proportion (>90%) of vinyl unsaturation at one of the chain ends.[60] This is also consistent with β-hydride elimination to monomer being the dominant termination reaction.

Vinyl terminated low molecular weight PEs are of interest due to the reactivity of the vinyl group. They may be used as intermediates in the formation of more complex polymer structures, for example as "macromonomers" for incorporation into a long-chain-branched PE system,[61] by further functionalisation to form end-functionalized PEs, or in the formation of block copolymers containing a PE segment and *e.g.* a polar polymer segment.

1.3.5.2 Poly(propene)

Salicylaldimine catalysts can produce a number of previously inaccessible poly(propene) (PP) products. In many cases the nature of the active species, and the mechanism for polymer insertion are unclear – hence precluding predictive design of catalyst systems. This is well put by Talarico and Cavallo:[56]

> "'Catalyst design', meaning the *rational* invention of a well-defined active species for a targeted application, is often associated with the metallocene

and post-metallocene breakthroughs in stereoselective olefin polymerization. The rapid and apparently endless implementation of new catalysts, leading to an amazing variety of largely unprecedented homopolymer and copolymer architectures, is actually perceived as a most convincing demonstration of the said association. In reality, *designing* one such catalyst from scratch is still a dream, and behind all reported discoveries is the classical mix of hard work and serendipity."

Syndiotactic Poly(propene)

Salicylaldimine catalysts have demonstrated the ability to generate a wide range of PP architectures, depending on the choice of ligand, metal centre, and co-catalyst/activator. Those based on titanium have shown the ability to produce highly syndiotactic PP (sPP) with very high peak melting temperatures (T_m).[47,53] This is somewhat surprising, since the precatalyst species preferentially form the C_2-symmetric *cis,trans,cis* (*i.e. cis*-N, *trans*-O) isomers. It has been assumed that some fluxional process of the active species is responsible for this behaviour,[16] and some theoretical (QM/MM-DFT) work[57] has suggested that the mechanism is a site-inversion between the Δ and Λ diastereoisomers of the proposed active species.

The polymerization mechanism in catalysts which produce sPP appears to be an initial 1,2-insertion of monomer followed by 2,1-insertion as the predominant propagation step.[53,62] This is a very unusual mechanism, and has led to some unique polymer structures from diene monomers.[63]

The zirconium and hafnium analogues appear to favour a 1,2 insertion mechanism, and produce only slightly syndiotactic PPs.[64]

Similarly to ethene polymerization, a bulky substituent *ortho* to the phenoxy-oxygen appears to be essential for high activity but in this case also for

syndioselectivity.[47,53] This is not in itself enough to explain the relationship between catalyst structure and resultant PP, however; it appears that changes to ligand, metal, co-catalyst (even down to variations in the batch of MAO used), all affect the syndiotacticity of the product.[59]

Isotactic Poly(propene)

Few examples of salicylaldimine ligands on zirconium and hafnium show any propene polymerization activity when activated with MAO, and those that do all have perfluorinated aryl substituents on the imine nitrogen, and produce very low molecular weight atactic PP (aPP) that may perhaps more accurately be described as oligomers.[64] This is consistent with QM/MM analysis of the possible transition states during propene polymerization[57] (*i.e.* to β-H elimination or to propagation) at different metal centres, which concur well with experimental results (*c.f.* §1.3.4.1).

When activated with $^{i}Bu_3Al/[(Ph_3C)B(C_6F_5)_4]$ (and hence presumably converted to salicylamine species, *q.v.* §1.2.2.2), some examples can produce moderately to highly isotactic PP (iPP).[65] The best performance comes from those with adamantyl substituents *ortho* to the salicylic oxygen, and cyclohexyl substituents on the imine nitrogen, which generate very isotactic PPs with extremely high peak melting temperatures (up to 165 °C).[66]

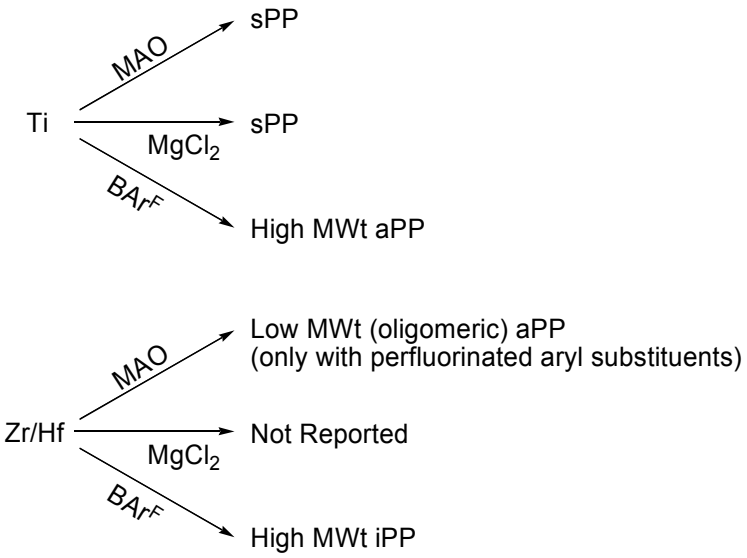

Figure 1.18 - Effect of metal centre and co-catalyst on propene polymerization

1.4 Conclusions

A wide range of salicylimine catalysts have been developed, and are capable of producing many polyolefinic materials, but there is currently little ability to *design* a catalyst in this series to produce a given product. Further, the reduced activity of most of these catalyst series at elevated temperatures presents a significant obstacle to industrial application of these systems. In addition, the majority of reported species possess an aniline moiety, which would render material produced with such catalysts unusable in many key applications.

At the time we began this work, the mechanism of catalyst deactivation was unknown, and no reported data differentiated between activity and productivity, which is fundamental to understanding the catalyst system during polymerization. We recognized the potential importance of these systems, and our investigations were intended to shed light on possible ways to enhance their industrial applicability.

1.5 References for Chapter 1

1 G. Natta, *Angew. Chem.*, 1956, **68**, 393-403; G. Natta, *J. Polym. Sci., Part A: Polym. Chem.*, 1955, **16**, 143-54; K. Ziegler, E. Holzkamp, H. Breil and H. Martin, *Angew. Chem.*, 1955, **67**, 541-7.

2 H. H. Brintzinger, D. Fischer, R. Mulhaupt, B. Rieger and R. M. Waymouth, *Angew. Chem., Int. Ed. Engl.*, 1995, **34**, 1143-70; M. Bochmann, *J. Chem. Soc., Dalton Trans.*, 1996, 255-70.

3 P. J. Shapiro, E. Bunel, W. P. Schaefer and J. E. Bercaw, *Organometallics*, 1990, **9**, 867-69; G. F. Schmidt, G. F. Timmers, G. W. Knight, S. Lai, P. N. Nickias, R. K. Rosen, J. C. Stevens and D. R. Wilson, EP0416815 (Dow Chemical Company), 1991; J. M. Canich, G. G. Hlatky and H. W. Turner, WO 92-00333 (Exxon Chemical Patents Inc), 1992; J. M. Canich, EP0420436 (Exxon Chemical Company), 1991.

4 W. Kaminsky, J. Kopf, H. Sinn and H. J. Vollmer, *Angew. Chem., Int. Ed. Engl.*, 1976, **15**, 629-30; H. Sinn, W. Kaminsky, H. J. Vollmer and R. Woldt, *Angew. Chem.*, 1980, **92**, 396-402; A. Andresen, H. G. Cordes, J. Herwig, W. Kaminsky, A. Merck, R. Mottweiler, J. Pein, H. Sinn and H. J. Vollmer, *Angew. Chem., Int. Ed. Engl.*, 1976, **15**, 630-32.

5 V. C. Gibson and S. K. Spitzmesser, *Chem. Rev.*, 2003, **103**, 283-315.

6 G. J. P. Britovsek, V. C. Gibson and D. F. Wass, *Angew. Chem., Int. Ed. Engl.*, 1999, **38**, 428-47.

7 A. Combes, *C. R. Hebd. Acad. Sci.*, 1889, **108**, 1252.

8 J. P. Collman, L. S. Hegedus, J. R. Norton and R. C. Finke, 'Principles and applications of organotransition metal chemistry', University Science Books, 1987.

9 S. N. Poddar and D. K. Biswas, *J. Inorg. Nucl. Chem.*, 1969, **31**, 565-67; J. P. Corden, W. Errington, P. Moore and M. G. H. Wallbridge, *Chem. Commun.*, 1999, 323-24; E. B. Tjaden, D. C. Swenson, R. F. Jordan and J. L. Petersen, *Organometallics*, 1995, **14**, 371-86; F. Corazza, E. Solari, C. Floriani, A. Chiesi-Villa and C. Guastini, *J. Chem. Soc., Dalton Trans.*, 1990, 1335-44.

10 T. Repo, M. Klinga, P. Pietikaeinen, M. Leskelae, A.-M. Uusitalo, T. Pakkanen, K. Hakala, P. Aaltonen and B. Loefgren, *Macromolecules*, 1997, **30**, 171-75.

11 L. K. Johnson, C. M. Killian and M. Brookhart, *J. Am. Chem. Soc.*, 1995, **117**, 6414-15; L. K. Johnson, S. Mecking and M. Brookhart, *J. Am. Chem. Soc.*, 1996, **118**, 267-68; C. M. Killian, D. J. Tempel, L. K. Johnson and M. Brookhart, *J. Am. Chem. Soc.*, 1996, **118**, 11664-65.

12 O. Daugulis and M. Brookhart, *Organometallics*, 2002, **21**, 5926-34; A. Daugulis, M. Brookhart and P. S. White, *Organometallics*, 2002, **21**, 5935-43.

13 S. Ittel, L. Johnson and M. Brookhart, *Chem. Rev.*, 2000, **100**, 1169-203.

14 P. A. Cameron, V. C. Gibson, C. Redshaw, J. A. Segal, A. J. P. White and D. J. Williams, *J. Chem. Soc., Dalton Trans.*, 2002, 415-22; V. C. Gibson, C. Newton, C. Redshaw, G. A. Solan, A. J. P. White and D. J. Williams, *J. Chem. Soc., Dalton Trans.*, 1999, 827-29.

15 B. L. Small, M. Brookhart and A. M. A. Bennett, *J. Am. Chem. Soc.*, 1998, **120**, 4049-50; G. J. P. Britovsek, V. C. Gibson, B. S. Kimberley, P. J. Maddox, S. J. McTavish, G. A. Solan, A. J. P. White and D. J. Williams, *Chem. Commun.*, 1998, 849-50.

16 J. Tian and G. W. Coates, *Angew. Chem.*, 2000, **39**, 3626-29; J. Tian, P. Hustad and G. Coates, *J. Am. Chem. Soc.*, 2001, **123**, 5134-35.

17 S. Matsui and T. Fujita, *Catal. Today*, 2001, **66**, 63-73.

18 H. Makio, N. Kashiwa and T. Fujita, *Adv. Synth. Catal.*, 2002, **344**, 477-93.

19 Y. Suzuki, H. Terao and T. Fujita, *Bull. Chem. Soc. Jpn.*, 2003, **76**, 1493-517.

20 S. Matsui, Y. Tohi, M. Mitani, J. Saito, H. Makio, H. Tanaka, M. Nitabaru, T. Nakano and T. Fujita, *Chem. Lett.*, 1999, 1065-66.

21 T. Fujita, Y. Tohi, M. Mitani, S. Matsui, J. Saito, M. Nitabaru, K. Sugi, H. Makio and T. Tsutsui, EP874005 (Mitsui Chemicals, Inc., Japan), 1998.

22 S. Matsui, M. Mitani, J. Saito, Y. Tohi, H. Makio, H. Tanaka and T. Fujita, *Chem. Lett.*, 1999, 1263-64.

23 S. Matsui, M. Mitani, J. Saito, N. Matsukawa, H. Tanaka, T. Nakano and T. Fujita, *Chem. Lett.*, 2000, 554-55.

24 S. Matsui, M. Mitani, J. Saito, Y. Tohi, H. Makio, N. Matsukawa, Y. Takagi, K. Tsuru, M. Nitabaru, T. Nakano, H. Tanaka, N. Kashiwa and T. Fujita, *J. Am. Chem. Soc.*, 2001, **123**, 6847-56.

25 Y. Tohi, H. Makio, S. Matsui, M. Onda and T. Fujita, *Macromolecules*, 2003, **36**, 523-25.

26 F. Milani, U. Casellato, P. A. Vigato, M. Vidali, D. F. Fenton and M. S. L. Gonzalez, *Inorg. Chim. Acta*, 1985, **103**, 15-18.

27 Y. Nakayama, H. Bando, Y. Sonobe and T. Fujita, *J. Mol. Catal. A: Chem.*, 2004, **213**, 141-50; Y. Nakayama, H. Bando, Y. Sonobe, Y. Suzuki and T. Fujita, *Chem. Lett.*, 2003, **32**, 766-67.

28 V. C. Gibson, S. Mastroianni, C. Newton, C. Redshaw, G. A. Solan, A. J. P. White and D. J. Williams, *J. Chem. Soc., Dalton Trans.*, 2000, 1969-72; D. J. Jones, V. C. Gibson, S. M. Green and P. J. Maddox, *Chem. Commun.*, 2002, 1038-39; D. J. Jones, V. C. Gibson, S. M. Green, P. J. Maddox, A. J. P. White and D. J. Williams, *J. Am. Chem. Soc.*, 2005, **127**, 11037-46.

29 T. R. Younkin, E. F. Conner, J. I. Henderson, S. K. Friedrich, R. H. Grubbs and D. A. Bansleben, *Science*, 2000, **287**, 460-62; D. A. Bansleben, S. K. Friedrich, T. R. Younkin, R. H. Grubbs, C. Wang and R. T. Li, 6410664 (Cryovac, Inc., USA), 2002.

30 J. Saito, M. Mitani, S. Matsui, Y. Tohi, H. Makio, T. Nakano, H. Tanaka, N. Kashiwa and T. Fujita, *Macromol. Chem. Phys.*, 2002, **203**, 59-65.

31 P. D. Knight, 'Chiral at Metal Catalyst Designs for Alkene Polymerisation and Hydroamination', Ph.D. Thesis, University of Warwick, Coventry, 2003.

32 P. R. Woodman, I. J. Munslow, P. B. Hitchcock and P. Scott, *J. Chem. Soc., Dalton Trans.*, 1999, 4069-76.

33 P. D. Knight, A. J. Clarke, B. S. Kimberley, R. A. Jackson and P. Scott, *Chem. Commun.*, 2002, 352-53.

34 P. D. Knight, G. Clarkson, M. L. Hammond, B. S. Kimberley and P. Scott, *J. Organomet. Chem.*, 2005, **690**, 5125-44.

35 E. Chen and T. Marks, *Chem. Rev.*, 2000, **100**, 1391-434.

36 R. W. Chesnut, R. R. Cesati, C. S. Cutler, S. L. Pluth and J. A. Katzenellenbogen, *Organometallics*, 1998, **17**, 4889-96; D. A. Cogan, G. C. Liu, K. J. Kim, B. J. Backes and J. A. Ellman, *J. Am. Chem. Soc.*, 1998, **120**, 8011-19; M. Hayashi, K. Tanaka and N. Oguni, *Tetrahedron: Asymmetry*, 1995, **6**, 1833-36.

37 S. Reinartz, A. F. Mason, E. B. Lobkovsky and G. W. Coates, *Organometallics*, 2003, **22**, 2542-44.

38 Y. Inoue, T. Nakano, H. Tanaka, N. Kashiwa and T. Fujita, *Chem. Lett.*, 2001, 1060-61.

39 P. G. Cozzi, C. Floriani, A. Chiesi-Villa and C. Rizzoli, *Inorg. Chem.*, 1995, **34**, 2921-30; P. G. Cozzi, E. Gallo, C. Floriani, A. Chiesi-Villa and C. Rizzoli, *Organometallics*, 1995, **14**, 4994-96.

40 L. K. Johnson, A. M. A. Bennett, S. D. Ittel, L. Wang, A. Parthasarathy, E. Hauptman, R. D. Simpson, J. Feldman and E. B. Coughlin, WO9830609 (E.I. Du Pont De Nemours and Company), 1998.

41 G. W. Coates, S. Reinartz and A. F. Mason, WO2004/058777 (Cornell Research Foundation, Inc., USA), 2004.

42 E. Zurek and T. Ziegler, *Faraday Discuss.*, 2003, **124**, 93-109; E. Zurek and T. Ziegler, *Organometallics*, 2002, **21**, 83-92; E. Zurek and T. Ziegler, *Prog. Polym. Sci.*, 2004, **29**, 107-48; W. Kaminsky and A. Laban, *Appl. Catal. A-Gen.*, 2001, **222**, 47-61; J. J. Eisch, S. I. Pombrik and G. X. Zheng, *Organometallics*, 1993, **12**, 3856-63; R. F. Jordan, W. E. Dasher and S. F. Echols, *J. Am. Chem. Soc.*, 1986, **108**, 1718-19.

43 J. L. Eilertsen, J. A. Støvneng, M. Ystenes and E. Rytter, *Inorg. Chem.*, 2005, **44**, 4843-51; M. Ystenes, J. L. Eilertsen, J. K. Liu, M. Ott, E. Rytter and J. A. Støvneng, *J. Polym. Sci., Part A: Polym. Chem.*, 2000, **38**, 3106-27; K. P. Bryliakov, E. P. Talsi and M. Bochmann, *Organometallics*, 2004, **23**, 149-52; K. P. Bryliakov, N. V. Semikolenova, D. V. Yudaev, V. A. Zakharov, H. H. Brintzinger, M. Ystenes, E. Rytter and E. P. Talsi, *J. Organomet. Chem.*, 2003, **683**, 92-102.

44 H. Makio and T. Fujita, *Macromol. Symp.*, 2004, **213**, 221-33.

45 K. P. Bryliakov, E. A. Kravtsov, D. A. Pennington, S. J. Lancaster, M. Bochmann, H. H. Brintzinger and E. P. Talsi, *Organometallics*, 2005, **24**, 5660-64.

46 Y. Tohi, T. Nakano, H. Makio, S. Matsui, T. Fujita and T. Yamaguchi, *Macromol. Chem. Phys.*, 2004, **205**, 1179-86.

47 R. Furuyama, J. Saito, S. Ishii, M. Mitani, S. Matsui, Y. Tohi, H. Makio, N. Matsukawa, H. Tanaka and T. Fujita, *J. Mol. Catal. A: Chem.*, 2003, **200**, 31-42.

48 P. A. Deck, C. L. Beswick and T. J. Marks, *J. Am. Chem. Soc.*, 1998, **120**, 1772-84.

49 A. D. Horton and J. deWith, *Chem. Commun.*, 1996, 1375-76; H. Mack and M. S. Eisen, *J. Organomet. Chem.*, 1996, **525**, 81-87.

50 J. D. Scollard and D. H. McConville, *J. Am. Chem. Soc.*, 1996, **118**, 10008-09; J. D. Scollard, D. H. McConville, N. C. Payne and J. J. Vittal, *Macromolecules*, 1996, **29**, 5241-43.

51 N. Matsukawa, S. Matsui, M. Mitani, J. Saito, K. Tsuru, N. Kashiwa and T. Fujita, *J. Mol. Catal. A: Chem.*, 2001, **169**, 99-104.

52 M. Mitani, R. Furuyama, J. Mohri, J. Saito, S. Ishii, H. Terao, N. Kashiwa and T. Fujita, *J. Am. Chem. Soc.*, 2002, **124**, 7888-89; J. Saito, M. Mitani, J. Mohri, Y. Yoshida, S. Matsui, S. Ishii, S. Kojoh, N. Kashiwa and T. Fujita, *Angew. Chem.*, 2001, **40**, 2918-20; M. Mitani and T. Fujita, *ACS Symp. Ser.*, 2003, **857**, 26-45; M. Mitani, T. Nakano and T. Fujita, *Chem. Eur. J.*, 2003, **9**, 2396-403; S. C. F. Kui, N. Y. Zhu and M. C. W. Chan, *Angew. Chem. Int. Ed.*, 2003, **42**, 1628-32; R. Furuyama, J. Saito, S. Ishii, H. Makio, M. Mitani, H. Tanaka and T. Fujita, *J. Organomet. Chem.*, 2005, **690**, 4398-413; S. Ishii, R. Furuyama, N. Matsukawa, J. Saito, M. Mitani, H. Tanaka and T. Fujita, *Macromol. Rapid. Commun.*, 2003, **24**, 452-56.

53 M. Mitani, R. Furuyama, J. Mohri, J. Saito, S. Ishii, T. Terao, T. Nakano, H. Tanaka and T. Fujita, *J. Am. Chem. Soc.*, 2003, **125**, 4293-305.

54 M. C. W. Chan, S. C. F. Kui, J. M. Cole, G. J. McIntyre, S. Matsui, N. Y. Zhu and K. H. Tam, *Chem. Eur. J.*, 2006, **12**, 2607-19.

55 V. Busico, G. Talarico and R. Cipullo, *Macromol. Symp.*, 2005, **226**, 1-16.

56 G. Talarico, V. Busico and L. Cavallo, *J. Am. Chem. Soc.*, 2003, **125**, 7172-73.

57 G. Talarico, V. Busico and L. Cavallo, *Organometallics*, 2004, **23**, 5989-93.

58 U. Stehling, J. Diebold, R. Kirsten, W. Röll, H. H. Brintzinger, S. Jüngling, R. Mülhaupt and F. Langhauser, *Organometallics*, 1994, **13**, 964-70.

59 M. Mitani, J. Saito, S. I. Ishii, Y. Nakayama, H. Makio, N. Matsukawa, S. Matsui, J. I. Mohri, R. Furuyama, H. Terao, H. Bando, H. Tanaka and T. Fujita, *Chem. Rec.*, 2004, **4**, 137-58.

60 S. Ishii, M. Mitani, J. Saito, S. Matsuura, S. Kojoh, N. Kashiwa and T. Fujita, *Chem. Lett.*, 2002, 740-41.

61 D. Yan, W. J. Wang and S. Zhu, *Polymer*, 1999, **40**, 1737-44.

62 J. Saito, M. Mitani, M. Onda, J. Mohri, J. Ishi, Y. Yoshida, T. Nakano, H. Tanaka, T. Matsugi, S. Kojoh, N. Kashiwa and T. Fujita, *Macromol. Rapid. Commun.*, 2001, **22**, 1072-75; P. Hustad, J. Tian and G. Coates, *J. Am. Chem. Soc.*, 2002, **124**, 3614-21; M. Lamberti, D. Pappalardo, A. Zambelli and C. Pellecchia, *Macromolecules*, 2002, **35**, 6478-78.

63 P. Hustad and G. Coates, *J. Am. Chem. Soc.*, 2002, **124**, 11578-79.

64 H. Makio, Y. Tohi, J. Saito, M. Onda and T. Fujita, *Macromol. Rapid. Commun.*, 2003, **24**, 894-99.

65 J. Saito, M. Onda, S. Matsui, M. Mitani, R. Furuyama, H. Tanaka and T. Fujita, *Macromol. Rapid. Commun.*, 2002, **23**, 1118-23.

66 A. Prasad, H. Makio, J. Saito, M. Onda and T. Fujita, *Chem. Lett.*, 2004, **33**, 250-51.

2 C2–bridged Salicylaldiminato Complexes

2.1 Introduction

One of the key issues concerning the Mitsui salicylaldimine catalysts[1] is the loss of productivity at elevated temperatures (See §1.2.2, §1.3.3). One possible cause of catalyst deactivation is 1,2-Migratory Insertion of a metal-bound alkyl into the imine C=N unit, and previous researchers within our laboratory have investigated this process in the tetradentate biaryl–bridged system **1**.[2,3]

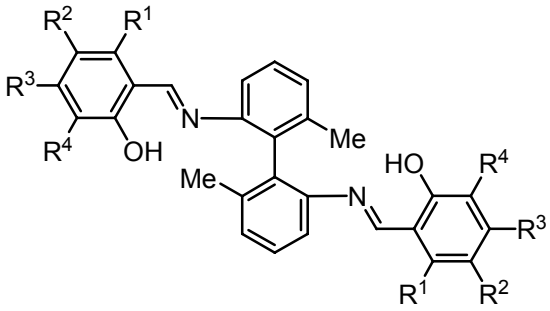

1

Figure 2.1 Biaryl precursor and ligand system

As discussed in §1.2.2.1, methyl substitution at the R^1 positions of **1** resulted in steric blocking of the MI reaction, and the complexes were shown to decompose instead *via* a slower radical pathway when a benzyl co-ligand was present. Such modified biaryl complexes are long-lived catalysts for ethylene polymerization, albeit with far lower activity than the analogous unbridged analogues.

The same increase in longevity was not observed for the unbridged salicylaldimine species. This was attributed to the increased flexibility of such complexes allowing the methyl group to move away from the site where it could block the MI.

We proposed that the reduction in activity observed in the biaryl-bridged systems **1** compared to unbridged systems was due to increased crowding at the active site during polymerization. Thus, lengthening the bridge between the aryl functionalities may be expected to reduce the constraint in the complexes, and hopefully provide active catalysts whilst still providing enough rigidity for the methyl substituent to be effective in retarding MI reactions.

Thakkar and Patil have previously synthesised Cu(II), Ni(II) and Co(II) complexes of ligands such as **2**, but their work was limited to characterization of the metal complexes and did not extend to investigations of reactivity.[4]

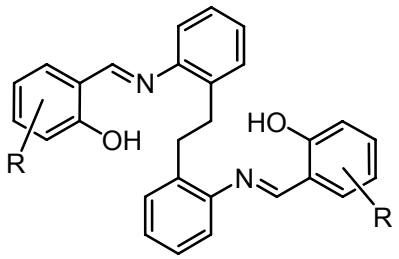

2

Fujita has previously investigated conceptually similar tetradentate ligands such as **3** (Figure 2.2), containing salicylaldimine units bridged through the imine unit, with varying length methylene chains ($n = 2 - 6$).[5] Ethene polymerization productivity was reported to increase with increasing n, and activity is reported to be higher at elevated temperature. However, the catalysts were only tested for very short periods (2 or 5 minutes),* and correspondingly the issue of deactivation was not addressed. Furthermore, the change from the aryl-substituted imines to these alkyl-substituted species may reasonably be expected to alter the properties of the catalyst system.

* In their paper, Fujita *et al.* do not give details of the polymerization times at elevated temperature. We have calculated the reaction times from the reported productivities.

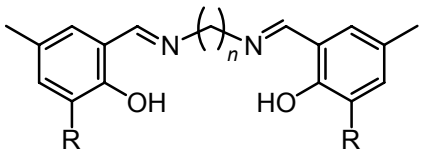

3

Figure 2.2 - N-Bridged salicylaldimines

2.2 Bibenzyl systems

2.2.1 Synthesis of proligands, H_2L^{1-4}

Salicylaldehydes were synthesised via the method reported by Hofsløkken[6] and optimised by Dr. Paul Knight in this laboratory (Scheme 2.1).

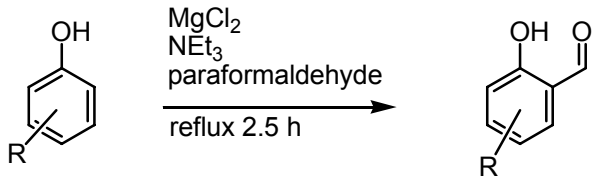

Scheme 2.1 - Synthesis of substituted salicylaldehydes

The imine proligands shown in Table 2.1 were synthesised by condensation between 1,1'-ethylenedianiline and the appropriate salicylaldehyde in good yield, as shown in Scheme 2.2. Initially, we concentrated on the species containing a ^{t}Bu substituent *ortho* to the phenoxy-oxygen (*i.e.* L^1 and L^2), since steric bulk in this position is believed to be essential for activity of phenoxy-imine catalysts. The species with less bulky substituents were investigated later, in response to our attempts to form metal alkyls. The methoxy-substituted species H_2L^5 was investigated following the results discussed in Chapter 3. For comparison, the unbridged ligands HL^6 and HL^7 were also used, as prepared by Dr Paul Knight in this laboratory (Figure 2.3)[2,7].

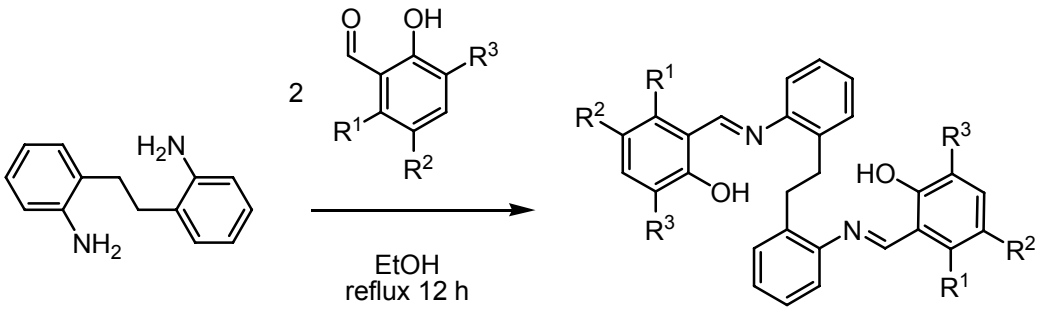

Scheme 2.2 – Synthesis of bibenzyl proligands

	R^1	R^2	R^3	Yield
H_2L^1	H	Me	^{t}Bu	86%
H_2L^2	Me	H	^{t}Bu	95%
H_2L^3	H	Me	Me	92%
H_2L^4	Me	H	Me	89%
H_2L^5	H	OMe	^{t}Bu	71%

Table 2.1 – Proligands synthesised

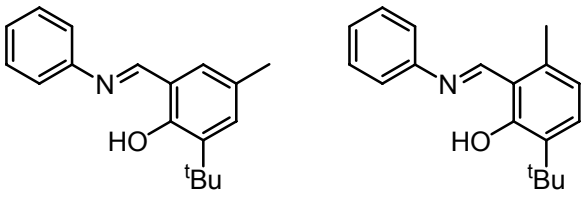

HL^6 HL^7

Figure 2.3 - Unbridged proligands for comparison with H_2L^{1-5}

2.2.2 Synthesis and characterization of metal chloride complexes

The species $[L^nMCl_2]$ (n = 1, 2, M = Ti, Zr) were synthesised in good yield (~60-70%) *via* the routes shown in Scheme 2.3, and were purified by sublimation (*vide infra*). The unbridged titanium complexes $[L^n{}_2TiCl_2]$ (n = 6, 7) were synthesised in the same fashion. Attempts to make $[L^5MCl_2]$ (M = Ti, Zr) *via* salt-metathesis (Li, Na, K) resulted in intractable mixtures which decomposed upon attempted sublimation.

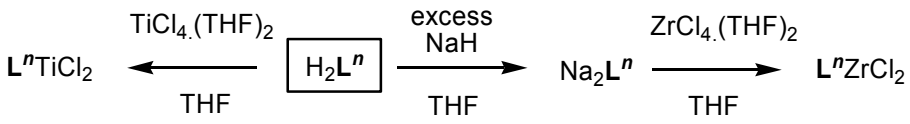

Scheme 2.3 – Synthesis of metal chloride complexes

2.2.2.1 Zirconium chloride complexes

The zirconium chloride complexes [L^nZrCl_2] (n = 1,2) were synthesised by salt metathesis between the sodium salts $Na_2\mathbf{L^1}$ and $Na_2\mathbf{L^2}$ and [$ZrCl_4(THF)_2$]. The products were isolated by sublimation at ~300 °C and 10^{-6} bar. ^{1}H NMR studies suggest that there are two products formed, in a ratio of approximately 1:4. The minor product gave sharp signals in ^{1}H NMR spectra at 298 K, whereas the major product gave much broader signals. Upon cooling to 183 K, the ^{1}H NMR signals from the major product became sharp. The signals from the minor product are consistent with a C_2-symmetrical *cis*-α species (Figure 2.4). The major product is an unsymmetrical species, *i.e.* the *cis*-β isomer. Since the exchange process causing line broadening evidently does not facilitate exchange between the two isomers on this timescale it is likely to be associated with conformational fluxionality in the nine-membered chelate structure.

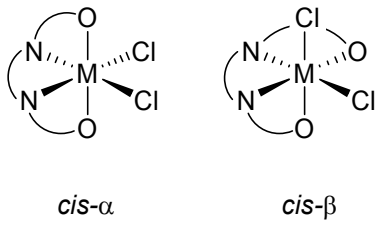

Figure 2.4 - *cis*-α and *cis*-β isomers

2.2.2.2 Titanium chloride complexes

Reaction of $H_2\mathbf{L^1}$ and $H_2\mathbf{L^2}$ with [$TiCl_4(THF)_2$] yielded crude products with ^{1}H NMR spectra which indicated the presence of –OH groups, suggesting that species such as

[H**L**^{n}TiCl$_{x}$(THF)$_{y}$] were present. After sublimation at ~300 °C and 10^{-6} bar however, the –OH resonance is not detected, and the desired [TiL^{n}Cl$_2$] (n = 1,2) complexes were isolated. ^{1}H NMR spectrum shows the presence of one unsymmetrical compound, which we assign as the *cis*-β isomer. In contrast to the zirconium species, these resonances are sharp at 298K.

The molecular structure of [L^{2}TiCl$_2$] was determined by Dr Paul O'Shaugnessey using single-crystal X-ray diffractometry (XRD). The structure of the complex was thus confirmed as the *cis*-β isomer (Figure 2.6). To our knowledge this is the first example of a *cis*-β (or indeed a *cis,cis,cis*) structure of a titanium salicylaldimine. A number of *cis,trans,cis* (*c.f. cis*-α) structures have been reported however,[7-10] and the bond distances and angles for [L^{2}TiCl$_2$] are unremarkable compared to these – for example [(**4**)$_2$TiCl$_2$] reported by Coates *et al.*[9] (Table 2.2).

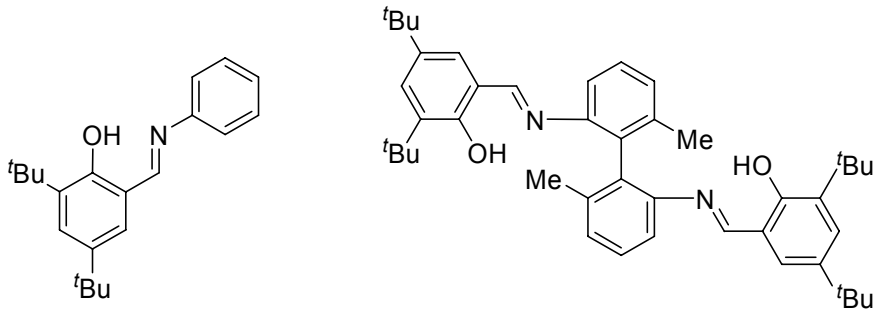

4 **5**

Figure 2.5 - Proligands used in comparison complexes

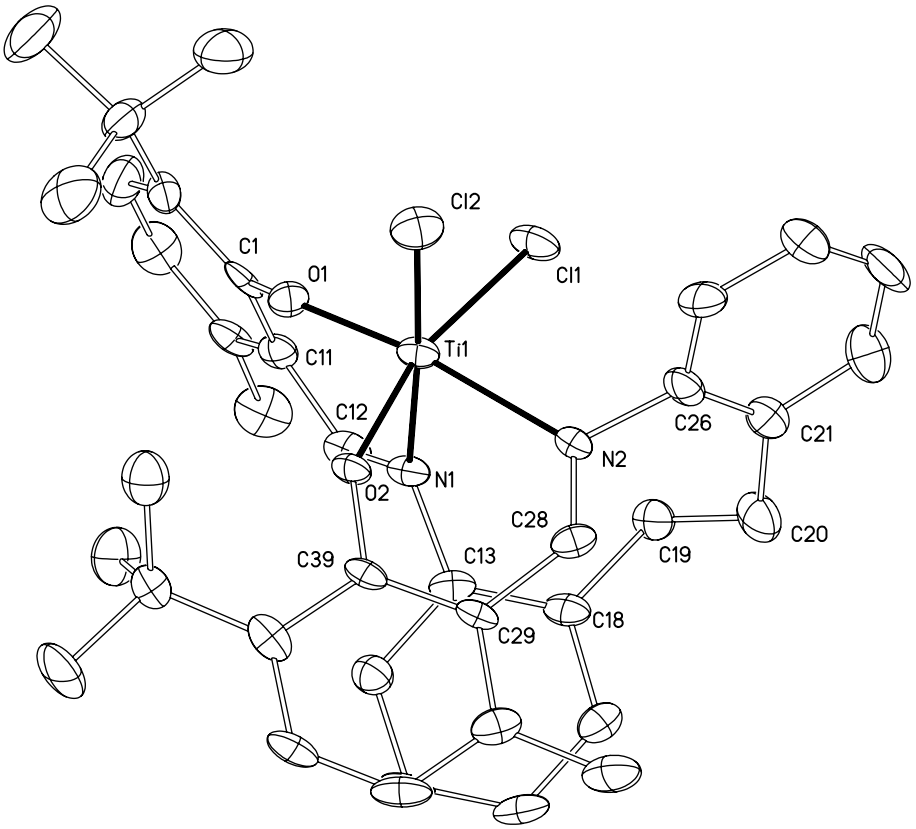

Figure 2.6 – Molecular structure of $[L^2TiCl_2]$ (Hydrogen atoms omitted for clarity). Probability ellipsoids are set to the 50% level

$[L^2TiCl_2]$		$[(4)_2TiCl_2]$[9]	
Bond	**Length (Å)**	**Bond**	**Length (Å)**
Ti(1)-O(1)	1.828(3)	Ti(1)-O(1)	1.8343(19)
Ti(1)-O(2)	1.837(3)	Ti(1)-O(2)	1.8390(19)
Ti(1)-N(1)	2.240(4)	Ti(1)-N(1)	2.202(2)
Ti(1)-N(2)	2.239(4)	Ti(1)-N(2)	2.219(2)
Ti(1)-Cl(1)	2.3174(14)	Ti(1)-Cl(1)	2.3098(9)
Ti(1)-Cl(2)	2.3075(14)	Ti(1)-Cl(2)	2.3175(8)
Bonds	**Angle (°)**	**Bonds**	**Angle (°)**
O(1)-Ti(1)-N(2)	170.38(13)	O(1)-Ti(1)-O(2)	171.39(8)
O(1)-Ti(1)-N(1)	80.69(13)	O(1)-Ti(1)-N(1)	81.06(8)
O(2)-Ti(1)-N(2)	80.18(13)	O(2)-Ti(1)-N(2)	79.91(8)
O(2)-Ti(1)-N(1)	85.12(13)	O(1)-Ti(1)-N(2)	92.36(9)
N(2)-Ti(1)-N(1)	89.93(13)	N(1)-Ti(1)-N(2)	83.49(8)
Cl(2)-Ti(1)-Cl(1)	95.59(5)	Cl(1)-Ti-Cl(2)	98.58(3)
C(1)-O(1)-Ti(1)	140.4(3)	O(2)-Ti(1)-N(1)	94.21(8)
C(39)-O(2)-Ti(1)	145.3(3)		

Table 2.2 - Selected bond angles and distances for $[L^2TiCl_2]$ with comparison to the reported molecular structure of $[(4)_2TiCl_2]$

Although the geometry at the metal is similar between the catalyst reported here and those previously reported, there are significant differences between the steric environments of the active sites (Figure 2.7).

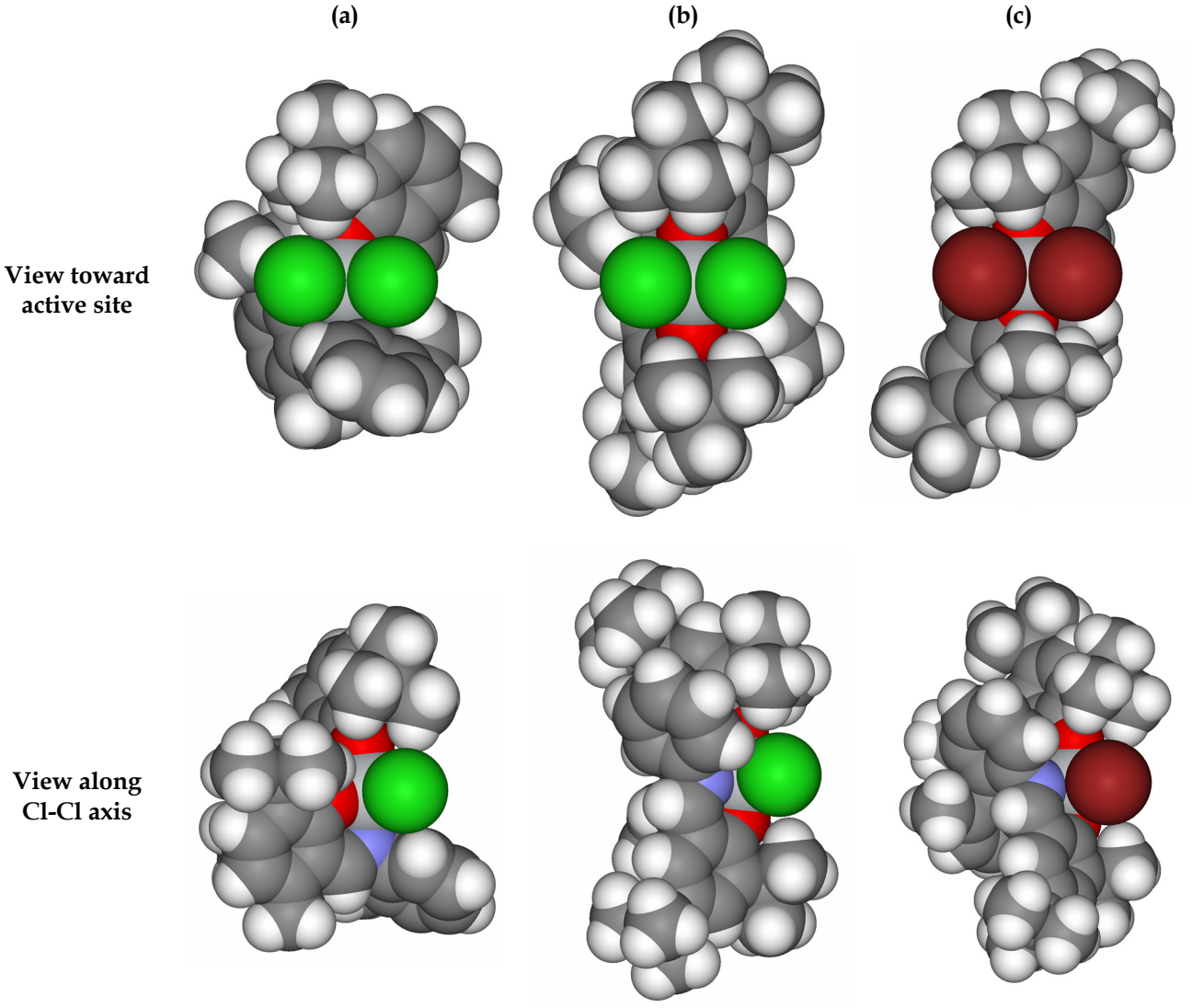

Figure 2.7 - Space filling models of [L²TiCl₂] (a) from XRD structure compared to [(4)₂TiCl₂] (b) and [(5)TiBr₂] (c) from reported XRD structures[9,10]

In [(**4**)$_2$TiCl$_2$] and [(**5**)TiBr$_2$] the halide ligands are equivalent, due to the C_2-symmetrical geometry of the systems, whereas in [L²TiCl$_2$] the chlorides are inequivalent, due to the C_1-symmetrical *cis*-β geometry.

[(**4**)$_2$TiCl$_2$] is relatively uncongested around the active site, in comparison to [(**5**)TiBr$_2$]. This increased congestion of the active site has been previously reported

to be responsible for a substantial reduction in catalytic activity of the zirconium analogues, compared to unbridged catalysts.[2,3] The active site of [L^2TiCl_2] is considerably more congested than that of the unbridged [(**4**)$_2$$TiCl_2$]; an aryl group is forced toward the active site, restricting approach to both chloride ligands from below (as depicted in Figure 2.7).

2.3 Polymerization Testing

Upon activation with MAO, the titanium and zirconium chloride complexes of **L**^{1} and **L**^{2} were found to catalyse ethene polymerization at ambient and elevated temperatures.

2.3.1 Methodology

2.3.1.1 Schlenk Test

The most common method of testing catalytic activity is what might be called a "Schlenk-test," whereby a reaction is allowed to proceed for a known period of time before quenching. The "activity" reported is actually the bulk productivity over the measured timeframe. These catalysts were tested using this methodology, primarily to allow for comparison with other work underway or recently completed within the group.[2,3]

2.3.1.2 Gas Pressure Burette

In order to quantify productivity of the catalysis over time, and thus gain information on catalyst lifetime, we constructed a gas pressure burette system to facilitate ethene uptake measurements during the polymerization reactions. In such systems, gas is allowed to flow from a storage tank through a regulator into the

reaction vessel. By measuring the change in pressure of the storage tank, the gas uptake can be calculated.

Gas Systems

The equipment was constructed as shown in schematically in Figure 2.8 (Page 41), details are given in Appendix 1. The equipment is operated as follows: prior to a reaction, ethene is passed through a drying train consisting of BASF R3-11G deoxygenating agent and 3Å molecular sieves (E-2), and a filter (E-3), and then stored in an appropriately sized pressure burette (E-4, E-5, or E-6) at *ca*. 20 bar. During the reaction, the supply valve (V-5) is closed, and gas passes from the burette through the regulator (V-8) into the reaction vessel (E-8) at between 1 and 7 bar as appropriate.

Data Acquisition and Processing

The pressure in the gas pressure burette is measured by a pressure transducer (I-1), and the temperature in the reactor is measured by a thermocouple (I-3). Data from the sensors is digitised by process meters (I-5 and I-6), and sampled at a selectable frequency by an attached PC (I-4), usually 1 s^{-1}.

We wrote custom data acquisition software using the Java programming language,[11] utilising the open-source libraries JFreeChart[12] and RXTX[13] for chart display and RS232 port control respectively. The software is controlled through a graphical user interface, and outputs data in CSV format.

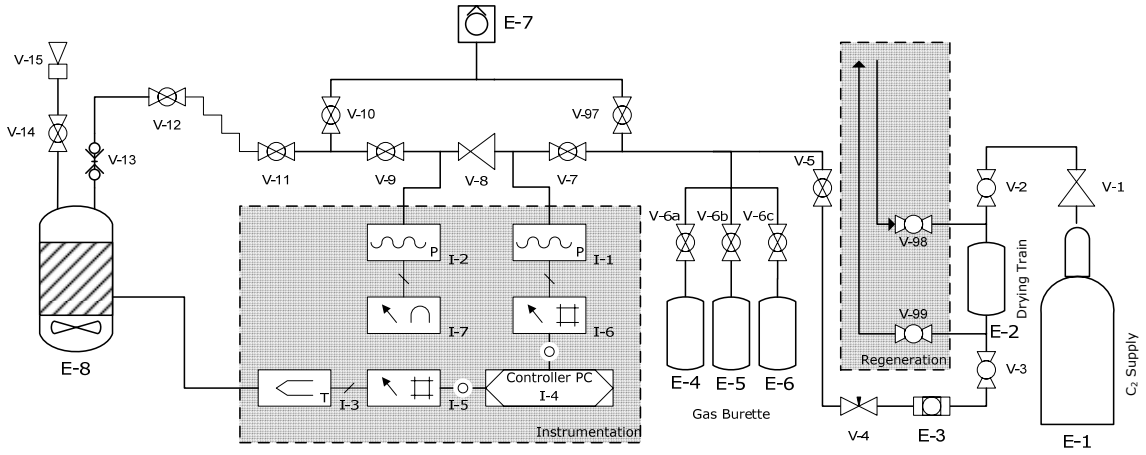

Figure 2.8 - Gas Pressure Burette Schematic

The control software performs the conversion from pressure in the burette to moles of gas taken up, by applying the second-order virial equation of state[14] (Equation 2.1), due to the non-ideal behaviour of ethene.

$$pV_{\mathrm{m}} = \mathrm{R}T\left(1+\frac{\mathrm{B}}{V_{\mathrm{m}}}\right)$$

Equation 2.1

$$\left(\frac{\mathrm{B}}{V}\right)n^2 + n + \frac{-pV}{\mathrm{R}T} = 0$$

Equation 2.2

B = 2nd virial coefficient

n = number of mols

P = Pressure

R = Gas Constant

T = Temperature

V = Total volume

V_{m} = Molar Volume

This may be rearranged to the quadratic form shown in Equation 2.2, which may in turn be solved using the standard numerical quadratic solution, resulting in the form shown in Equation 2.3, which is solved by the software for each data point.

$$n = \frac{-1 \pm \sqrt{1 - 4\left(\frac{B}{V}\right)\left(\frac{-pV}{RT}\right)}}{2\left(\frac{B}{V}\right)}$$

Equation 2.3

Following the reaction, the pressure dataset is processed in Microcal Origin[15] by applying a Savitzky-Golay smoothing method with 5th order polynomial[16] to return the 1st derivative of the data, with an aperture of ±25 s. The Savitsky-Golay function is appropriate for smoothing experimental results due to its sensitivity to short-duration events in the input data. In some cases, where the ethene uptake rate is very low, a 120 point FFT filter is applied to the derivative data, to remove high-frequency noise.

2.3.2 Results

2.3.2.1 Initial results

When activated with MAO, the precatalysts [$L^n TiCl_2$] (n = 1,2,6,7) were active for ethene polymerization,* the results are shown in Table 2.3. The experiments with

* Conditions: 3 μmol precatalyst, 500 ml toluene inc. 4ml 10% MAO/toluene, 1.2 bar C_2. Under these conditions, the polymer produced has a "stringy" consistency, necessitating powerful overhead stirring of the reaction.

longer reaction times show lower measured productivities (Figure 2.9) and only limited variation in product molecular weights.

Precatalyst	Time (min)	Polymer Yield (g)	Productivity (kg mol^{-1} bar^{-1} h^{-1})	M_n (u)	M_w (u)	PDi
[L^{1}TiCl$_2$]	15	0.33	3.7 x 10^2	101,000	204,000	2.0
[L^{1}TiCl$_2$]	60	0.45	1.3 x 10^2	113,000	233,000	2.1
[L^{1}TiCl$_2$]	120	0.35	4.9 x 10^1	121,000	256,000	2.0
[L^{2}TiCl$_2$]	15	0.94	1.0 x 10^3	182,000	398,000	2.2
[L^{2}TiCl$_2$]	60	1.13	3.1 x 10^2	117,000	377,000	3.2
[L^{2}TiCl$_2$]	120	1.17	1.6 x 10^2	137,000	370,000	2.7
[L^{6}TiCl$_2$]	60	1.27	3.5 x 10^2	110,000	299,000	2.7
[L^{7}TiCl$_2$]	60	0.67	1.9 x 10^2	61,300	256,000	4.2

Table 2.3 - Initial productivity results for L^{n}TiCl$_2$ species at 50 °C

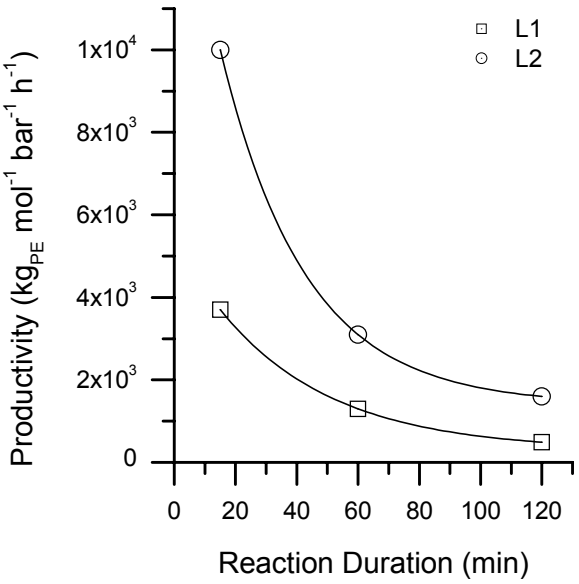

Figure 2.9 - Initial productivity results for L^{n}TiCl$_2$ species at 50 °C

2.3.2.2 Activity profiling

The catalysts were tested using the gas pressure burette apparatus, utilizing a much lower catalyst loading to facilitate easier stirring. The activity profiles of the

titanium species are shown in Figure 2.10, at 25 °C and 50 °C,* and the experimental results are summarized in Table 2.4.

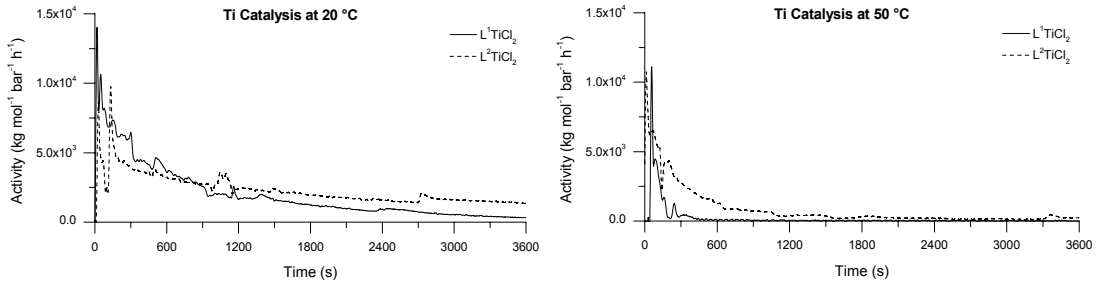

Figure 2.10 Reaction profiles for [L^{n}TiCl$_2$] at 20 °C (left) and 50 °C (right)

Precatalyst	Temp. (°C)	Yield (g)	Productivity (kg mol^{-1} bar^{-1} h^{-1})	M_n (u)	M_w (u)	PDi
[L^{1}TiCl$_2$]	25	3.72	2060	142,000	309,000	2.2
[L^{2}TiCl$_2$]	25	4.34	2452	195,000	449,000	2.3
[L^{1}TiCl$_2$]	50	0.58	321	56,200	214,000	3.8
[L^{2}TiCl$_2$]	50	1.51	791	179,000	450,000	2.5

Table 2.4 - L^{n}TiCl$_2$ ethene polymerization results

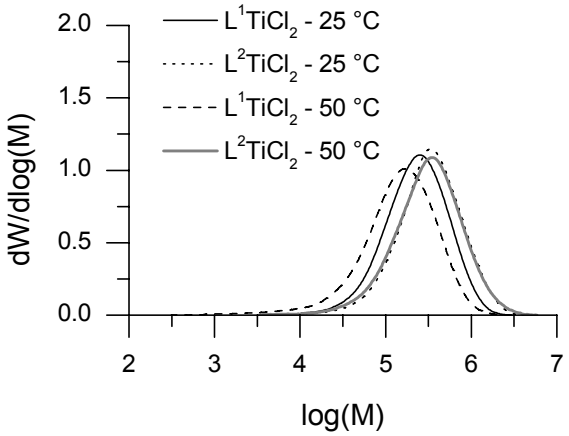

Figure 2.11 - GPC Results for [L^{n}TiCl$_2$] Catalysis

It is clear from these charts that the variation of substitution has affected the course of the polymerization reaction. At 20 °C, both complexes show an initial high

* Conditions: 1.5 μmol precat., 100 ml toluene inc. 5ml 10% MAO/toluene, 1.2 bar C_2, 1 h

activity, followed by a gradual loss of activity. The "protected" [L^2TiCl_2] species shows a slower loss of activity than the unprotected L^1 species. At 50 °C, the effect is more pronounced, with both species suffering rapid loss of activity. However, whereas the unprotected species shows almost no activity after 600 s, the protected species still shows activity of around 200 kg_{PE} mol^{-1} bar^{-1} h^{-1} after an hour (Figure 2.12).

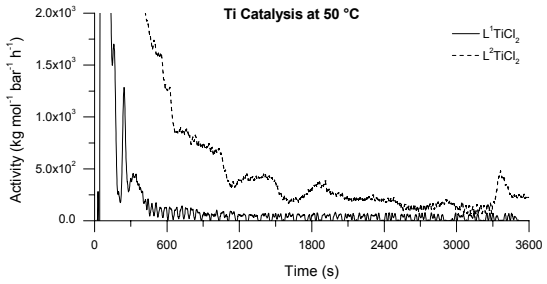

Figure 2.12 – [$L^n TiCl_2$] species at 50 °C, expanded vertical scale

The "protected" [L^2TiCl_2] catalyst also produces polymer with higher MWt than [L^1TiCl_2], which suggests that the rate of polymer chain termination or transfer is lower for the L^2 species.

The zirconium complexes were also tested,* and found to have much lower productivities. The ethene uptake was too low to obtain useful reaction profile data, but the results are summarized in Table 2.5. In all cases, the MWDs were multimodal (Figure 2.13), and it was possible to deconvolute the separate components.

* Conditions: 100 ml toluene inc. 5ml 10% MAO/toluene, 1.2 bar C_2, 1 h

Precatalyst	Cat. (mmol)	Temp. (°C)	Yield (g)	Productivity (kg mol^{-1} bar^{-1} h^{-1})	M_n (u)	M_w (u)	PDi
[L^1ZrCl_2]	2.8	20	0.13	39	900	31,400	(34.9)
High					*6,800*	*52,800*	*7.8*
Low					*400*	*550*	*1.4*
[L^2ZrCl_2]	1.5	20	0.20	114	2,400	55,800	(23.3)
High					*253,000*	*434,000*	*1.7*
Mid					*6,300*	*11,900*	*1.9*
Low					*400*	*520*	*1.3*
[L^1ZrCl_2]	6.0	50	trace	trace	–	–	–
[L^2ZrCl_2]	6.0	50	0.10	14	3,470	45,800	(13.2)
High					*86,900*	*131,000*	*1.5*
Low					*2,670*	*10,300*	*3.9*

High, Mid, Low refer to the MWt of the peak in question.

Table 2.5 - L^{n}ZrCl$_2$ ethene polymerization results

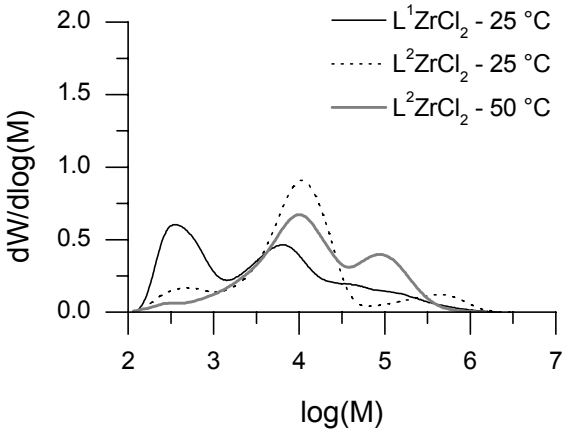

Figure 2.13 - GPC Results for L^{n}ZrCl$_2$ Catalysis

2.3.2.3 Industrially-Relevant Conditions

In collaboration with Theo Smit (Imperial College, London), we tested the titanium catalyst systems using an autoclave system, under conditions somewhat different to those we normally employ.* The activity profiles are shown below (Figure 2.14). It

* 1 L autoclave reactor, 10 µmol catalyst, 400 ml isobutane, 4 bar C_2, 2 mmol MAO scavenger, catalysts pre-activated with 200 eq. MAO before injection. C_2 uptake measured with a gas-flow meter.

can be seen that the gas-uptake profiles recorded are very similar to those we observed using our gas pressure burette equipment.

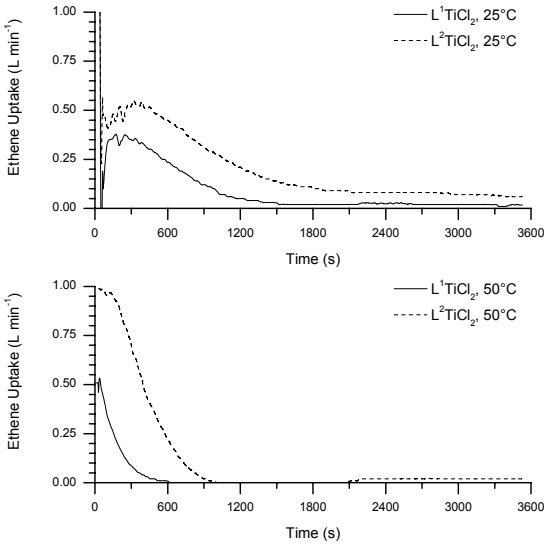

Figure 2.14 - Gas Uptake for [L^{n}TiCl$_2$] at 25 °C (left) and 50 °C (right)

2.4 Stilbene-based Complexes

2.4.1 Proligand Synthesis

In an attempt to increase the rigidity of the ligand system around the metal, we synthesized analogues of L^1 and L^2 utilizing a diaminostilbene backbone. 2,2′-diaminostilbene was synthesized in two steps from 2-nitrobenzyl chloride, using the methods of Bischoff and Thiele (Scheme 2.4).[17]

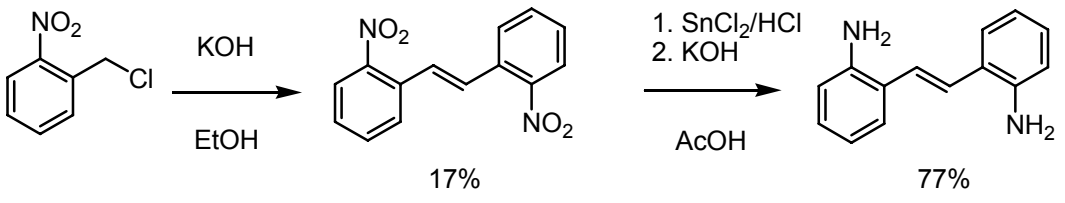

Scheme 2.4 - Synthesis of 2,2'-diaminostilbene

The ligands L^8 and L^9 were synthesized via condensation with the appropriate salicylaldehyde (Scheme 2.5).

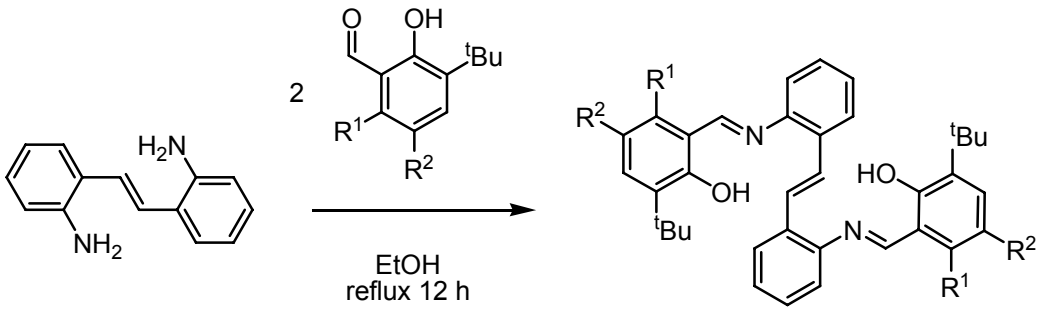

Scheme 2.5 - Synthesis of stilbene-based proligands

	R^1	R^2	Yield
H_2L^8	H	Me	93%
H_2L^9	Me	H	95%

Table 2.6 - Stilbene proligands synthesized

2.4.2 Complexation Behaviour

Attempts to make the species [$L^{8,9}TiCl_2$] yielded products with NMR spectra more complex than expected and which could not be assigned initially. However, a crystal of [L^8TiCl_2] suitable for X-Ray structure determination was grown from DCM/Pentane, and the molecular structure is shown in Figure 2.16. The structure of one metal unit is shown in Figure 2.17.

The complex is an oxygen-bridged dimer in which the ligand has cyclized to form a quinoline unit (Figure 2.15). The source of the oxygen can not be determined with any certainty, but inadvertent ingress of water, or degradation of THF would seem to be the most probable explanations.

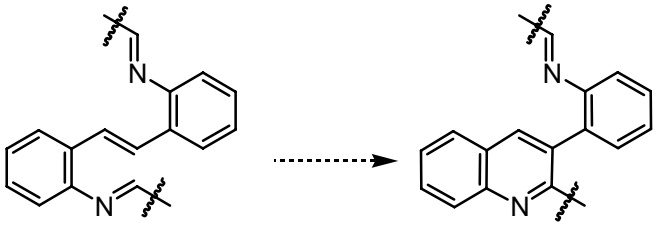

Figure 2.15 - Cyclization of L^8

The asymmetric unit contains the quinoline complex, one chloride ligand, titanium and bridging oxygen, with a dimer in the unit cell. The bridging oxygen lies on a special position. There is a disordered molecule of DCM present; the disorder was modelled as a rotation about the Cl-Cl axis with major to minor occupancies of 55:45.

The bond angles throughout the quinoline unit are 120°, and a hydrogen at C(11) was found in a difference Fourier map, demonstrating that C(11) is sp^2 hybridised. No hydrogen was found at N(99). Together, this is good evidence for ligand having being oxidized to the quinoline.

The titanium centres are 5-coordinate (slightly distorted trigonal bipyramidal), and it is of note that the angles through the phenoxy donors differ significantly – 165° for C(41)-O(1)-Ti(1) *vs.* 138° for C(7)-O(2)-Ti(1). The bond lengths from the titanium centre to the ligands all compare well with examples of oxo-bridged titanium species,[18] although as there are no X-Ray structures of such 5-co-ordinate (N,O,O,O,Cl) O-bridged titanium species recorded in the literature, comparisons are necessarily indirect.

Bond	Length (Å)
Ti(1)-O(1)	1.819(4)
Ti(1)-O(2)	1.843(4)
Ti(1)-O(3)	1.8214(10)
Ti(1)-N(1)	2.190(5)
Ti(1)-Cl(1)	2.3403(19)

Bonds	Angle (°)
O(1)-Ti(1)-O(2)	126.52(18)
O(2)-Ti(1)-O(3)	111.75(14)
O(2)-Ti(1)-O(1)	126.52(18)
O(2)-Ti(1)-N(1)	81.67(18)
Cl(1)-Ti(1)-N(1)	172.88(14)
C(38)-C(11)-C(13)	120.7(6)
C(41)-O(1)-Ti(1)	165.7(4)
C(7)-O(2)-Ti(1)	138.1(4)

Table 2.7 - Selected bond lengths and angles for "L^8 Ti".

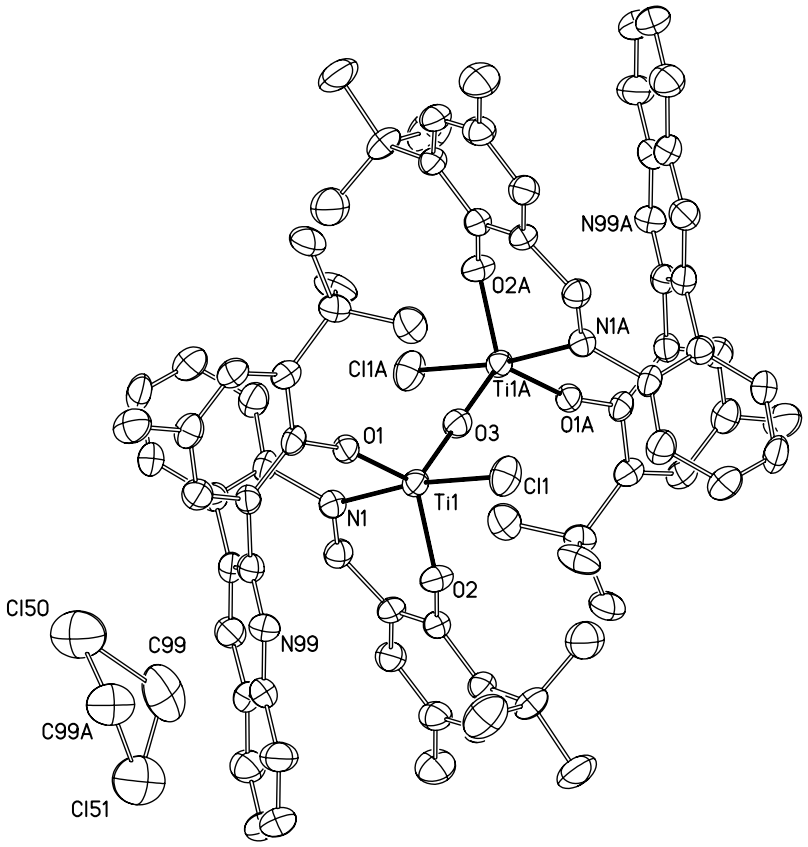

Figure 2.16 - Molecular structure of "L[8] Ti" dimer (Hydrogen atoms omitted for clarity).

Probability ellipsoids are given at the 50% level.

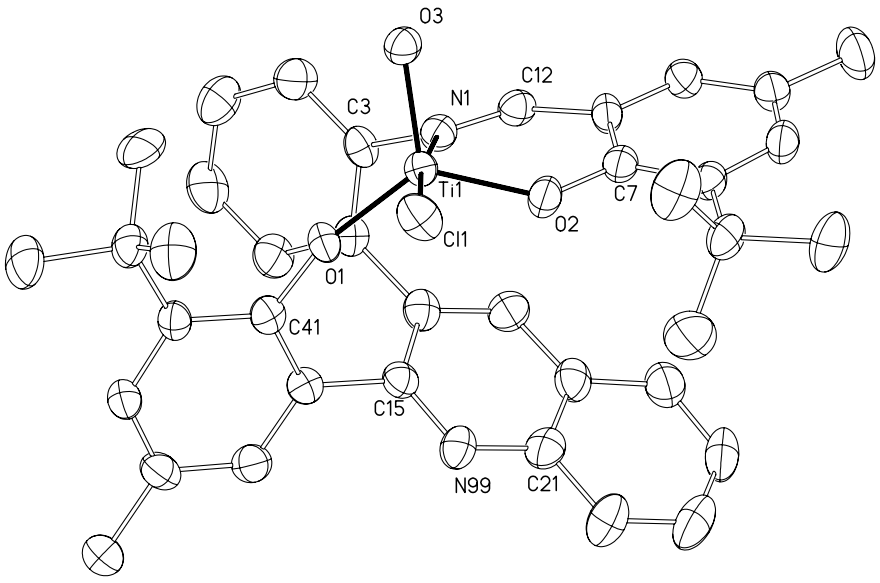

Figure 2.17 - Molecular Structure of symmetry-independent part of "L[8] Ti"

The NMR spectrum appears to be consistent with overlapping spectra of two compounds, one of which is the quinoline system, and one which is most likely to be some isomer of a dihydroquinoline, although the complexity of the spectrum precludes complete assignment.

This compound was essentially inactive for ethylene polymerization, which is unsurprising given the absence of available *cis*-situated co-ordination sites (*q.v.* §1.1.1). On the basis of these results, we decided not to investigate this system further.

2.5 Conclusions

Attempting to increase the lifetime of salicylaldimine catalysts by sterically blocking a proposed 1,2-Migratory Insertion to the imine functionality were partly successful; the "protected" species indeed showed a longer lifetime than the "unprotected" analogues. However, they are still deactivated at elevated temperatures.

Catalysis with the $[L^2MCl_2]$ species produced higher MWt PE than catalysis with the L^1 analogues, with a similar activity initially. This suggests that the rate of chain transfer is lower for these species. The most commonly observed chain-transfer mechanisms in single-site catalysts are β-H elimination (resulting in a vinyl end-group),[19] or transfer of the polymer chain to aluminium species present in the mixture.[20] Both transfer mechanisms depend on a balance between the steric and electronic nature of the active site. To speculate, transfer to aluminium may be slowed by a sterically encumbered active site preventing approach of aluminium species, and β-H elimination may be favoured if the congestion similarly prevents approach of ethene monomer.

Since the initial activities of $[L^1TiCl_2]$ and $[L^2TiCl_2]$ are similar, it seems unlikely that the active site of one compound is significantly more congested than for the

other. The X-Ray structure of [L^2TiCl_2] shows that it is unlikely that the different substitution of L^1 will significantly affect the active site geometry. Therefore, it seems probable that the difference in the polymer produced is not due to gross variation of geometry, but more likely due to some electronic effect. This may be variation of the electronic nature of the phenoxy-donor due to the differing substitution, or some more subtle interaction between the imine N and some other component of the reaction mixture (most likely some aluminium alkyl species) which is affected by the steric blocking.

Attempts to make complexes of salicyl-stilbene ligands yielded a mixture of products of an unexpected electrocyclization reaction.

Given the results presented above, we decided to investigate a ligand series which should be intrinsically less vulnerable to migratory insertion to the imine bond, and this work is discussed in Chapter 3.

2.6 References for Chapter 2

1 S. Matsui and T. Fujita, *Catal. Today*, 2001, **66**, 63-73; J. Tian and G. W. Coates, *Angew. Chem.*, 2000, **39**, 3626-29; J. Tian, P. Hustad and G. Coates, *J. Am. Chem. Soc.*, 2001, **123**, 5134-35; S. Matsui, M. Mitani, J. Saito, Y. Tohi, H. Makio, N. Matsukawa, Y. Takagi, K. Tsuru, M. Nitabaru, T. Nakano, H. Tanaka, N. Kashiwa and T. Fujita, *J. Am. Chem. Soc.*, 2001, **123**, 6847-56.

2 P. D. Knight, 'Chiral at Metal Catalyst Designs for Alkene Polymerisation and Hydroamination', Ph.D. Thesis, University of Warwick, Coventry, 2003.

3 P. D. Knight, A. J. Clarke, B. S. Kimberley, R. A. Jackson and P. Scott, *Chem. Commun.*, 2002, 352-53.

4 N. V. Thakkar and R. M. Patil, *Synth. React. Inorg. Met.-Org. Chem*, 2000, **30**, 1159-74.

5 S. Ishii, M. Mitani, J. Saito, S. Matsuura, R. Furuyama and T. Fujita, *Stud. Surf. Sci. Catal.*, 2003, **145**, 49-54.

6 N. U. Hofsløkken and L. Skattebøl, *Acta Chem. Scand.*, 1999, **53**, 258-62.

7 P. D. Knight, G. Clarkson, M. L. Hammond, B. S. Kimberley and P. Scott, *J. Organomet. Chem.*, 2005, **690**, 5125-44.

8 R. K. J. Bott, D. L. Hughes, M. Schormann, M. Bochmann and S. J. Lancaster, *J. Organomet. Chem.*, 2003, **665**, 135; D.Owiny, S.Parkin and F.T.Ladipo, *J. Organomet. Chem.*, 2003, **678**, 134; A. F. Mason, J. Tian, P. D. Hustad, E. B. Lobkovsky and G. W. Coates, *Isr. J. Chem.*, 2002, **42**, 301; S. Matsui, Y. Tohi, M. Mitani, J. Saito, H. Makio, H. Tanaka, M. Nitabaru, T. Nakano and T. Fujita, *Chem. Lett.*, 1999, 1065-66; M. Mitani, R. Furuyama, J. i. Mohri, J. Saito, S. Ishii, H. Terao, N. Kashiwa and T. Fujita, *J. Am. Chem. Soc.*, 2002, **124**, 7888-89.

9 S. Reinartz, A. F. Mason, E. B. Lobkovsky and G. W. Coates, *Organometallics*, 2003, **22**, 2542-44.

10 P. R. Woodman, N. W. Alcock, I. J. Munslow, C. J. Sanders and P. Scott, *J. Chem. Soc., Dalton Trans.*, 2000, 3340-46.

11 Sun Microsystems, 'Java 1.5' - http://java.sun.com/

12 D. Gilbert and T. Morgner, 'JFreeChart 0.96' - http://www.jfree.org/jfreechart/

13 K. Jarvi, 'RXTX 2.1' - http://users.frii.com/jarvi/rxtx/

14 P. W. Atkins, 'Physical chemistry', 6th ed., Oxford University Press, 1998.

15 OriginLab Corporation, 'Origin 7.0 SR1' - http://www.originlab.com/

16 A. Savitsky and M. J. E. Golay, *Anal. Chem.*, 1964, **36**, 1627-39.

17 J. Thiele and O. Dimroth, *Chem. Ber.*, 1895, **28**, 1411-14; C. A. Bischoff, *Chem. Ber.*, 1888, **21**, 2071-78.

18 A. Kayal, A. F. Ducruet and S. C. Lee, *Inorg. Chem.*, 2000, **39**, 3696-704; M. Mazzanti, J. M. Rosset, C. Floriani, A. Chiesi-Villa and C. Guastini, *J. Chem. Soc., Dalton Trans.*, 1989, 953-57.

19 S. Ishii, M. Mitani, J. Saito, S. Matsuura, S. Kojoh, N. Kashiwa and T. Fujita, *Chem. Lett.*, 2002, 740-41; N. Kawahara, S. Kojoh, S. Matsuo, H. Kaneko, T. Matsugi, Y. Toda, A. Mizuno and N. Kashiwa, *Polymer*, 2004, **45**, 2883-88; L. Resconi, I. Camurati and O. Sudmeijer, *Top. Catal.*, 1999, **7**, 145-63; L. Resconi, R. L. Jones, A. L. Rheingold and G. P. A. Yap, *Organometallics*, 1996, **15**, 998-1005; U. Stehling, J. Diebold, R. Kirsten, W. Roll, H. H. Brintzinger, S. Jungling, R. Mulhaupt and F. Langhauser, *Organometallics*, 1994, **13**, 964-70; L. Resconi, F. Piemontesi, G. Franciscono, L. Abis and T. Fiorani, *J. Am. Chem. Soc.*, 1992, **114**, 1025-32; W. Kaminsky, A. Ahlers and N. Mollerlindenhof, *Angew. Chem., Int. Ed. Engl.*, 1989, **28**, 1216-18.

20 L. Resconi, S. Bossi and L. Abis, *Macromolecules*, 1990, **23**, 4489-91; J. C. W. Chien and B. P. Wang, *J. Polym. Sci., Part A: Polym. Chem.*, 1988, **26**, 3089-102.

3 Salicyloxazoline Systems

3.1 Introduction

Our attempts to block the Migratory Insertion reaction sterically (described in Chapter 2) showed only limited effectiveness – although the catalytic lifetime of the "protected" species was longer than that of the "unprotected" analogue, neither could be described as long-lived. Given these results, we proposed a modification to the ligand system which should render the complexes considerably more resistant to attack at the imine bond, by incorporation of the imine function within an oxazoline ring. The presence of the oxo-functionality in the oxazoline may also be expected to alter the chemistry of such systems in comparison to salicylaldimine systems.

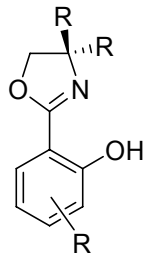

Figure 3.1 - Salicyloxazoline Ligand

Group 4 complexes containing such salicyloxazoline ligand systems have previously been investigated by Floriani,[1] (see §1.2.2.3) but were found to give only very low activity for ethylene polymerisation, perhaps because they did not possess bulky substituents *ortho* to the phenoxy-oxygen, and bulk in this position is reported to be essential for the activity of the analogous salicylaldimine catalysts[2-4] (see §1.3.2.1).

3.2 Synthesis of Salicyloxazoline Proligands HL10-13

A wide selection of salicylic acids are available commercially, and others are accessible in good yield from the respective phenols (See Scheme 3.1).[5]

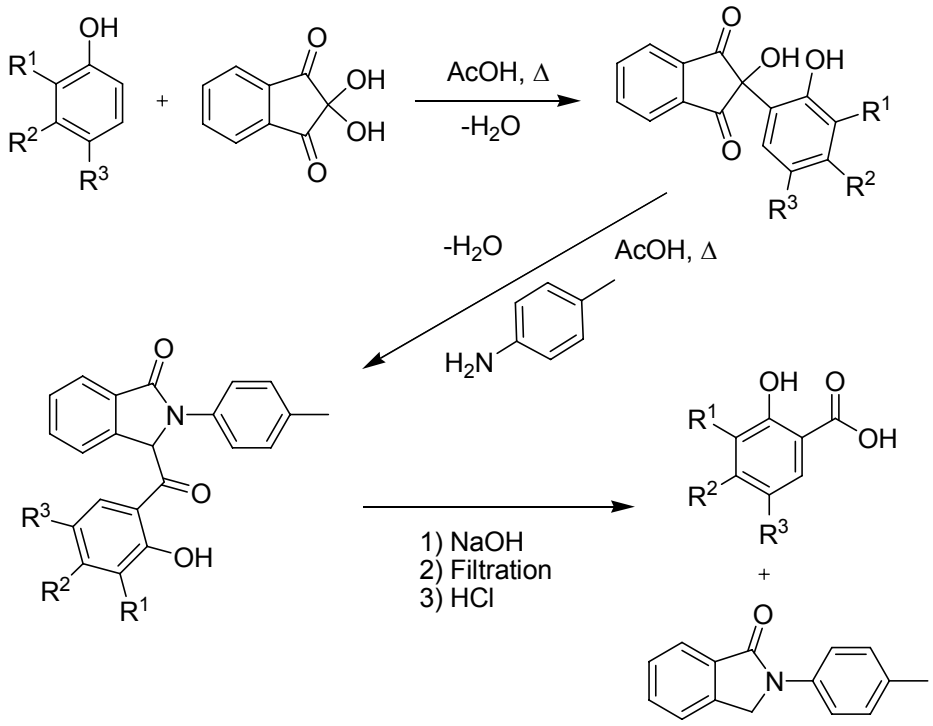

Scheme 3.1 - Synthesis of Substituted Salicylic Acids

The synthesis of salicyloxazolines by reaction of salicylic acids with 2-aminoalcohol in the presence of CCl_4, PPh_3 and a base such as triethylamine (TEA) was originally reported by Vorbrüggen.[6] We optimized the conditions, as shown in Scheme 3.2 below. It appears that small variations in the equivalences make little difference to the final yield.

This route is convenient, as a wide range of 2-aminoalcohols is available, including chiral non-racemic species. This work is however only concerned with the achiral analogues symmetrically substituted at the oxazoline 4-position.

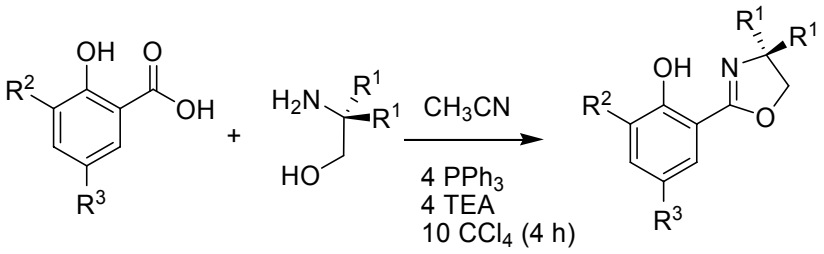

Scheme 3.2 - Synthesis of Salicyloxazolines

	R^1	R^2	R^3	Yield
HL[10]	H	^{t}Bu	^{t}Bu	47%
HL[11]	Me	^{t}Bu	^{t}Bu	46%
HL[12]	Me	^{i}Pr	^{i}Pr	33%
HL[13]	Ph[a]	^{t}Bu	^{t}Bu	11%

[a] *Vide Infra*

Table 3.1 - Salicyloxazoline Proligands Synthesized

H**L**[13] is a benzoxazole species (Figure 3.2), synthesized in a similar manner from 3,5-di-*tert*-butylsalicylic acid and 2-hydroxyaniline. We felt that this species would provide an interesting link to the salicylaldimine catalysts, due to the presence of the aromatic substituent α to the imine nitrogen. The archetypical[3,7] salicylaldimine proligand H**L**[14] was synthesized for comparison.

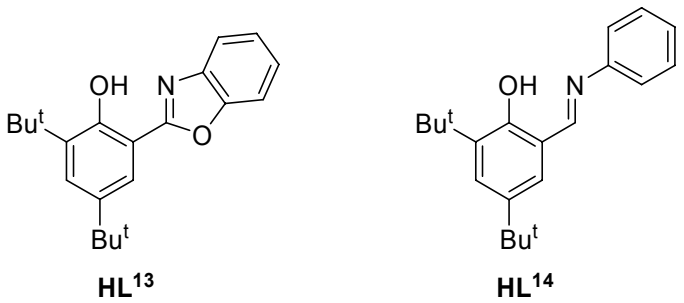

Figure 3.2 – Further proligands, HL[13] and HL[14]

3.3 The Effect of Steric Bulk – Synthesis and Polymerization Testing of Metal Chloride Complexes of L10-14

Various species [$\mathbf{L}^{n}{}_2MCl_2$] were synthesized either *via* the salt-metathesis route shown in Scheme 3.3, or in one case by direct reaction between [$TiCl_4$] with H$\mathbf{L}^{10}$. Products were purified by sublimation or recrystallization.

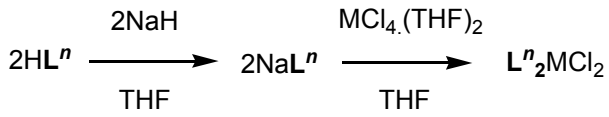

Scheme 3.3 - Salt-metathesis synthesis of metal chloride complexes

Initially, we synthesized a library of salicyloxazoline complexes with varying steric bulk at the R^1 (*i.e.* the oxazoline 4-position, α- to the nitrogen) and R^2 (*i.e.* the phenol 2-position, *ortho*- to the oxygen) positions, *viz.* [$\mathbf{L}^{n}{}_2MCl_2$] (n = 10, 11, 12, M = Ti, Zr). For further comparison, we synthesized the hafnium complexes of H$\mathbf{L}^{10}$ and H$\mathbf{L}^{11}$, and the zirconium complex of the salicylbenzoxazole ligand H$\mathbf{L}^{13}$. Attempts to make the titanium complex of H$\mathbf{L}^{13}$ resulted in an intractable mixture of products. Since the polymerization activity and products can depend strongly on reaction conditions, we also synthesized the titanium and zirconium complexes of the salicylaldimine ligand H$\mathbf{L}^{14}$ for direct comparison. The yields of these complexes are shown in Table 3.2.

	$\mathbf{L}^{10}$	$\mathbf{L}^{11}$	$\mathbf{L}^{12}$	$\mathbf{L}^{13}$	$\mathbf{L}^{14}$
Ti	63%	70%	35%	–	60%
Zr	20%	44%	6%	39%	65%
Hf	82%	36%	–	–	–

Table 3.2 - Yields of L^nMCl_2 Complexes

3.4 Structural Characterization of Complexes

Some of these metal chloride complexes demonstrate very broad ^{1}H NMR spectra at room temperature. Variable temperature NMR experiments were conducted on selected species to investigate the nature of the dynamic process.

Energies of activation $\Delta G^{\ddagger}$ may be calculated using the Eyring equation, in the form shown in Equation 3.1.[8,*]

$$\Delta G^{\ddagger} = aT_c\left[9.972 + \log\left(\frac{T_c}{\delta\upsilon}\right)\right]$$

Equation 3.1

a = 1.914×10^{-2} kJ mol^{-1} K^{-1}

T_c = Coalescence Temperature

The Eyring equation may also be presented in the form:

$$a\left[\log\frac{k}{T} - 10.319\right] = \frac{-\Delta H^{\ddagger}}{T} + \Delta S^{\ddagger}$$

Equation 3.2

Thus, if it is possible to determine the rate of exchange across a range of temperatures, a plot of $a\left[\log\frac{k}{T} - 10.319\right]$ *vs.* $\frac{1}{-T}$ should be a straight line with intercept $\Delta S^{\ddagger}$ and gradient $\Delta H^{\ddagger}$.

---

[*] See Appendix 2 for the derivation of these forms of the Eyring equation. There is also a contribution from the coupling energy, as this is a coalescing AB system. However, this contribution is 2 orders of magnitude lower than the uncertainty in the measurement for these systems and is ignored here.

3.4.1 $[L^{10}{}_2MCl_2]$

3.4.1.1 Zirconium and Hafnium

The $\mathbf{L^{10}}$ species of zirconium and hafnium both consist of a single C_2-symmetric isomer (which we assign to be *cis,trans,cis* on the basis of XRD and DFT results for related species, *q.v.* §3.4.5, Chapters 1 & 5) which undergoes exchange between enantiomers. Selected spectra of the Zr complex are shown in Figure 3.3 (Hf is similar).

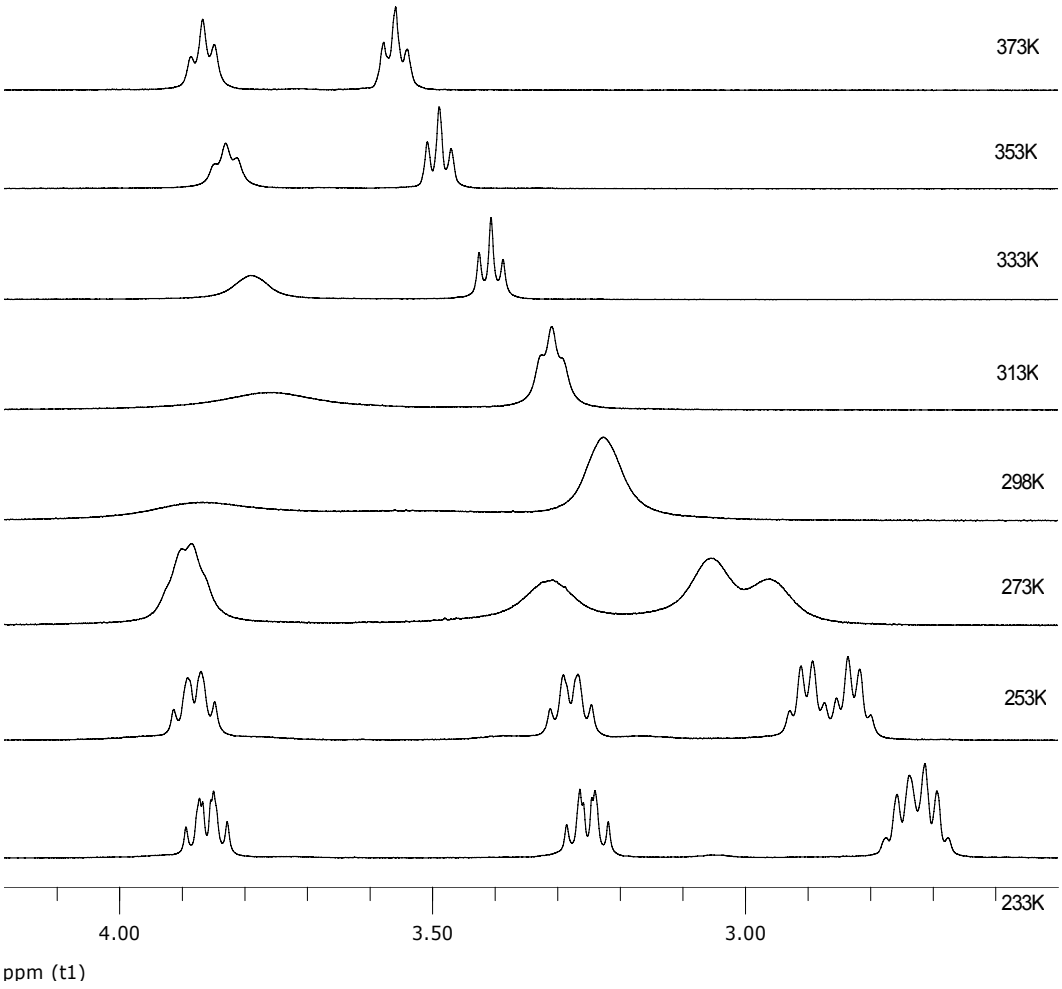

Figure 3.3 – Exchange behaviour in the oxazoline CH_2CH_2 region of ^1H NMR spectrum of $[L^{10}{}_2ZrCl_2]$

The calculated $\Delta G^{\ddagger}_{Tc}$ values for the exchange are 57±2 kJ mol^{-1} for the zirconium complex, and 63±2 for the hafnium analogue.* These values may not be compared directly however, as the contribution from $\Delta S^{\ddagger}$ is temperature dependent ($\Delta G^{\ddagger}_{T} = \Delta H^{\ddagger} - T\Delta S^{\ddagger}$).

We calculated the rate of exchange for [$\mathbf{L^{10}}_2MCl_2$] (M = Zr, Hf) throughout the slow-exchange regime (233 – 273 K for Zr, 263 – 313 K for Hf) by iterative fitting to a simulation of the ABCD spin system of the oxazoline CH_2-CH_2 protons. A non-exchanging fit was performed using the NUMARIT algorithm,[9] and then the rate of exchange was determined iteratively using MEXICO,[10] both algorithms as implemented in Spinworks 2.5.[11] The results are shown in Figure 3.4 ([$\mathbf{L^{10}}_2ZrCl_2$]) and Figure 3.5 ([$\mathbf{L^{10}}_2HfCl_2$]).

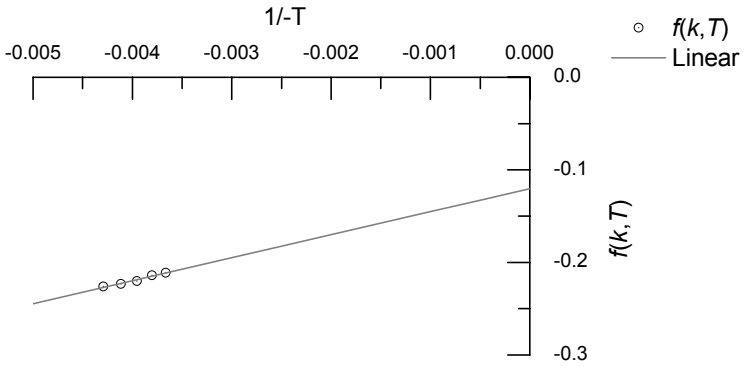

Figure 3.4 - Eyring plot for [$\mathbf{L^{10}}_2ZrCl_2$] (r^2 = 0.986); $f(k,T) = \mathbf{a}\left[\log\frac{k}{T} - 10.319\right]$

* It is possible to calculate $\Delta G^{\ddagger}$ separately for each of the two sets of coalescing signals, the precise results are 57.3 (T_c = 298 K) and 57.1 kJ mol^{-1} (T_c = 308 K) for Zr and 62.3 (T_c = 323 K) and 59.3 kJ mol^{-1} (T_c = 308 K) for Hf. Accurate determination of T_c is the major term in the reported uncertainty.

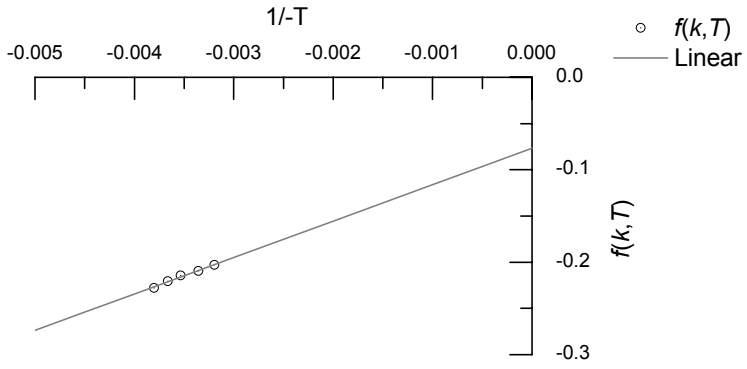

Figure 3.5 - Eyring plot for $[L^{10}{}_2HfCl_2]$ (r^2 = 0.994); $f(k,T) = a\left[\log\frac{k}{T} - 10.319\right]$

Linear regression of the data points using Origin 7[12] gives the thermodynamic parameters $\Delta H^{\ddagger}$, $\Delta S^{\ddagger}$ and thus $\Delta G^{\ddagger}$ (Table 3.3).

	$\Delta H^{\ddagger}$ (kJ mol^{-1})	ΔS (J K^{-1} mol^{-1})	$\Delta G^{\ddagger}_{298\ K}$ (kJ mol^{-1})
$[L^{10}{}_2ZrCl_2]$	25±3	-120±10	61±5
$[L^{10}{}_2HfCl_2]$	39±2	-77±9	62±5

Table 3.3 – Thermodynamic parameters from NMR lineshape analysis. The given uncertainties are the standard errors from the regression analysis

Values of $\Delta G^{\ddagger}$ at the various coalescence temperatures calculated from these parameters coincide in all cases with the $\Delta G^{\ddagger}$ values calculated from the measurement of T_c, within experimental uncertainty (Table 3.4).

	T_c	$\Delta G^{\ddagger}$ (kJ mol^{-1}) (from T_c)	$\Delta G^{\ddagger}$ (kJ mol^{-1}) (calc.)
$[L^{10}{}_2ZrCl_2]$	298	57.3±2	60.8±5
	308	57.1±2	62.0±5
$[L^{10}{}_2HfCl_2]$	308	59.3±2	62.7±5
	323	62.3±2	63.9±5

Table 3.4 – Comparison of calculated $\Delta G^{\ddagger}$ values using T_c and lineshape analysis

In related bis(chelate) species, similar processes have been assigned to either an in-place trigonal (*i.e.* Bailar) twist,[13,14] or to an N-dissociative mechanism involving a five-coordinate intermediate.[15]

The somewhat negative $\Delta S^{\ddagger}$ implies an ordered transition state, which is suggestive of an in-place rearrangement. Furthermore, the thermodynamic parameters we observe correlate well with previously reported values for zirconium diamine-bis(phenolato) complexes, which undergo interconversion between diastereomers due to a non-dissociative rearrangement ($\Delta H^{\ddagger}$ = 35.9±0.8 kJ mol^{-1}, $\Delta S^{\ddagger}$ = -105±5 J K^{-1} mol^{-1}).[14]

However, as the ligands in our systems are unsymmetrical, a trigonal (Bailar) or rhombic (Ray-Dutt) twist[16] would result not in an inversion, but rather an inter-conversion between different diastereomers (Figure 3.6). The observed NMR spectra are consistent with one C_2-symmetric species undergoing inversion, but there is no evidence for the presence of other diastereomers. It seems likely that the other diastereomers have much higher energies, and thus may be expected to rapidly interconvert *via* further twists before falling into the energy well of the other *cis,trans,cis* enantiomer.

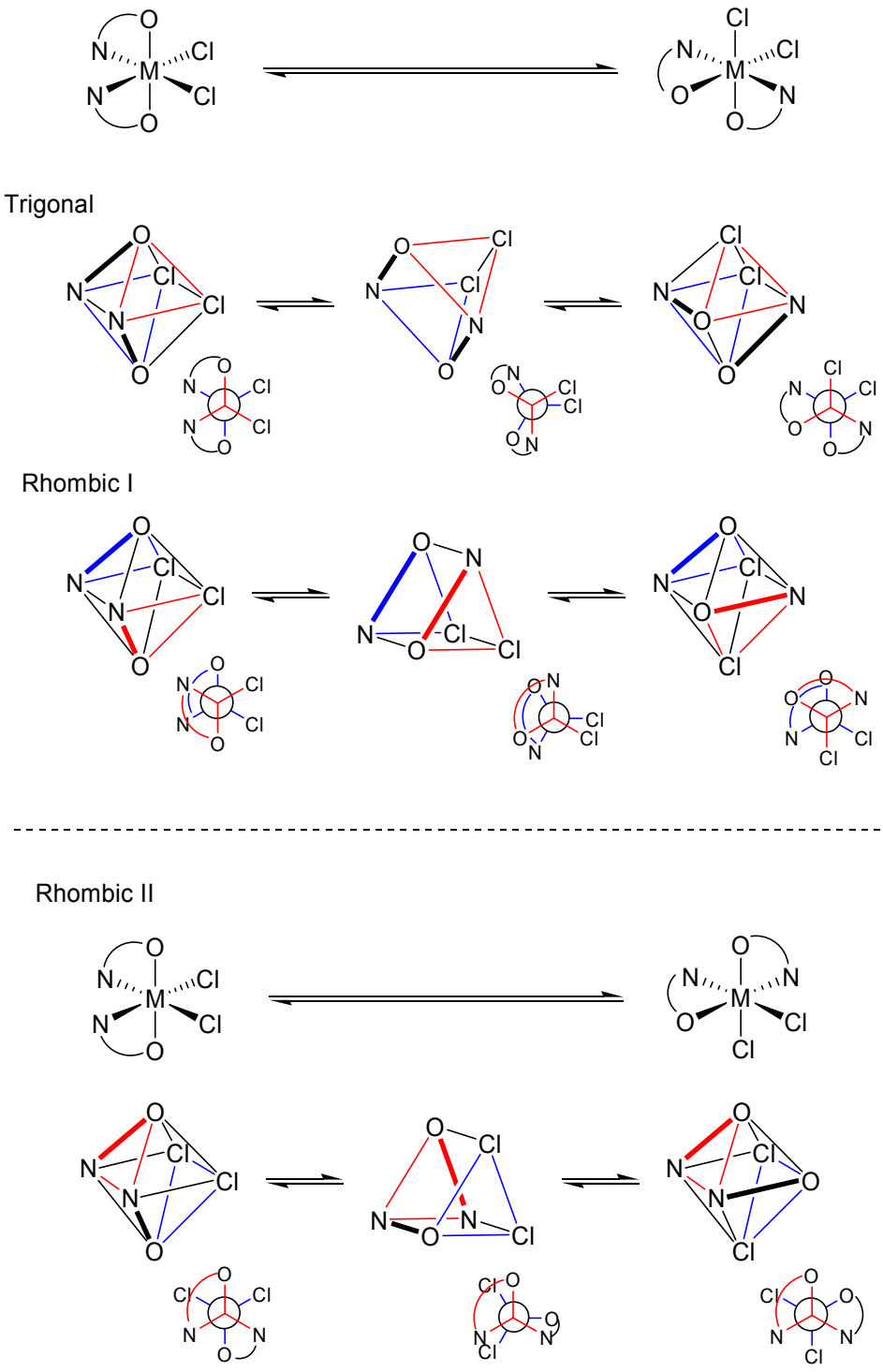

Figure 3.6 – Trigonal and rhombic twists

3.4.1.2 Titanium

[$\mathbf{L^{10}}_2TiCl_2$] consists of two species in a ratio of ~2:1. The major product has a spectra consistent with a C_2-symmetric complex, and a minor product which we could not fully assign, but appears to arise from an unsymmetrical complex.

VT NMR studies (Figure 3.7) show that the minor, unsymmetrical species demonstrates typical exchange behaviour (although the signal is not fully sharpened by 373 K in toluene) with $\Delta G^{\ddagger}_{Tc} = 66 \pm 2$ kJ mol^{-1} (T_c = 323 K). The complexity and degree of overlap of the signals rendered them unusable for generation of an Eyring plot.

Importantly, the resonances from the major product remain sharp across the range of temperatures accessible to us. Therefore, the fluxional behaviour *does not facilitate exchange between species*. This strongly suggests that there are two compounds present, rather than two stereoisomers.

The mass spectrum of the compound shows some evidence for the presence of higher molecular weight material, leading us to suspect that the minor species is an oxygen-bridged dimer of the type [$\mathbf{L^{10}}_2TiCl(\mu\text{-}O)TiCl\mathbf{L^{10}}_2$], although without further evidence this must remain entirely speculative.

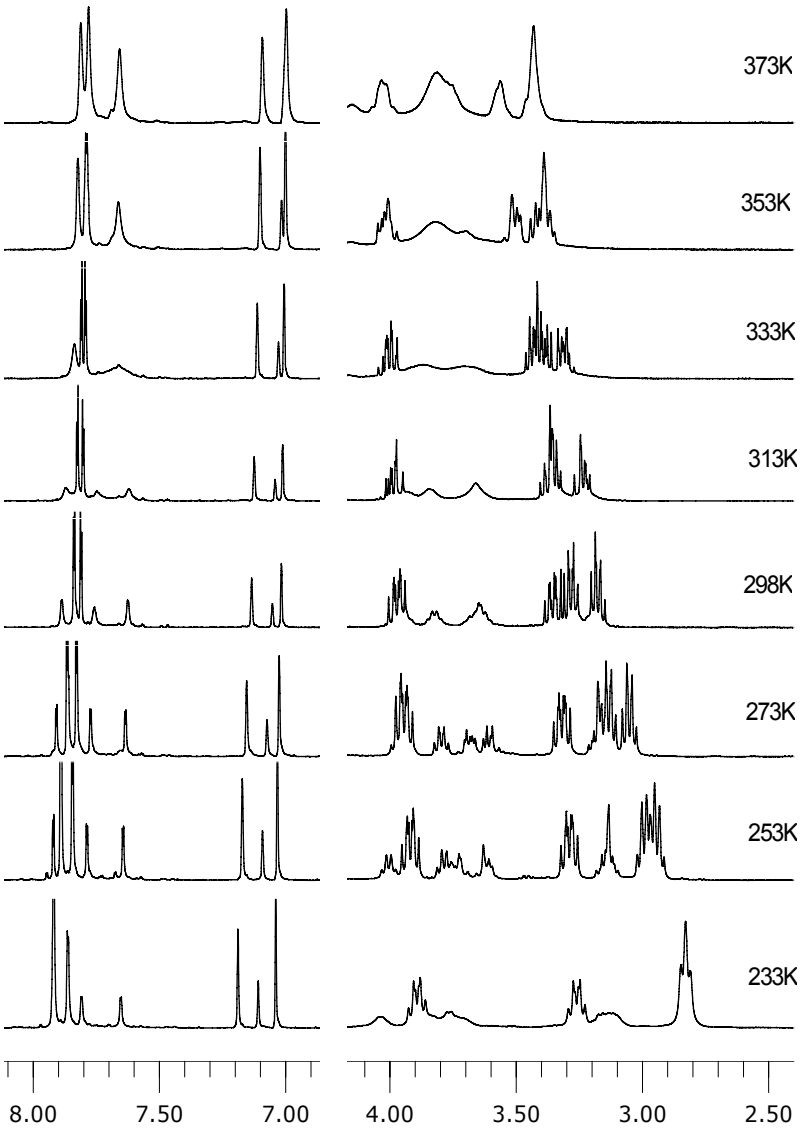

Figure 3.7 - Exchange behaviour in aryl and oxazoline CH_2CH_2 regions of ^1H NMR spectrum of [$L^{10}_2TiCl_2$]

3.4.2 [$L^{11}_2MCl_2$]

The ^1H NMR spectra of [$\mathbf{L^{11}}_2MCl_2$] consist of a single set of resonances consistent with a C_2-symmetric isomer which do not demonstrate any noticeable line broadening over the range of temperatures accessible to us. This is consistent with the process causing the broadening of the $\mathbf{L^{10}}$ species being a nondissociative twist, as the increased steric bulk provided by the methyl substituents on the oxazoline

ring would be expected to present a significant hindrance to a twist rearrangement on any axis.

3.4.3 [$L^{13}_2ZrCl_2$]

The ^{1}H NMR spectrum of the benzoxazole complex [$\mathbf{L^{13}_2}ZrCl_2$] shows very broad resonances at 298 K, which sharpen upon heating or cooling. The spectrum is consistent with a C_2-symmetric complex in the slow exchange regime undergoing a fluxional exchange and sharpening to the time-averaged signals in the fast-exchange regime.

3.4.4 [$L^{14}_2MCl_2$]

Although the original reports of the salicylaldimine catalysts by Fujita *et al.* make no mention of the presence of multiple isomers,[4,7,17] it has been the experience of our laboratory that multiple isomers are indeed observed.[18] Later publications by Fujita have discussed the observed isomers in the context of forming multimodal polymeric materials[19] (*c.f.* §1.2.1).

3.4.4.1 Titanium

The spectra obtained from [$L^{14}_2TiCl_2$] show two sets of resonances in a ratio of ~2:1. The major product has a spectra consistent with a symmetrical complex, and the minor set appear to arise from an unsymmetrical complex. Neither set of resonances demonstrate any noticeable line broadening over the range of temperatures accessible to us. There is no evidence for higher molecular-weight species in the mass spectrum, suggesting that the unsymmetrical species is unlikely to be a dimeric species.

3.4.4.2 Zirconium

Similarly to the titanium analogue, spectra obtained from [$L^{14}{}_2ZrCl_2$] also show two sets of resonances, the ratio between products is ~5:1. The major product has a spectrum consistent with a symmetrical complex, and the minor set appear to arise from an unsymmetrical complex.

The assignment of the aryl region of the ^1H NMR spectrum of [$\mathbf{L^{14}}_2ZrCl_2$] at 263 K is shown in Figure 3.8. At this temperature the major isomer is sharp but the minor is very broad, making the assignment clearer. The aryl region of the ^1H NMR spectra from 203-363 K are shown in Figure 3.9.

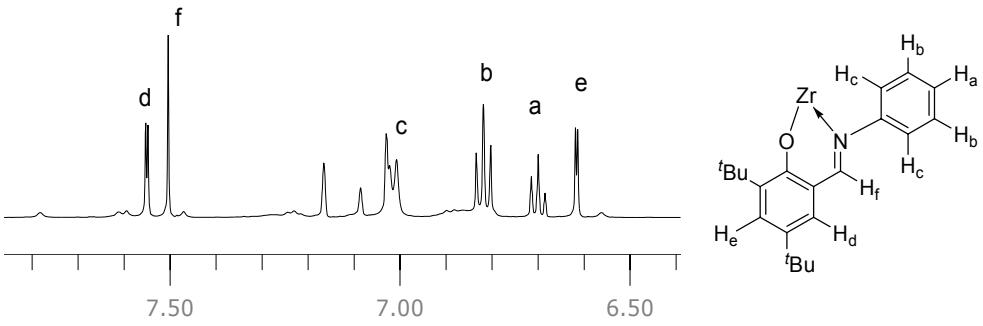

Figure 3.8 - Assignment of aryl region of [$L^{14}{}_2ZrCl_2$] (at 263K)

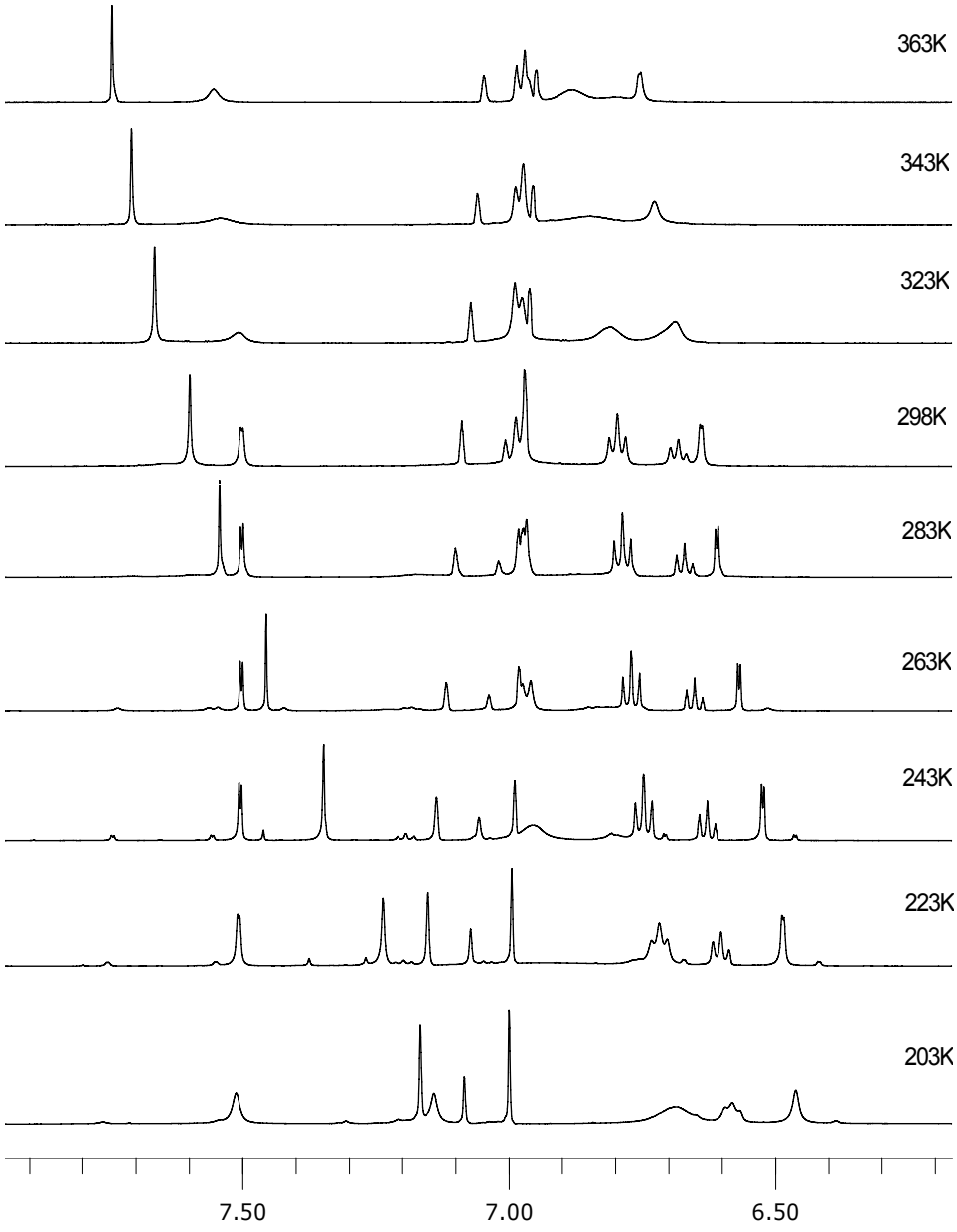

Figure 3.9 – Exchange behaviour in aryl region of ^{1}H NMR spectrum of [$L^{14}_2ZrCl_2$]

The presence of a minor, unsymmetrical (or C_1 symmetrical) isomer is most clear around 233 K, and this spectrum is shown below (Figure 3.10). At this temperature, one of the aryl signals from the major (C_2-symmetric) isomer is significantly broadened, masking some of the aryl signals from the minor isomer. As the temperature is increased, all the signals broaden, before the two sets of signals coalesce at around 333 K.

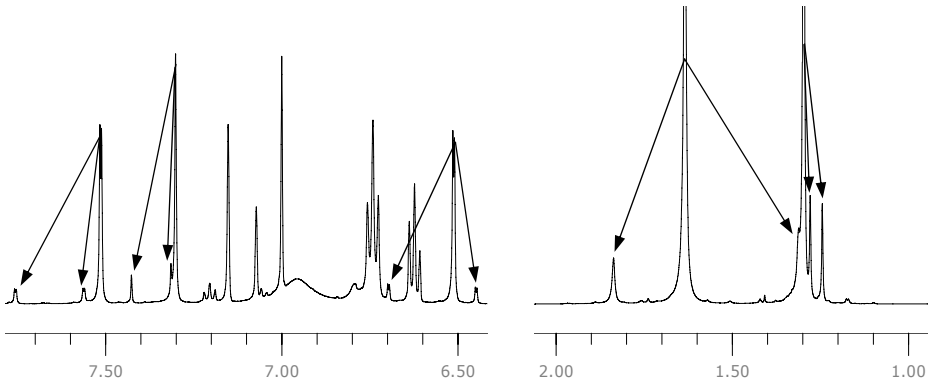

Figure 3.10 - Unsymmetrical minor isomer in [$L^{14}_2ZrCl_2$] (233 K); arrows indicate exchange between major and minor species

3.4.5 Molecular Structure of [$L^{11}_2TiCl_2$]

The molecular structure of [$\mathbf{L^{11}}_2TiCl_2$] was determined by single-crystal X-ray diffractometry (crystals grown from DCM/pentane), and is shown in Figure 3.11. It can be seen that the ligands have adopted an essentially C_2-symmetrical *cis*,*trans*,*cis* arrangement around the metal centre.

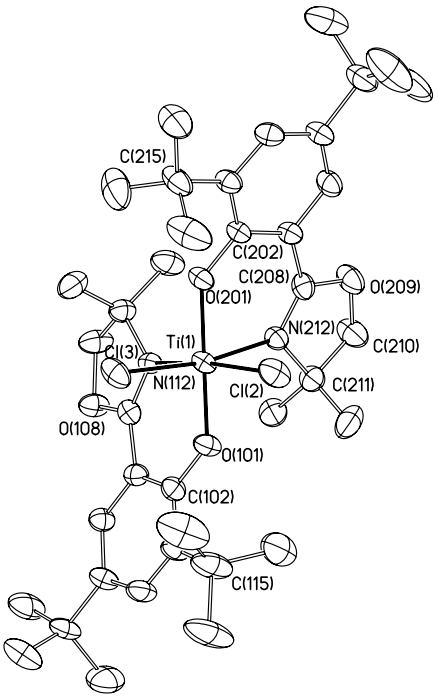

Figure 3.11 – Molecular structure of [$L^{11}_2TiCl_2$] (Hydrogen atoms omitted for clarity). Probability ellipsoids are set to the 50% level

In this system, compared to the salicylaldimine [$L^{14}{}_2TiCl_2$], whose molecular structure has been reported by Coates,[20] the two ligand *tert*-butyl groups are forced further toward the active site – the "bite angle" between the two ^{t}Bu groups through the titanium centre is more acute (140.33° *vs.* 161.09°), the distance between them is shorter (8.652 Å *vs.* 9.069 Å), and the distance from the metal centre to the centroid of the ^{t}Bu moieties is further (1.561 Å *vs.* 0.755 Å). This increased congestion at the active site is clearly visible in space-filling models of the species (Figure 3.12).

[$L^{11}{}_2TiCl_2$]		**[$L^{14}{}_2TiCl_2$][20]**	
Bond	**Length (Å)**	**Bond**	**Length (Å)**
Ti(1)-O(101)	1.864(2)	Ti(1)-O(1)	1.8343(19)
Ti(1)-O(201)	1.878(2)	Ti(1)-O(2)	1.8390(19)
Ti(1)-N(112)	2.183(3)	Ti(1)-N(1)	2.202(2)
Ti(1)-N(212)	2.174(3)	Ti(1)-N(2)	2.219(2)
Ti(1)-Cl(2)	2.3192(11)	Ti(1)-Cl(1)	2.3098(9)
Ti(1)-Cl(3)	2.3227(10)	Ti(1)-Cl(2)	2.3175(8)
C(115)-C(215)	8.652	C(18)-C(35)	9.069
Ti(1)-[C(115):C(215)]	1.561[a]	Ti(1)-[C(18):C(35)]	0.755[a]
Bonds	**Angle (°)**	**Bonds**	**Angle (°)**
O(101)-Ti(1)-O(201)	178.35(9)	O(1)-Ti(1)-O(2)	171.39(8)
O(101)-Ti(1)-N(112)	82.58(9)	O(1)-Ti(1)-N(1)	81.06(8)
O(201)-Ti(1)-N(212)	82.51(9)	O(2)-Ti(1)-N(2)	79.91(8)
O(101)-Ti(1)-N(212)	96.15(10)	O(1)-Ti(1)-N(2)	92.36(9)
N(112)-Ti(1)-N(212)	83.53(9)	N(1)-Ti(1)-N(2)	83.49(8)
Cl(2)-Ti-Cl(3)	100.08(4)	Cl(1)-Ti-Cl(2)	98.58(3)
O(201)-Ti(1)-N(112)	96.29(9)	O(2)-Ti(1)-N(1)	94.21(8)
C(115)-Ti(1)-C(215)	140.33	C(18)-Ti(1)-C(35)	161.09

[a] *I.e.* the distance from the metal to the centroid between the quarternary carbon atoms of the ^{t}Bu groups over the active site.

Table 3.5 - Selected bond angles and distances for [L^2TiCl_2] with comparison to the reported molecular structure of [$L^{14}{}_2TiCl_2$]

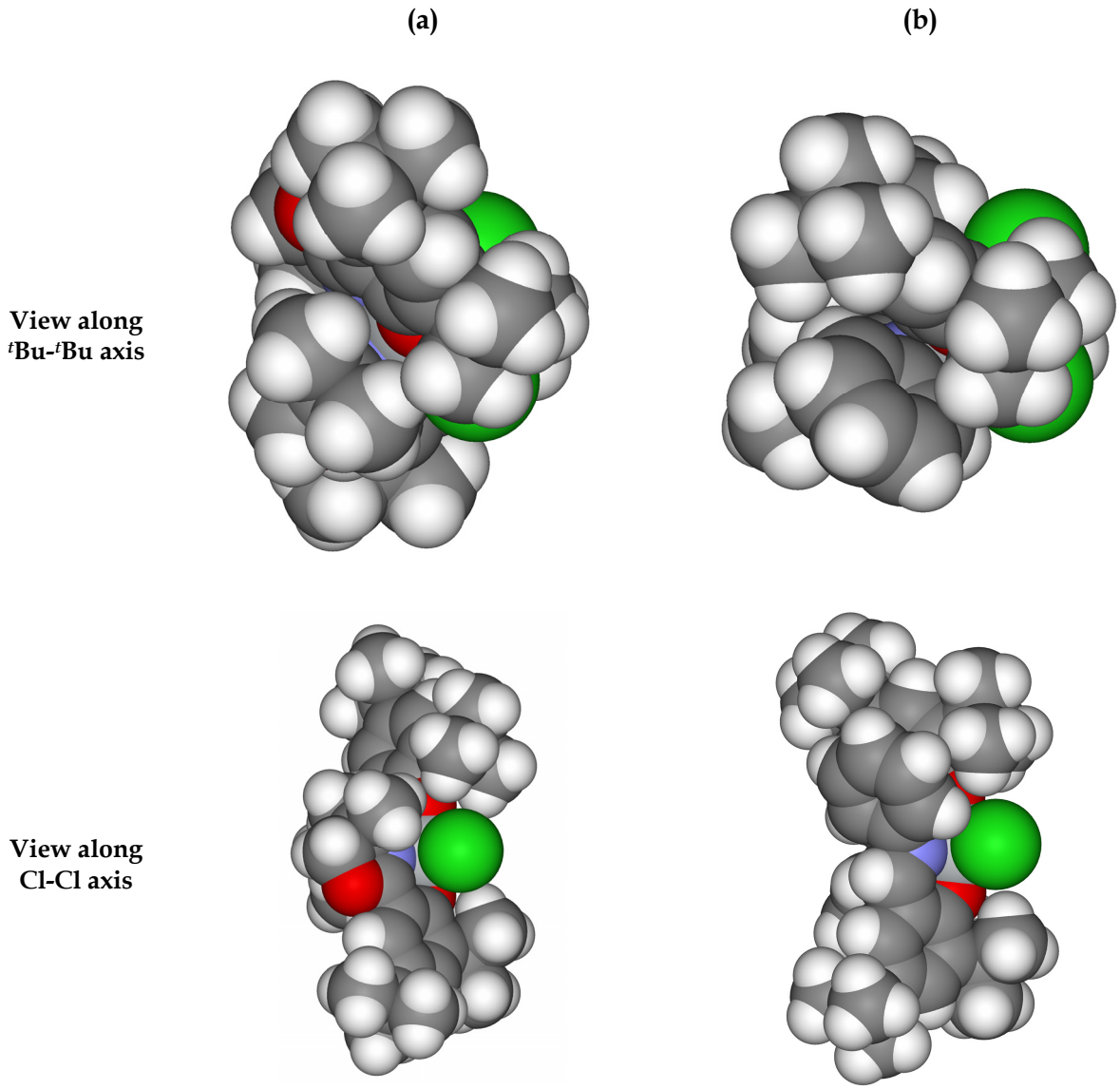

Figure 3.12 – Space-filling models of [$L^{11}_2TiCl_2$] (a) from XRD structure and [$L^{14}_2TiCl_2$] (b) from reported XRD structure[20]

3.5 Ligand Stability to MAO

In order to determine whether the oxazoline ligand itself was stable in the presence of MAO, we treated a quantity of [$\mathbf{L^{11}}_2ZrCl_2$] with 10% MAO/toluene for 1 h, and after *cautious* hydrolysis with water and subsequent extraction, recovered H$\mathbf{L^{11}}$ in

good yield, demonstrating that the ligand is not directly attacked (*e.g.* ring-opened) by the aluminium species in the polymerization reaction.

3.6 Initial Polymerization Trials

We screened the metal chloride complexes for activity in ethene polymerization using crude "Schlenk Test" productivity measurements (see §2.3.1.1).* Upon activation with MAO, the precatalysts [$L^n{}_2MCl_2$] were active for ethene polymerization; the results are summarized in Table 3.6, and shown graphically in Figure 3.13. It should be noted that themocontrol was not attempted for this series of trials. The experiments utilising the more productive catalysts became noticeably warm at the start.

The polymer products were analysed by Gel Permeation Chromatography (GPC) to determine their Molecular Weight (MWt) distributions, and the results are shown graphically in Figure 3.14.

Precatalyst	Precatalyst (µmol)	Yield (g)	Productivity (kg mol^{-1} bar^{-1} h^{-1})	M_n (u)	M_w (u)	PDi[a]
[$\mathbf{L^{10}}_2TiCl_2$]	18	0.21	10	8,255	229,000	(28)
[$\mathbf{L^{11}}_2TiCl_2$]	18	2.71	125	124,500	174,000	1.4
[$\mathbf{L^{12}}_2TiCl_2$]	18	0.12	5	2,325	75,250	(33)
[$\mathbf{L^{10}}_2ZrCl_2$]	14	1.05	62	840	127,500	(150)
[$\mathbf{L^{11}}_2ZrCl_2$]	16	5.75	308	765	28,300	(37)
[$\mathbf{L^{12}}_2ZrCl_2$]	14	0.04	2	2,015	346,500	(175)
[$\mathbf{L^{13}}_2ZrCl_2$]	14	3.60	216	495	5,040	(10)
[$\mathbf{L^{10}}_2HfCl_2$]	13	0.05	3	2,720	241,000	(89)
[$\mathbf{L^{11}}_2HfCl_2$]	14	1.73	107	490	28,300	(58)

[a] numbers in brackets represent multimodal polymer products

Table 3.6 – Initial polymerization results from L^nMCl_2 precatalysts

* Conditions: 175 ml toluene, 1000 eq. MAO, 1.2 bar C_2, 60 min

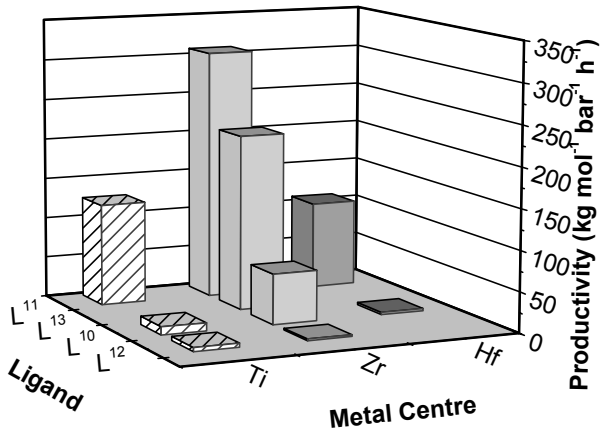

Figure 3.13 – Graph to show productivities from Initial Trials

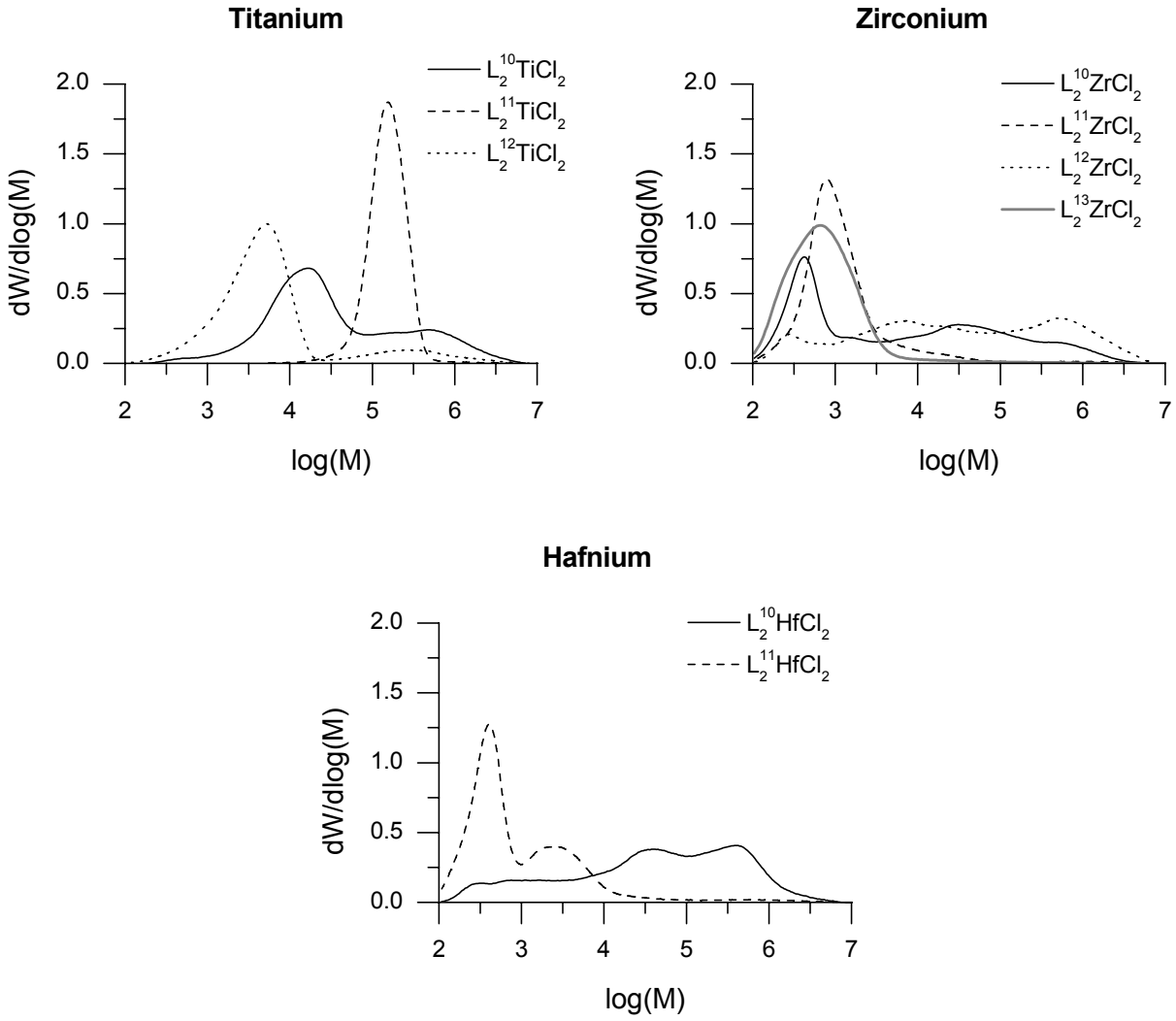

Figure 3.14 - MWDs from Initial Trials

This preliminary trial demonstrates that the system is active for ethene polymerization. Productivities vary in the order Zr > Ti > Hf, and $\mathbf{L^{11}} > \mathbf{L^{13}} > \mathbf{L^{10}} > \mathbf{L^{12}}$.

With the exception of $[\mathbf{L^{11}}_2TiCl_2]$, the oxazoline catalysts produce multimodal polymers under these conditions. The catalysts based on $\mathbf{L^{10}}$ produce higher molecular-weight polymer than those based on $\mathbf{L^{11}}$, but with lower productivity. Those based on $\mathbf{L^{12}}$ produce multimodal polymer with very low activity. Molecular weight varies in the order Ti > Zr > Hf.

The $[\mathbf{L^{13}}_2ZrCl_2]$ produces a broad molecular weight distribution, at low molecular weight.

Given the preliminary nature of these results, we will not discuss this data in detail at this point, but rather in §3.9, in comparison to other polymerization methodologies (*vide infra*).

3.7 High–Throughput (HT) Trials

3.7.1 Methodology

In order to generate further information regarding the ethene polymerization behaviour of this series of catalysts, we conducted a series of experiments using high-throughput methodology, utilizing an Argonaut Endeavor reactor, with the assistance of Dr Stefan Spitzmesser (BP/Innovene). We investigated only the titanium and zirconium complexes, and of these, only the more active species, namely $[\mathbf{L^{11}}_2TiCl_2]$, $[\mathbf{L^{11}}_2ZrCl_2]$ and $[\mathbf{L^{13}}_2ZrCl_2]$. For comparison, we also tested the salicylaldimine catalysts $[\mathbf{L^{14}}_2TiCl_2]$ and $[\mathbf{L^{14}}_2ZrCl_2]$.

The Endeavor reactor contains eight reaction vessels, each of which was loaded with 5 ml of solvent. We tested each catalyst under the following conditions (Table 3.7):*

Conditions	Temp. (°C)	Hexene (ml)
1	30	0.5
2	30	–
3	50	–
4	70	–

Table 3.7 – Conditions for High Throughput screen

3.7.2 Productivity

The results are shown in Table 3.8, and graphically in Figure 3.15. We believe that the result from the test of [$\mathbf{L^{11}}_2ZrCl_2$] under condition 4 is unreliable.†

* Common Conditions: 10 bar C_2, 5 ml Toluene, 600 eq MAO, 30 min

† The productivity under these conditions is disproportionately large, and the molecular weight distribution for the produced polyethene is considerably different to the other catalyst/conditions sets in the series. We believe that the most likely explanation is contamination of the reaction by another, more potent, catalyst which had previously been tested. The design of the equipment makes this somewhat likely, with catalyst solutions or suspensions being injected through 0.5 mm bore tubing. This tubing is readily blocked, and it seems that an amount of catalyst from a previous test had become lodged in the injector system, and entered the reaction, causing high activity and different product distribution. Unfortunately, due to the protocol for work-up of the product this error was not noted during the period when we had access to the Endeavor reactor, so the run could not be repeated. Thus, this datapoint is not shown in Figure 3.15.

Precatalyst	Conditions	Catalyst Load (μmol)	Yield [a] (g)	Productivity (kg mol^{-1} bar^{-1} h^{-1})
[$\mathbf{L^{11}}_2TiCl_2$]	1	1	0.114	2.3×10^1
[$\mathbf{L^{11}}_2TiCl_2$]	2	1	0.185	3.7×10^1
[$\mathbf{L^{11}}_2TiCl_2$]	3	1	0.212	4.2×10^1
[$\mathbf{L^{11}}_2TiCl_2$]	4	1	0.087	1.7×10^1
[$\mathbf{L^{11}}_2ZrCl_2$]	1	0.1	0.357	7.1×10^2
[$\mathbf{L^{11}}_2ZrCl_2$]	2	0.1	0.263	5.3×10^2
[$\mathbf{L^{11}}_2ZrCl_2$]	3	0.1	0.289	5.8×10^2
[$\mathbf{L^{11}}_2ZrCl_2$]	4[b]	0.1	0.591	1.2×10^3
[$\mathbf{L^{13}}_2ZrCl_2$]	1	0.1	0.180	3.6×10^2
[$\mathbf{L^{13}}_2ZrCl_2$]	2	0.1	0.183	3.7×10^2
[$\mathbf{L^{13}}_2ZrCl_2$]	3	0.1	0.094	1.9×10^2
[$\mathbf{L^{13}}_2ZrCl_2$]	4	0.1	0.075	1.5×10^2
[$\mathbf{L^{14}}_2TiCl_2$]	1	1	0.366	7.3×10^1
[$\mathbf{L^{14}}_2TiCl_2$]	2	1	0.593	1.2×10^2
[$\mathbf{L^{14}}_2TiCl_2$]	3	1	0.368	7.4×10^1
[$\mathbf{L^{14}}_2TiCl_2$]	4	1	0.371	7.4×10^1
[$\mathbf{L^{14}}_2ZrCl_2$]	1	0.1	0.501	1.0×10^3
[$\mathbf{L^{14}}_2ZrCl_2$]	2	0.1	0.330	6.6×10^2
[$\mathbf{L^{14}}_2ZrCl_2$]	3	0.1	0.425	8.5×10^2
[$\mathbf{L^{14}}_2ZrCl_2$]	4	0.1	0.438	8.8×10^2

[a] Assuming all MAO is converted to Al_2O_3
[b] We believe that this result should be discounted – *vide supra*

Table 3.8 – Productivity Results from HT trial

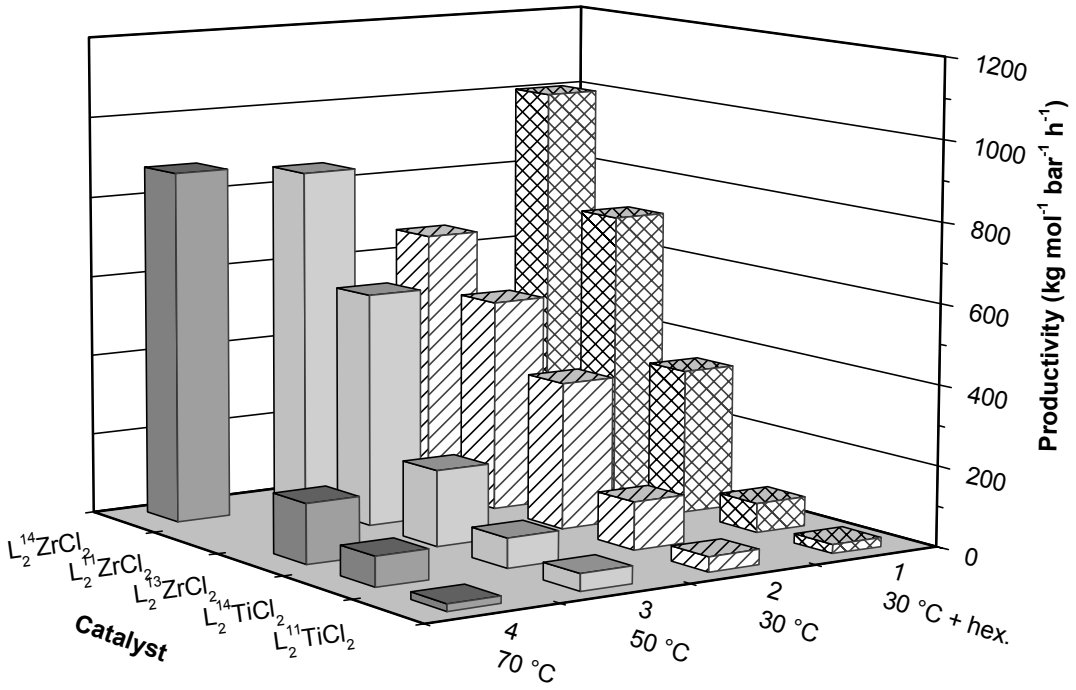

Figure 3.15 - Graph to show productivities from HT trial

3.7.3 Hexene Incorporation

Attempts to press the product into films suitable for IR analysis of hexene incorporation and DSC studies were unsuccessful. The increased productivities noted when hexene is present in the system suggest some interaction with the system, but it is not possible to determine whether it has been incorporated into the polymer under these conditions.

3.7.4 Polymer Characterization

The polymers produced were analysed using GPC, and the results are shown in Table 3.9.

Precatalyst	Conditions	M_n (u)	M_w (u)	Modality	PDi
[$\mathbf{L^{11}}_2TiCl_2$]	1	101,200	325,600	1	3.2
[$\mathbf{L^{11}}_2TiCl_2$]	2	127,900	372,500	1	2.9
[$\mathbf{L^{11}}_2TiCl_2$]	3	67,400	344,300	1	5.1
[$\mathbf{L^{11}}_2TiCl_2$]	4	53,600	262,700	2	(4.9)
[$\mathbf{L^{11}}_2ZrCl_2$]	1	1,700	14,800	2	(8.5)
[$\mathbf{L^{11}}_2ZrCl_2$]	2	2,100	19,700	2	(9.3)
[$\mathbf{L^{11}}_2ZrCl_2$]	3	3,800	34,200	2	(9.1)
[$\mathbf{L^{11}}_2ZrCl_2$]	4[b]	2,400	5,200	1	2.2[a]
[$\mathbf{L^{13}}_2ZrCl_2$]	1	700	1,000	1	1.3[a]
[$\mathbf{L^{13}}_2ZrCl_2$]	2	600	1,000	1	1.5[a]
[$\mathbf{L^{13}}_2ZrCl_2$]	3	700	1,000	1	1.5[a]
[$\mathbf{L^{13}}_2ZrCl_2$]	4	800	1,100	1	1.5[a]
[$\mathbf{L^{14}}_2TiCl_2$]	1	4,5200	122,100	1	2.7
[$\mathbf{L^{14}}_2TiCl_2$]	2	96,900	270,800	1	2.8
[$\mathbf{L^{14}}_2TiCl_2$]	3	89,600	275,300	1	3.1
[$\mathbf{L^{14}}_2TiCl_2$]	4	39,300	215,700	2	(5.5)
[$\mathbf{L^{14}}_2ZrCl_2$]	1	2,600	41,100	2	(15.9)
[$\mathbf{L^{14}}_2ZrCl_2$]	2	2,500	26,000	2	(10.3)
[$\mathbf{L^{14}}_2ZrCl_2$]	3	–	–		–[c]
[$\mathbf{L^{14}}_2ZrCl_2$]	4	3,500	72,200	2	(20.8)

[a] Molecular weight very low, so low confidence in PDi numbers
[b] We believe that the reaction under these conditions should be discounted – *vide supra*
[c] Sample unsuitable for GPC analysis

Table 3.9 – Polymer Characterization from HT trial

3.7.4.1 Comparison with Salicylaldimine Catalysts under HT Conditions

Figure 3.16 shows the molecular weight distributions over the range of temperatures tested, for the titanium and zirconium **L**^{11} and **L**^{14} systems. Both systems appear to show two distinct modes in the molecular weight distributions. For the titanium systems, increased temperature appears to favour the lower MWt mode in both ligand systems. In the zirconium systems however, increased temperature favours the higher MWt mode.

At a titanium centre, the salicyloxazoline system produces higher molecular weight polymer compared to the salicylaldimine. At a zirconium centre, the molecular weight is lower, but a higher proportion of the polymer is in the higher molecular weight mode compared to the product generated by the salicylaldimine system.

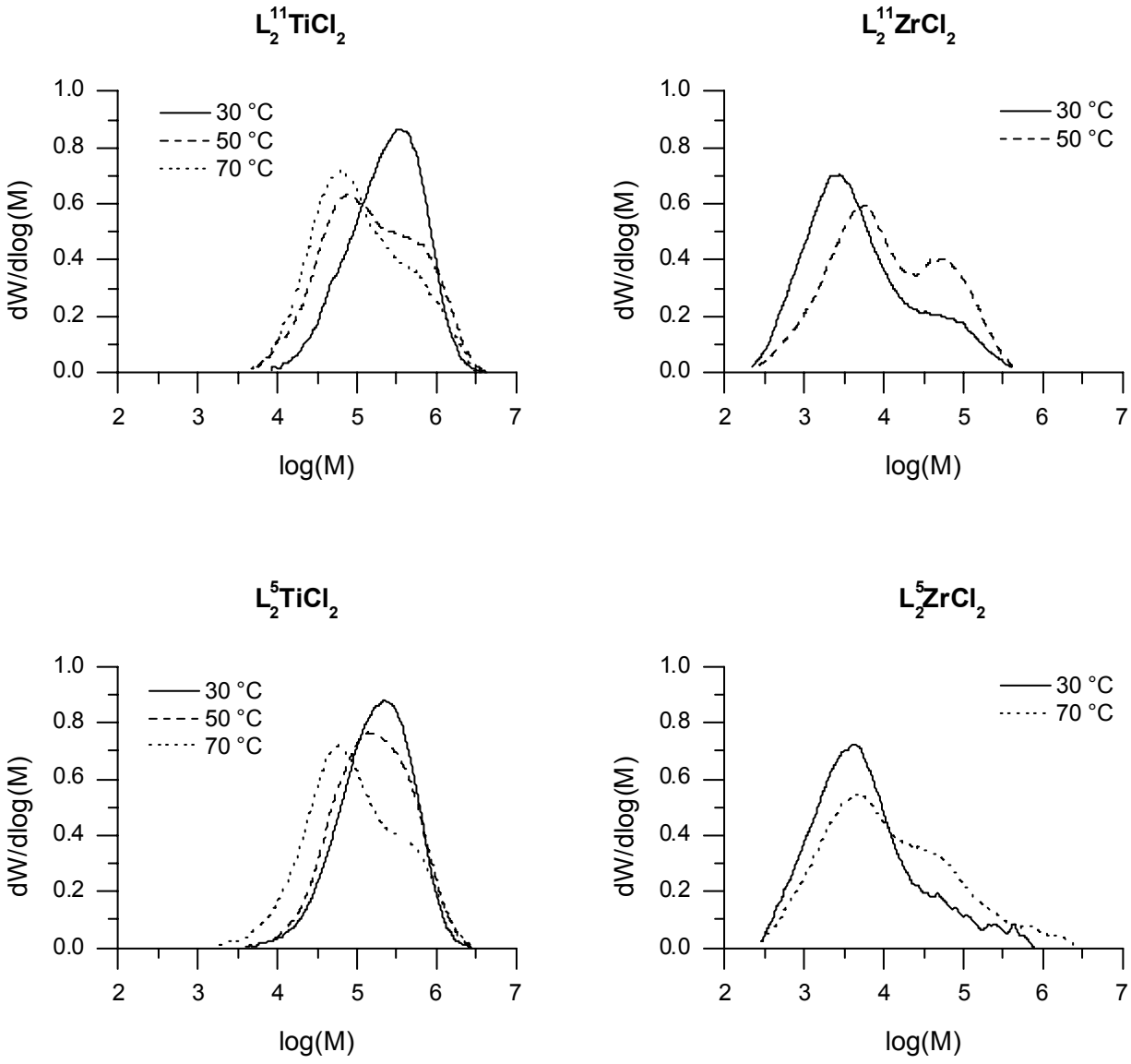

Figure 3.16 - MWDs for L^{11} and L^{14} catalysts obtained under HT conditions

3.7.4.2 Benzoxazole System

In contrast, the benzoxazole system [$\mathbf{L^{13}}_2ZrCl_2$] produces very low molecular weight polymer with a unimodal weight distribution (Figure 3.17). Structurally, the ligand is more similar than the other salicyloxazolines to the salicylaldimine ligand tested, but it generates substantially different polymer nonetheless.

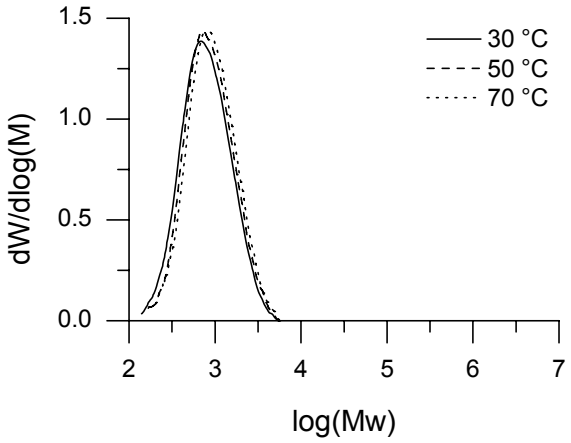

Figure 3.17 - MWDs for [$L^{13}_2ZrCl_2$] in HT trial

3.7.5 Conclusions from HT Trials

The similarities between the behaviour of the salicylaldimine and salicyloxazoline catalyst systems suggest that the active species are closely related. The similar variations of polymer MWD with varying conditions are particularly striking. The lower MWt of the polymer produced by the benzoxazole-based catalyst suggests that this system may have a higher susceptibility to chain-transfer reactions during the polymerization; although being structurally more similar to the salicylaldimines, it behaves in a significantly different manner.

The reactor volume in the Endeavor is very small. Although it is well stirred, and despite using low catalyst loading we felt that there was a significant possibility that the reactions may be diffusion limited under these conditions, especially as the volume of polymer in the reactor rises.

Hence while the Endeavor reactor records the uptake of gas to each reactor, we have low confidence in the data obtained this way. As such, we still did not have a reliable measure of the lifetime of the catalysts. This data was obtained using the gas burette system discussed in Chapter 2.

3.8 Reaction Profiles

We conducted a series of experiments to measure the uptake of ethene by these catalyst systems at 25 and 50 °C, using the gas burette apparatus described in Chapter 2. The productivity and MWt data are presented in Table 3.11. Where possible, a half-life ($\tau_{½}$) has been calculated for the catalyst decay (*vide infra*, §3.8.5).

3.8.1 [$L^{14}_2MCl_2$]

We initially tested the unbridged salicylaldimine catalysts [$\mathbf{L^{14}}_2MCl_2$] (M = Ti, Zr) – which have been previously reported as long-lived.[7,21,*]

[$\mathbf{L^{14}}_2TiCl_2$] shows good stability at 25 °C ($\tau_{½}$ = 3060 s), and gradual decay in activity at 50 °C ($\tau_{½}$ = 1610 s) (Figure 3.18).

This catalyst shows higher initial activity at 50 °C than at 25 °C, but the higher rate of decay at elevated temperature reduces this difference over the course of the run. Although the increase in measured ethene uptake is small (a factor of 2 at the start of the run), it is significant; at 50 °C the concentration of ethene in solution is approximately 60% of that at 25 °C.[22] Assuming that the rate of polymerization has non-zero order in monomer concentration,[23] this will affect the observed "activity".

The zirconium analogue [$\mathbf{L^{14}}_2ZrCl_2$] shows much higher initial activity, but far lower stability; at 25 °C the activity drops relatively steeply ($\tau_{½}$ = 640 s), whereas at 50 °C the system is essentially inactive after 300 s ($\tau_{½}$ = 60 s).

---

[*] Conditions: 100 ml toluene inc. 5 ml 10% w/v MAO/toluene solution, 1.2 bar C_2,1 h

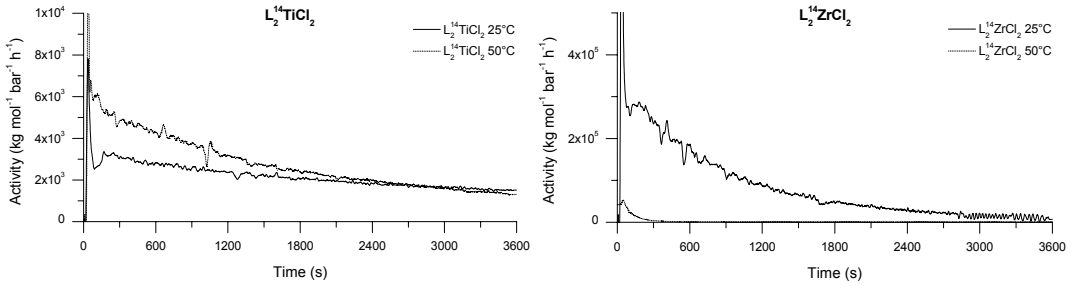

Figure 3.18 - Reaction profiles for [$L^{14}_2MCl_2$]

This is further evidence of how dramatically the choice of metal centre affects the course of the polymerization, with the titanium system exhibiting good stability, and the zirconium system rapid decay of activity. It should be noted that although the decrease in activity for the zirconium system at 25 °C is pronounced, the system still shows an activity of *ca.* 5 × 10^4 kg mol^{-1} bar^{-1} h^{-1}) after 30 min – *i.e.* very highly active on the "Gibson scale."[24]

3.8.2 [$L^{10}_2MCl_2$]

We tested the Zr and Ti complexes of **L**[10] under similar conditions. The activities of the catalysts formed from both metal species are low, with the zirconium species demonstrating a somewhat higher activity and productivity (Figure 3.19).

The zirconium system appears to gradually increase in activity over the first 1200 s of the reaction, before gradually decreasing after that point. The titanium system shows gradual decrease in activity from an initial peak.

Given the low activity, and the difficulties involved in measuring uptake at this level without substantially changing the reaction conditions, we did not test these catalysts at 50 °C.

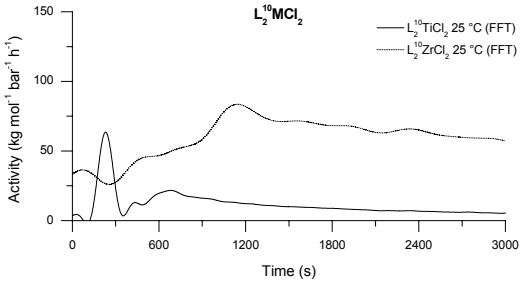

Figure 3.19 - Reaction profiles for [$L^{10}_2MCl_2$] (M = Ti, Zr)

3.8.3 [$L^{11}_2MCl_2$]

In comparison with the systems utilizing **L**^{10}, those using **L**^{11} show substantially higher activities.

[**L**$^{11}_2TiCl_2$] shows good stability at both 25 °C and 50 °C ($\tau_{½}$ = 4060 s, 2340 s respectively), (Figure 3.20). With a zirconium centre, the results are strikingly similar to those for the salicylaldimine catalyst [**L**$^{14}_2ZrCl_2$]. At 25 °C the activity drops relatively steeply ($\tau_{½}$ = 930 s), whereas at 50 °C the system is essentially inactive after 300 s ($\tau_{½}$ = 50 s).

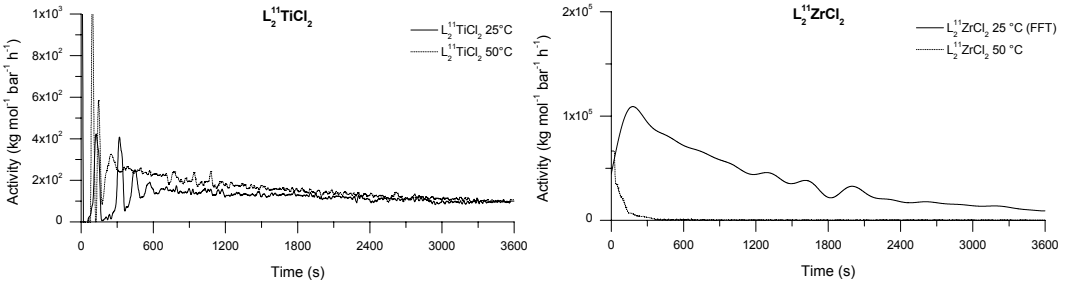

Figure 3.20 - Reaction profiles for [$L^{11}_2MCl_2$]

At 25 °C the hafnium analogue shows behaviour intermediate between the zirconium and titanium species, with gradual decay in activity ($\tau_{½}$ = 2630 s), and an activity approximately twice that of the titanium species. This system was not tested at 50 °C.

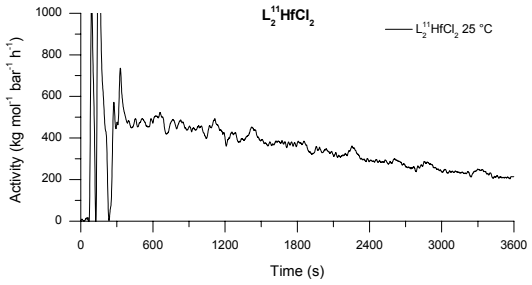

Figure 3.21 - Reaction profile for [$L^{11}_2HfCl_2$]

3.8.4 [$L^{13}_2ZrCl_2$]

The salicylbenzoxazole species [$\mathbf{L^{13}}ZrCL_2$] suffered very rapid deactivation at 25 °C ($\tau_{½}$ = 50 s), and was effectively inactive at 50 °C – no uptake of gas was measured and only a trace of polymer was recovered.

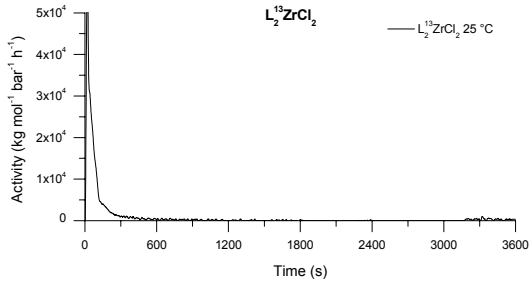

Figure 3.22 - Reaction profile for [$L^{13}_2ZrCl_2$]

3.8.5 Productivity/Activity Measurements and Polymer Characterization

3.8.5.1 Least-squares fitting

An equation to represent the decay of activity over time was obtained by an iterative least-squares fitting of the data to a first-order exponential decay of the form $y = A\exp(-(x - x_0)/t_1) + y_0$, using Origin 7 (Table 3.10).[12] Where the activity of a catalyst dropped to a constant value during the reaction, y_0 was calculated, in all other cases, it was set to 0. The fit was constrained such that $x_0 \geq 0$. The half-life is given by $\tau_{½} = t_1 \ln(2) + x_0$ and A represents the initial activity of the system at $t = x_0$.

Precatalyst	Temp. (°C)	Data start (s)	y_0[a]	x_0	A	t_1	r²	$\tau_{½}$
[$\mathbf{L^{11}}_2TiCl_2$]	25	600	[0]	0	1.70×10^2	5860	0.851	4060
[$\mathbf{L^{11}}_2TiCl_2$]	50	300	[0]	80	2.63×10^2	3270	0.946	2340
[$\mathbf{L^{11}}_2ZrCl_2$]	25	200	[0]	0	1.15×10^5	1350	0.988	930
[$\mathbf{L^{11}}_2ZrCl_2$]	50	50	240	0	6.23×10^4	80	0.986	50
[$\mathbf{L^{11}}_2HfCl_2$]	25	350	[0]	30	5.66×10^2	3750	0.950	2630
[$\mathbf{L^{13}}_2ZrCl_2$]	25	35	140	10	5.60×10^4	50	0.987	50
[$\mathbf{L^{14}}_2TiCl_2$]	25	200	[0]	0	3.18×10^3	4420	0.972	3060
[$\mathbf{L^{14}}_2TiCl_2$]	50	200	[0]	0	5.47×10^3	2320	0.985	1610
[$\mathbf{L^{14}}_2ZrCl_2$]	25	200	[0]	0	3.27×10^5	930	0.989	640
[$\mathbf{L^{14}}_2ZrCl_2$]	50	70	520	0	7.56×10^4	90	0.989	60

[a] y_0 and A have the units kg mol^{-1} bar^{-1} h^{-1}, x_0, t_1 and $\tau_{½}$ have units s

Table 3.10 – Least-squares fitting results for activity profiles for [L^nMCl_2]

3.8.5.2 Productivity

The detail of the reactions conducted is shown in Table 3.11, including the results of polymer characterization by GPC.

Precatalyst	Temp. (°C)	Catalyst (mol)	Yield (g)	Productivity$_{60}$ (kg mol^{-1} bar^{-1} h^{-1})	M_n (u)	M_w (u)	PDi
[$\mathbf{L^{10}}_2TiCl_2$]	25	1.8×10^{-5}	0.19	8.8	7,300	10,600	(15)[a]
[$\mathbf{L^{10}}_2ZrCl_2$]	25	3.1×10^{-6}	0.15	40	760	77,000	(102)[a]
[$\mathbf{L^{10}}_2HfCl_2$]	25	1.3×10^{-5}	trace	–	–	–	–
[$\mathbf{L^{11}}_2TiCl_2$]	25	6.9×10^{-6}	1.60	1.7×10^2	88,500	160,000	1.8
[$\mathbf{L^{11}}_2TiCl_2$]	50	7.7×10^{-6}	1.09	1.3×10^2	129,000	172,000	1.3
[$\mathbf{L^{11}}_2ZrCl_2$]	25	1.3×10^{-8}	0.61	3.9×10^4	1,900	9,400	(5.0)[a]
[$\mathbf{L^{11}}_2ZrCl_2$]	50	2.6×10^{-7}	0.32	1.0×10^3	510	770	1.5
[$\mathbf{L^{11}}_2HfCl_2$]	25	7.0×10^{-6}	2.91	3.5×10^2	1,200	39,400	(33)[a]
[$\mathbf{L^{13}}_2ZrCl_2$]	25	2.5×10^{-7}	0.72	2.4×10^3	710	1,100	1.6
[$\mathbf{L^{13}}_2ZrCl_2$]	50	2.5×10^{-7}	trace	–	–	–	–
[$\mathbf{L^{14}}_2TiCl_2$]	25	1.4×10^{-6}	3.73	2.3×10^3	233,000	470,000	2.0
[$\mathbf{L^{14}}_2TiCl_2$]	50	1.4×10^{-6}	4.62	2.8×10^3	125,000	276,000	2.2
[$\mathbf{L^{14}}_2ZrCl_2$]	25	1.3×10^{-8}	1.28	8.3×10^4	16,200	55,400	2.5
[$\mathbf{L^{14}}_2ZrCl_2$]	50	6.4×10^{-7}	1.82	2.4×10^3	870	11,900	(13.7)[a]

[a] Multimodal MWt distribution observed.

Table 3.11 - Results from activity profiling reactions for [$L^n{}_2MCl_2$]*

* Conditions: 100 ml toluene inc. 5ml 10% w/v MAO/toluene solution, 1.2 bar C_2,1 h

3.8.5.3 Polymer Characterization

The MWDs obtained are shown graphically in Figure 3.23, and are clearly very similar to those obtained from the non-thermocontrolled initial trials. The polymers produced by the various methodologies will be compared in detail in §3.9.2.

The salient features of the MWDs obtained are:

- The salicyloxazoline catalysts demonstrate behaviour very similar to the corresponding salicylaldimine species.
- Titanium catalysts generate higher MWt polymers than the corresponding zirconium species
- **L**^{10} species produce broad, multimodal distributions
- **L**^{11} species produce much tighter distributions; [**L**$^{11}_2$$TiCl_2$] is unimodal, whereas [**L**$^{11}_2$$ZrCl_2$] demonstrates a minor mode with higher MWt. [**L**$^{11}_2$$HfCl_2$] shows a bimodal distribution, favouring the higher MWt mode somewhat
- [**L**$^{13}_2$$ZrCl_2$] produces unimodal polymer with a low molecular weight
- Increasing the temperature from 25 °C to 50 °C results in a lower MWt of the product for the **L**^{11} species

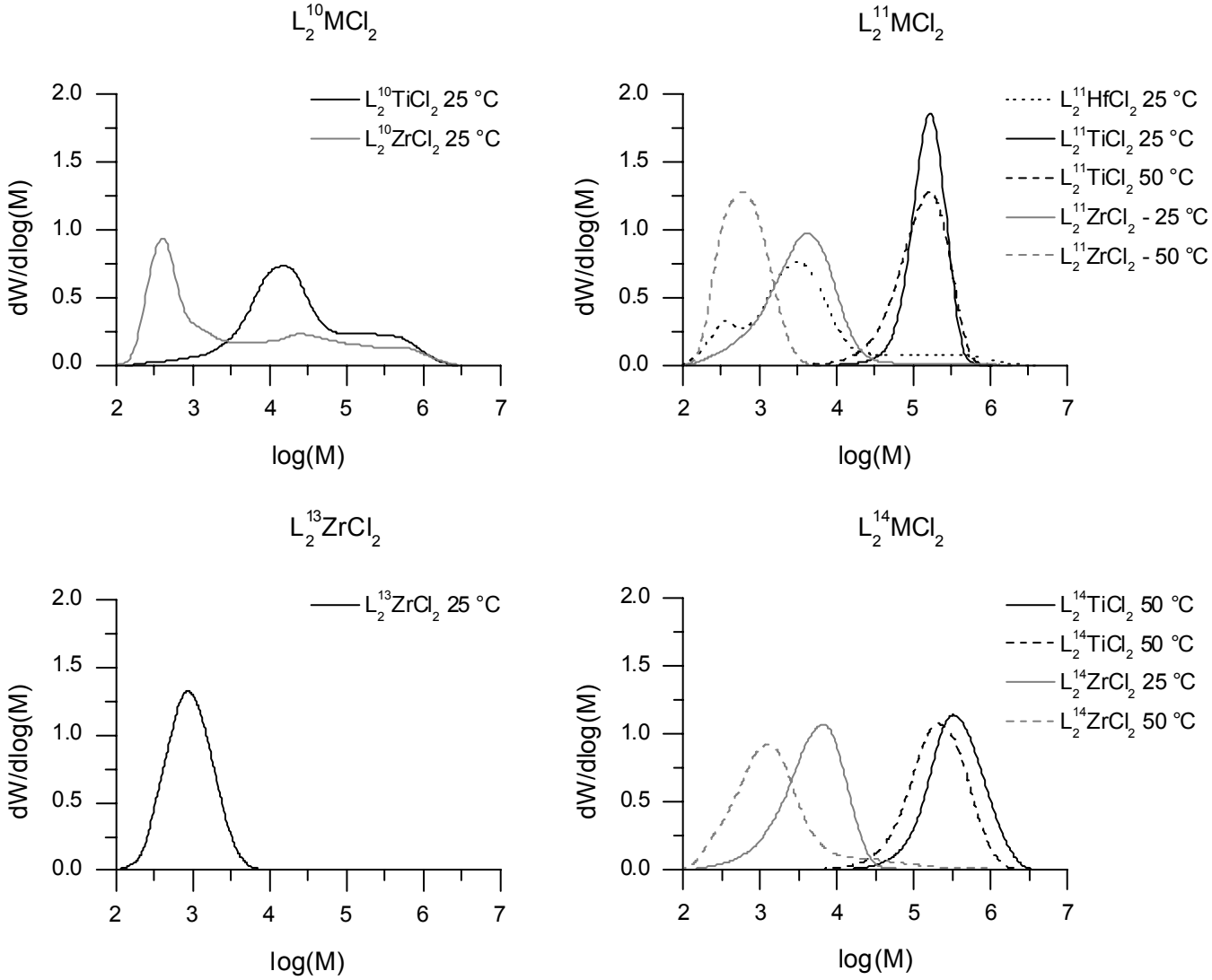

Figure 3.23 – MWDs from profiling reactions

3.9 Comparison of Different Methodologies

3.9.1 Catalyst Productivity *vs.* Activity

It is clear that the different methods we have used to conduct polymerization reactions have resulted in significantly different observed productivities and activities. Table 3.12 summarizes the productivity and activity data presented above.

Precatalyst	Temp. (°C)[a]	Productivity$_{60}$ (Initial)[b]	Productivity$_{60}$ (HT)[b]	Productivity$_{60}$ (Profiled)[b]	Activity$_{t0}$ (Profiled)[b,c]
[**L**$^{10}_2$TiCl$_2$]	low	10	–	8.8	–
[**L**$^{10}_2$ZrCl$_2$]	low	62	–	40	–
[**L**$^{10}_2$HfCl$_2$]	low	3	–	–	–
[**L**$^{11}_2$TiCl$_2$]	low	1.3×10^2	37	1.7×10^2	1.7×10^2
[**L**$^{11}_2$TiCl$_2$]	50	–	42	1.3×10^2	2.6×10^2
[**L**$^{11}_2$ZrCl$_2$]	low	3.1×10^2	5.3×10^2	3.9×10^4	1.2×10^5
[**L**$^{11}_2$ZrCl$_2$]	50	–	5.8×10^2	1.0×10^3	6.2×10^4
[**L**$^{11}_2$HfCl$_2$]	low	1.1×10^2	–	3.5×10^2	5.7×10^2
[**L**$^{13}_2$ZrCl$_2$]	low	2.2×10^2	3.7×10^2	2.4×10^3	5.6×10^4
[**L**$^{13}_2$ZrCl$_2$]	50	–	1.9×10^2	trace	–
[**L**$^{14}_2$TiCl$_2$]	low	–	1.2×10^2	2.3×10^3	3.2×10^3
[**L**$^{14}_2$TiCl$_2$]	50	–	74	2.8×10^3	5.5×10^3
[**L**$^{14}_2$ZrCl$_2$]	low	–	6.6×10^2	8.3×10^4	3.3×10^5
[**L**$^{14}_2$ZrCl$_2$]	50	–	8.5×10^2	2.4×10^3	7.6×10^4

[a] "low" = ambient temperature for initial trials, 30 °C for HT trials, 25 °C for profile trials
[b] units for all productivity measurements are kg mol^{-1} bar^{-1} h^{-1}
[c] from linear regression analysis (*q.v.* Table 3.10)

Table 3.12 - Comparison of productivities & activities from different methodologies

Upon comparison of the productivities recorded in our initial screening tests with those obtained during the carefully-controlled profiling tests, it is clear that the initial screening tests significantly underestimated the potential productivity of some of these catalysts – specifically [**L**$^{11}_2$ZrCl$_2$] and [**L**$^{13}_2$ZrCl$_2$]. This is not surprising given the results presented in §3.8 which clearly demonstrate the sensitivity of these systems to elevated temperature; in the initial trials the temperature was observed to rise - this would have lead to a rapid deactivation of the catalyst.

Comparison of the data from the HT trials with those recorded in our laboratory is less straightforward, due to the different conditions. The HT results consistently give productivity values an order of magnitude lower than those observed during our profiling reactions. Although the difference in temperature may be expected to influence the productivities observed, under HT conditions raising the temperature from 30 °C to 50 °C has only minimal effect on the observed productivity of the systems tested whereas a similar rise from 25 °C to 50 °C results in an order of

magnitude decrease in productivity for the zirconium systems when measured in our laboratory. From the activity profile data it is clear that this lower productivity at elevated temperature is a result of decreasing activity during the course of the reaction rather than lower initial activity (*q.v.* §3.8).

There are at least two possible explanations for this behaviour, *viz*.: i) At 10 bar the catalysts do not deactivate so readily. We will show in §4.6 that this is unlikely to be the case. ii) The experimental methodology employed during the HT trials leads to limited sensitivity towards differences in activity, as a result of diffusion limitation (*q.v.* §3.7.5).

3.9.2 Polymer Properties

The MWDs of the polymers produced during the initial trials correlate almost perfectly with those recorded at 25 °C with effective thermocontrol. The only notable exception is [$\mathbf{L^{11}}_2HfCl_2$] which produces bimodal polymer; without thermocontrol the lower MWt mode is somewhat favoured whereas with thermocontrol the higher MWt mode is. The similarity between the polymer products with and without thermocontrol strongly suggests that the deactivation mechanism is absolute; the catalyst decomposes into an essentially inactive compound rather than some other catalytically active species.

The polymers produced during the high-throughput trials show some similarities with those produced in our laboratory: titanium produces higher MWt products than zirconium with both $\mathbf{L^{11}}$ and the analogous salicylaldimine $\mathbf{L^{14}}$ as ligands. On closer inspection, however, there are significant differences between the products.

Most significantly, under the HT conditions, clearly bimodal MWDs were observed in most cases, whereas in the results from our laboratory one mode

dominates. Comparison of the GPC traces for the zirconium species shows this effect most clearly* (the appropriate data for [$\mathbf{L^{11}}_2ZrCl_2$] are reproduced in Figure 3.24 and those for [$\mathbf{L^{14}}_2ZrCl_2$] in Figure 3.25).

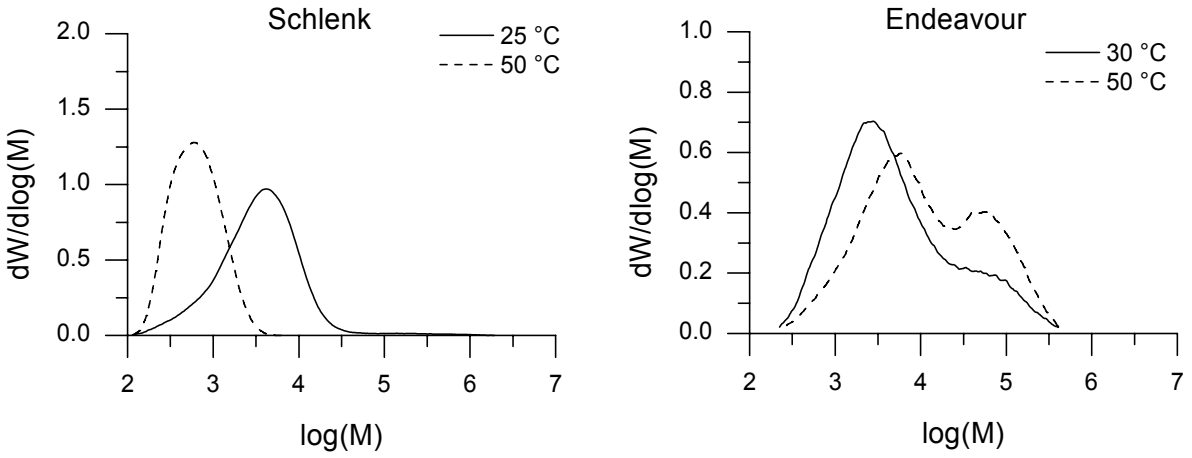

Figure 3.24 - Comparison of Schlenk and Endeavor products for [$L^{11}_2ZrCl_2$]

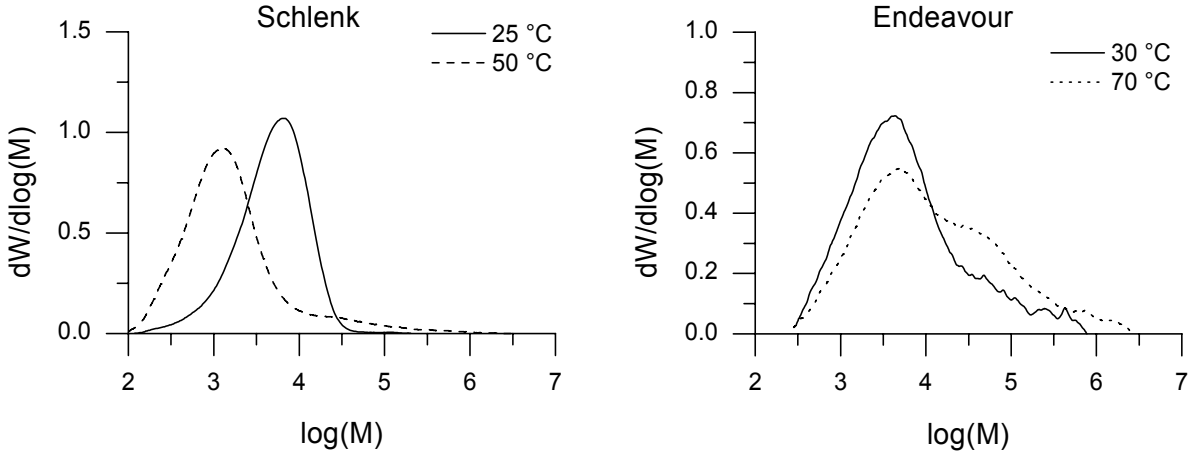

Figure 3.25 - Comparison of Schlenk and Endeavor products for [$L^{14}_2ZrCl_2$]

---

* *N.B.* the polymers produced from the Schlenk tests and from the Endeavor reactor were analysed under different (although similar) GPC conditions (those from the Schlenk tests were analysed by RAPRA Ltd, and those from the Endeavor by Innovene). We analysed some samples using both methods, the results obtained demonstrated excellent degree of correlation. See §6.1.4 for details of GPC techniques.

It should be noted that although the products obtained under profiling conditions are predominantly unimodal, they all demonstrate a tail of material in the high MWt region of the spectrum. These GPC data were obtained using a refractive index detector, but a differential pressure (viscosity) detector was online during the runs, and Figure 3.26 shows the chromatogram obtained for the product of [$\mathbf{L^{11}}_2ZrCl_2$] under Schlenk conditions at 25 °C (*cf.* Figure 3.24 [left]). Although the overall molecular weight of the polymer is low, these data clearly show the presence of higher MWt material (higher MWt material has a shorter retention time in GPC).

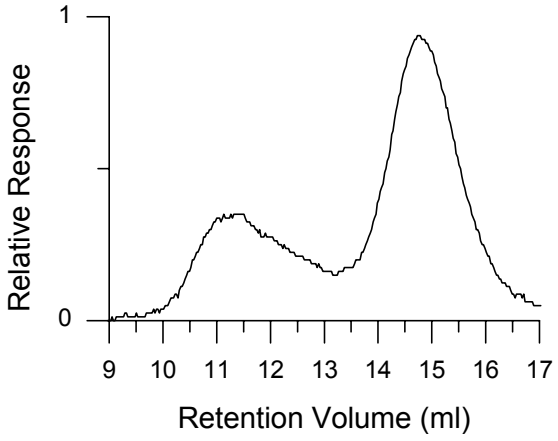

Figure 3.26 - Differential pressure chromatogram of [$\mathbf{L^{11}}_2ZrCl_2$] Schlenk product, 25 °C

Under the Endeavor conditions, increased temperature favoured increased molecular weight, whereas under Schlenk conditions the opposite is true.

3.10 Summary and Conclusions

We have presented a new series of catalysts based on salicyloxazoline ligands. In order to obtain highly-active catalyst systems it is necessary for the salicyloxazoline ligand to possess steric bulk at two positions; *ortho* to the phenoxy-donor, and α to the oxazoline nitrogen donor. Those systems based on zirconium show very high activity, those on titanium somewhat lower. The performance of the benzoxazole

system [$L^{13}_2ZrCl_2$] is interesting, demonstrating a high initial activity but a rapid deactivation.

We have unambiguously shown that the salicylaldimine catalysts suffer from rapid deactivation at 50 °C and, surprisingly, that the salicyloxazoline catalysts suffer similar deactivation. Hence, we began investigating another possible mechanism for catalyst deactivation, and this work is discussed in Chapter 4.

3.11 References for Chapter 3

1 P. G. Cozzi, C. Floriani, A. Chiesi-Villa and C. Rizzoli, *Inorg. Chem.*, 1995, **34**, 2921-30; P. G. Cozzi, E. Gallo, C. Floriani, A. Chiesi-Villa and C. Rizzoli, *Organometallics*, 1995, **14**, 4994-96.

2 R. Furuyama, J. Saito, S. Ishii, M. Mitani, S. Matsui, Y. Tohi, H. Makio, N. Matsukawa, H. Tanaka and T. Fujita, *J. Mol. Catal. A: Chem.*, 2003, **200**, 31-42.

3 T. Fujita, Y. Tohi, M. Mitani, S. Matsui, J. Saito, M. Nitabaru, K. Sugi, H. Makio and T. Tsutsui, EP874005 (Mitsui Chemicals, Inc., Japan), 1998; S. Matsui and T. Fujita, *Catal. Today*, 2001, **66**, 63-73.

4 S. Matsui, M. Mitani, J. Saito, N. Matsukawa, H. Tanaka, T. Nakano and T. Fujita, *Chem. Lett.*, 2000, 554-55.

5 I. J. Munslow, *SyntheticPages*, 2001, http://www.syntheticpages.org/pages/6; G. Schmitt, N. D. An, J. P. Poupelin, J. Vebrel and B. Laude, *Synthesis*, 1984, 758-60.

6 H. Vorbrüggen and K. Krolikiewicz, *Tetrahedron Lett.*, 1981, **22**, 4471-74; H. Vorbrüggen and K. Krolikiewicz, *Tetrahedron*, 1993, **49**, 9353-72.

7 S. Matsui, M. Mitani, J. Saito, Y. Tohi, H. Makio, N. Matsukawa, Y. Takagi, K. Tsuru, M. Nitabaru, T. Nakano, H. Tanaka, N. Kashiwa and T. Fujita, *J. Am. Chem. Soc.*, 2001, **123**, 6847-56.

8 J. Sandström, 'Dynamic NMR spectroscopy', Academic Press, 1982.

9 A. R. Quirt and J. S. Martin, *J. Magn. Reson.*, 1971, **5**, 318-327.

10 A. D. Bain and G. J. Duns, *Can. J. Chem.*, 1996, **74**, 819-24; A. D. Bain, 'MEXICO 3.0' - http://www.chemistry.mcmaster.ca/~bain/mexmanc.html

11 University of Manitoba, 'Spinworks 2.5.3' - http://www.umanitoba.ca/chemistry/nmr/spinworks/index.html

12 OriginLab Corporation, 'Origin 7.0 SR1' - http://www.originlab.com/

13 L. Kakaliou, W. J. Scanlon, B. X. Qian, S. W. Baek, M. R. Smith and D. H. Motry, *Inorg. Chem.*, 1999, **38**, 5964-77; M. Rahim, N. J. Taylor, S. X. Xin and S. Collins, *Organometallics*, 1998, **17**, 1315-23; E. Otten, P. Dijkstra, C. Visser, A. Meetsma and B. Hessen, *Organometallics*, 2005, **24**, 4374-86; J. C. Bailar, *J. Inorg. Nucl. Chem.*, 1958, **8**, 165; F. A. Cotton and G. Wilkinson, 'Advanced inorganic chemistry: a comprehensive text', 5th ed ed., Wiley, 1988, pp. 1323-24.

14 T. Toupance, S. R. Dubberley, N. H. Rees, B. R. Tyrrell and P. Mountford, *Organometallics*, 2002, **21**, 1367-82.

15 X. H. Bei, D. C. Swenson and R. F. Jordan, *Organometallics*, 1997, **16**, 3282-302; E. J. Crust, A. J. Clarke, R. J. Deeth, C. Morton and P. Scott, *Dalton Trans.*, 2004, 4050-58; H. M. Gau and R. C. Fay, *Inorg. Chem.*, 1990, **29**, 4974-83; T. Tsukahara, D. C. Swenson and R. F. Jordan, *Organometallics*, 1997, **16**, 3303-13.

16 E. L. Muetterties, *J. Am. Chem. Soc.*, 1968, **90**, 5097-102.

17 S. Matsui, M. Mitani, J. Saito, Y. Tohi, H. Makio, H. Tanaka and T. Fujita, *Chem. Lett.*, 1999, 1263-64; S. Matsui, Y. Tohi, M. Mitani, J. Saito, H. Makio, H. Tanaka, M. Nitabaru, T. Nakano and T. Fujita, *Chem. Lett.*, 1999, 1065-66.

18 P. D. Knight, 'Chiral at Metal Catalyst Designs for Alkene Polymerisation and Hydroamination', Ph.D. Thesis, University of Warwick, Coventry, 2003.

19 Y. Tohi, H. Makio, S. Matsui, M. Onda and T. Fujita, *Macromolecules*, 2003, **36**, 523-25; Y. Tohi, T. Nakano, H. Makio, S. Matsui, T. Fujita and T. Yamaguchi, *Macromol. Chem. Phys.*, 2004, **205**, 1179-86.

20 S. Reinartz, A. F. Mason, E. B. Lobkovsky and G. W. Coates, *Organometallics*, 2003, **22**, 2542-44.

21 J. Saito, M. Mitani, S. Matsui, Y. Tohi, H. Makio, T. Nakano, H. Tanaka, N. Kashiwa and T. Fujita, *Macromol. Chem. Phys.*, 2002, **203**, 59-65.

22 M. Atiqullah, H. Hammawa and H. Hamid, *Eur. Polym. J.*, 1998, **34**, 1511-20; J. Wu, Q. Pan and G. L. Rempel, *J. Appl. Polym. Sci.*, 2005, **96**, 645-49.

23 K. Vanka, Z. T. Xu and T. Ziegler, *Organometallics*, 2004, **23**, 2900-10; T. Ziegler, K. Vanka and Z. T. Xu, *C. R. Chim.*, 2005, **8**, 1552-65.

24 G. J. P. Britovsek, V. C. Gibson and D. F. Wass, *Angew. Chem., Int. Ed. Engl.*, 1999, **38**, 428-47.

4 p-Methoxy-substituted Salicyloxazoline Catalysts

4.1 Introduction

Given the results of Chapter 3, we returned to the basic question of what process was responsible for the deactivation of salicyl-imine catalysts. Fujita has proposed that loss of ligand to aluminium species present in the reaction mixture may be responsible,[1] and a recent study by Talsi *et al.* has directly observed this ligand-loss process in salicylaldimine catalysts possessing perfluoroaryl functionality.[2]

Fujita has reported that modification of salicylaldimine catalysts by addition of a methoxy substituent *para* to the phenoxy oxygen increased the productivity of the system at higher temperatures[3] (*q.v.* §1.3.3). Although the results show promise, the methodology employed makes it impossible to determine whether the effect of the substituent is to retard decomposition or rather to increase the underlying activity of the system. We decided to investigate the effect on the salicyloxazoline systems, using essentially the same methodology employed in Chapter 3.

4.2 Synthesis of Proligand HL15

In order to test the effect of an electron-donating substituent at the *para*-position on the phenol functionality of the salicyloxazoline catalysts, we synthesized a further ligand, H**L**^{15}, utilising the same route discussed previously (*q.v.* §3.2), *i.e.* reaction of 4-*tert*-butyl, 5-methoxysalicylic acid with 2-amino, 2-methylpropan-1-ol.

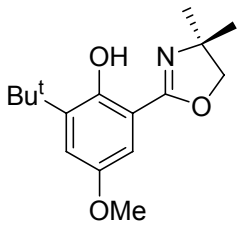

HL^{15}

Figure 4.1 - Salicyloxazoline Proligand with Electron Donor Substituent

4.3 Synthesis of Complexes of L15

The metal chloride complexes [$\mathbf{L^{15}}_2MCl_2$] (M = Ti, Zr, Hf) were synthesized by salt metathesis as described previously (*q.v.* §3.3). Complexes were purified by sublimation (at *ca.* 250 °C, 10^{-7} bar) or recrystallization from boiling toluene.

4.3.1 Structure of Complexes

^{1}H NMR spectra of the complexes [$\mathbf{L^{15}}_2MCl_2$] (M = Ti, Zr, Hf) each consist of a single set of resonances, consistent with C_2-symmetrical complexes. There is no notable line-broadening as the samples are heated to 373 K.

Despite persistent efforts, we were unable to grow crystals of any [$\mathbf{L^{15}}_2MCl_2$] complex suitable for structure determination.

4.4 High Throughput Polymerization Trials

We conducted trials of [$\mathbf{L^{15}}_2TiCl_4$] and [$\mathbf{L^{15}}_2ZrCl_4$] on the Endeavor reactor (*q.v.* §**3.7**), under the conditions shown in Table 4.1 (The titanium system was only tested under conditions 1-4).

Conditions	Temp. (°C)	Time (min)	C_2 (bar)	H_2 (bar)‡‡‡‡	Hexene (ml)
1	30	30	10	–	0.5
2	30	30	10	–	–
3	50	30	10	–	–
4	70	30	10	–	–
5	70	30	5	–	–
6	70	30	10.5	0.5	–
7	90	30	10	–	–
8	105	30	10	–	–

Table 4.1 – Conditions for HT trial of $L^{15}MCl_2$ Systems

4.4.1 Productivity

The results are shown in Table 4.2, and graphically in Figure 4.2. The productivities of the **L**[11] analogues are reproduced on that figure for ease of comparison. The systems based on **L**[15] demonstrate higher productivities than those based on **L**[14] under all conditions.

Precatalyst	Conditions	Catalyst Load (μmol)	Yield [a] (g)	Productivity (kg mol^{-1} bar^{-1} h^{-1})
[$\mathbf{L}^{15}_2TiCl_2$]	1	1.0	0.188	3.8×10^1
[$\mathbf{L}^{15}_2TiCl_2$]	2	1.0	0.453	9.1×10^1
[$\mathbf{L}^{15}_2TiCl_2$]	3	1.0	0.398	8.0×10^1
[$\mathbf{L}^{15}_2TiCl_2$]	4	1.0	0.305	6.1×10^1
[$\mathbf{L}^{15}_2ZrCl_2$]	1	0.1	0.484	9.7×10^2
[$\mathbf{L}^{15}_2ZrCl_2$]	2	0.1	0.559	1.1×10^3
[$\mathbf{L}^{15}_2ZrCl_2$]	3	0.1	0.428	8.6×10^2
[$\mathbf{L}^{15}_2ZrCl_2$]	4	0.1	0.238	4.8×10^2
[$\mathbf{L}^{15}_2ZrCl_2$]	5	0.1	0.068	2.7×10^2
[$\mathbf{L}^{15}_2ZrCl_2$]	6	0.1	0.173	3.5×10^2
[$\mathbf{L}^{15}_2ZrCl_2$]	7	0.1	0.286	5.7×10^2
[$\mathbf{L}^{15}_2ZrCl_2$]	8	0.1	0.100	2.0×10^2

[a] Assuming all MAO is converted to Al_2O_3

Table 4.2 – Productivity Results from HT trial of $L^{15}MCl_2$ Systems

‡‡‡‡ The Endeavor system pressurises the reactor to the desired pressure of hydrogen, then adds ethene to the desired total pressure. The partial pressure of H_2 is not maintained during the run. Thus, if the polymerization is consuming hydrogen, the gas composition will vary through the run.

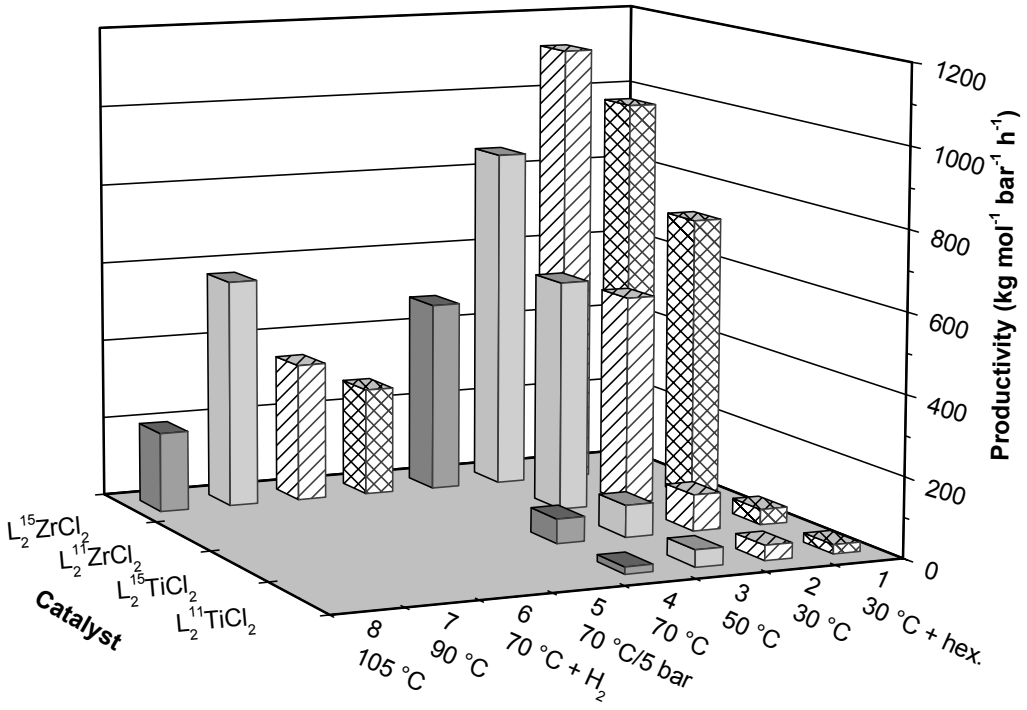

Figure 4.2 - Graph to show productivities from HT trial of L^{15} systems. L^{11} systems shown for comparison

4.4.2 Hexene Incorporation

We were again unable to perform IR analysis of the polymers produced, to determine hexene incorporation. We were, however, able to determine the melting properties of the polymers produced by [$\mathbf{L^{15}}ZrCl_2$] under conditions 1 and 2, *i.e.* at 30 °C, with and without hexene present in the system (Table 4.3). There is a small difference in the melting points of the two polymers, but this alone is insufficient evidence for incorporation of hexene.

Precatalyst	Conditions	T_m (°C)	ΔH_m (J/g)
[$\mathbf{L^{15}}_2TiCl_2$]	1	134.46	201.25
[$\mathbf{L^{15}}_2TiCl_2$]	2	137.76	212.16

Table 4.3 – Polymer Characterization from HT trial

4.4.3 Polymer Characterization

The polymers produced were analysed by GPC; the results are shown in Table 4.4.

Precatalyst	Conditions	M_n (u)	M_w (u)	Modality	PDi
[$\mathbf{L^{15}}_2TiCl_2$]	1[a]	–	–	–	–
[$\mathbf{L^{15}}_2TiCl_2$]	2[b]	569,900	1,963,000	1	3.4
[$\mathbf{L^{15}}_2TiCl_2$]	3	132,500	502,300	1	3.8
[$\mathbf{L^{15}}_2TiCl_2$]	4[a]	–	–	–	–
[$\mathbf{L^{15}}_2ZrCl_2$]	1	7,000	54,300	1	7.8
[$\mathbf{L^{15}}_2ZrCl_2$]	2	19,900	136,600	1	6.9
[$\mathbf{L^{15}}_2ZrCl_2$]	3	5,200	98,900	2	(19.2)
[$\mathbf{L^{15}}_2ZrCl_2$]	4	17,300	53,200	1	3.1
[$\mathbf{L^{15}}_2ZrCl_2$]	5	4,100	49,500	2	(12.2)
[$\mathbf{L^{15}}_2ZrCl_2$]	6	2,200	23,200	2	(10.4)
[$\mathbf{L^{15}}_2ZrCl_2$]	7[a]	–	–	–	–
[$\mathbf{L^{15}}_2ZrCl_2$]	8[a]	–	–	–	–

[a] Sample unsuitable for GPC analysis
[b] MWt exceeds calibrated range for this GPC system.

Table 4.4 – Polymer Characterization from HT trial

4.4.3.1 Titanium System

The MWDs for [$\mathbf{L^{15}}TiCl_2$] are shown in Figure 4.3. The polymer has a higher molecular weight than is observed for the comparable $\mathbf{L^{14}}$ and $\mathbf{L^{11}}$ systems under the same conditions, and the PDi is also higher. Whereas the MWD produced by [$\mathbf{L^{11}}TiCl_2$] at 50 °C is clearly bimodal, the $\mathbf{L^{15}}$ species produces a less clear distribution. There appears to be a shoulder on the main mode, and a tail to low MWt.

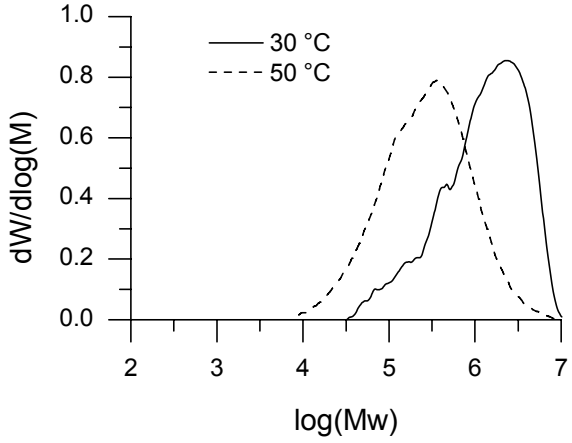

Figure 4.3 – MWDs for [$\mathbf{L^{15}}_2TiCl_2$] in HT trial

4.4.3.2 Zirconium System

The MWDs for [$\mathbf{L^{15}}ZrCl_2$] are shown in Figure 4.4. In comparison with the $\mathbf{L^{11}}$ and $\mathbf{L^{14}}$ analogues, this system produces higher MWt polymer. The response to change of temperature is also dissimilar. At 30 °C, a broad unimodal distribution is evident, with a tail to low MWt. At 50 °C, the distribution is bimodal, but at 70 °C the distribution is unimodal with a lower PDi (3.1, *vs.* 6.9 at 30 °C).

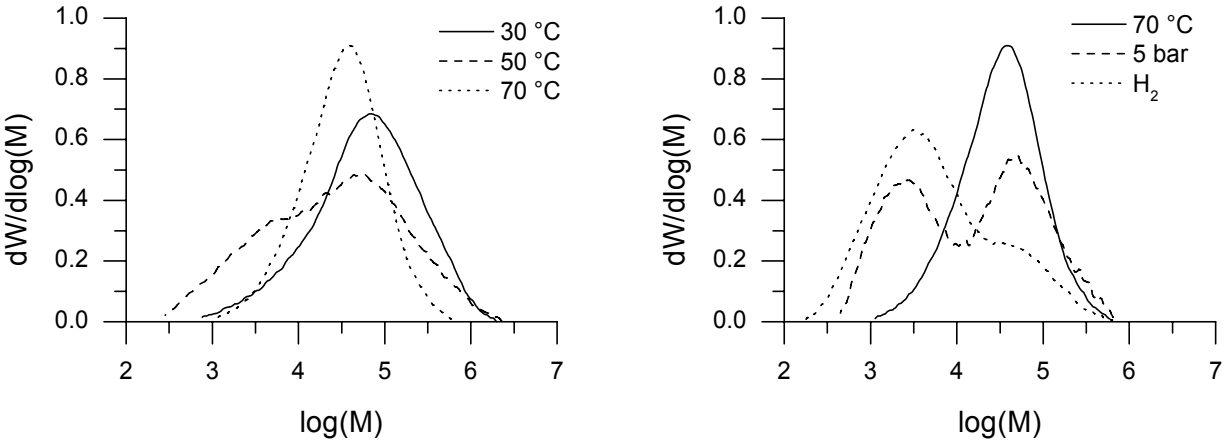

Figure 4.4 - MWDs for [$\mathbf{L^{15}}_2ZrCl_2$] in HT trial, varying temperature (l) and variation of gas mixture (r)

Variation of the gas mixture similarly has a clear effect on the MWD of the polymers produced. Reduction of the ethene pressure to 5 bar results in a bimodal distribution, with the higher MWt slightly favoured, whereas addition of H_2 results in a bimodal distribution with the lower molecular weight favoured.

There appear to be at least two distinct modes of polymerization occurring, and variations in the reaction conditions vary the proportion of the product polymer in each mode.

4.5 Reaction Profiles

We measured the catalytic profiles of these catalysts using the same methodology discussed previously (*c.f.* §2.3.1.2).

[**L$^{15}_2$**TiCl$_2$] shows good stability at 25 °C ($\tau_{½}$ = 3950 s), and less stability at 50 °C ($\tau_{½}$ = 2890 s). Similarly to the salicylaldimine [**L$^{14}_2$**TiCl$_2$], this catalyst shows higher activity at elevated temperature.

[**L$^{15}_2$**ZrCl$_2$] demonstrates fair stability at 25 °C ($\tau_{½}$ = 2280 s), and somewhat lower stability at 50 °C ($\tau_{½}$ = 1490 s).

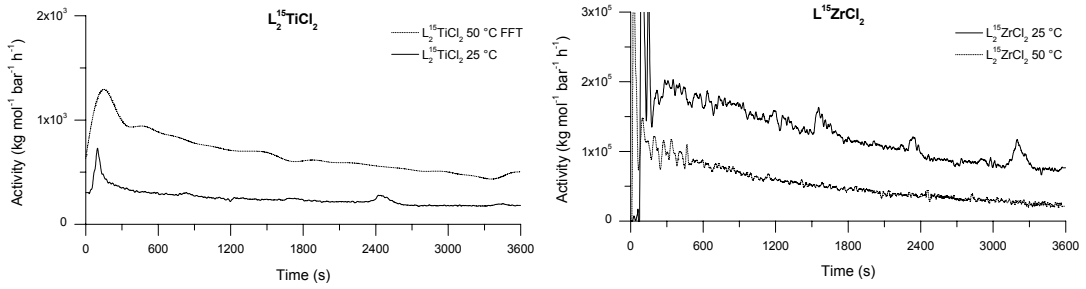

Figure 4.5 - Reaction profiles for [L^{15}MCl$_2$]

4.5.1 Productivity/Activity Measurements and Polymer Characterization

4.5.1.1 Least Squares Fitting

The reaction profile data were analysed numerically using the same methodology as discussed previously (*q.v.* §3.8.5.1), and the results are shown below (Table 4.5).

Precatalyst	Temp. (°C)	Data start (s)	y_0[a]	x_0	A	t_1	r^2	$\tau_{½}$
[L^{15}TiCl$_2$]	25	250	[0]	0	3.33 × 10^2	5180	0.860	3590
[L^{15}TiCl$_2$]	50	300	[0]	0	9.92 × 10^2	4170	0.966	2890
[L^{15}ZrCl$_2$]	25	300	[0]	0	2.10 × 10^5	3280	0.941	2280
[L^{15}ZrCl$_2$]	50	150	[0]	0	1.09 × 10^5	2150	0.958	1490

[a] y_0 and A have units kg mol^{-1} bar^{-1} h^{-1}, x_0, t_1 and $\tau_{½}$ have units s

Table 4.5 - Least-squares fitting results for activity profiles for [L$^{15}_2$MCl$_2$]

4.5.1.2 Productivity

The detail of the reactions conducted is shown in Table 4.6, including the results of polymer characterization by GPC.

Precatalyst	Temp. (°C)	Catalyst (mol)	Yield (g)	Productivity$_{60}$ (kg mol^{-1} bar^{-1} h^{-1})	M_n (u)	M_w (u)	PDi
[**L**$^{15}_2$TiCl$_2$]	25	1.4 × 10^{-5}	4.20	2.57 × 10^2	420,000	719,000	1.7
[**L**$^{15}_2$TiCl$_2$]	50	1.5 × 10^{-6}	1.30	7.24 × 10^2	321,000	595,000	1.9
[**L**$^{15}_2$ZrCl$_2$]	25	1.4 × 10^{-8}	2.64	1.57 × 10^5	95,600	423,000	(4.4)[a]
[**L**$^{15}_2$ZrCl$_2$]	50	1.4 × 10^{-8}	0.89	5.27 × 10^4	4,960	80,600	(16.3)[a]

[a] Multimodal MWt distribution observed.

Table 4.6 - Results from activity profiling reactions for [L$^{15}_2$MCl$_2$]§§§§

4.5.1.3 Polymer Characterization

The MWDs obtained are shown graphically in Figure 4.6, in comparison to the equivalent distributions obtained from the HT experiments. It can be seen that there is a much closer correlation between the two sets of data than was the case for the catalysts based on **L**^{11} and **L**^{14} discussed previously (*c.f.* §3.9.2).

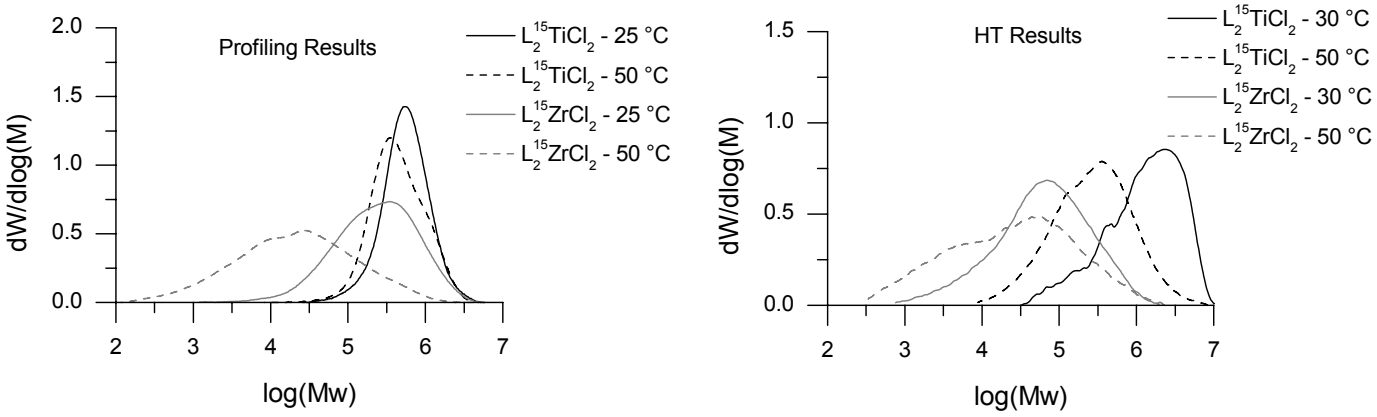

Figure 4.6 - MWDs from profiling reactions (l) in comparison to MWDs from HT Trial (r)

§§§§ Conditions: 100 ml toluene inc. 5 ml 10% w/v MAO/toluene solution, 1.2 bar C_2,1 h

4.6 Industrially Relevant Conditions

As a further test of the catalytic behaviour, we tested ethene polymerization with [$\mathbf{L^{15}}_2ZrCl_2$] and [$\mathbf{L^{11}}_2ZrCl_2$] in a 5 L autoclave reactor,[*****] with the assistance of Dr Stefan Spitzmesser (Innovene). The reaction involving [$\mathbf{L^{11}}_2ZrCl_2$] was stopped after 30 min as no further ethene uptake was measured.

The summarized reaction details are given in Table 4.7, and the ethene uptake profile in Figure 4.7. The products were characterized by GPC, and the MWD plots are shown in Figure 4.8.

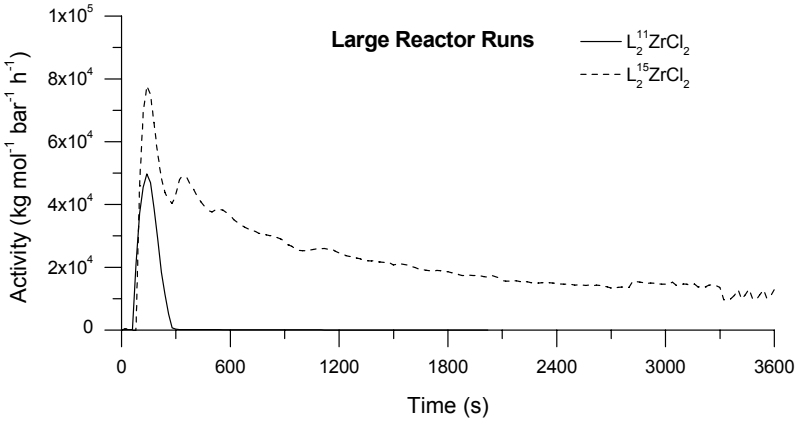

Figure 4.7 – Reaction profiles from large reactor trial of [$\mathbf{L^{11,15}}_2ZrCl_2$]

Precatalyst	Temp (°C)	Time (min)	Catalyst (mol)	Yield (g)	Productivity (kg mol^{-1} bar^{-1} h^{-1})	M_n (u)	M_w (u)	PDi
[$\mathbf{L^{11}}_2ZrCl_2$]	80	30	2.0×10^{-6}	22	4.40×10^3	8,900	214,000	(24.06)[a]
[$\mathbf{L^{15}}_2ZrCl_2$]	80	60	2.0×10^{-6}	414	4.14×10^4	122,000	745,000	6.11

[a] Multimodal MWt distribution observed.

Table 4.7 - Results from large reactor trial of [$\mathbf{L^{11,15}}_2ZrCl_2$]

[*****] Conditions: 1.8 L isobutane, 2.0 µmol catalyst, 1000 eq. MAO, 10 bar C_2, 30 min (L^{11}), 60 min (L^{15}), 80 °C

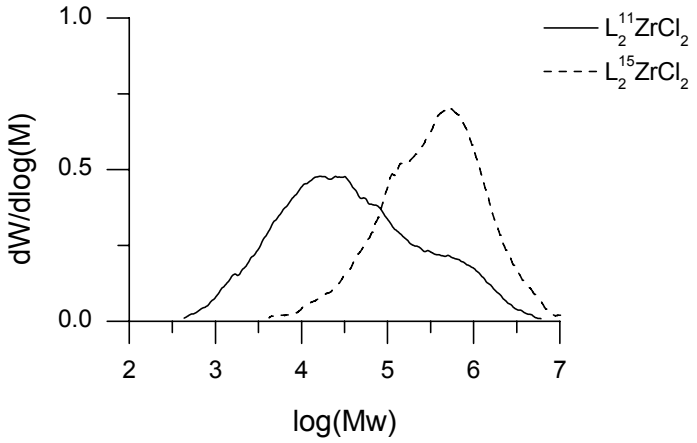

Figure 4.8 - MWDs from large reactor trial

The reactions under these conditions corroborate the results obtained using our gas pressure burette, as well as those obtained during the high-throughput tests. Although quantitative comparisons are of limited use due to the different conditions, it is clear that the main features are similar; [$\mathbf{L^{11}}_2ZrCl_2$] is rapidly deactivated whereas [$\mathbf{L^{15}}_2ZrCl_2$] shows greater stability and produces material with higher MWt. Under these conditions, the molecular weights of the products of both catalyst systems are somewhat higher than when tested in our gas pressure burette and in the Endeavor reactor.

4.7 Propene Polymerization

The [$\mathbf{L^{15}}_2MCl_2$] (M = Ti, Zr) catalysts were active toward polymerization of propene.* The titanium species produced poly(propene) with an activity of 0.87 kg mol^{-1} bar^{-1} h^{-1}. Comparison of the ^{13}C NMR spectrum of the polymer product with reported data for salicylaldimine products[4] suggests that the product is syndiotactic-enriched, but that it demonstrates a significant degree of

* Conditions: 95 ml heptane, 5 ml 10%w/v MAO/toluene solution, 5 bar C_3, 2 h (Ti), 3 h (Zr)

regioinversion. The product was characterized by GPC (M_n = 20,300 u, M_w = 167,000 u, PDi = 8.2); the MWD appears to be predominantly one mode, with shoulders to high and low MWt.

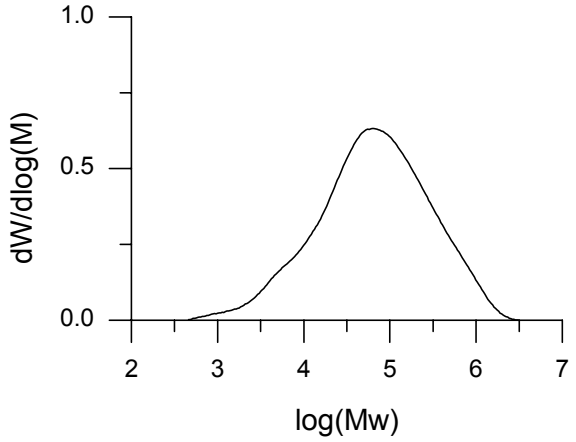

Figure 4.9 - MWD of poly(propene) produced by [$L^{15}_2TiCl_2$]

The zirconium based catalyst was found to produce oligomers with an activity of 4.8 kg mol^{-1} bar^{-1} h^{-1}. The molecular weight was too low for GPC analysis, but NMR analysis suggests a degree of polymerization of about 18 (*i.e.* M_n around 800).

The productivity of the titanium systems for propene polymerization is somewhat lower than the reported productivities of titanium salicylaldimine catalysts,[5] which are typically in the region of 2 – 6 kg mol^{-1} bar^{-1} h^{-1}. Productivities were reported to increase somewhat when the steric bulk *ortho* to the phenoxy donor was reduced, giving productivities in the range 30 – 70 kg mol^{-1} bar^{-1} h^{-1}. Propene polymerization was not reported for the salicylaldimine catalysts incorporating a methoxy moiety.

4.8 Effect of Methoxy Substitution on Catalytic Behaviour

4.8.1 Stability

The methoxy-substituted catalysts utilizing **L^{15}** show enhanced stability in comparison to the *tert*-butyl substituted species utilizing **L^{11}**.

Ligand	Ti (25 °C)	Zr (25 °C)	Ti (50 °C)	Zr (50 °C)
L^{11}	4060	930	2340	50
L^{15}	3590	2280	2890	1490

Table 4.8 - Comparison of half lives (s) of L^{11} and L^{15} catalysts

For the titanium species, the stability at 25 and 50 °C is similar between **L^{11}** and **L^{15}** catalysts. Both titanium catalysts can reasonably be described as long lived at both temperatures.

The effect is more dramatic on the zirconium species however - the deactivation of [**L^{11}**$ZrCl_2$] (which is rapid at 25 °C and almost immediate at 50 °C) is significantly retarded by the OMe substitution.

4.8.2 Activity

The **L^{15}** catalysts demonstrate initial activities (from linear regression analysis) which are approximately double the initial activities of the **L^{15}** species Table 4.9).

Ligand	Ti (25 °C)	Zr (25 °C)	Ti (50 °C)	Zr (50 °C)
L^{11}	1.70×10^2	1.15×10^5	2.63×10^2	6.23×10^4
L^{15}	3.33×10^2	2.10×10^5	9.92×10^2	1.09×10^5

Table 4.9 – Comparison of initial activities (kg mol^{-1} bar^{-1} h^{-1})

of L^{11} and L^{15} catalysts

4.8.3 Polymer Properties

The polymers produced by the catalysts utilizing **L^{15}** have significantly higher MWt than those produced by **L^{11}** catalysts.

Ligand	Ti (25 °C)	Zr (25 °C)	Ti (50 °C)	Zr (50 °C)
L^{11}	88,500 (1.8)	1,900 (5.0[a])	129,000 (1.3)	510 (1.5)
L^{15}	420,000 (1.7)	95,600 (4.4[a])	321,000 (1.9)	4,960 (16.3[a])

[a] Multimodal MWt distribution observed

Table 4.10 – Comparison of product M_n from L^{11} and L^{15} catalysts

(all units are u, PDi in brackets)

It is interesting that the zirconium systems using L^{15} have higher M_n values, but also higher polydispersity (Figure 4.10); the distribution has been *extended* into the higher MWt region, rather than being *displaced* there.

There appear to be two modes present in the product, but both have higher molecular weights than the modes present in the product of the L^{11} catalyst.

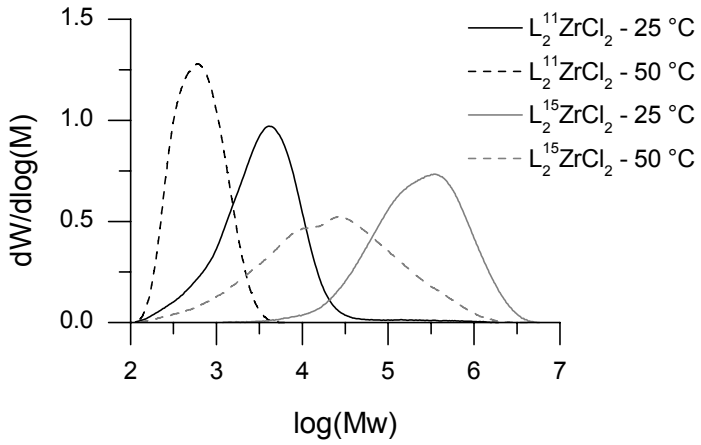

Figure 4.10 - Comparison of L^{11} and L^{14} zirconium catalysts

Thus, methoxy-substitution of the phenoxy donor affects not only the deactivation mechanism during the polymerization, but also the chain transfer or termination mechanisms.

4.9 Summary and Conclusions

A modification to the ligand system presented in Chapter 3, which is proposed to strengthen the bond between phenoxy-oxygen and metal centre, resulted in

significant improvements in stability of the catalysis at 50 °C, leading to the conclusion that the primary deactivation mechanism is not 1,2-migratory insertion to the imine bond, but is more likely to be loss of ligand from the catalyst to aluminium species present in the polymerization.

Those catalysts based on zirconium are extremely active for the polymerization of ethene, and moderately productive for the oligomerization of propene, whereas those based on titanium are highly active for the polymerization of ethene, and active for the polymerization of propene, producing syndiotactic-enriched PP with moderate productivity.

In light of the mixtures of isomers observed for some of the catalysts presented here and in Chapter 3, and in order to investigate the possible nature of the active species, we decided to attempt to investigate the nature of that species directly, and this work is discussed in Chapter 5.

4.10 References for Chapter 4

1 H. Makio and T. Fujita, *Macromol. Symp.*, 2004, **213**, 221-33.

2 K. P. Bryliakov, E. A. Kravtsov, D. A. Pennington, S. J. Lancaster, M. Bochmann, H. H. Brintzinger and E. P. Talsi, *Organometallics*, 2005, **24**, 5660-64.

3 N. Matsukawa, S. Matsui, M. Mitani, J. Saito, K. Tsuru, N. Kashiwa and T. Fujita, *J. Mol. Catal. A: Chem.*, 2001, **169**, 99-104.

4 M. Mitani, R. Furuyama, J. Mohri, J. Saito, S. Ishii, T. Terao, T. Nakano, H. Tanaka and T. Fujita, *J. Am. Chem. Soc.*, 2003, **125**, 4293-305.

5 R. Furuyama, J. Saito, S. Ishii, H. Makio, M. Mitani, H. Tanaka and T. Fujita, *J. Organomet. Chem.*, 2005, **690**, 4398-413.

5 Structure and Activation of Imine Catalysts

5.1 Introduction

Metallocene and post-metallocene catalyst systems are primarily differentiated from the older Ziegler-Natta technologies by having well-defined active sites, and therefore studies into the nature of the active sites of such species are of great interest.[1-3] The catalytically-active species are generally believed to be coordinatively unsaturated alkyl cation species (*vide infra*). There are several possible ways to form such species; the method most commonly applied during polymerization reactions is the treatment of a metal halide with MAO, which alkylates and ionizes the metal centre. MAO is typically present in significant excess, and its structure is poorly understood and probably poorly-defined.[4-7] This precludes unequivocal structural assignment of cations formed with it, although spectroscopic techniques have recently been used to investigate such species with some success.[8,9]

As an alternative to MAO, the most commonly employed reagents are the various non-coordinating perfluoryarylborane and perfluoroarylborate species.[1,10] The most commonly employed are $B(C_6F_5)_3$, $[PhNMe_2H][B(C_6F_5)_4]$ and $[CPh_3][B(C_6F_5)_4]$, which are capable of abstracting metal-bound alkyl species. In order to use such activators with metal chloride complexes, the complex is treated with an alkylating agent such as triisobutylaluminium.

5.2 Synthesis of Metal Benzyl Complexes

We synthesized the metal benzyl species $[\mathbf{L}^n{}_2M(CH_2Ph)_2]$ (n = 10-12,15, M = Zr, Hf) by protonolysis between the proligand HL^n with $[M(CH_2Ph)_4]$ in toluene, pentane or diethyl ether, with the exclusion of light. The products were isolated by

recrystallization from pentane. The low yields represent difficulties in isolating the product rather than a low conversion; mixing ligand with metal precursor in a young's-tap NMR tube led to 100% conversion. Attempts to form the titanium benzyl species yielded intractable mixtures.

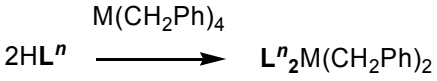

Figure 5.1 – Protonolysis synthesis of metal benzyl complexes

	L^{10}	L^{11}	L^{12}	L^{15}
Zr	44%	27%	26%	31%
Hf	52%	30%	32%	37%

Table 5.1 – Isolated yields of [L^nM($CH_2Ph)_2$] complexes

5.2.1 Molecular Structures of [$L_2Hf(CH_2Ph)_2$] complexes

The molecular structures of [$\mathbf{L^{10}}Hf(CH_2Ph)_2$] and [$\mathbf{L^{12}}Hf(CH_2Ph)_2$] were determined by single-crystal X-ray diffractometry, and are shown in Figure 5.2. Both compounds have adopted C_2-symmetric *trans,cis,cis*-geometries (*i.e.* the oxygen atoms are mutually *trans*). There are only minor differences between the structures of these two compounds, despite the significant reduction in steric bulk around the phenolate functionality in the $\mathbf{L^{12}}$ species.

As far as we are aware, these are the first reported [L_2HfX_2] (L = N,O-donor, X = halide or alkyl) structures, although the structure of the alkyl cation of a closely related species has been previously presented,[11] and these structures are unremarkable compared to this.

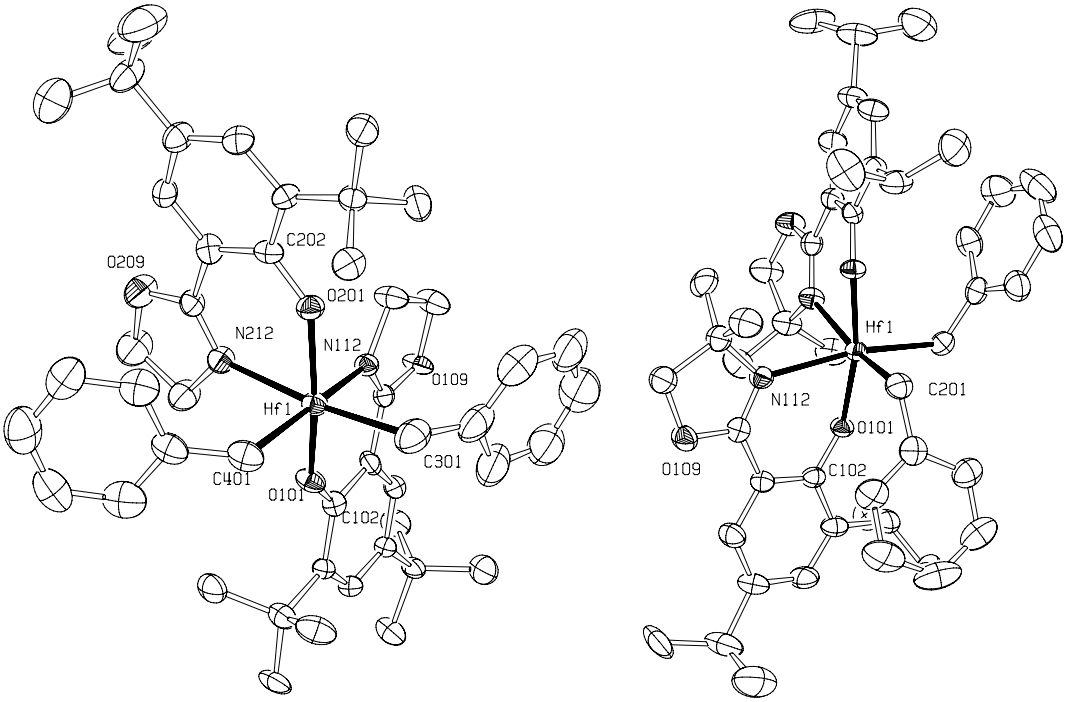

$[L^{10}{}_2Hf(CH_2Ph)_2]$ **$[L^{12}{}_2Hf(CH_2Ph)_2]$**

Figure 5.2 - Molecular structures of $[L^{10}{}_2Hf(CH_2Ph)_2]$ and $[L^{12}{}_2Hf(CH_2Ph)_2]$ (Hydrogen atoms omitted for clarity). Probability ellipsoids are set to the 50% level

$[L^{10}{}_2Hf(CH_2Ph)_2]$		$[L^{12}{}_2Hf(CH_2Ph)_2]^a$	
Bond	**Length (Å)**	**Bond**	**Length (Å)**
Hf(1)-O(101)	2.013(3)	Hf(1)-O(101)	2.003(2)
Hf(1)-O(201)	2.005(3)		
Hf(1)-N(112)	2.300(4)	Hf(1)-N(112)	2.351(3)
Hf(1)-N(212)	2.336(4)		
Hf(1)-C(301)	2.279(6)	Hf(1)-C(201)	2.272(4)
Hf(1)-C(401)	2.272(5)		
Bonds	**Angle (°)**	**Bonds**	**Angle (°)**
O(201)-Hf(1)-O(101)	159.64(13)	O(101)#1-Hf(1)-O(101)	168.03(14)
O(101)-Hf(1)-N(112)	76.35(14)	O(101)-Hf(1)-N(112)	77.25(11)
O(201)-Hf(1)-N(212)	76.21(14)	O(101)-Hf(1)-N(112)#1	94.11(11)
C(301)-Hf(1)-N(212)	173.4(2)	C(201)-Hf(1)-N(112)#1	167.31(14)
N(112)-Hf(1)-N(212)	82.72(14)	N(112)#1-Hf(1)-N(112)	88.70(16)
C(401)-Hf(1)-C(301)	92.4(2)	C(201)#1-Hf(1)-C(201)	93.3(2)
O(101)-Hf(1)-N(212)	88.39(14)		
C(102)-O(101)-Hf(1)	145.1(3)	C(102)-O(101)-Hf(1)	141.5(3)
C(202)-O(201)-Hf(1)	144.2(3)		

[a] Structure has crystallographic C_2 symmetry

Table 5.2 - Selected bond angles and lengths for $[L^{10}{}_2Hf(CH_2Ph)_2]$ and $[L^{12}{}_2Hf(CH_2Ph)_2]$

5.3 Cation Synthesis and Stability

5.3.1 Ionization Using Perfluoroarylboron Compounds

We attempted to form the alkyl cations $[\mathbf{L}^{n}{}_2Zr(CH_2Ph)]^+$ (n = 11,15) by reaction of $[\mathbf{L}^{n}{}_2Zr(CH_2Ph)_2]$ with $B(C_6F_5)_3$ or $[PhNMe_2H][B(C_6F_5)_4]$ in d_5-bromobenzene in Young's tap NMR tubes.

Reactions of both complexes with $B(C_6F_5)_3$ lead to products with complicated ^1H NMR spectra suggestive of rapid decomposition. We repeated the reaction of $[\mathbf{L}^{11}{}_2Zr(CH_2Ph)_2]$ with $B(C_6F_5)_3$ at -78 °C by distilling d_2-dichloromethane onto the mixed solids, and transferring the NMR tube to the spectrometer at this temperature, but extensive decomposition was apparent immediately.

Reaction of $[\mathbf{L}^{11}{}_2Zr(CH_2Ph)_2]$ with $[PhNMe_2H][B(C_6F_5)_4]$ in CD_5Br led to the production of a major component with ^1H NMR signals consistent with the formation of an alkyl cation (Figure 5.3). The system is chiral, and the single CH_2Ph group gives rise to a pair of AB doublets around 2.9 and 3.1 ppm. The oxazoline CH_2 groups give a similar signal at 3.6 ppm, with matching Me signals at 0.7 and 1.1 ppm. The aromatic CH resonances from L^{11} appear at 7.81 and 7.87 ppm. This spectrum is consistent with a five-coordinate species $[L^{11}{}_2Zr(CH_2Ph)][B(C_6F_5)_4]$; the presence of an additional ligand such as $PhNMe_2$ would lead to inequivalence of the two L^{11} ligands.

A minor unsymmetrical species is also present (see doublet signals in aromatic region, and overlapping signals 3.7-4.2 ppm). Notably, no corresponding zirconium CH_2Ph signal was detected; perhaps the alkyl cation decomposes *via* loss of a benzyl radical[12] or α-elimination. The mixture gradually decomposed further over a period of hours. Upon standing for several days, the mixture became a deep blue colour.

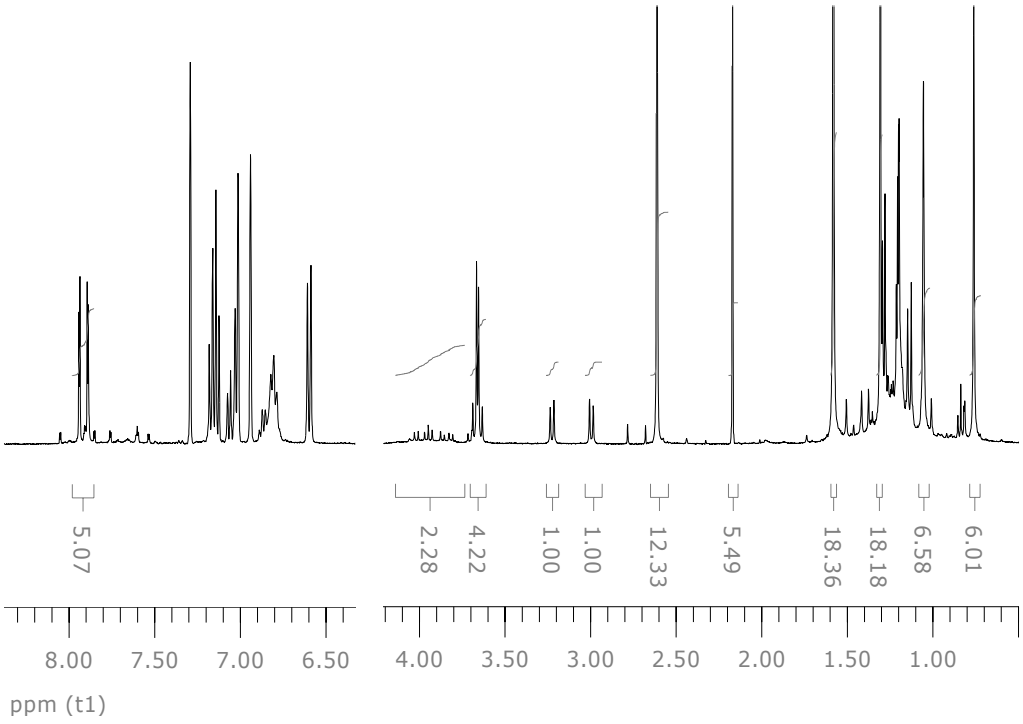

Figure 5.3 - Aryl and alkyl regions of ^{1}H NMR spectrum of [L$^{11}_2$Zr(CH$_2$Ph)]$^+$

Reaction of [**L**$^{15}_2$Zr(CH$_2$Ph)$_2$] with [PhNMe$_2$H][B(C$_6$F$_5$)$_4$] gave a product with a ^{1}H NMR spectrum consistent with an alkyl cation; only this time the product was relatively clean. The alkyl region is shown in Figure 5.4, the aromatic region is complicated by overlapping signals. The very sharp singlet marked * is not consistent with any part of the expected cation spectrum. After standing for 48 h, a fine colourless precipitate had formed, and the integrals of the peaks assigned to the cation reduced to 30% of their original values (in comparison to the integral of the residual solvent protium signals), and the integral of the unidentified peak (*) grew to 4 times its original value.

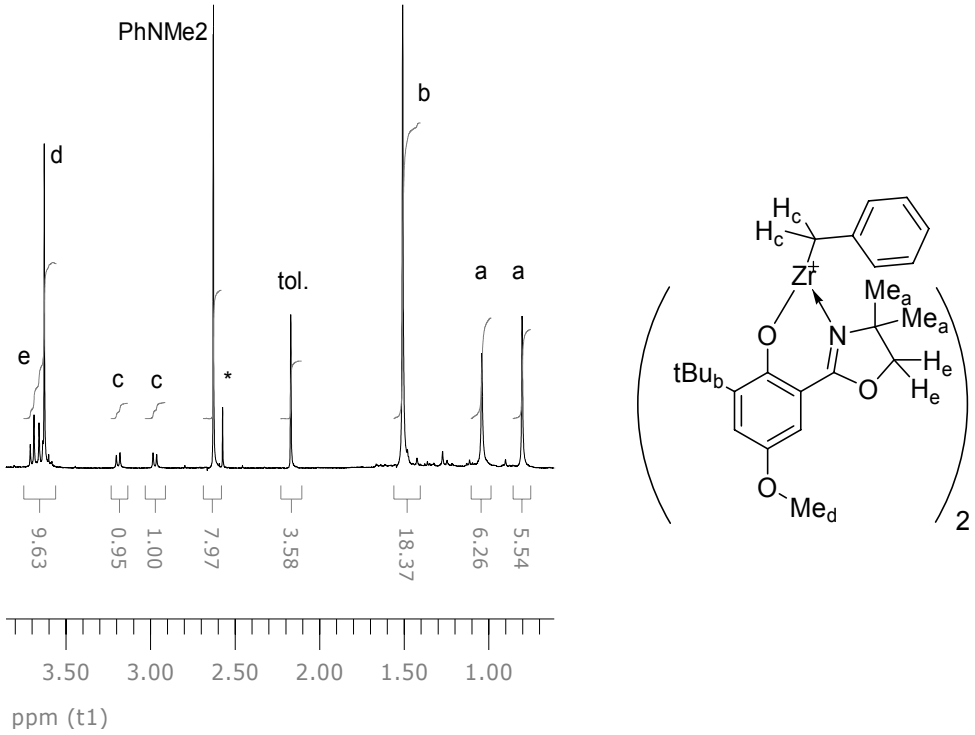

Figure 5.4 - Alkyl region of ^{1}H NMR spectrum of $[L^{15}_2Zr(CH_2Ph)]^+$

5.3.2 Ionization using MAO

Whilst studies using stoichiometric borate species as ionizers/counterions may be informative as to nature of a cationic species, ultimately studies using the same agents as in a polymerization reaction (*i.e.* MAO) should be more relevant, especially since the method of decomposition is of interest.

Makio and Fujita,[13] and a more recently Talsi *et al.*[8] have investigated the reaction of the perfluorinated titanium salicylaldimine complex [$\mathbf{L}_2TiCl_2$] [H**L** = 2-*tert*-butyl-6-{(perfluorophenylimino)methyl}phenol] with MAO, utilizing NMR spectroscopy. The latter study confirms that the salicylaldimine was decomposed to $LAlMe_2$ with $\tau_{½}$ around 1 h.

We investigated the species [$\mathbf{L}^n_2MCl_2$] (n = 11,15, M = Ti, Zr) by direct reaction with TMA-depleted MAO in d_5-bromobenzene, in Young's tap NMR tubes.

For comparison, we also synthesized [$\mathbf{L}^n$AlMe$_2$] (n = 11,15) compounds by reaction of H$\mathbf{L}^n$ with TMA (20 eq.) in d_5-bromobenzene. A range of [**L**AlMe$_2$] (**L** = imine or salicylaldimine ligand) complexes have been previously synthesized using a similar route.[14]

5.3.2.1 [$\mathbf{L}^{11}{}_2$MCl$_2$]

Upon treatment of the $\mathbf{L}^{11}$ complexes (Figure 5.5, A, Ti is similar) with MAO, multiple unidentified species are initially generated (B). After standing for 24 h, [$\mathbf{L}^{11}{}_2$MCl$_2$] is completely converted to $\mathbf{L}^{11}$AlMe$_2$ (C, D). The fate of the metal is unclear.

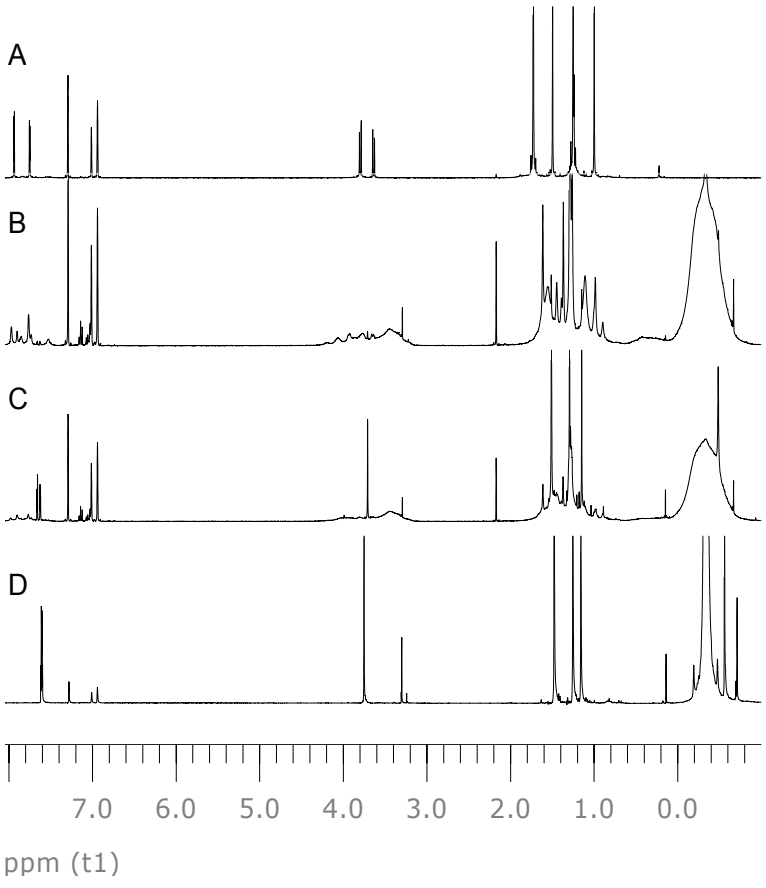

Figure 5.5 - ^{1}H NMR spectra of A: [$\mathbf{L}^{11}{}_2$ZrCl$_2$], B: [$\mathbf{L}^{11}{}_2$ZrCl$_2$] + MAO, C: [$\mathbf{L}^{11}{}_2$ZrCl$_2$] + MAO + 24 h, D: H$\mathbf{L}^{11}$ + TMA

The multiple signals generated initially may represent a mixture of the various possible isomers. Such mixtures of isomers in salicylaldimine catalyst have been proposed to be responsible for forming multimodal poly(ethene).[15]

5.3.2.2 [$L^{15}_2MCl_2$]

The **L**^{15} complexes demonstrate different behaviour, immediately forming a new species, consistent with a reaction with MAO to form [$L^{15}_2M(Me)]^+$[$Me(MAO)]^-$, but not with formation of **L**$^{15}AlMe_2$. The ^1H NMR spectrum of the zirconium species is shown in Figure 5.6 (B) (The sharp singlet at ~3.6 ppm is caused by the OMe protons). This species has an element of chirality, as the oxazoline CH_2 protons still appear as an AB doublet (around 3.6 and 3.8 ppm), and the C(CH_3)$_2$ signals are two singlets (at around 1.0 and 1.5 ppm). In the spectrum of [**L**$^{15}AlMe_2$] (C) this element of chirality is not present. The spectrum of the mixture of [**L**$^{15}_2ZrCl_2$] with MAO was unchanged after standing for 48 h at room temperature.

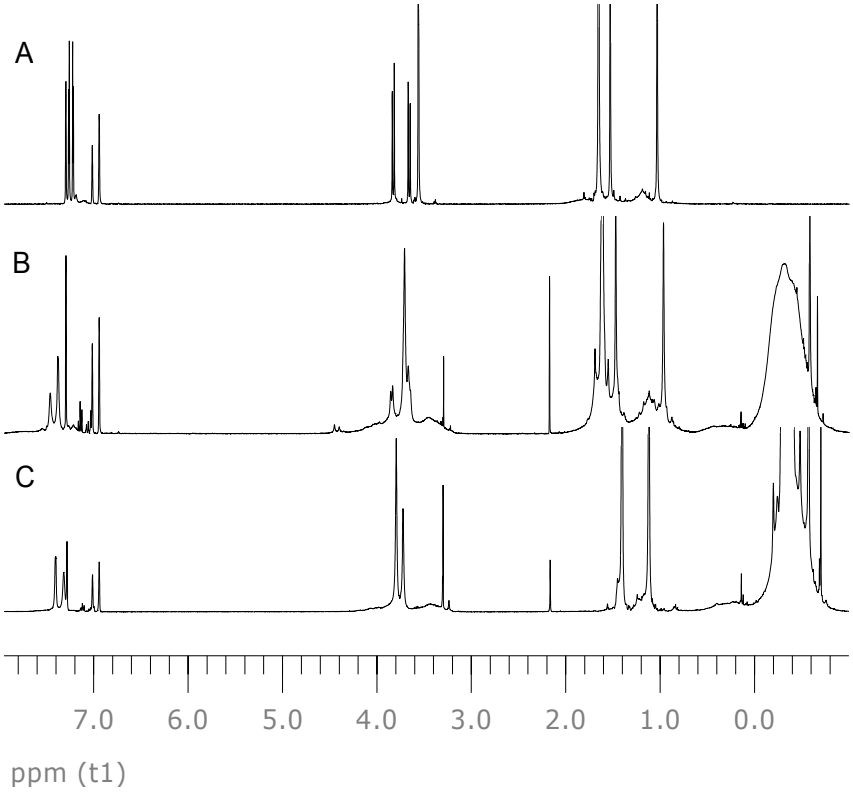

Figure 5.6 – ^{1}H NMR spectra of A: [$L^{15}_2ZrCl_2$], B: [$L^{15}_2ZrCl_2$] + MAO, C: HL^{15} + TMA + MAO

5.3.3 Conclusions from Cation Studies

These results offer direct evidence that the effect of the methoxy substituent on **L^{15}** is to prevent loss of ligand from the complex to aluminium. Whereas [$\mathbf{L}^{11}_2ZrCl_2$] forms a mixture of species on treatment with MAO, the methoxy-substituted **L^{15}** analogue appears to form just one. The **L^{11}** species is converted to [$\mathbf{L}^{11}AlMe_2$] over ~24 h at room temperature, whereas the **L^{15}** analogue shows no conversion.

Reactions of [$PhNMe_2H$][$B(C_6F_5)_4$] with [$\mathbf{L}^{n}_2Zr(CH_2Ph)_2$] ($n$ = 11,15) yield products with a ^{1}H NMR spectra consistent with alkyl cations. The **L^{15}** cation is relatively stable, but the **L^{11}** analogue appears to suffer some other decomposition mechanism in the absence of aluminium, leading to unsymmetrical species which go on to decay further. The methoxy-substituted catalyst does not appear to decompose *via* this pathway; rather the cations formed slowly decompose to species

which are not detected by NMR spectroscopy (this may simply be due to precipitation, or, in the case of titanium, reduction to the 3^+ state.[8]).

5.4 Modelling Catalyst Species

5.4.1 Isomeric Nature

With Dr Stefan Spitzmesser at Innovene, we have calculated ΔE_f for the precatalysts [$\mathbf{L^{11}}_2ZrCl_2$] and [$\mathbf{L^{15}}_2ZrCl_2$] using DFT* (Density Functional Theory); the relative energies of the various *cis*-Cl isomers are shown in Figure 5.7, and the structures themselves in Figure 5.8.

	$\mathbf{L^{11}}_2\mathbf{ZrCl_2}$	$\mathbf{L^{15}}_2\mathbf{ZrCl_2}$
Cis,cis,trans	1.3	-10.9
Cis,cis,cis	3.3	-2.3
Cis,trans,cis	0.0	0.0

All units are kJ mol^{-1}

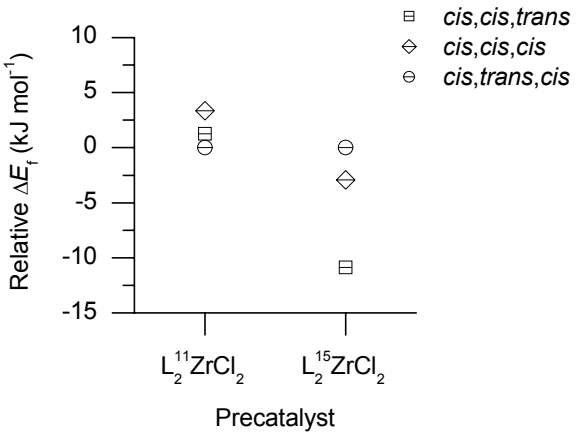

Figure 5.7 - Formation Energies of isomers, relative to *cis,trans,cis*

* DMol^3 software, with double-ζ basis set, single polarization function, and utilizing the Becke exchange functional (B88)[16] in combination with the Perdew-Wang correlation functional (P91).[17] See §0 for full details of calculation methodology.

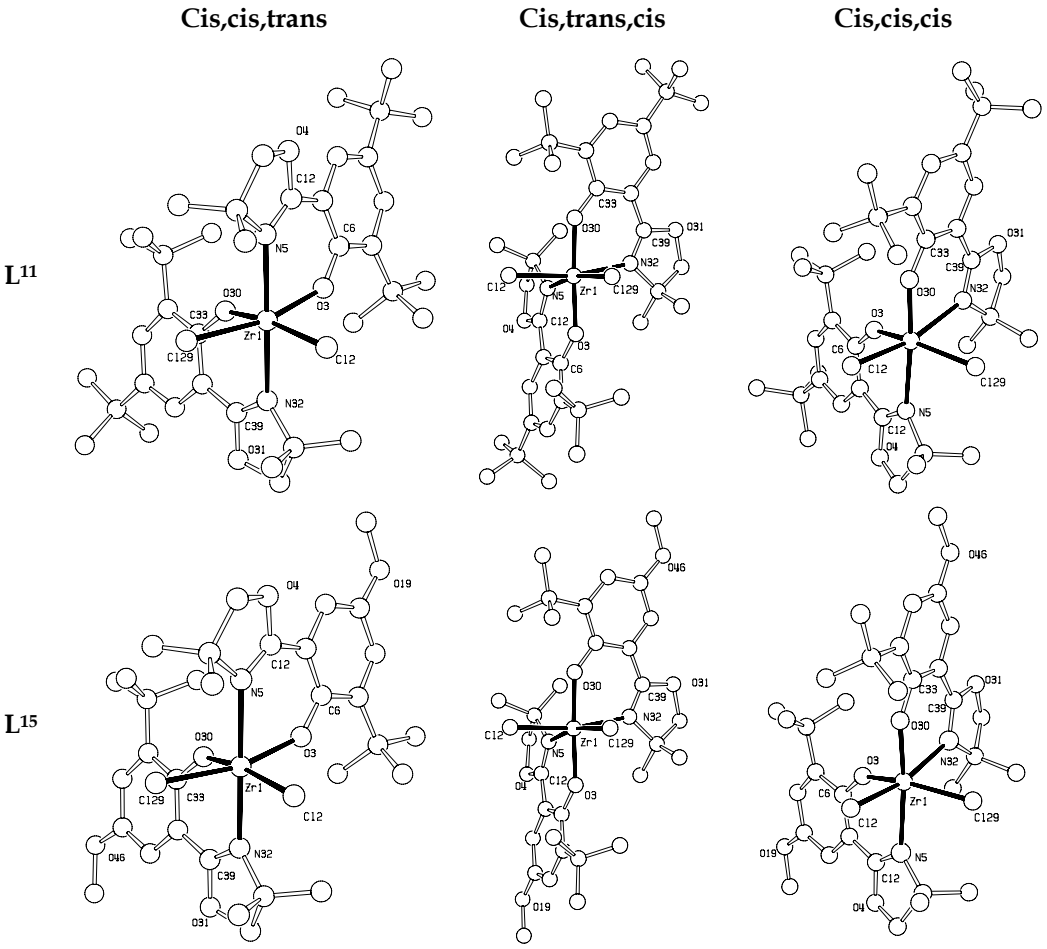

Figure 5.8 - Optimized structures of [$L^n{}_2ZrCl_2$] (n = 11, 15)

The difference between the energies of these isomers is relatively small; in related work in our group utilizing chiral salicyloxazoline ligands,[18] the difference between isomers is of the order of 35 kJ mol^{-1}.

If the various isomers are able to interchange, we would expect to see a statistical (Boltzmann) distribution between isomers, with occupancies as shown in Table 5.3. However, only one isomer is observed in the NMR spectra of both species (*q.v.* §3.4.2, §4.3.1). Whereas this may be valid for [$L^{15}{}_2ZrCl_2$], on the basis of these calculations we would expect to see a mixture of isomers for [$\mathbf{L^{11}}_2ZrCl_2$]. The reason for this discrepancy is unclear, but it seems most likely to arise from the DFT calculations' neglect of solvent effects, although this should not vary significantly between isomers.

	$L^{11}_2ZrCl_2$	$L^{15}_2ZrCl_2$
Cis,cis,trans	14%	96%
Cis,cis,cis	32%	3%
Cis,trans,cis	54%	1%

Table 5.3 – Calculated distribution of isomers

5.4.2 Effect of Methoxy Substituent

It has been proposed that the effect of the methoxy substituent in salicylaldimine catalysts is to strengthen the bonds between the zirconium centre and the ligands.[19] If this is indeed the case, it should result in those bonds in [$\mathbf{L^{15}}_2ZrCl_2$] being shorter than the equivalent bonds in [$\mathbf{L^{11}}_2ZrCl_2$].

The methoxy substituent is in conjugation with the aryl system in all the calculated structures of [$\mathbf{L^{15}}_2ZrCl_2$] (the dihedral angle between the O-Me bond and the aryl is <0.1°, consistent with sp^2 hybridization which is indicative of conjugation with the aryl system). However, comparison of the calculated structures shows that the methoxy substituent has only a very minor effect on the length of the Zr-O bonds (< 0.6 pm, Table 5.4).

Ligand	Bond	*Cis,cis,trans* Length (Å)	*Cis,trans,cis* Length (Å)	*Cis,cis,cis* Length (Å)
$\mathbf{L^{11}}$	Zr(1)-O(3)	2.047	2.056	2.042
	Zr(1)-O(30)	2.056	2.055	2.013
$\mathbf{L^{15}}$	Zr(1)-O(3)	2.041	2.051	2.042
	Zr(1)-O(30)	2.056	2.051	2.010

Table 5.4 – Calculated lengths of Zr-O bonds in various isomers of [$L^n_2ZrCl_2$] (n = 11, 15)

The 4-methoxy substituted salicylaldimine species previously reported by Fujita were crystallographically characterized* as having Zr-N bonds which were shorter (by 0.074 Å) than the 4-hydro analogues.[19,20] Comparison of our calculated structures again shows only very slight differences in the length of these bonds, between the structures of complexes utilizing $\mathbf{L^{11}}$ *vs.* $\mathbf{L^{15}}$.

Ligand	Bond	*Cis,cis,trans* Length (Å)	*Cis,trans,cis* Length (Å)	*Cis,cis,cis* Length (Å)
$\mathbf{L^{11}}$	Zr(1)-N(5)	2.385	2.428	2.457
	Zr(1)-N(32)	2.383	2.430	2.472
$\mathbf{L^{15}}$	Zr(1)-N(5)	2.391	2.436	2.463
	Zr(1)-N(32)	2.381	2.435	2.472

Table 5.5 - Calculated lengths of Zr-N bonds in various isomers with $[L^n_2ZrCl_2]$ (n = 11, 15)

It seems therefore that the effect of the methoxy substituent is not to strengthen the metal-ligand bonds in a straightforward manner: the calculated bond lengths do not support such an effect. There are several further possibilities as to how the methoxy substituent may prevent loss of ligand to aluminium, however.

The lowest energy isomer is predicted to be *cis,trans,cis* for $[\mathbf{L^{11}}_2ZrCl_2]$, and *cis,cis,trans* for the $\mathbf{L^{15}}$ analogue (*vide supra*). It is possible that the *cis,cis,trans* isomer disfavours ligand loss. This appears feasible; a close examination of the calculated structures shows that the *cis,cis,trans* isomer appears to be somewhat more congested around the phenoxy-oxygen than the *cis,trans,cis*.

Secondly, it is possible that the methoxy substituent has some other direct effect. For example, MAO may co-ordinate to it directly, and therefore not be suitably

* The original paper discussing this work does not mention the crystallographic structure determination; the bond lengths were presented in the later review article without associated crystallographic information. As far as we are aware, the full crystal structures have never been published.

oriented to accept the salicyloxazoline ligand. Since the structure of MAO is still poorly understood,[5] this is merely speculative however.

Thirdly, the increased electron density at the phenoxy-oxygen may interfere with the mechanism of ligand-loss to aluminium. It is clear that although the bond lengths are similar between **L**^{11} and **L**^{15} species there is nonetheless an electronic effect at the metal centre, favouring the *cis,cis,trans* isomer in the **L**^{15} complex.

Some related work within our group, utilizing complexes of the type [Cp****L**ZrCl$_2$] (Cp* = 1,2,3,4,5-pentamethylcyclopentadienyl) has shown that for those species the methoxy substituent has no effect on the lifetime of catalysis (direct reaction with MAO has not been attempted);[21] this is consistent with a change in geometry being responsible for inhibiting ligand loss, since any electronic effect would be expected to similarly affect the half-sandwich complexes.

5.4.3 Catalytic Cycle

The catalytically-active species for olefin polymerization are generally believed to be coordinatively unsaturated metal alkyl complexes,[3,4,7,22] operating *via* the Cossée mechanism (Figure 5.9).[23] The olefin approaches the alkyl cation (**A**), forming a π-complex (π). A 4-membered transition state (**TS**) leads to insertion of the olefin, and the resultant polymeryl chain is stabilized by a γ-agostic interaction (γ), before rearranging to be stabilized by a β-agostic interaction (β).

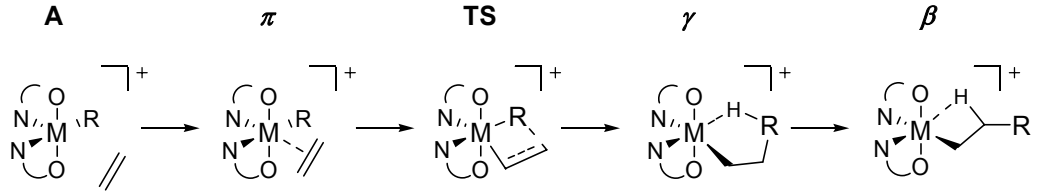

Figure 5.9 - Cossée mechanism

Using DFT, we modelled the expected intermediates in polymerization of ethene using [$\mathbf{L^{15}_2ZrCl_2}$], where R = Me (The key stages are shown in Figure 5.10, for the *trans*-O isomer).

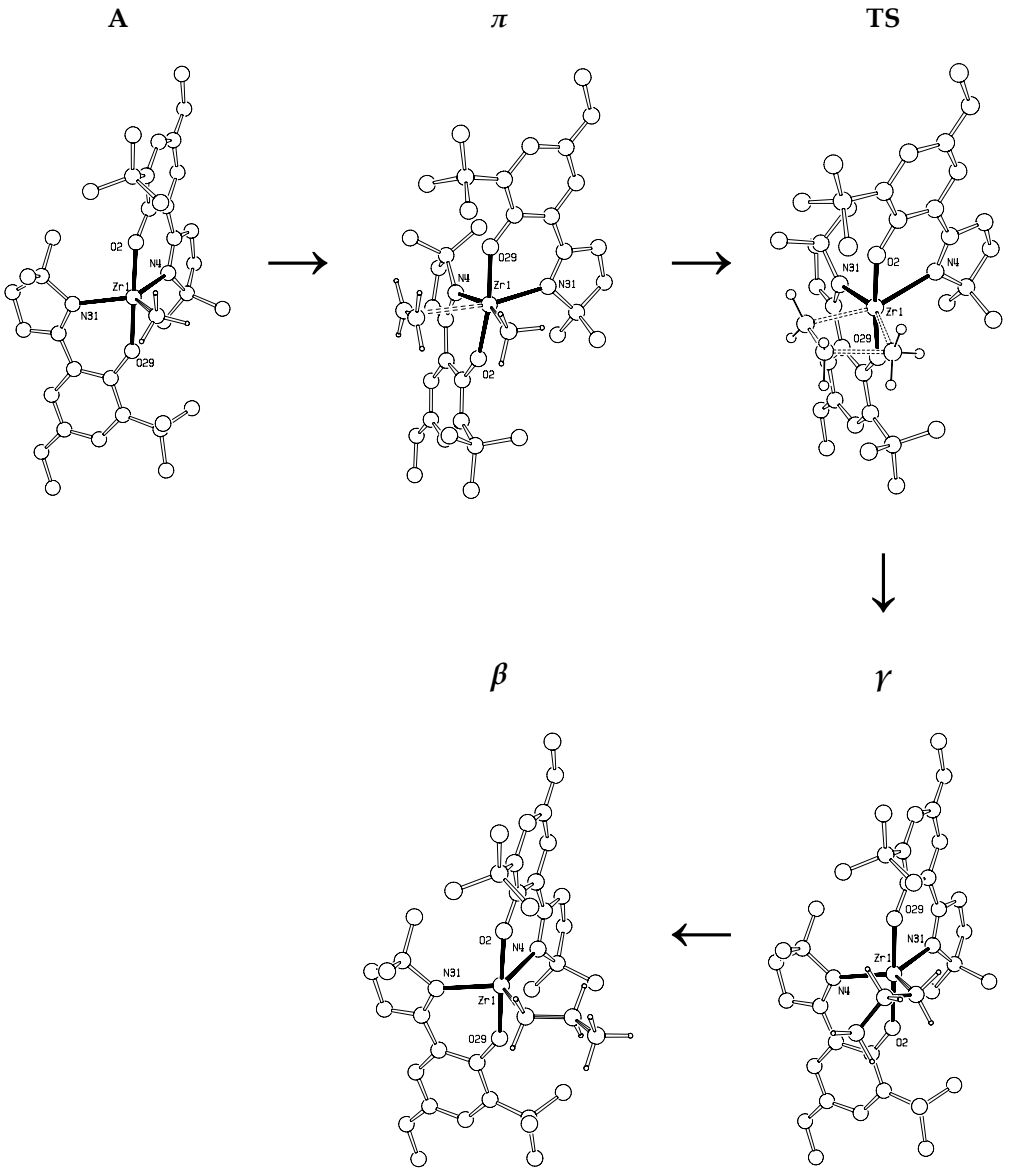

Figure 5.10 - Modelling Catalytic Process for *trans*-O [$\mathbf{L^{15}_2ZrCl_2}$]

The structures β and γ do not show any evidence of agostic interaction; if such interaction were present it we would expect to observe lengthened C-H bonds, and shorter Zr-H distances. Although the calculations were initiated from geometries consistent with agostic interactions, in all cases the optimizations have led to

5-coordinate structures with no such agostic interaction. This result is significant, as calculations for related [Cp*$\mathbf{L}$ZrCl$_2$] complexes using the same methodology clearly show agostic interactions.[21]

The calculated energies (relative to the *trans*-O isomer of A) are shown in Figure 5.11. Whereas the *cis,trans,cis* (*i.e. trans*-O) isomer of the dichloride complex is highest in energy (*vide supra*), in the methyl cation the *trans*-NO isomer has the highest energy. This may be rationalized if the reduction in steric demand around the metal centre stabilizes the *cis,trans,cis* structure more than it stabilizes the *cis,cis,cis*. Careful examination of the structures confirms that this is likely; in the *cis,trans,cis* dichloride structure the ligands are substantially distorted from planar co-ordination due to steric repulsion from the oxazoline dimethyl moiety. In the *cis,cis,cis* dichloride complex the ligands are more planar. Upon formation of the methyl cations, the situation is reversed (Table 5.6).

Isomer	**Ligand 1**		**Ligand 2**	
	dichloride	Me cation	dichloride	Me cation
cis,trans,cis	-23.37°	-2.46°	-22.85°	0.36°
cis,cis,cis	-3.61°	-18.93°	4.02°	6.88°

Table 5.6 – Dihedral angles between N-Zr-O-C for each ligand in [$\mathbf{L^{15}_2ZrCl_2}$] isomers

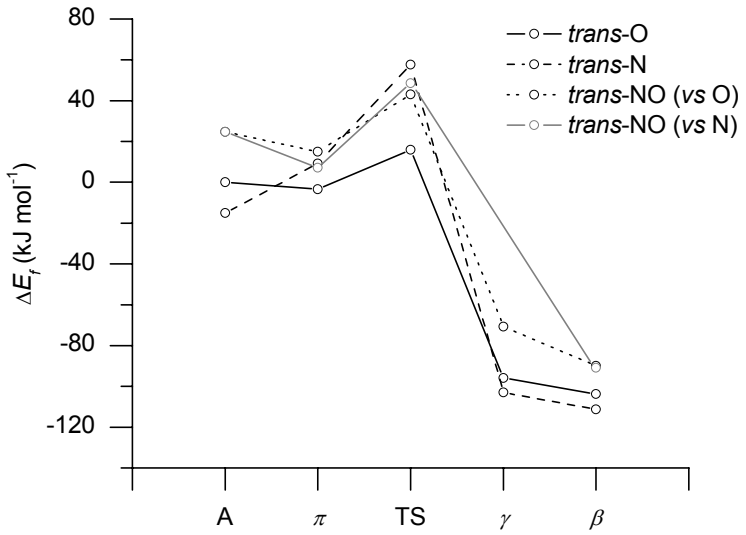

Figure 5.11 – Reaction energy profiles for C_2 polymerization with isomers of [$L^{15}{}_2ZrCl_2$] (relative to *trans*-O: A)

	A	π	**TS**	γ	β
***trans*-O**	0	-3.3	15.9	-95.8	-103.8
***trans*-N**	-15.1	9.2	57.7	-102.9	-111.3
***trans*-NO (*vs.* O)**	24.7	15.1	43.1	-70.7	-90.0
***trans*-NO (*vs.* N)**	24.7	7.1	48.5	–	-90.8

Table 5.7 - Calculated energies (in kJ mol^{-1}) for C_2 polymerization with various isomers of [$L^{15}{}_2ZrCl_2$]

No stable [$L^{15}{}_2$Zr(Me)(ethene)]$^+$ species (*c.f.* π in Figure 5.10) could be found where the N donors were *trans*; the energy given above is not optimized. The high $\Delta E^{\ddagger}$ probably reflects the disfavourable nature of co-ordinating ethene to this species. This may have implications for the nature of the active species in the polymerization; although the *cis,cis,trans* dichloride complex is lowest in energy, at the equivalent methyl cation it appears to be energetically disfavourable to co-ordinate ethene, *i.e.* although this isomer is predicted to be the thermodynamically most stable isomer, it is unlikely to be catalytically active in polymerization.

The "free" methyl cations (**A**) may be expected to undergo facile interchange *via* a rotational or pseudo-rotational (Berry twist) mechanism, and should have a

statistical distribution. This raises the possibility that only a minority of the available catalyst molecules will be active at any given time.

It has been suggested that electronic as well as steric flexibility in the salicylaldimine catalysts may play a role in their high activity, with the Zr-N bond *trans* to the polymeryl chain calculated to lengthen by ~0.1 Å upon formation of the ethene π-complex.[24] We calculate that the same behaviour should occur in $[\mathbf{L^{15}}_2Zr(Me)]^+$ (Table 5.8).

Bond	A	π	γ
Zr(1)-N(4)	2.293	2.504	2.295
Zr(1)-N(31)	2.283	2.257	2.285
Zr(1)-O(2)	2.037	2.043	2.041
Zr(1)-O(29)	2.035	2.034	2.041

Table 5.8 – Calculated bond lengths (Å) for *trans*-O $\mathbf{L^{15}}_2$Zr species

5.4.4 Conclusions from DFT Modelling

We have calculated the energies of the various possible isomers of $[\mathbf{L^{11}}_2ZrCl_2]$ and $[\mathbf{L^{15}}_2ZrCl_2]$, and the reaction pathways for the various isomers of the $\mathbf{L^{15}}$ species. We have shown that the influence of the methoxy substituent is not a straightforward strengthening of the metal-ligand bonds and propose instead that the effect is an electronic one, favouring a different isomer.

We have come to the unexpected conclusion that the lowest energy isomer of $[L^{15}_2ZrCl_2]$ is unlikely to be catalytically active. It is tempting to speculate that this isomer represents a "resting state" of the catalyst which is not active, but also not susceptible to ligand loss to aluminium.

However, there are several factors which are not included in these computational results, but which may be expected to influence the results. Firstly, the solvation energy is not modelled. It may be reasonable to assume that this will be similar between the different isomers, and should not affect the relative results.[25]

Secondly, the counterion is not modelled in our calculations. It has previously been shown that for metallocene systems with stoichiometric activators that the counterion can strongly influence the catalytic process.[1,4,25] This presents a particular problem where the counterion is MAO, the structure of which is still a matter of considerable debate (*vide supra*). In calculations of the insertion of ethene at a zirconocene centre,[4] the presence of one possible form of MAO was calculated to reduce the activation barrier by 1-2 kJ mol^{-1}. Interestingly, this study also calculated a significant increase in the activation barrier (~24 kJ mol^{-1}) when a solvent (toluene) was modelled with the MAO counterion, but not with the naked cation.

In summary, whilst we believe that these computational results are of interest (especially for the purposes of comparison with other studies), the difficulty involved in including MAO in the calculations of the reaction pathways probably presents a significant barrier to accurate modelling.

5.5 References for Chapter 5

1 E. Chen and T. Marks, *Chem. Rev.*, 2000, **100**, 1391-434.

2 V. C. Gibson and S. K. Spitzmesser, *Chem. Rev.*, 2003, **103**, 283-315.

3 G. J. P. Britovsek, V. C. Gibson and D. F. Wass, *Angew. Chem., Int. Ed. Engl.*, 1999, **38**, 428-47.

4 E. Zurek and T. Ziegler, *Faraday Discuss.*, 2003, **124**, 93-109.

5 J. L. Eilertsen, J. A. Støvneng, M. Ystenes and E. Rytter, *Inorg. Chem.*, 2005, **44**, 4843-51.

6 M. Ystenes, J. L. Eilertsen, J. K. Liu, M. Ott, E. Rytter and J. A. Støvneng, *J. Polym. Sci., Part A: Polym. Chem.*, 2000, **38**, 3106-27.

7 E. Zurek and T. Ziegler, *Prog. Polym. Sci.*, 2004, **29**, 107-48.

8 K. P. Bryliakov, E. A. Kravtsov, D. A. Pennington, S. J. Lancaster, M. Bochmann, H. H. Brintzinger and E. P. Talsi, *Organometallics*, 2005, **24**, 5660-64.

9 K. P. Bryliakov, N. V. Semikolenova, D. V. Yudaev, V. A. Zakharov, H. H. Brintzinger, M. Ystenes, E. Rytter and E. P. Talsi, *J. Organomet. Chem.*, 2003, **683**, 92-102; K. P. Bryliakov, E. P. Talsi and M. Bochmann, *Organometallics*, 2004, **23**, 149-52.

10 M. Bochmann, *J. Organomet. Chem.*, 2004, **689**, 3982-98.

11 P. G. Cozzi, E. Gallo, C. Floriani, A. Chiesi-Villa and C. Rizzoli, *Organometallics*, 1995, **14**, 4994-96.

12 P. D. Knight, A. J. Clarke, B. S. Kimberley, R. A. Jackson and P. Scott, *Chem. Commun.*, 2002, 352-53.

13 H. Makio and T. Fujita, *Macromol. Symp.*, 2004, **213**, 221-33.

14 D. Pappalardo, C. Tedesco and C. Pellecchia, *Eur. J. Inorg. Chem.*, 2002, 621-28.

15 Y. Tohi, T. Nakano, H. Makio, S. Matsui, T. Fujita and T. Yamaguchi, *Macromol. Chem. Phys.*, 2004, **205**, 1179-86.

16 A. Becke, *Phys. Rev. B*, 1988, **38**, 3098.

17 J. P. Perdew, K. Burke and Y. Wang, *Phys. Rev. B*, 1996, **54**, 16533-39.

18 I. Westmoreland, 'Chiral Architectures for Group 4 Metals', University of Warwick, Coventry, 2004; I. Westmoreland, I. J. Munslow, A. J. Clarke, G. Clarkson, R. J. Deeth and P. Scott, *J. Organomet. Chem.*, In Press.

19 N. Matsukawa, S. Matsui, M. Mitani, J. Saito, K. Tsuru, N. Kashiwa and T. Fujita, *J. Mol. Catal. A: Chem.*, 2001, **169**, 99-104.

20 H. Makio, N. Kashiwa and T. Fujita, *Adv. Synth. Catal.*, 2002, **344**, 477-93.

21 S. R. Coles, S. K. Spitzmesser and P. Scott, Unpublished Results

22 S. Matsui and T. Fujita, *Catal. Today*, 2001, **66**, 63-73; E. Zurek and T. Ziegler, *Organometallics*, 2002, **21**, 83-92; W. Kaminsky and A. Laban, *Appl. Catal. A-Gen.*, 2001, **222**, 47-61; J. J. Eisch, S. I. Pombrik and G. X. Zheng, *Organometallics*, 1993, **12**, 3856-63; R. F. Jordan, W. E. Dasher and S. F. Echols, *J. Am. Chem. Soc.*, 1986, **108**, 1718-19; M. Bochmann, *J. Chem. Soc., Dalton Trans.*, 1996, 255-70.

23 P. Cossée, *J. Catal.*, 1964, **3**, 80-88.

24 S. Matsui, M. Mitani, J. Saito, Y. Tohi, H. Makio, N. Matsukawa, Y. Takagi, K. Tsuru, M. Nitabaru, T. Nakano, H. Tanaka, N. Kashiwa and T. Fujita, *J. Am. Chem. Soc.*, 2001, **123**, 6847-56.

25 I. E. Nifant'ev, L. Y. Ustynyuk and D. N. Laikov, *Organometallics*, 2001, **20**, 5375-93.

6 Experimental Procedures

6.1 General Procedures

Where required, procedures were carried out under an atmosphere of argon using a dual-manifold vacuum/argon line and standard Schlenk procedures, and an MBraun argon-atmosphere dry-box. NMR samples were made up in Young's type concentric stopcock tubes and sealed under argon. Solvents were dried over sodium wire (except dichloromethane), and then distilled over K (tetrahydrofuran), Na (toluene), Na/K alloy (pentane), or CaH_2 (dichloromethane), under an atmosphere of N_2. Deuterated solvents were freeze-thaw degassed and dried by refluxing over CaH_2 (dichloromethane, bromobenzene) or molten K (all others) *in vacuo*, and then distilled to a Rotaflo ampoule and stored in the dry-box. All glassware was stored in an oven (>373 K) prior to use. Chemicals were purchased from Aldrich, Acros, Fluorochem or Fluka, and used without further purification unless otherwise noted. $[M(CH_2Ph)_4]$ (M = Ti,Zr,Hf) were prepared in our laboratory according to published procedures[1]

NMR spectra were recorded at ~298 K on Bruker DPX300, DPX400, AC400 or DRX500 spectrometers unless otherwise noted. Spectra were referenced internally via residual protio-solvent resonances relative to tetramethylsilane (δ = 0). Microanalyses were conducted by Warwick Analytical Services Ltd, or by Medac Ltd.

6.1.1 General Procedure for MAO activated Ethylene Polymerization

To toluene under argon in a round-bottom flask with several quick-fit ports was added the appropriate quantity of MAO as a 10% w/v solution in toluene. The

solution was stirred gently until it reached a constant temperature. The vessel was evacuated, and then charged with ethylene at 1.2 bar, and the rate of stirring increased to 400 rpm. The solution was stirred until ethylene uptake ceased, and the appropriate precatalyst was injected as a toluene solution. The pressure of ethylene and rate of stirring were maintained for the duration of the experiment. After the appropriate time, the reaction was stopped by addition of MeOH (20 ml), and removal of the ethylene atmosphere. The polymer product was precipitated by pouring onto a solution of 5 % HCl in MeOH (~800 ml), and stirring for ~4 h. The product was recovered by filtration, and washed with 5 % HCl in MeOH followed by acetone. The polymer product was dried by heating to 70 °C *in vacuo* for 24 h.

6.1.2 Ethylene polymerization in "Endeavor" reactor

The "Endeavor" reactor is a parallel screening device containing 8 individual high-pressure reactors. These were prepared by inserting a pre-weighed glass liner and attaching a plastic (PEEK) impeller for stirring. A solution of MAO in toluene (4 cm^3, 0.15 M) was then injected into each vessel under an inert atmosphere. Hexene (0.5 ml) was then injected into the appropriate vessels. The vessels were then purged and heated to the appropriate temperatures. Hydrogen gas (0.5 bar) was introduced if required, followed by a constant supply of ethylene (10 bar), and the stirring was switched on. Then a solution of the catalyst in toluene (5 mM for a 1 μM injection, 0.5 mM for a 0.1 μM injection) was then made, and pre-activated with MAO (10 eq., 0.5 M). The catalyst solution (0.2 ml) was injected into the vessel, followed by toluene (0.8 ml) to wash the syringe through. The ethylene uptake of the each vessel was monitored from the moment of injection for 30 minutes, whereupon the vessels were purged, returned to an inert atmosphere, and cooled to 30 ^oC. The polymers produced were then dried and weighed to obtain the final

productivity value for each catalyst, allowing for the residual weight of aluminium species present in the polymer.

6.1.3 Ethylene polymerization in 5 L autoclave

A catalyst solution was prepared by dissolving the appropriate precatalyst (2.0 µmol) in toluene (15.7 ml) followed by the addition of MAO (3.9 ml, 0.5 M in toluene, 1000 eq. Al/Zr) to reach a final catalyst concentration of 0.1 mM. 10 ml of this catalyst solution were immediately transferred into a 5 L autoclave containing isobutane (1.8 L), MAO (2.0 ml, 0.5 M in toluene, 1000 eq Al/Zr) and ethylene (10 bar) at 80 °C. The polymerization reaction was stopped after the appropriate time by venting all volatiles.

6.1.4 GPC Analysis

Samples generated in our laboratory were analysed by RAPRA Ltd. Samples generated using the Endeavor reactor were analysed by Innovene.

6.1.4.1 Rapra Ltd.

A single solution of each sample was prepared by adding 15 ml of solvent to 15 mg of sample and heating at 190 °C for 20 min with shaking to dissolve. Each sample solution was then filtered through a metal sinter at 160 °C and part of each filtered solution transferred to glass sample vials. The vials were then placed in a heated sample compartment and after an initial delay of thirty minutes to allow the samples to equilibrate thermally, injection of part of the contents of each vial was carried out automatically.

Instrument:	Polymer Laboratories GPC220,
Columns:	PLgel guard plus 2 x mixed bed-B, 30 cm, 10 microns,
Solvent:	1,2,4-trichlorobenzene with anti-oxidant,
Flow-rate:	1.0 ml/min (nominal),
Temperature:	160 °C (nominal),
Detector:	refractive index (a Viscotek differential pressure detector was also online, but the data was not used for the traces reported, unless otherwise mentioned).

Table 6.1 - Chromatographic details for RAPRA analysis

Data capture and subsequent data handling was carried out using Viscotek 'Trisec' 3.0 software.

The GPC system used for the work was calibrated with polystyrene and a mathematical procedure involving the use of literature viscosity constants has been applied to the calibration to allow for the difference in chemical type between the sample and the calibrants (the Mark Houwink parameters used are identified below). The results are therefore expressed as for polyethene.

	Polystyrene (calibrants)	**Polyethene**
A	0.707	0.725
Log K	-3.917	-3.391

Table 6.2 – Mark Houwink parameters for RAPRA analysis

6.1.4.2 Innovene

A single solution of each sample was prepared by adding 10 ml of solvent to 4.5 mg of sample and shaking in a PL SP260 dissolution rig at 160 °C for 120 minutes. 2 ml

of each filtered solution were transferred to glass sample vials, which were then placed in a heated sample compartment and injection of part of the contents of each vial was carried out automatically.

Instrument:	Polymer Laboratories GPC220
Columns:	PLgel HTS-B (150 x 7.5 mm) for rapid GPC
Solvent:	1,2,4-trichlorobenzene with 1 g/l BHT
Flow-rate:	1.0 ml/min (nominal)
Temperature:	160 °C (nominal)
Detector:	refractive index.

Table 6.3 - Chromatographic details for RAPRA analysis

Data capture and subsequent data handling was carried out using PL Cirrus GPC Online software (v 1.2).

The GPC system used for the work was calibrated with polystyrene and a mathematical procedure involving the use of literature viscosity constants has been applied to the calibration to allow for the difference in chemical type between the sample and the calibrants (the Mark Houwink parameters used are identified below). The results are therefore expressed as for polyethene.

	Polystyrene (calibrants)	**Polyethene**
A	0.707	0.725
K	12.1	40.6

Table 6.4 – Mark Houwink parameters for RAPRA analysis

6.1.5 Molecular Modeling Details

All geometry optimizations were performed with the DMol[3] Density Functional Theory (DFT) code[2] as implemented in the Accelrys MaterialsStudio (versions 3.1 and 3.2).[3] DMol[3] utilizes a basis set of numeric atomic functions, which are exact

solutions to the Kohn-Sham equations for the atoms. These basis sets are generally more complete than a comparable set of linearly independent Gaussian functions, and have smaller basis set superposition errors. In the present study, a polarized split valence basis set (termed "double numeric polarized" (DNP)) was used, *i.e.* a double-ζ basis set with polarization functions (functions with angular momentum one higher than that of the highest occupied orbital in the free atom: 2p for H; 3d for C, N, O; 5p for Zr). All geometry optimizations employed delocalized internal coordinates.[4]

The generalized gradient approximation (GGA) functional utilizing the Becke exchange functional (B88)[5] in combination with the Perdew-Wang correlation functional (P91)[6] was used for all geometry optimizations. The convergence criteria for these optimizations consisted of threshold values of 2×10^{-5} Ha, 0.004 Ha $Å^{-1}$ and 0.005 Å for energy, gradient and displacement convergence, respectively, while a self consistent field (SCF) density convergence threshold value of 1×10^{-5} was specified.

Preliminary transition state geometries were obtained by the integrated linear synchronous transit/quadratic synchronous transit (LST/QST) algorithm[7] available in MaterialsStudio. These preliminary structures were then subjected to full TS optimizations using an eigenvector following algorithm. All transition structure geometries exhibited only one imaginary frequency in the reaction coordinate. All calculated reaction energies were derived from the total electronic energies of the geometries after optimization.

6.1.6 Synthesis of Metal Reagents

6.1.6.1 $[ZrCl_4(THF)_2]$[8]

A Schlenk vessel with stirrer bar was charged with zirconium tetrachloride (15.8 g, 67.8 mmol) and dichloromethane (80 ml). The suspension was stirred vigorously and THF (12.1 ml, 149 mmol) was added dropwise. The solid material dissolved upon addition of THF. The solution was filtered, pentane (80 ml) was added and the solution kept at –30 °C overnight. A white crystalline solid was obtained, which was filtered, washed with pentane and dried *in vacuo*, yielding $[ZrCl_4(THF)_2]$ (22.22 g, 87 %).

6.1.6.2 $[TiCl_4(THF)_2]$[8]

A Schlenk vessel with stirrer bar was charged with dichloromethane (30 ml) and titanium tetrachloride (2.9 ml, 26.4 mmol). The solution was stirred vigorously and THF (9 ml, 111.1 mmol) was added dropwise over 1 h. The solution was stirred for a further 20 min. Pentane (60 ml) was added, and then the solution was cooled to –30 °C and kept overnight to yield a bright yellow crystalline solid. This was recovered by filtration and dried *in vacuo*, yielding $[TiCl_4(THF)_2]$ (8.1 g, 92 %).

6.2 Bibenzyl Proligands

6.2.1 2-hydroxy-3-*tert*-butyl-6-methylbenzaldehyde

To 2-*tert*-butyl-5-methylphenol (16.5 g, 0.10 mol) in dry acetonitrile (500 ml) under argon was added dry TEA (55 ml), followed by dry $MgCl_2$ (14.4 g, 0.15 mol). The mixture was stirred for 30 min. Dry paraformaldehyde (21 g, 0.70 mol) was added, and the mixture was heated at reflux for 2 h, before being allowed to cool to rt. The product was extracted with Et_2O (7 × 100 ml), dried ($MgSO_4$) and filtered through

celite. The solvent was then removed *in vacuo*. Distillation under reduced pressure (125 – 150 °C, 10^{-2} bar) yielded the desired product as a yellow-green oil (3.8 g, 18%).

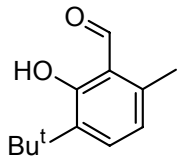

^{1}H NMR 400 MHz ($CDCl_3$): δ ppm 12.76 (s, 1H, OH), 10.29 (s, 1H, Ar–C*H*=O), 7.38 (d, 1H, Ar*H*, $^3J_{HH}$ = 8 Hz), 6.64 (d, 1H, Ar*H*, $^3J_{HH}$ = 8 Hz), 2.55 (s, 3H, Ar-CH_3), 1.43 (s, 9H, C(CH_3)$_3$)

^{13}C{^{1}H} NMR 100 MHz ($CDCl_3$): δ ppm 195.6 (Ar–*C*H=O), 162.7, 139.5, 136.2, 134.3, 120.9, 118.2 (Ar), 34.4 (*C*(CH$_3$)$_3$), 29.1 (C(*C*H$_3$)$_3$), 17.6 (Ar–CH$_3$)

MS (EI$^+$): m/z 192 (M$^+$)

6.2.2 H_2L^1

To 3-*tert*-butyl-2-hydroxy-5-methylbenzaldehyde (2.00 g, 10.40 mmol) was added 2,2'-diaminobibenzyl (1.06 g, 5.00 mmol), and then EtOH (~40 ml). The solution was heated at reflux for 18 h, during which time it turned bright orange. The mixture was cooled to 0 °C, and the powder product was recovered by filtration and then washed with ice-cold EtOH. H_2L^1 was recovered as a yellow-orange powder (2.40 g, 86%).

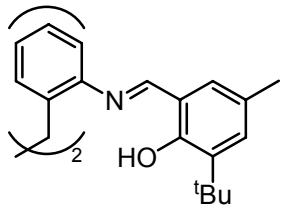

^{1}H NMR 300 MHz ($CDCl_3$): δ ppm 13.96 (s, 2H, OH), 8.46 (s, 2H, N=C*H*), 7.45 (dd, 2H, Ar*H*, $^3J_{HH}$ = 8 Hz, $^4J_{HH}$ = 2 Hz), 7.23 (td, 2H, Ar*H*, $^3J_{HH}$ = 8 Hz, $^4J_{HH}$ = 2 Hz), 7.23 (d, 2H, Ar*H*, $^3J_{HH}$ = 8 Hz), 7.13 (tt, 2H, Ar*H*, $^3J_{HH}$ = 8 Hz, $^4J_{HH}$ = 1 Hz), 7.05 (dd, 2H,

Ar*H*, $^{3}J_{HH}$ = 8 Hz, $^{4}J_{HH}$ = 1 Hz), 7.03 (d, 2H, Ar*H*, $^{4}J_{HH}$ = 2 Hz), 3.07 (s, 4H, Ar–CH_2), 2.33 (s, 6H, Ar–CH_3), 1.53 (s, 18H, C(CH_3)$_3$)

^{13}C{^{1}H} NMR 75 MHz ($CDCl_3$): δ ppm 161.6 (N=*C*H), 158.2, 147.0, 137.3, 135.8, 130.6, 126.8, 118.8 (Ar), 131.3, 130.3, 127.3, 126.7, 117.6 (ArH), 34.6 (*C*(CH$_3$)$_3$), 33.9 (Ar–*C*H$_2$), 29.2 (C(*C*H$_3$)$_3$), 18.76 (Ar–*C*H$_3$)

MS (EI$^+$): m/z 560 (M$^+$)

EA: found (calc) C: 80.97 (81.39), H: 7.90 (7.91), N: 5.11 (5.00)

6.2.3 H_2L^2

To 2-hydroxy-3-*tert*-butyl-6-methylbenzaldehyde (1.82 g, 9.47 mmol) was added 2,2'-diaminobibenzyl (0.994 g, 4.68 mmol), and then EtOH (~40 ml). The solution was heated at reflux for 18 h, during which time it turned bright orange. The mixture was cooled to 0 °C, and the powder product was recovered by filtration and then washed with ice-cold EtOH. H_2L^2 was recovered as a yellow-orange powder (2.50 g, 95%).

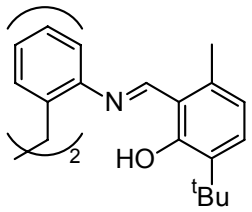

^{1}H NMR 400 MHz ($CDCl_3$): δ ppm 14.97 (s, 2H, OH), 8.86 (s, 2H, N=C*H*), 7.48 (d, 2H, Ar*H*, $^{3}J_{HH}$ = 8 Hz), 7.27 (d, 2H, Ar*H*, $^{3}J_{HH}$ = 8 Hz), 7.23 (t, 2H, Ar*H*, $^{3}J_{HH}$ = 8 Hz), 7.11 (t, 2H, Ar*H*, $^{3}J_{HH}$ = 8 Hz), 7.05 (d, 2H, Ar*H*, $^{3}J_{HH}$ = 8 Hz), 6.64 (d, 2H, Ar*H*, $^{3}J_{HH}$ = 8 Hz), 3.08 (s, 4H, Ar–CH_2), 2.49 (s, 6H, Ar–CH_3), 1.50 (s, 18H, C(CH_3)$_3$)

^{13}C{^{1}H} NMR 100 MHz ($CDCl_3$): δ ppm 160.6 (N=*C*H), 161.7, 147.2, 137.3, 135.9, 135.8, 130.7, 130.5, 127.3, 126.8, 119.9, 117.8, 117.0 (Ar), 34.6 (*C*(CH$_3$)$_3$), 33.9 (Ar–*C*H$_2$), 29.2 (C(*C*H$_3$)$_3$), 18.76 (Ar–*C*H$_3$)

MS (EI^+): m/z 560 (M^+)

EA: found (calc) C: 81.44 (81.39), H: 7.92 (7.91), N: 5.01 (5.00)

6.2.4 H_2L^3

To 2-hydroxy-3,5-dimethylbenzaldehyde (0.920 g, 6.13 mmol) in EtOH was added 2,2′-diaminobibenzyl (0.594 g, 2.80 mmol), with stirring. The mixture was stirred at room temperature for 18 h, during which time it turned bright orange. The mixture was cooled to 0 °C, and the powder product was recovered by filtration and then washed with ice-cold EtOH. The supernatant was cooled to 5 °C for 3 days, and another crop of orange powder was recovered by filtration and washing with EtOH. The crops were combined, leaving H_2L^3 as an orange powder (1.22 g, 92%).

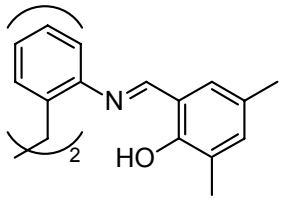

^{1}H NMR 400 MHz ($CDCl_3$): δ ppm 13.84 (s, 2H, OH), 8.05 (S, 2H, N=C*H*), 7.26–6.8 (m, 12H, Ar*H*), 3.07 (s, 4H, Ar–CH_2), 2.32 (s, 6H, Ar–CH_3), 2.28 (s, 6H, Ar–CH_3)

^{13}C{^{1}H} NMR 100 MHz ($CDCl_3$): δ ppm 163.3 (N=CH), 157.5, 148.3, 135.6, 135.4, 130.8, 130.3, 127.7, 127.6, 126.8, 126.7, 118.7, 118.6 (Ar), 33.6 (Ar–CH_2), 20.8, 15.9 (Ar–CH_3)

MS (EI^+): m/z 476 (M^+)

EA: found (calc) C: 80.71 (80.64), H: 6.78 (6.77), N: 5.84 (5.88)

6.2.5 H_2L^4

To 2-hydroxy-3,6-dimethylbenzaldehyde (1.06 g, 7.06 mmol) in an RBF was added 2,2′-diaminobibenzyl (0.750 g, 3.54 mmol). EtOH (~40 ml) was added, and the mixture was warmed gently to aid dissolution. The mixture was stirred at room

temperature for 66 h, during which time it turned bright orange. The mixture was cooled to 0 °C, and the powder product was recovered by filtration and then washed with ice-cold EtOH. The supernatant was concentrated *in vacuo*, then cooled to 5 °C for 7 days, and another crop of orange-yellow powder was recovered by filtration and washed with EtOH. The crops were combined, leaving H_2L^4 as an orange powder (1.5 g, 89%).

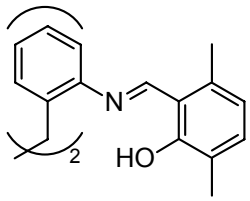

^{1}H NMR 400 MHz ($CDCl_3$): δ ppm 14.29 (s, 2H, OH), 8.65 (S, 2H, N=C*H*), 7.20 (m, 4H, 2 overlapping Ar*H* signals), 7.09 (m, 4H, 2 overlapping Ar*H* signals), 6.93 (d, 2H, Ar*H*), 6.59 (d, 2H, Ar*H*), 3.10 (s, 4H, Ar–CH_2), 2.46 (s, 6H, Ar–CH_3), 2.24 (s, 6H, Ar–CH_3)

^{13}C{^{1}H} NMR 100 MHz ($CDCl_3$): δ ppm 161.0 (N=*C*H), 160.8, 148.2, 137.3, 135.9, 134.6, 130.9, 127.6, 127.0, 124.8, 120.6, 118.5, 117.0 (Ar), 33.5 (Ar–*C*H_2), 19.3, 15.9 (Ar–*C*H_3)

MS (EI^+): m/z 476 (M^+)

EA: found (calc) C: 80.14 (80.64), H: 6.87 (6.77), N: 5.91 (5.88)

6.2.6 $HL^{5\,(9)}$

To 3-*tert*-butyl-2-hydroxy-5-metoxybenzaldehyde (1.61 g, 7.83 mmol) was added 2,2'-diaminobibenzyl (0.79 g, 3.72 mmol), and then EtOH (~40 ml). The solution was heated at reflux for 18 h, during which time it turned bright orange. The mixture was cooled to 0 °C, and the powder product was recovered by filtration and then

washed with ice-cold EtOH. H_2L^5 was recovered as a yellow-orange powder (1.71 g, 74%).

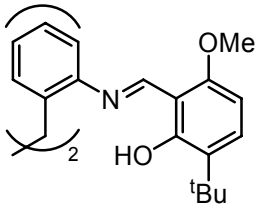

^{1}H NMR 400 MHz ($CDCl_3$): δ ppm 13.73 (s, 2H, OH), 8.43 (S, 2H, N=C*H*), 7.42–6.69 (m, 12H, Ar*H*), 3.81 (s, 6H, OMe), 3.06 (s, 4H, Ar–CH_2), 2.32 (s, 6H, Ar–CH_3), 2.28 (s, 18H, C(CH_3)$_3$)

^{13}C{^{1}H} NMR 100 MHz ($CDCl_3$): δ ppm 162.6 (N=*C*H), 155.1, 151.4, 146.9, 139.2, 135.8, 130.6, 127.3, 126.8, 119.2, 118.4, 117.6, 111.8 (Ar), 55.76 (O*C*H$_3$), 33.8 (Ar-*C*H$_2$) 33.7 (*C*(CH$_3$)$_3$), 29.1 (C(*C*H$_3$)$_3$)

6.3 Bibenzyl Complexes

6.3.1 [L^1ZrCl_2]

To H_2L^1 (0.537 g, 0.959 mmol) in a Schlenk tube was added NaH (92 mg, 3.8 mmol) under argon. THF (~20 ml) was added, and the mixture was stirred for 18 h. The solution was filtered *via* cannula into a Schlenk tube containing $ZrCl_4$.2THF (0.359 g, 0.952 mmol) at 0 °C, and the mixture was stirred for 66 h. A fine precipitate was allowed to settle out. The solution was filtered *via* cannula, and then the solvent was removed *in vacuo*, leaving a yellow solid. Sublimation at ~175 °C and 10^{-6} bar yielded [L^1ZrCl_2] (0.457 g, 67%).

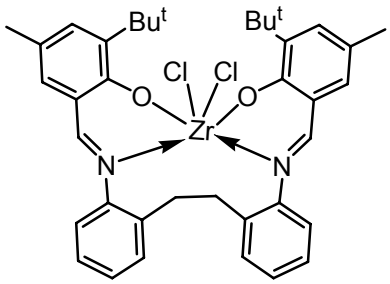

NMR shows that there are two products: a sharp symmetrical one (*cis*-α), and a much broader unsymmetrical one (*cis*-β), in a ratio of approximately 1:4.

^{1}H NMR 400 MHz (CD_2Cl_2):

cis-α (298K): δ ppm 8.05 (s, 2H, N=C*H*), 7.60 (d, 2H, Ar, $^3J_{HH}$ = 7 Hz), 7.40 (s, 2H, Ar), 7.18 (d, 2H, Ar*H*, $^3J_{HH}$ = 7 Hz), 7.00 (m, 4H, Ar*H*), 6.87 (d, 2H, Ar*H*), 3.07 (s, 2H, Ar–CH_2, $^2J_{HH}$ = 13Hz), 2.65 (d, 2H, Ar–CH_2, $^2J_{HH}$ = 13Hz), 2.28 (s, 6H, Ar–CH_3), 1.56 (s, 18H, C(CH_3)$_3$)

cis-β (298K): δ ppm 8.13 (br, 1H, N=C*H*), 7.97 (br, 1H, N=C*H*), 7.6–7.0 (br, 9H, Ar*H*), 6.5 (br, 2H, Ar*H*), 6.3 (br, 1H, Ar*H*), 3.6 (br, 1H, Ar–CH_2), 3.5 (br, 1H, Ar–CH_2), 3.3 (br, 1H, Ar–CH_2), 3.0 (br, 1H, Ar–CH_2), 2.3 (br, 3H, Ar–CH_3), 2.2 (br, 3H, Ar–CH_3), 1.6 (br, 9H, C(CH_3)$_3$), 1.4 (br, 9H, C(CH_3)$_3$)

cis-α (183K): δ ppm 8.06 (s, 2H, N=C*H*), 7.49 (d, 2H, Ar*H*, $^3J_{HH}$ = 8 Hz), 7.34 (s, 2H, Ar*H*), 7.19(d, 2H, Ar*H*, overlapping *cis*–β signal), 6.99 (t, 2H, Ar*H*, $^3J_{HH}$ = 8 Hz), 6.93 (t, 2H, Ar, $^3J_{HH}$ = 8 Hz), 6.86 (s, 2H, Ar*H*), 3.04 (d, 2H, Ar–CH_2, $^2J_{HH}$ = 12Hz), 2.57 (d, 2H, Ar–CH_2, $^2J_{HH}$ = 12Hz), 2.21 (s, 6H, Ar–CH_3), 1.46 (s, 18H, C(CH_3)$_3$, overlapping *cis*–β signal)

cis-β (183K): δ ppm 8.16 (br, 1H, N=C*H*), 7.92 (br, 1H, N=C*H*), 7.47 (d, 1H, Ar*H*, $^3J_{HH}$ = 8 Hz), 7.43 (s, 1H, Ar), 7.35 (d, 1H, Ar*H*), 7.27-7.20 (m, 4H, Ar*H*, overlapping *cis*–α signal), 7.16 (s, 1H, Ar*H*), 6.93 (t, 1H, Ar*H*, $^3J_{HH}$ = 8 Hz), 6.47 (s, 1H, Ar*H*), 6.44 (s, 1H, Ar*H*, $^3J_{HH}$ = 8 Hz), 6.22 (s, 1H, Ar*H*, $^3J_{HH}$ = 8 Hz), 3.43 (m, 1H, Ar–CH_2), 3.32-

3.25 (m, 2H, Ar–CH_2), 2.94 (m, 1H, Ar–CH_2), 2.29 (s, 3H, Ar–CH_3), 2.15 (s, 3H, Ar–CH_3), 1.46 (s, 9H, C(CH_3)$_3$, overlapping *cis*–α signal), 1.32 (s, 9H, C(CH_3)$_3$)

MS (EI$^+$): m/z 718 (M$^+$), 683 ([M - Cl]$^+$), 647 ([M - 2Cl]$^+$)

EA: found (calc for $C_{38}H_{42}Cl_2N_2O_2Zr$) C: 62.29 (63.31), H: 5.60 (5.87), N: 3.76 (3.89)

6.3.2 [L^{2}ZrCl$_2$]

To H_2L^2 (0.580 g, 1.04 mmol) in a Schlenk tube was added NaH (110 mg, 4.6 mmol) under argon. THF (~200 ml) was added, and the mixture was stirred for 18 h. The solution was filtered *via* cannula into a Schlenk tube containing $ZrCl_4$.2THF (0.392 g, 1.04 mmol) in THF at 0 °C, and the mixture was stirred for 18 h. A fine precipitate was allowed to settle out. The solution was filtered *via* cannula, and then the solvent was removed *in vacuo*, leaving a yellow solid. Sublimation at ~305 °C and 10^{-6} bar yielded [L^{1}ZrCl$_2$] (0.500 g, 67%).

NMR suggests that there are two products: a sharp symmetrical product (*cis*-α), and a much broader unsymmetrical one (*cis*-β), in a ratio of approximately 1:4.

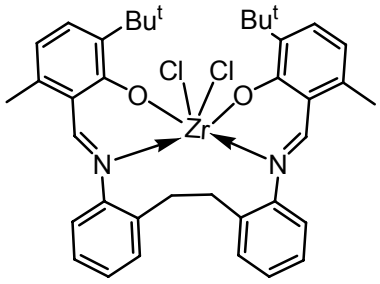

^{1}H NMR 400 MHz (CD_2Cl_2):

cis-α (298 K): δ ppm 8.47 (s, 2H, N=C*H*), 7.62 (d, 2H, Ar*H*, $^3J_{HH}$ = 9 Hz), 7.45 (d, 2H, Ar*H*, $^3J_{HH}$ = 8 Hz), 7.21 (d, 2H, Ar*H*, $^3J_{HH}$ = 8 Hz), 6.97 (m, 4H, Ar*H*), 6.66 (d, 2H, Ar*H*, $^3J_{HH}$ = 8 Hz), 3.10 (d, 2H, ArCH_2, $^2J_{HH}$ = 12 Hz), 2.72 (d, 2H, Ar–CH_2, $^2J_{HH}$ = 13 Hz), 2.30 (s, 6H, Ar–CH_3), 1.56 (s, 18H, C(CH_3)$_3$).

cis-β (298 K): δ ppm 8.40 (br, 2H, N=C*H*), 7.43 (br, Ar–*H*), 7.36 (d, 2H, Ar–*H*, $^3J_{HH}$ = 8 Hz), 7.18 (br, Ar*H*), 6.68 (br, Ar*H*), 3.48 (br, 4H, Ar–CH_2), 2.28 (br, 6H, *Me*), 1.51 (br, 18H, C(CH_3)$_3$).

cis-β (253 K): δ ppm 7.57 (s, 1H, N=C*H*), 7.55 (s, 1H, N=C*H*), 7.56 (d, 1H, Ar*H*, $^3J_{HH}$ = 8 Hz), 7.53 (d, 1H, Ar*H*, $^3J_{HH}$ = 8 Hz), 7.39 – 7.31 (m, 4H, Ar*H*), 7.27 (t, 1H,Ar*H*, $^3J_{HH}$ = 7 Hz), 7.03 (t, 1H, Ar*H*, $^3J_{HH}$ = 8 Hz), 6.84 (d, 1H, Ar*H*, $^3J_{HH}$ = 8 Hz), 6.54 (d, 1H, Ar*H*, $^3J_{HH}$ = 8 Hz), 6.50 (t, 1H, Ar*H*, $^3J_{HH}$ = 8 Hz), 6.33 (d, 1H, Ar*H*, $^3J_{HH}$ = 7 Hz), 3.55 (m, 1H, Ar–CH_2), 3.49 (m, 1H, Ar–CH_2), 3.35 (m, 1H, Ar–CH_2), 3.00 (m, 1H, Ar–CH_2), 2.40 (s, 3H, Ar–CH_3), 2.11 (s, 3H, Ar–CH_3), 1.55 (s, 9H, C(CH_3)$_3$), 1.39 (s, 9H, C(CH_3)$_3$).

$^{13}C\{^1H\}$ NMR 100 MHz (CD_2Cl_2): *cis*-α and *cis*-β, δ ppm 169.6 (N=*C*H), 148.1, 140.3, 136.7, 135.9, 134.6, 133.9, 130.9, 127.0, 126.7, 125.8, 122.3), 122.1 (*Ar*), 34.8 (Ar–*C*H_2), 33.3 (*C*Me$_3$), 29.7, 29.5 (C(*C*H_3)$_3$), 19.0 (Ar–*C*H_3)

MS (EI^+): m/z 703 ($[M–CH_3]^+$), 648 ($[M–(Cl)_2]^+$)

EA: found (calc for $C_{38}H_{42}Cl_2N_2O_2Zr$) C: 63.96 (63.31), H: 5.96 (5.87), N: 3.74 (3.89)

6.3.3 [L^1TiCl_2]

To H_2L^1 (0.492 g, 0.879 mmol) in a Schlenk tube was added $TiCl_4$.2THF (0.291 g, 0.87 mmol), under argon. Toluene (~20 ml) was added, and the mixture was stirred for 66 h. The solvent was removed *in vacuo*, leaving a red solid. Sublimation at 250 °C and 10^{-6} bar yielded [L^1TiCl_2] (0.343 g, 58%).

NMR suggests that there is one *cis*–β unsymmetrical product.

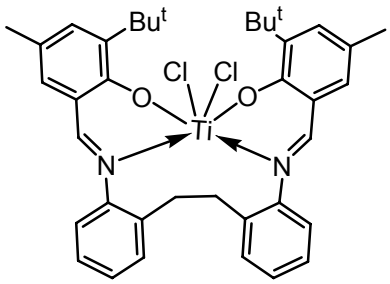

^{1}H NMR 400 MHz (CD_2Cl_2): δ ppm 8.00 (s, 1H, N=C*H*), 7.75 (s, 1H, N=C*H*), 7.72 (d, 1H, Ar*H*, $^{3}J_{HH}$ = 8 Hz), 7.35 (s, 1H, Ar*H*), 7.17–7.04 (m, 6H, Ar*H*), 6.93 (t, 1H, Ar*H*, $^{3}J_{HH}$ = 8 Hz), 6.40 (t, 1H, Ar*H*, $^{3}J_{HH}$ = 8 Hz), 6.40 (s, 1H, Ar*H*), 6.18 (d, 1H, Ar*H*, $^{3}J_{HH}$ = 8 Hz), 3.45 (m, 1H, Ar–CH_2), 3.3 (m, 1H, Ar–CH_2), 3.05 (m, 1H, Ar–CH_2), 2.8 (m, 1H, Ar–CH_2), 2.27 (s, 3H, Ar–CH_3), 2.11 (s, 3H, Ar–CH_3), 1.5 (s, 9H, C(CH_3)$_3$), 1.3 (s, 9H, C(CH_3)$_3$)

^{13}C{^{1}H} NMR 100 MHz (CD_2Cl_2): δ ppm 171.4, 167.1 (N=*C*H), 161.6, 160.2, 154.7, 149.9, 139.7, 138.1, 137.3, 133.9, 132.1, 131.6, 126.6, 125.0 (Ar), 36.6, 35.7, (Ar–*C*H_2), 30.4, 30.2, (C(*C*H_3)$_3$), 27.3 (*C*(CH$_3$)$_3$), 21.4, 21.1 (Ar–*C*H_3)

MS (EI$^+$): m/z 676 (M$^+$), 641 ([M – Cl]$^+$), 605 ([M – 2Cl]$^+$)

EA: found (calc for $C_{38}H_{42}Cl_2N_2O_2Ti$) C: 67.01 (67.36), H: 6.14 (6.25), N: 4.25 (4.13)

6.3.4 [L^{2}TiCl$_2$]

To H_2L^2 (0.582 g, 1.04 mmol) in a Schlenk tube was added $TiCl_4$.2THF (0.347 g, 10.4 mmol) under argon. Toluene (~20 ml) was added, and the mixture was stirred for 18 h. The solvent was removed *in vacuo*, leaving a red solid. Sublimation at 305 °C and 10^{-6} bar yielded [L^{2}TiCl$_2$] (0.482 g 68%).

NMR suggests that there is one *cis*–β unsymmetrical product.

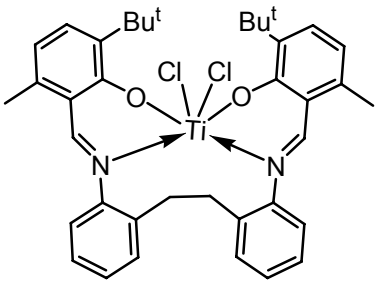

^{1}H NMR 400 MHz (CD_2Cl_2): δ ppm 8.38 (s, 1H, N=C*H*), 8.31 (s, 1H, N=C*H*), 7.6 (d, 1H, Ar*H*, $^{3}J_{HH}$ = 8 Hz), 7.57 (d, 1H, Ar*H*, $^{3}J_{HH}$ = 8 Hz), 7.35–7.17 (m, 5H, Ar*H*), 7.03 (t, 1H, Ar*H*, $^{3}J_{HH}$ = 8 Hz), 6.91 (d, 1H, Ar*H*, $^{3}J_{HH}$ = 8 Hz), 6.58 (d, 1H, Ar*H*, $^{3}J_{HH}$ = 8 Hz), 6.50 (t, 1H, Ar*H*, $^{3}J_{HH}$ = 8 Hz), 6.32 (d, 1H, Ar*H*, $^{3}J_{HH}$ = 8 Hz), 3.6–3.5 (m, 2H, Ar–CH_2), 3.3 (m, 1H, Ar–CH_2), 2.9 (m, 1H, Ar–CH_2), 2.42 (s, 3H, Ar–CH_3), 2.08 (s, 3H, Ar–CH_3), 1.59 (s, 9H, C(CH_3)$_3$), 1.43 (s, 9H, C(CH_3)$_3$)

^{13}C{^{1}H} NMR 100 MHz (CD_2Cl_2): δ ppm 168.7, 164.1 (N=*C*H), 134.0, 133.8, 131.1, 128.5, 128.1, 128.1, 127.0, 126.8, 126.3, 124.8, 124.6, 124.4 (Ar *C*–H), 155.2, 150.1, 140.9, 140.4, 140.3, 136.1, 135.8, 125.5, 123.5 (quarternary Ar *C*), 36.9, 35.6 (Ar–*C*H_2), 27.2 (*C*(CH$_3$)$_3$), 30.4, 30.3, (C(*C*H$_3$)$_3$), 20.2, 19.3 (*C*H$_3$)

MS (EI$^+$): m/z 676 (M$^+$), 641 ([M – Cl]$^+$), 605 ([M – 2Cl]$^+$)

EA: found (calc for $C_{38}H_{42}Cl_2N_2O_2Ti$) C: 67.85 (67.36), H: 6.27 (6.25) N: 4.35 (4.13)

6.3.5 [L$^{(1,2)}$M(CH$_2$Ph)$_2$]

To the appropriate ligand (~10 mg, 0.18 mmol) in a young's-tap NMR tube was added [M(CH$_2$Ph)$_4$] (M = Ti, Zr, 1 eq) in d$_8$-toluene, under argon. The tube was sealed, and shaken.

The NMR spectra of the Zr reactions could not be interpreted – no tractable products could be distinguished. The Ti reactions showed very complicated ^{1}H NMR spectra, suggesting a mix of more than one product, and a number of peaks between 3-5 ppm indicate the presence of breakdown products[9].

6.4 Stilbene Ligands

6.4.1 2,2'-dinitrostilbene (2,2'-DNS)[11]

To 2-nitrobenzyl chloride (5.05 g, 29.43 mmol) in EtOH (20 ml) was added slowly KOH (8.26 g, 148 mmol) in warm EtOH (50 ml) with vigorous stirring. The mixture became warm. The mixture was stirred overnight, and a yellow precipitate was recovered by filtration, washed with EtOH, and recrystallized from ethyl acetate, yielding 2,2'-dinitrostilbene as needle like yellow crystals (1.39 g, 18%).

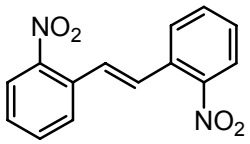

^{1}H NMR 400 MHz ($CDCl_3$): δ ppm 8.04 (dd, $^{4}J_{HH}$ = 1 Hz, $^{3}J_{HH}$ = 8 Hz, 2H, Ar*H*), 7.81 (dd, $^{4}J_{HH}$ = 1 Hz, $^{3}J_{HH}$ = 8 Hz, 2H, Ar*H*), 7.67 (td, $^{4}J_{HH}$ = 1 Hz, $^{3}J_{HH}$ = 8 Hz, 2H, Ar*H*), 6.57 (s, 2H, C*H*=C*H*), 7.48 (td, $^{4}J_{HH}$ = 1 Hz, $^{3}J_{HH}$ = 8 Hz, 2H, Ar*H*)

^{13}C{^{1}H} NMR 100 MHz ($CDCl_3$): δ ppm 147.9, 133.7, 132.6, 129.1, 128.9 124.9 (Ar) 130.0 (*C*=*C*)

EA: found (calc for $C_{14}H_{10}N_2O_4$) C: 62.12 (62.22), H: 3.69 (3.73), N: 10.21 (10.37)

MS (EI^+): m/z 270 (M^+)

6.4.2 2,2'-diaminostilbene (2,2'-DAS)[12]

To $SnCl_2$ (15.4 g, 81.9 mmol) suspended in glacial acetic acid (40 ml) was added concentrated HCl until all $SnCl_2$ had dissolved (~20 ml). To this was added 2,2'-DNS (1.34 g, 4.96 mmol). The mixture was stirred for 15 minutes at room temperature, and then gradually warmed to 70 °C. The mixture was stirred at that temperature for 1 h, and then allowed to cool to room temperature. A yellow precipitate (2,2-DAS.2(HCl)) was recovered by filtration, and washed with glacial

acetic acid. This was then dissolved in hot water, and basified with KOH, causing a flocculent yellow precipitate to form. After cooling, the precipitate was extracted with Et_2O, and dried over $MgSO_4$. The solvent was removed *in vacuo*, and the yellow solid remaining was recrystallized from toluene, leaving 2,2'-diaminostilbene as bright yellow flake-like crystals (0.80 g, 77%).

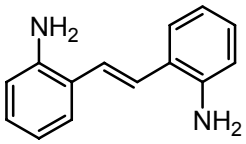

^{1}H NMR 400 MHz ($CDCl_3$): δ ppm 7.40 (dd, $^4J_{HH}$ = 1 Hz, $^3J_{HH}$ = 8 Hz, 2H, Ar*H*), 7.12 (td, $^4J_{HH}$ = 1 Hz, $^3J_{HH}$ = 8 Hz, 2H, Ar*H*), 7.03 (s, 2H, C*H*=C*H*), 6.81 (td, $^4J_{HH}$ = 1 Hz, $^3J_{HH}$ = 8 Hz, 2H, Ar*H*), 6.72 (dd, $^4J_{HH}$ = 1 Hz, $^3J_{HH}$ = 8 Hz, 2H, Ar*H*), 5-2.5 (v. br, ~6H, NH_3)

^{13}C{^{1}H} NMR 100 MHz ($CDCl_3$): δ ppm 143.9, 128.7, 127.2, 124.1, 119.2, 116.2 (Ar) 125.9 (*C*=*C*)

EA: found (calc for $C_{14}H_{14}N_2$) C: 79.96 (79.97), H: 6.72 (6.71), N: 13.38 (13.32)

MS (EI^+): m/z 120 (M^+)

6.4.3 H_2L^8

To 2,2'-DAS (0.569 g, 2.71 mmol) and 2-hydroxy,3-*tert*-butyl,5-methylbenzaldehyde (1.13 g, 5.96 mmol) was added EtOH, and the mixture was stirred at reflux for 18 h, during which time a yellow precipitate formed. The mixture was cooled, and the precipitate recovered by filtration. Washing with EtOH yielded H_2L^8 as a yellow powder (1.38 g, 93%).

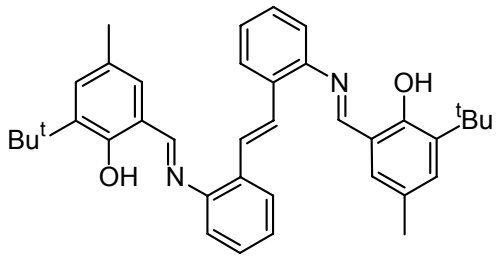

^{1}H NMR 400 MHz ($CDCl_3$): δ ppm 8.45 (s, 2H, N=C*H*), 7.81 (dd, $^{4}J_{HH}$ = 2 Hz, $^{3}J_{HH}$ = 8 Hz, 2H, Ar*H*), 7.6 (s, 2H, C*H*=C*H*), 7.34-7.24 (m, 2H, overlapping Ar*H* signals), 7.10 (dd, $^{4}J_{HH}$ = 2 Hz, $^{3}J_{HH}$ = 8 Hz, 2H, Ar*H*), 7.05 (d, $^{4}J_{HH}$ = 2 Hz, 2H, Ar*H*), 2.32 (s, 6H, Ar-CH_3), 1.50 (s, 18H, C(CH_3)$_3$)

^{13}C{^{1}H} NMR 100 MHz ($CDCl_3$): δ ppm 163.71 (N=*C*H), 158.55, 146.76, 137.45, 131.70, 131.67, 130.46, 128.72, 127.11, 126.88, 126.17, 118.96, 118.70 (Ar), 126.04, (*C*=*C*), 34.89 (*C*(CH_3)$_3$), 29.39 (C(*C*H_3)$_3$), 20.71 (Ar-*C*H_3)

MS (EI^+): m/z 558(M^+)

EA: found (calc for $C_{38}H_{42}N_2O_2$) C: 80.19 (81.68), H: 7.53 (7.58), N: 4.86 (5.01)

6.4.4 H_2L^9

To 2,2′-DAS (0.193 g, 0.92 mmol) and 2-hydroxy,3-*tert*-butyl,6-methylbenzaldehyde (0.390 g, 2 eq) in an RBF was added EtOH. The mixture was stirred at reflux for 24 h, during which time an orange precipitate formed. The mixture was cooled, and the precipitate recovered by filtration. Washing with EtOH yielded H_2L^9 as an orange powder (0.49 g, 95%).

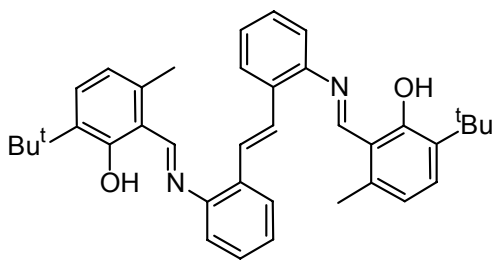

^{1}H NMR 400 MHz (CD_2Cl_2): δ ppm 14.95 (s, 2H, OH), 9.02 (s, 2H, N=C*H*), 7.88 (d, $^{3}J_{HH}$ = 8 Hz, 2H, Ar*H*), 7.69 (s, 2H, C*H*=C*H*), 7.42-7.21 (m, 10H, overlapping Ar*H* signals), 6.70 (d, $^{3}J_{HH}$ = 8 Hz, 2H, Ar*H*), 2.54 (s, 6H, Ar-CH_3), 1.51 (s, 18H, C(CH_3)$_3$)

^{13}C{^{1}H} NMR 100 MHz (CD_2Cl_2): δ ppm 162.0 (N=CH), 147.2, 146.8, 138.3, 132.1, 127.6, 117.6 (Ar), 131.2, 129.3, 127.3, 126.4, 120.5, 119.3 (ArH), 126.2, (*C*=*C*), 35.6 (*C*(CH$_3$)$_3$), 29.39 (C(*C*H$_3$)$_3$), 19.0 (Ar-*C*H$_3$)

MS (EI$^+$): m/z 558 (M$^+$)

EA: found (calc for $C_{38}H_{42}N_2O_2$) C: 81.41 (81.68), H: 7.60 (7.58), N: 5.11 (5.01)

6.5 Salicyloxazoline Proligands

6.5.1 3-tert-butyl-2-hydroxy-5-methoxybenzoic acid

To a hot solution of ninhydrin (24 g, 0.14 mol) in acetic acid was added 4-hydroxy,3-*tert*-butylanisole (24.3 g, 0.14 mol). The mixture was heated to reflux for 2.5 h and then allowed to cool to room temperature, affording yellow crystals which were recovered by suction (31.3 g, not dried).

The crystalline product was added to acetic acid, and 4-methylaniline (19.7 g, 0.184 mol) was added. The mixture was heated to reflux for 24 h, and then allowed to cool to room temperature before being poured into water (500 ml). An unpleasant sticky precipitate formed, and the mixture was stirred with an overhead stirrer for 18 h to break up the lumps. The solid material was recovered by suction filtration (no. 3 sinter), stirred with Et_2O for 15 min and then collected by suction filtration, yielding a yellow powder (33.5 g).

The product was added to a solution of NaOH (2M, ~100 ml), heated to reflux for 15 min, and then allowed to cool to room temperature. A white precipitate was removed by suction filtration and washed with water. The washings were

combined with the yellow filtrate, and acidified with HCl (conc.). The resulting white precipitate was isolated by vacuum filtration, washed with cold water and recrystallized from EtOH/H_2O, giving the title compound as a fine white powder (8.75 g 28%).

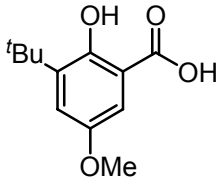

^{1}H NMR 400 MHz ($CDCl_3$): δ ppm 10.85 (br. s, 1H, COO*H*), 7.27, 7.12 (2 × d, $^4J_{HH}$ = 2 Hz, 1H, Ar*H*), 4.70 (br. S, 1H, O*H*), 3.74 (s, 3H, OCH_3), 1.37 (s, 9H, C(CH_3)$_3$)

^{13}C{^{1}H} NMR 100 MHz ($CDCl_3$): δ ppm 175.0 (*C*OOH), 156.9, 151.2 , 139.9 , 124.2 (Ar), 123.9, 108.8 (ArH), 55.7 (OCH_3), 35.1 (*C*(CH_3)$_3$), 29.3 (C(*C*H_3)$_3$)

EA: found (calc for $C_{12}H_{16}O_4$) C: 64.31 (64.27), H: 7.07 (7.19), N: 0.13 (0.00)

MS (ESI): m/z 223 (M+)

6.5.2 HL[10]

To 3,5-di-*tert*-butyl salicylic acid (2.49 g, 10.0 mmol) in a Schlenk vessel was added PPh_3 (10.4 g, 39.6 mmol), and the atmosphere in the vessel replaced with argon. Acetonitrile (~25 ml), and then triethylamine (5.5 ml, 55 mmol) were added, with stirring. 2-Aminoethanol (0.60 g, 10 mmol) was injected in a small volume of acetonitrile. CCl_4 (9.5 ml, 39 mmol) was added dropwise over 3 hours. The mixture was stirred for 48 hours, after which time the solution was filtered, washed through with a little Et_2O, which caused a further precipitation, this precipitate was also removed by filtration. The solvents were removed *in vacuo*, and the product extracted with hexane (3 × 100 ml). The combined extracts were dried *in vacuo*, and the pale yellow powder was purified by flash chromatography on a silica column,

eluted with hexane-ethyl acetate (50:1), affording HL^{11} as a pale yellow powder (1.3 g, 47%) after removal of solvent.

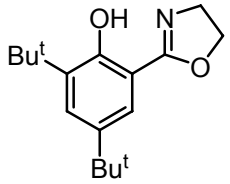

^{1}H NMR 400 MHz ($CDCl_3$): δ ppm 12.47 (s, 1H, O*H*), 7.44 (d, $^4J_{HH}$ = 2.5 Hz, 1H, Ar*H*), 7.33 (d, $^4J_{HH}$ = 2.5 Hz, 1H, Ar*H*), 4.30 (t, $^3J_{HH}$ = 9 Hz, 2H, CH_2), 3.99 (t, $^3J_{HH}$ = 9 Hz, 2H, Ar*H*), 1.34 (s, 9H, C(CH_3)$_3$), 1.21 (s, 9H, C(CH_3)$_3$)

^{13}C{^{1}H} NMR 100 MHz ($CDCl_3$): δ ppm 167.1 (N=*C*–O), 156.8, 140.0, 136.4 (Ar), 127.9, 122.2 (Ar *C*-H), 109.9 (Ar), 66.5, 53.4 (*C*H_2), 35.2, 34.3 (*C*(CH$_3$)$_3$), 31.5, 29.5 (C(*C*H$_3$)$_3$)

EA: found (calc for $C_{17}H_{25}NO_2$) C: 74.20 (74.14), H: 9.35 (9.15), N: 4.98 (5.09)

MS (EI): m/z 275 (M+)

IR (ATR): cm^{-1}: 2956, 1636 (C=N), 1596, 1438, 1370, 1251, 1216, 1187, 1099, 1013, 960, 890, 799, 780, 722

6.5.3 HL^{11}

To 3,5-di-*tert*-butyl salicylic acid (2.5 g, 10.0 mmol) in a Schlenk vessel was added PPh_3 (10.4 g, 39.6 mmol), and the atmosphere in the vessel replaced with argon. Acetonitrile (~25 ml), and then triethylamine (6 ml, 60 mmol) were added, with stirring. 2-amino-2-methyl-1-propanol (0.89 g, 10 mmol) was injected in a small volume of acetonitrile. CCl_4 (10 ml, 40 mmol) was added dropwise over 3 hours. The mixture was stirred for 48 hours, after which time the solution was filtered, washed through with a little Et_2O, which caused a further precipitation, this

precipitate was also removed by filtration. The solvents were removed *in vacuo*, and the product extracted with hexane (3 × 100 ml). The combined extracts were dried *in vacuo*, and the pale yellow powder was purified by flash chromatography on a silica column, eluted with hexane-ethyl acetate (50:1), affording HL^{10} as a pale yellow powder (1.4 g, 46%) after removal of solvent.

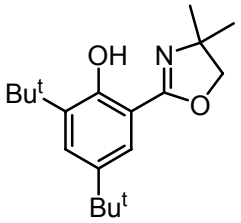

^{1}H NMR 400 MHz ($CDCl_3$): δ ppm 12.60 (s, 1H, O*H*), 7.54 (d, $^4J_{HH}$ = 2 Hz, 1H, Ar*H*), 7.44 (d, $^4J_{HH}$ = 2 Hz, 1H, Ar*H*), 4.09 (s, 2H, CH_2), 1.46 (s, 9H, C(CH_3)$_3$), 1.40 (s, 6H, CH_3) 1.32 (s, 9H, C(CH_3)$_3$)

^{13}C{^{1}H} NMR 100 MHz ($CDCl_3$): δ ppm 164.3 (N=*C*–O), 156.8, 140.0, 136.3 (Ar), 127.8, 122.0 (Ar *C*-H), 109.9 (Ar), 78.1 (*C*H_2), 67.0 (*C*(CH_3)$_2$), 35.1, 34.2 (*C*(CH_3)$_3$), 31.5, 29.5 (C(*C*H_3)$_3$), 28.6 (*C*H_3)

EA: found (calc for $C_{19}H_{29}NO_2$) C: 75.14 (75.21), H: 9.63 (9.63), N: 4.62 (4.51)

MS (EI): m/z 303 (M+), 288 ([M-CH_3]$^+$)

IR (ATR): cm^{-1}: 2963, 2137, 1634 (C=N), 1595, 1438, 1366, 1251, 1183, 1098, 978, 891, 805, 781, 721

6.5.4 HL^{12}

To 3,5-di-isopropylsalicylic acid (2.45 g, 11 mmol) in a Schlenk vessel was added PPh_3 (11.5 g, 43.8 mmol), and the atmosphere in the vessel replaced with argon. Acetonitrile (~25 ml), and then triethylamine (6 ml, 60 mmol) were added, with stirring. 2-amino-2-methyl-1-propanol (0.98 g, 11 mmol) was injected in a small volume of acetonitrile. CCl_4 (10.6 ml, 108 mmol) was added dropwise over 4 hours.

The mixture was stirred for 48 hours, after which time the solution was filtered, washed through with a little Et_2O, which caused a further precipitation, this precipitate was also removed by filtration. The solvents were removed *in vacuo*, and the product extracted with hexane (3 × 100 ml). The combined extracts were dried *in vacuo*, and the pale yellow powder was purified by flash chromatography on a silica column, eluted with hexane-ethyl acetate (50:1), affording HL[13] as a pale yellow crystalline solid (1.01 g, 33%) after removal of solvent.

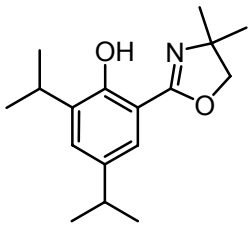

^{1}H NMR 400 MHz ($CDCl_3$): δ ppm 12.25 (s, 1H, O*H*), 7.27 (d, $^4J_{HH}$ = 2 Hz, 1H, Ar*H*), 7.09 (d, $^4J_{HH}$ = 2 Hz, 1H, Ar*H*), 4.00 (s, 2H, CH_2), 3.30 (sept., $^3J_{HH}$ = 7 Hz, 1H, C*H*(CH_3)$_2$), 2.77 (sept., $^3J_{HH}$ = 7 Hz, 1H, C*H*(CH_3)$_2$), 1.30 (s, 6H, CH_3), 1.18 (d, 6H, $^3J_{HH}$ = 7 Hz, CH(CH_3)$_2$), 1.15 (d, 6H, $^3J_{HH}$ = 7 Hz, CH(CH_3)$_2$)

^{13}C{^{1}H} NMR 100 MHz ($CDCl_3$): δ ppm 164.1 (N=*C*–O); 155.5, 138.5, 135.7 (Ar), 128.5, 122.3 (Ar *C*–H), 109.9 (Ar), 78.3 (*C*(CH_3)$_2$), 67.0 (*C*H_2), 33.6 (*C*H(CH_3)$_2$), 28.6 (*C*H_3), 27.1 (*C*H(CH_3)$_2$), 24.2, 22.5 (CH(*C*H_3)$_2$)

EA: found (calc for $C_{17}H_{25}NO_2$) C: 74.01 (74.14), H: 9.15 (9.15), N: 5.03 (5.09)

MS (EI): m/z 275 (M+), 260 ([M – CH_3]$^+$), 188 ([M – 4CH_3, H]$^+$)

IR (ATR): cm–1: 2962, 2137, 1674, 1635 (C=N), 1597, 1455, 1365, 1249, 1193, 1168, 1092, 978, 944, 888, 799, 785, 745

6.5.5 HL[13]

To 3,5-di-*tert*-butyl salicylic acid (2.03 g, 8.1 mmol) in a Schlenk vessel was added PPh_3 (8.5 g, 33 mmol) and 2-aminophenol (0.89 g, 8.1 mmol), and the atmosphere in the vessel was replaced with argon. Acetonitrile (~25 ml), and then triethylamine (4.5 ml, 45 mmol) were added, with stirring. CCl_4 (7.8 ml, 81 mmol) was added dropwise over 4 hours. The mixture was stirred for 48 hours, after which time the solution was filtered, washed through with a little Et_2O, which caused a further precipitation, this precipitate was also removed by filtration. The solvents were removed in vacuo, and the product extracted with hexane (3 × 100 ml). The combined extracts were dried *in vacuo*, and the pale yellow powder was purified by flash chromatography on a silica column, eluted with hexane-ethyl acetate (50:1), affording HL[12] as a fine white powder (0.30 g, 11%) after removal of solvent.

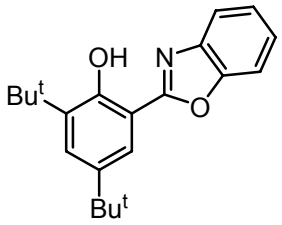

^{1}H NMR 400 MHz ($CDCl_3$): δ ppm 11.95 (s, 1H, O*H*), 7.92 (d, $^4J_{HH}$ = 2 Hz, 1H, Ar*H*), 7.71 (m, 1H, Ar*H*), 7.62 (m, 1H, Ar*H*), 7.52 (d, $^4J_{HH}$ = 2 Hz, 1H, Ar*H*), 1.50 (s, 9H, C(CH_3)$_3$), 1.39 (s, 9H, C(CH_3)$_3$)

^{13}C{^{1}H} NMR 100 MHz ($CDCl_3$): δ ppm 164.0 (benzoxazole N=*C*-O), 155.9, 149.1, 141.1, 140.1, 137.2, 128.5, 125.1, 124.6, 121.3, 113.0, 110.6, 109.8 (Ar), 35.3, 34.5 (*C*(CH$_3$)$_3$), 31.5, 29.5 (C(*C*H$_3$)$_3$)

EA: found (calc for $C_{21}H_{25}NO_2$) C: 78.13 (77.98), H: 7.89 (7.79), 4.33 (4.33)

MS (EI$^+$): m/z 323 (M$^+$), 308 ([M–CH$_3$]$^+$)

IR (ATR): cm^{-1} 2959, 2361, 1624 (C=N), 1545, 1454, 1437, 1361, 1247, 1176, 1109, 1089, 953, 886, 868, 804, 776, 758, 743, 700, 668

6.5.6 HL[15]

To 3-*tert*-butyl,5-methoxysalicylic acid (1.90 g, 8.05 mmol) in a Schlenk vessel was added PPh_3 (8.45 g, 32 mmol), and the atmosphere in the vessel replaced with argon. Acetonitrile (~25 ml), and then triethylamine (4.25 ml, 42 mmol) were added, with stirring. 2-amino-2-methyl-1-propanol (0.79 g, 8.9 mmol) was injected in a small volume of acetonitrile. CCl_4 (7.7 ml) was added dropwise over 4 hours. The mixture was stirred for 48 hours, after which time the solution was filtered, washed through with a little Et_2O, which caused a further precipitation, this precipitate was also removed by filtration. The solvents were removed in vacuo, and the product extracted with hexane (3 × 100 ml). The combined extracts were dried *in vacuo*, and the pale yellow powder was purified by flash chromatography on a silica column, eluted with hexane-ethyl acetate (50:1), affording HL[15] as a pale yellow crystalline solid (1.2 g, 54%) after removal of solvent.

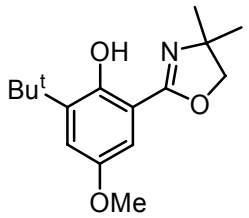

^{1}H NMR 400 MHz ($CDCl_3$): δ ppm 12.34 (s, 1H, O*H*), 7.02 (s, 2H, Ar*H*), 4.08 (s, 2H, CH_2), 3.77 (s, 3H, OCH_3), 1.42 (s, 9H, C(C*H*3)3), 1.40 (s, 6H, C(CH_3)$_2$)

^{13}C{^{1}H} NMR 100 MHz ($CDCl_3$): δ ppm 164.1 (N=C-O), 153.8, 151.0, 138.8, 119.5, 111.0, 107.4 (Ar), 78.2 (OCH_2), 67.3 (*C*(CH_3)$_2$), 55.7 (OCH3), 35.0 (*C*(CH_3)$_3$, 29.3 (C(*C*H3)$_3$), 28.6 (C(*C*H_3)$_2$)

EA: found (calc for $C_{16}H_{23}NO_3$) C: 69.09 (69.29), H: 8.36 (8.36), N: 5.04 (5.05)

MS (ESI): m/z 278 (M+)

IR (ATR): cm^{-1}: 2951 (C-H), 1631 (C=C), 1596 (C=N), 1469, 1449, 1431, 1411, 1390, 1368, 1332, 1288, 1270, 1233, 1203, 1169, 1089, 1060, 1021, 980, 948, 931, 902, 883, 851, 788, 777, 748, 654

6.6 Salicyloxazalinato Complexes

6.6.1 Chloride Complexes

6.6.1.1 General Procedure for Synthesis of $L^{n}_2MCl_2$ Complexes

To the appropriate ligand (100-500 mg) in a Schlenk vessel under argon was added NaH (2 eq), and then THF (~20 ml) with stirring. The mixture was left stirring for ~20 h. Stirring was ceased, allowing excess NaH to settle out. The solution was filtered *via* cannula into another Schlenk vessel containing MCl_4 or $MCl_4.THF_2$ (0.5 eq) as appropriate, with stirring. Stirring was continued for ~20 h, and then ceased to allow NaCl precipitate to settle, before removal of the solvent *in vacuo*, extraction in DCM and filtration of the solution *via* cannula. The solvent was removed *in vacuo*, yielding a crude product which was purified by sublimation or recrystallization, as appropriate.

6.6.1.2 $[L^{10}_2TiCl_2]$

To $TiCl_4$ (0.46 ml of 10% v/v solution in DCM, 0.42 mmol) in DCM being stirred in a Schlenk vessel under argon, at –78 °C was added HL^{10} (0.240 g, 0.84 mol) in DCM. The vessel was allowed to warm to room temperature, and stirring was continued for 16 h. The solution was filtered *via* cannula, and the volatiles where removed *in vacuo*. The solid was sublimated at 275 °C, 10^{-6} bar, yielding $[L^{10}_2TiCl_2]$ as a red powder (0.179 g, 63%).

NMR spectra suggest the presence of two isomers, predominantly a C_2–symmetric *cis,trans,cis* species, with a further unsymmetrical species present, in a ratio of approximately 2:1. The ^{1}H signals from the oxazoline CH_2-CH_2 protons or both isomers overlap considerably, precluding detailed assignment of this region of the spectrum.

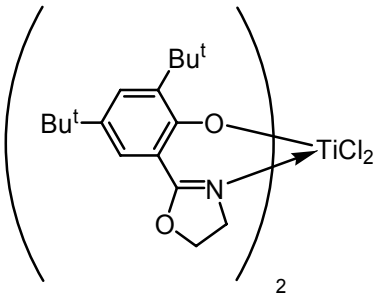

Resonances arising from the minor isomer are enclosed in square brackets in the ^{1}H spectrum. Signal was too low for assignment of minor isomer peaks in ^{13}C NMR. Integrals are consistent within each species.

^{1}H NMR 500 MHz (d_8-toluene, 253 K): δ ppm [7.87, 7.85, 7.74, 7.60 (4 × d, $^4J_{HH}$ = 2 Hz, 1H, Ar*H*)], 7.85, 7.80 (2 × d, $^4J_{HH}$ = 2 Hz, 1H, Ar*H*), 2.8–4.7 (overlapping multiplets from both isomers, 4H from each, C*H*$_2$–C*H*$_2$), 1.85, 1.31 (2 × s, 9H, ^{t}Bu), [1.40, 1.31, 1.27, 1.23 (4 × s, 9H, ^{t}Bu)]

^{13}C{^{1}H} NMR 125 MHz (d_8-toluene): δ ppm 166.3 (N=*C*), 162.4, 142.9, 139.1, (Ar) 130.7, 123.7 (Ar *C*–H), 115.4 (Ar), 79.2 (O–*C*H$_2$–CH$_2$-N), 54.6 (O–CH$_2$–*C*H$_2$-N), 35.8, 34.7 (*C*(CH$_3$)$_3$), 31.5, 30.17 (C(*C*H$_3$)$_3$)

EA: found (calc for $C_{34}H_{48}N_2O_4Cl_2Ti$) C: 59.64 (61.18), H: 7.01 (7.25), N: 3.98 (4.20)

MS (EI$^+$): m/z 666 (M$^+$), 631 ([M–Cl]$^+$), 596 ([M–2Cl]$^+$)

6.6.1.3 [$L^{10}{}_2ZrCl_2$]

Following the general method, L^{10} (0.152 g, 0.529 mmol), NaH (35 mg, 1.5 mmol), and [$ZrCl_4$] (83 mg, 0.356 mmol) were used. The mixture turned from pale to slightly darker yellow. The crude product was purified by sublimation at 275-300 °C, 10^{-6} bar, yielding [$L^{10}{}_2ZrCl_2$] as a yellow solid (99.9 mg, 20%).

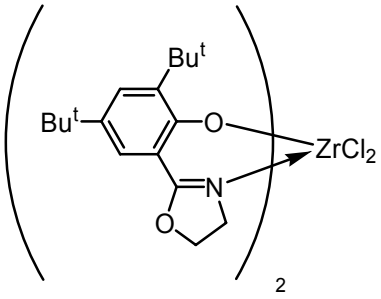

^{1}H NMR 400 MHz (CD_2Cl_2): δ ppm 7.68 (d, $^4J_{HH}$ = 2.5 Hz, 1H, Ar*H*), 7.63 (d, $^4J_{HH}$ = 2.5 Hz, 1H, Ar*H*), 4.48 (br. m, 2H, CH_2), 3.7-4.2 (br, 2H, CH_2), 1.50 (s, 9H, ^{t}Bu), 1.29 (s, 9H, ^{t}Bu)

^{13}C{^{1}H} NMR 100 MHz (CD_2Cl_2): δ ppm 169.5 (N=*C*), 159.9, 142.5, 139.0 (Ar) 131.3, 124.3 (Ar *C*–H), 113.7 (Ar) 68.2 (*C*H_2), 35.6, 34.8 (*C*(CH_3)$_3$), 31.5 29.8 (C(*C*H_3)$_3$)

EA: found (calc for $C_{34}H_{48}N_2O_4Cl_2Zr$) C: 57.28 (57.44), H: 6.71 (6.81), N: 4.02 (3.61)

MS (EI$^+$): m/z 708 (M^+), 694 ([M–CH_3]$^+$)

6.6.1.4 [$L^{10}{}_2HfCl_2$]

Following the general method, L^{11} (0.175 g, 0.61 mmol), NaH (30 mg) and [$HfCl_4$] (100 mg, 0.31 mmol) were used. The mixture turned pale yellow. The solid was recrystallized from DCM/Pentane, yielding [$L^{11}{}_2HfCl_2$] as a pale yellow crystalline solid (0.210 g, 82%).

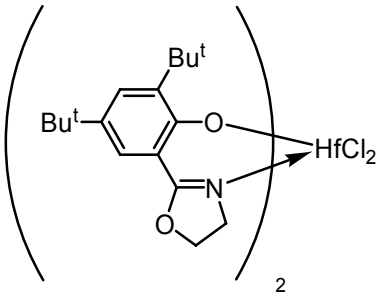

^{1}H NMR 500 MHz (d_8-toluene, 253K): δ ppm 7.87 (d, $^{4}J_{HH}$ = 2.5 Hz, 1H, Ar*H*), 7.85 (d, $^{4}J_{HH}$ = 2.5 Hz, 1H, Ar*H*), 3.90, 3.27, 2.88, 2.82 (4 × m, 1H, CH_2), 1.81 (s, 9H, ^{t}Bu), 1.34 (s, 9H, ^{t}Bu)

^{13}C{^{1}H} NMR 100 MHz (C_6D_6): δ ppm 161.2, 141.6 (Ar) 131.1, 124.0 (Ar *C*–H), 113.7 (Ar), 67.1 (*C*H_2), 35.8, 34.5 (*C*(CH_3)$_3$), 31.5, 30.0 (C(*C*H_3)$_3$)

EA: found (calc for $C_{34}H_{48}N_2O_4Cl_2Hf$) C: 48.06 (51.16), H: 5.83 (6.06), N: 3.21 (3.51)

MS (CI$^+$): m/z 798 (M$^+$), 783 ([M–CH_3]$^+$) 763 ([M-Cl]$^+$)

6.6.1.5 [$L^{11}_2TiCl_2$]

Following the general method, L^{11} (0.330 g, 1.09 mmol), NaH (50 mg), and [$TiCl_4.THF_2$] (175 mg, 0.523 mmol), were used. The mixture turned deep red, and was then heated to 60 °C for 20 h, and then allowed to cool to room temperature, before filtering the solution *via* cannula. The solvent was removed *in vacuo*. The solid product was sublimated at 290 °C, yielding [$L^{11}_2TiCl_2$] as a red crystalline solid (0.285 g, 70%).

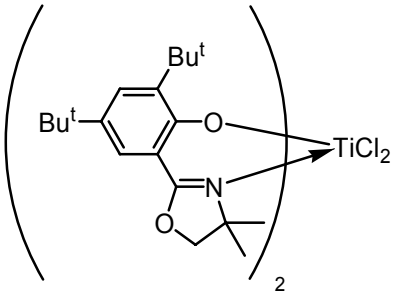

^{1}H NMR 400 MHz (CD_2Cl_2): δ ppm 7.80 (d, $^{4}J_{HH}$ = 2.5 Hz, 1H, Ar*H*), 7.75 (d, $^{4}J_{HH}$ = 2.5 Hz, 1H, Ar*H*), 4.31 (d, $^{2}J_{HH}$ = 8.5 Hz, 1H, CH_2), 3.98 (d, $^{2}J_{HH}$ = 8.5 Hz, 1H, CH_2), 1.64 (s, 3H, CH_3), 1.63 (s, 9H, ^{t}Bu), 1.39 (s, 9H, ^{t}Bu), 1.20 (s, 3H, CH_3)

^{13}C{^{1}H} NMR 100 MHz (CD_2Cl_2): δ ppm 167.8 (N=*C*), 162.3, 143.8, 138.5 (Ar) 131.4, 124.6 (Ar *C*–H), 117.4 (Ar), 79.7 (O-*C*-C(CH_3)$_2$), 71.8 (C-*C*(CH_3)$_2$-N), 35.7, 34.9 (*C*(CH_3)$_3$), 31.5, 30.5 (C(*C*H_3)$_3$), 28.8, 25.9 (C(*C*H_3)$_2$)

EA: found (calc for $C_{36}H_{56}N_2O_4Cl_2Ti$) C: 62.84 (63.07), H: 7.78 (7.80), N: 3.87 (3.76)

MS (EI^{+}): m/z 722 (M^{+}), 687 ([M–Cl]$^{+}$), 652 ([M–2Cl]$^{+}$), 420 ([M-L^{11}]$^{+}$), 302 ([L^{11}]$^{+}$)

6.6.1.6 [$L^{11}_2ZrCl_2$]

Following the general method, L^{11} (0.318 g, 1.05 mmol), NaH (48 mg), and [$ZrCl_4$] (118 mg, 0.506 mmol), were used. The mixture turned yellow. The crude product was recrystallized from DCM/Pentane, yielding [$L^{11}_2ZrCl_2$] as a pale yellow crystalline solid (0.180 g, 44%).

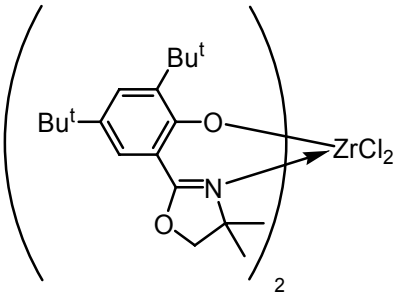

^{1}H NMR 400 MHz (CD_2Cl_2): δ ppm 7.80 (d, $^{4}J_{HH}$ = 2.5 Hz, 1H, Ar*H*), 7.71 (d, $^{4}J_{HH}$ = 2.5 Hz, 1H, Ar*H*), 4.30 (d, $^{2}J_{HH}$ = 8.5 Hz, 1H, CH_2), 4.03 (d, $^{2}J_{HH}$ = 8.5 Hz, 1H, CH_2), 1.60 (s, 3H, CH_3), 1.59 (s, 9H, ^{t}Bu), 1.37 (s, 9H, ^{t}Bu), 1.22 (s, 3H, CH_3)

^{13}C{^{1}H} NMR 100 MHz (CD_2Cl_2): δ ppm 169.5 (N=*C*), 159.7, 142.1, 139.2, (Ar) 131.4, 124.5 (Ar *C*–H), 117.4 (Ar), 79.2 (O-*C*-C(CH_3)$_2$), 69.9 (C-*C*(CH_3)$_2$-N), 35.4, 34.6 (*C*(CH_3)$_3$), 31.3, 30.0 (C(*C*H_3)$_3$), 28.9, 26.3 (C(*C*H_3)$_2$)

EA: found (calc for $C_{36}H_{56}N_2O_4Cl_2Zr$) C: 59.55 (59.51), H: 7.28 (7.36), N: 3.74 (3.65)

MS (EI^+): m/z 766 (M^+), 751 ($[M–CH_3]^+$), 730 ($[M–Cl]^+$)

6.6.1.7 $[L^{11}{}_2HfCl_2]$

Following the general method, L^{11} (0.200 g, 0.63 mmol), NaH (30 mg, 2 eq), and $[HfCl_4]$ (105 mg, 0.327 mmol), were used. The mixture turned pale yellow. The crude product was recrystallized from DCM/Pentane, yielding $[L^{11}{}_2HfCl_2]$ as a pale yellow crystalline solid (0.185 g, 36%).

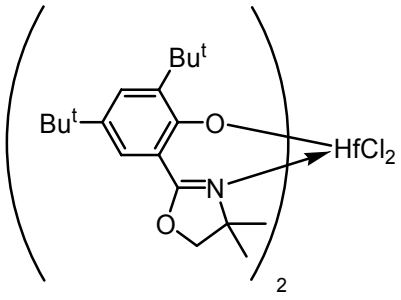

^1H NMR 400 MHz (C_6D_5Br): δ ppm 7.90 (d, $^4J_{HH}$ = 2.5 Hz, 1H, Ar*H*), 7.74 (d, $^4J_{HH}$ = 2.5 Hz, 1H, Ar*H*), 3.85 (d, $^2J_{HH}$ = 8.5 Hz, 1H, CH_2), 3.64 (d, $^2J_{HH}$ = 8.4 Hz, 1H, CH_2), 1.67 (s, 3H, CH_3), 1.49 (s, 9H, ^{t}Bu), 1.23 (s, 9H, ^{t}Bu), 1.00 (s, 3H, CH_3)

$^{13}C\{^1H\}$ NMR 100 MHz (CD_2Cl_2): δ ppm 160.7 (N=*C*), 141.5, 140.3, , (Ar) 131.6, 124.4 (Ar *C*–H), 114.9 (Ar), 79.0 (O-*C*-C$(CH_3)_2$), 69.8 (C-*C*$(CH_3)_2$-N), 35.5, 34.5 (*C*$(CH_3)_3$), 31.6, 30.5 (C(*C*$H_3)_3$), 28.9, 26.3 (C(*C*$H_3)_2$)

EA: found (calc for $C_{36}H_{56}N_2O_4Cl_2Hf$) C: 53.29 (53.43), H: 6.58 (6.61), N: 3.23 (3.28)

MS (EI^+): m/z 854 (M^+), 839 ($[M–CH_3]^+$), 819 ($[M–Cl]^+$)

6.6.1.8 $[L^{12}{}_2TiCl_2]$

Following the general method, L^{12} (0.233 g, 0.85 mmol), NaH (40 mg), and $[TiCl_4.THF_2]$ (140 mg, 0.419 mmol) were used. The mixture turned deep red, and stirring was continued for 20 h. The product precipitated out with the NaCl by-

product. The crude reaction mixture was dried *in vacuo*, and then sublimated at 275 °C, 10^{-6} bar, yielding [$L^{12}{}_2TiCl_2$] as a red crystalline solid (0.098 g, 35%).

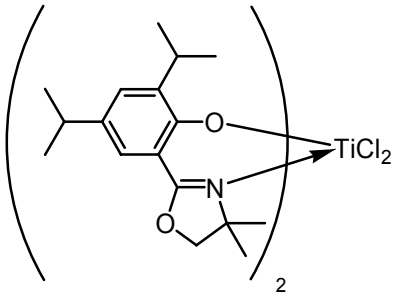

^{1}H NMR 400 MHz (CD_5Br): δ ppm 7.75 (d, $^4J_{HH}$ = 2 Hz, 1H, Ar*H*), 7.46 (d, $^4J_{HH}$ = 2 Hz, 1H, Ar*H*), 3.89 (sept., $^3J_{HH}$ = 7 Hz, 1H C*H*(CH_3)$_2$), 3.83 (d, $^3J_{HH}$ = 8 Hz, 1H, O–C*H*$_2$) 3.61 (d, $^3J_{HH}$ = 8 Hz, 1H, O–C*H*$_2$) 2.81 (sept., $^3J_{HH}$ = 7 Hz, 1H C*H*(CH_3)$_2$), 1.76 (s, 3H, CH_3) 1.53 (d, $^3J_{HH}$ = 7 Hz, 3H, CH(C*H*$_3$)$_2$) 1.38 (d, $^3J_{HH}$ = 7 Hz, 3H, CH(C*H*$_3$)$_2$) 1.20 (d, $^3J_{HH}$ = 7 Hz, 3H, CH(C*H*$_3$)$_2$) 1.19 (d, $^3J_{HH}$ = 7 Hz, 3H, CH(C*H*$_3$)$_2$) 0.94 (s, 3H, C*H*$_3$)

^{13}C{^{1}H} NMR 100 MHz (CD_5Br): , 137.0, 133.1, 120.2, 111.8, 75.5, 66.4, 29.6, 24.9, 20.2, 20.0, 19.8, 18.0, 23.8, 22.5

EA: found (calc for $C_{34}H_{48}N_2O_4Cl_2Ti$) C: 60.95 (61.18) H: 7.14 (7.25), N: 4.16 (4.20)

MS (EI$^+$): m/z 666 (M^+), 631 ([M–Cl]$^+$)

6.6.1.9 [$L^{12}{}_2ZrCl_2$]

Following the general method, L^{12} (0.441 g, 1.6 mmol), NaH (77 mg), and [$ZrCl_4$] (187 mg, 0.802 mmol) were used. The mixture turned yellow. After stirring for 20 h, stirring was ceased, and the product precipitated out with the NaCl by-product. The product was extracted with THF (3 × 10 ml), and the solvent was removed *in vacuo*, and the resulting powder then sublimated at 275 °C, 10^{-6} bar, yielding a yellow solid (0.066 g, 6%). The ^{1}H NMR spectrum appears to show the presence of two isomers

in a ratio of approximately 4:1, with many overlapping peaks, precluding detailed assignment of many regions of the spectrum.

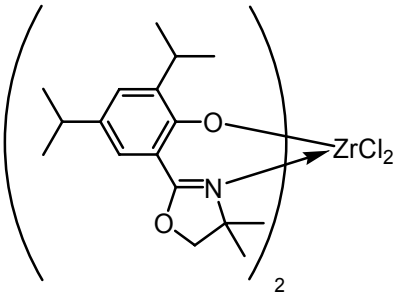

^{1}H NMR 400 MHz (d_5-pyridine): δ ppm 7.83 (d, $^{4}J_{HH}$ = 2 Hz, 1H, Ar*H*), 7.63 (d, $^{4}J_{HH}$ = 2 Hz, 1H, Ar*H*), 3.6-4.3 (m, 6H, overlapping signals from O-CH_2, CH(CH_3)$_2$), 2.8-3.0 (m, 2H, overlapping signals from CH(CH_3)$_2$ from both isomers). 1.92 (s, 3H, CH_3), 1.35-1.50 (m, 12H, overlapping CH_3 signals) 1.15-1.30 (m, 18H, overlapping CH_3 signals)

The product was not sufficiently soluble in any deuterated solvent available to us for determination of the ^{13}C NMR spectrum.

EA: found (calc for $C_{34}H_{48}N_2O_4Cl_2Zr$) C: 56.58 (57.44) H: 6.74 (6.81), N: 3.90 (3.94)

MS (EI$^+$): m/z 708 (M^+), 694 (M-CH_3]$^+$), 673 ([M-Cl]$^+$)

6.6.1.10 [L$^{13}_2$ZrCl$_2$]

Following the general method, L^{12} (0.250 g, 0.77 mmol), NaH (40 mg) and [$ZrCl_4$] (90 mg) were used. The mixture turned deep red. The solid was sublimated at 280 °C, 10^{-6} bar, yielding [L$^{13}_2$ZrCl$_2$] as a pale yellow microcrystalline solid (0.242 g, 39%).

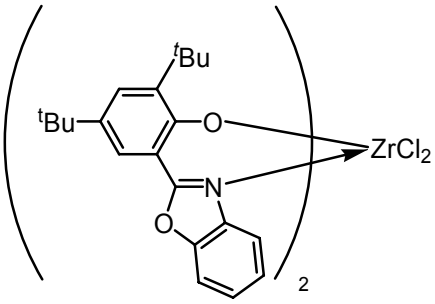

^{1}H NMR 400 MHz (CD_2Cl_2): δ ppm 7.95 (d, $^{4}J_{HH}$ = 2 Hz, 1H, Ar) 7.65 (br. s, 1H, Ar), 7.47 (br. m, 2H, 2 overlapping Ar), 7.20 (br. m, 1H, Ar), 7.01 (br. s, 1H, Ar), 1.52 (br. a, 9H, C(CH_3)$_3$), 1.31 (s, 9H, C(CH_3)$_3$)

^{13}C{^{1}H} NMR 100 MHz (CD_2Cl_2): δ ppm 165.6 (N=C–O), 159.2, 148.2, 143.8, 138.2, 136.5 (Ar), 131.8, 126.8, 126.0, 123.4 (ArH), 114.6 (Ar), 111.1 (ArH), 35.8, 35.0 (C(CH_3)$_3$), 31.5, 29.8(C(CH_3)$_3$)

EA: found (calc for $C_{42}H_{48}N_2O_4Cl_2Zr$) C: 62.50 (62.51), H: 6.12 (6.00), N: 3.47 (3.47)

MS (EI^{+}): m/z 806 (M^{+}), 791 ([M-CH_3]$^{+}$), 769 ([M-Cl]$^{+}$), 737 ([M-2Cl]$^{+}$)

6.6.1.11 [$L^{14}_2TiCl_2$]

Following the general method, L^{14} (0.335 g, 1.08 mmol), NaH (52 mg, 2 eq), and [$TiCl_4$].THF_2 (180 mg, 0.54 mmol), were used. The mixture turned deep red. The crude product was extracted with DCM and sublimated at 250 °C, 10^{-6} bar. A deep red microcrystalline solid was recovered (0.241 g, 60%).

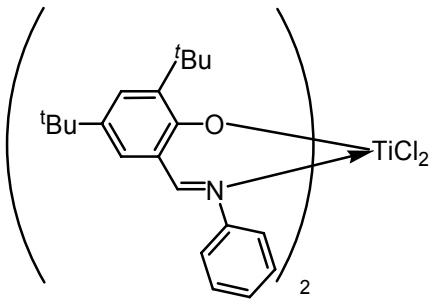

NMR spectra are extremely complicated due to overlapping signals from two isomers in a 7:4 ratio, and could not be fully assigned. Where possible, the signals from the major species are reported here.

^{1}H NMR (400 MHz CD_2Cl_2): δ ppm 8.00 (s, 1H, N=C*H*), 7.41 (d, $^{4}J_{HH}$ = 2.5 Hz, 1H, Ar*H*), 7.02 (d, $^{4}J_{HH}$ = 2.5 Hz, Ar*H*), 7.4-6.8 (m, many overlapping Ar signals), 1.24, 1.20 (2 × s, 9H, C(CH_3)$_3$)

^{13}C{^{1}H} NMR (CD_2Cl_2): δ ppm 167.7 (N=*C*),159.4, 152.8, 144.1, 137.9 (Ar), 132.5, 129.7, 128.8, 127.1, 123.7 (Ar *C*-H), 124.9 (Ar *C*-C=N), 35.4, 34.6 (2 × *C*(CH$_3$)$_3$), 31.4, 29.8 (C(*C*H$_3$)$_3$)

EA: found (calc for $C_{42}H_{52}N_2O_2Cl_2Ti$) C: 66.88 (68.57), H: 6.96 (7.12), N: 3.91 (3.81)

MS (EI$^+$): m/z 734 (M$^+$)

6.6.1.12 [L$^{14}_2$ZrCl$_2$]

Following the general method, L^{14} (0.430 g, 1.39 mmol), NaH (70 mg, 2 eq), and [$ZrCl_4$].THF_2 (165 mg, 0.71 mmol), were used. The mixture turned yellow. The crude product was extracted with DCM and sublimated at 265 °C, 10^{-6} bar. A yellow microcrystalline solid was recovered (0.351 g, 65%).

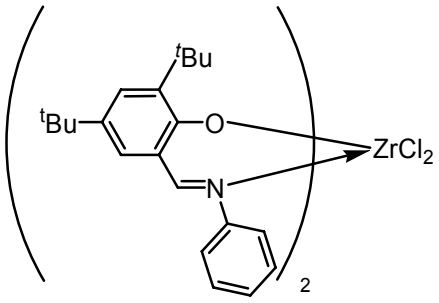

Compound is a mixture of 2 isomers in a 5:1 ratio. The major isomer is reported here.

^{1}H NMR (500 MHz toluene-d_8 363K): δ ppm 7.55 (d, $^{4}J_{HH}$ = 2.4 Hz, 1H, Ar*H*), 7.50 (s, 1H, N=C*H*), 7.01 (d, $^{3}J_{HH}$ = 7.5 Hz, 1H, Ar*H*) 6.82 (t, $^{3}J_{HH}$ = 7.5 Hz, 1H, Ar*H*), 6.70 (t, $^{3}J_{HH}$ = 7.5 Hz, 1H, Ar*H*), 6.62 (d, $^{4}J_{HH}$ = 2.4 Hz, Ar*H*), 1.61, 1.30 (2 × s, 9H, C(CH_3)$_3$)

^{13}C{^{1}H} NMR (100 MHz CD_2Cl_2): δ ppm 171.1 (N=*C*), 142.8, 138.8, 133.1 (Ar), 132.7, 130.3, 129.0, 127.0, 123.4 (Ar *C*-H), 123.0 (Ar), 35.4, 34.5 (2 × *C*(CH$_3$)$_3$), 31.4, 29.7 (C(*C*H$_3$)$_3$)

EA: found (calc for $C_{42}H_{52}N_2O_2Cl_2Zr$) C: 64.90 (64.76), H: 6.70 (6.73), N: 3.76 (3.60)

MS (EI$^+$): m/z 778 (M$^+$)

6.6.1.13 [L$^{15}_2$TiCl$_2$]

Following the general method, L^{15} (0.215 g, 1.13 mmol), NaH (40 mg, 2 eq), and [TiCl$_4$].THF$_2$ (132 mg, 0.395 mmol), were used. The mixture turned yellow. The crude product was recrystallized from boiling toluene, and then washed with cold pentane, yielding of [L$^{15}_2$TiCl$_2$] as a deep red crystalline solid (0.204 g, 57%).

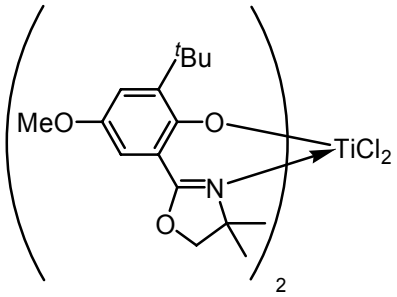

^{1}H NMR (400 MHz CD_2Cl_2): δ ppm 7.23 (m, 2H, Ar*H*), 4.28 (d, $^{2}J_{HH}$ = 8.4 Hz, 1H, CH_2), 3.95 (d, $^{2}J_{HH}$ = 8.4 Hz, 1H, CH_2), 3.81 (s, 3H, OCH_3), 1.59 (s, 3H, CH_3), 1.57 (s, 9H, ^{t}Bu) 1.17 (s, 3H, CH_3)

^{13}C{^{1}H} NMR (CD_2Cl_2): δ ppm 167.1 (N=*C*), 159.4, 153.6, 141.1 (Ar) 118.0 (Ar *C*–OMe) 122.5, 109.3 (Ar *C*–H), 79.7 (O-*C*-C(CH$_3$)$_2$), 72.0 (C-*C*(CH$_3$)$_2$-N), 56.0 (OCH$_3$), 35.6 (*C*(CH$_3$)$_3$), 30.3 (C(*C*H$_3$)$_3$), 28.8, 25.8 (C(*C*H$_3$)$_2$)

EA: found (calc for $C_{36}H_{44}N_2O_6Cl_2Ti$) C: 57.66 (57.24), H: 6.78 (6.60), N: 4.34 (4.17)

MS (EI^+): m/z 670 (M^+), 638 ($[M–Cl]^+$)

6.6.1.14 [$L^{15}{}_2ZrCl_2$]

Following the general method, L^{15} (0.439 g, 1.62 mmol), NaH (80 mg, 2 eq), and $[ZrCl_4].THF_2$ (300 mg, 0.795 mmol), were used. The mixture turned yellow. The crude product was recrystallized from boiling toluene, and then washed with cold pentane, yielding [$L^{15}{}_2ZrCl_2$] as a pale yellow crystalline solid (0.300 g, 52%).

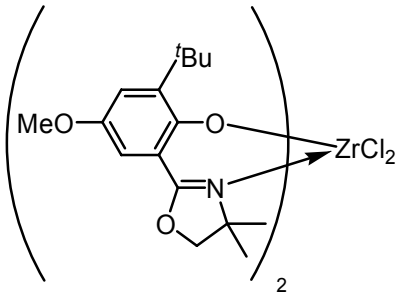

^1H NMR (CD_2Cl_2): δ ppm 7.26 (m, 2H, Ar*H*), 4.29 (d, $^2J_{HH}$ = 8.5 Hz, 1H, C*H*$_2$), 4.04 (d, $^2J_{HH}$ = 8.5 Hz, 1H, C*H*$_2$), 3.81 (s, 3H, OC*H*$_3$), 1.59 (s, 3H, C*H*$_3$), 1.58 (s, 9H, ^{t}Bu) 1.20 (s, 3H, C*H*$_3$)

$^{13}C\{^1H\}$ NMR (CD_2Cl_2): δ ppm 169.0 (N=*C*), 156.8, 152.4, 141.7 (Ar) 115.4 (Ar *C*–OMe) 122.8, 109.2 (Ar *C*–H), 79.2 (O-*C*-C(CH$_3$)$_2$), 70.1 (C-*C*(CH$_3$)$_2$-N), 55.8 (OCH$_3$), 35.3 (*C*(CH$_3$)$_3$), 29.7 (C(*C*H$_3$)$_3$), 28.8, 26.2 (C(*C*H$_3$)$_2$)

EA: found (calc for [$L^{15}{}_2ZrCl_2$] + 0.4 Toluene) C: 56.94 (55.61), H: 6.36 (6.33), N: 3.54 (3.43)

MS (EI^+): m/z 712 (M^+), 677 ($[M–Cl]^+$)

6.6.1.15 [$L^{15}{}_2HfCl_2$]

Following the general method, L^{15} (0.214 g, 0.79 mmol), NaH (40 mg, 2 eq), and $[HfCl_4]$ (128 mg, 0.399 mmol), were used. The mixture turned yellow. The crude

product was recrystallized from boiling toluene, and then washed with cold pentane, yielding [$L^{15}_2HfCl_2$] as a pale yellow crystalline solid (0.101 g, 32%).

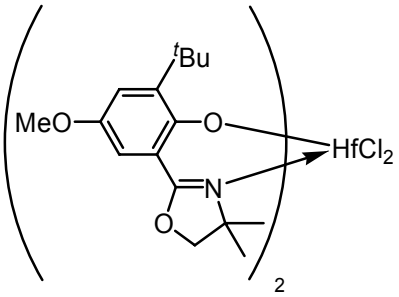

^{1}H NMR 400 MHz (CD_2Cl_2): δ ppm 7.28 (d, $^3J_{HH}$ = 3 Hz, 1H, Ar*H*), 7.25 (d, $^3J_{HH}$ = 3 Hz, 1H, Ar*H*), 4.33 (d, $^2J_{HH}$ = 8.5 Hz, 1H, CH_2), 4.04 (d, $^2J_{HH}$ = 8.5 Hz, 1H, CH_2), 3.82 (s, 3H, OCH_3), 1.61 (s, 3H, CH_3), 1.56 (s, 9H, ^{t}Bu) 1.23 (s, 3H, CH_3)

^{13}C{^{1}H} NMR 100 MHz (CD_2Cl_2): δ ppm 152.3, 142.6, 115.2 (Ar) 114.9 (Ar *C*–OMe) 123.4, 109.2 (Ar *C*–H), 79.6 (O-*C*-C(CH_3)$_2$), 70.4 (C-*C*(CH_3)$_2$-N), 56.0 (OCH_3), 35.4 (*C*(CH_3)$_3$), 30.0 (C(*C*H_3)$_3$), 29.0, 26.3 (C(*C*H_3)$_2$)

EA: found (calc for $C_{36}H_{44}N_2O_6Cl_2Hf$) C: 47.97 (47.92), H: 5.59 (5.53), N: 3.31 (3.49)

MS (EI$^+$): m/z 802 (M$^+$)

6.6.2 Benzyl Complexes

6.6.2.1 [$L^{10}_2Zr(CH_2Ph)_2$]

To H**L^{10}** (0.175 g, 0.61 mmol), in a Schlenk vessel under argon was added [$Zr(CH_2Ph)_4$] (0.139 g, 0.305 mmol), and pentane was added at -78 °C with stirring and the exclusion of light. The mixture was allowed to warm to room temperature, and stirred for 3 h. The product was recrystallized from pentane, yielding [$L^{10}_2Zr(CH_2Ph)_2$] as a pale yellow powder (0.110 g, 44%).

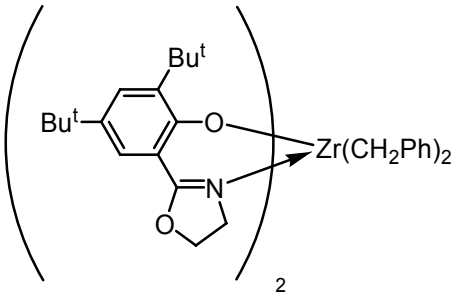

^{1}H NMR 400 MHz (C_6D_6): δ ppm 8.07 (d, $^{4}J_{HH}$ = 2 Hz, 1H, Ar*H*), 7.86 (br. s, 1H, Ar*H*), 6.9-7.2 (m, 4H, overlapping benzyl C_6H_5 signals), 6.75 (m, 1H, C_6H_5), 3-4 (br. m, 4H, CH_2–CH_2), 2.92 (br. s, 2H, CH_2Ph), 1.87 (br. s, 9H, C(CH_3)$_3$), 1.43 (s, 9H, C(CH_3)$_3$)

^{13}C{^{1}H} NMR 100 MHz (C_6D_6): δ ppm 174.3 (N=*C*), 168.9, 163.9, 161.0, 144.5, 112.5 (Ar), 130.9, 129.6, 128.7, 122.6, 120.4 (Ar *C*-H), 72.4 (O-*C*-C(CH$_3$)$_2$), 69.1 (*C*H$_2$Ph), 66.5 (O-*C*H$_2$-C), 55.7 (C-*C*H$_2$-N) 31.6, 30.3 (C(*C*H$_3$)$_3$), 34.5, 27.8 (*C*(CH$_3$)$_3$)

EA: found (calc for $C_{48}H_{62}N_2O_4Cl_2Zr$) C: 65.78 (70.11), H: 7.46 (7.60), N: 3.64 (3.41)

MS (EI$^+$): m/z 820 (M$^+$), 729 ([M–(CH$_2$Ph)]$^+$)

6.6.2.2 [L$^{10}_2$Hf(CH$_2$Ph)$_2$]

To [Hf(CH$_2$Ph)$_4$] (0.224 g, 0.41 mmol) in toluene (20 ml) in a Schlenk vessel under argon was added H**L^{10}** (0.237 g, 0.862 mmol) in toluene (10 ml) with stirring. Stirring was continued for 10 min, and then the solvent was removed *in vacuo*. Excess toluene was removed azeotropically with pentane, and the product was recrystallized from toluene/pentane, yielding the product as a pale yellow microcrystalline solid (196 mg, 52%).

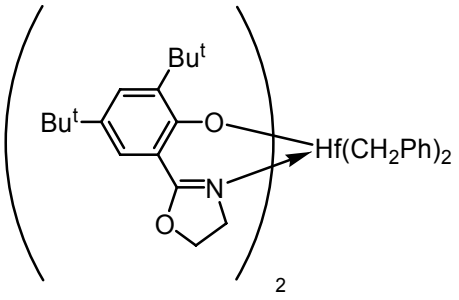

^{1}H NMR 400 MHz (C_6D_6): δ ppm 8.00 (br. s, 1H, Ar*H*), 7.92 (br. s, 1H, Ar*H*), 6.9-7.2 (m, 4H, overlapping benzyl C_6H_5 signals), 6.73 (m, 1H, C_6H_5), 2.6-3.6 (br. m, 6H, overlapping CH_2–CH_2, CH_2Ph), 1.91 (br. s, 9H, C(CH_3)$_3$), 1.38 (s, 9H, C(CH_3)$_3$)

^{13}C{^{1}H} NMR 100 MHz (C_6D_6): δ ppm 175.0 (N=*C*), 160.0, 152.2, 142.3, 137.2 (Ar), 130.3, 128.0, 127.1, 125.3, 118.1 (Ar *C*-H), 116.5 (Ar), 75.5 (O-*C*-C(CH_3)$_2$), 72.0 (*C*H_2Ph), 64.6 (O-*C*H_2-C), 52.3 (C-*C*H_2-N) 35.5, 34.6 (C(*C*H_3)$_3$), 30.2, 31.0 (*C*(CH_3)$_3$)

EA: found (calc for $C_{48}H_{62}N_2O_4Hf$) C: 61.22 (63.39), H: 6.86 (6.87), N: 3.03 (3.08)

MS (EI$^+$): m/z 910 (M^+), 819 ([M–(CH_2Ph)]$^+$)

6.6.2.3 [L^{11}$_2$Zr(CH_2Ph)$_2$]

To H**L^{11}** (0.320 g, 1.06 mmol), in a Schlenk vessel under argon was added [Zr(CH_2Ph)$_4$] (0.240 g, 0.527 mmol). Toluene (~10 ml) was added with stirring and the exclusion of light. The mixture was stirred for 30 min, and then the solvent was removed *in vacuo*. The product was recrystallized from pentane, yielding [L^{11}$_2$Zr(CH_2Ph)$_2$] as a deep yellow powder (0.250 g 27%).

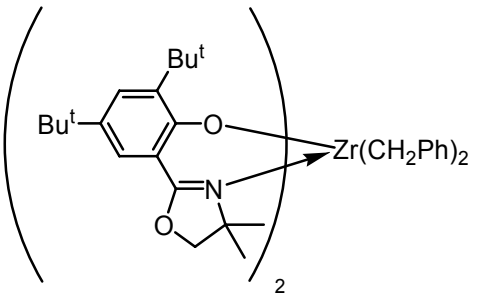

^{1}H NMR 400 MHz (d_8-toluene): δ ppm 8.03, 7.80 (2 × d, $^{4}J_{HH}$ = 3 Hz, 1H, Ar*H*), 6.89 (m, 4H, overlapping benzyl C_6H_5 signals), 6.60-6.66 (m, 1H, C_6H_5), 3.30, 3.20 (2 × d, $^{2}J_{HH}$ = 8 Hz, 1H, O–CH_2), 2.92, 2.80 (2 × d, 1H, $^{2}J_{HH}$ = 11 Hz, CH_2Ph), 1.78, 1.32 (2 × s, 9H, C(CH_3)$_3$), 0.98, 0.73 (2 × s, 3H, N–C(CH_3)$_2$)

^{13}C{^{1}H} NMR 100 MHz (d_8-toluene): δ ppm 168.3 (N=*C*), 161.0, 150.2, 141.1, 139.3 (Ar), 130.7, 127.8, 126.5, 124.8, 120.1 (Ar *C*-H), 116.5 (Ar), 78.0 (O-*C*-C(CH_3)$_2$), 72.0 (*C*H_2Ph), 69.2 (C-*C*(CH_3)$_2$-N), 35.9, 34.7 (*C*(CH_3)$_3$), 31.8, 31.7 (C(*C*H_3)$_3$), 27.7, 26.5 (C(*C*H_3)$_2$)

EA: found (calc for $C_{52}H_{70}N_2O_4Zr$) C: 69.50 (71.11), H: 8.00 (8.03), N: 3.08 (3.19)

MS (EI$^+$): m/z 878(M^+), 785 ([M–(CH_2Ph)]$^+$)

6.6.2.4 [L$^{11}_2$Hf(CH_2Ph)$_2$]

To H**L^{11}** (0.180 g, 0.57 mmol), in a Schlenk vessel under argon was added [Hf(CH_2Ph)$_4$] (0.155 g, 0.28 mmol). Toluene (~10 ml) was added with stirring and the exclusion of light. The mixture was stirred for 15 min, and then the solvent was removed *in vacuo*. The product was recrystallized from toluene/pentane, yielding [L$^{11}_2$Hf(CH_2Ph)$_2$] as a deep yellow powder (0.082 g, 30%).

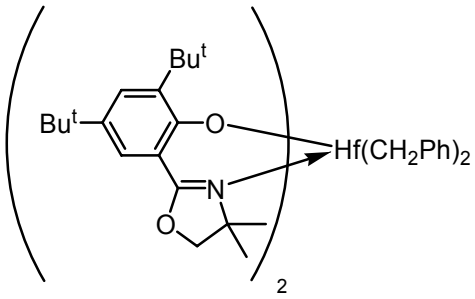

^{1}H NMR 300 MHz (C_6D_6): δ ppm 8.21, 7.95 (2 × d, $^{4}J_{HH}$ = 2.6 Hz, 1H, Ar*H*), 7.1 (m, 4H, overlapping benzyl C_6H_5 signals), 6.80 (tt, $^{3}J_{HH}$ = 7.1 Hz, $^{4}J_{HH}$ = 1.6 Hz, 1H,

C_6H_5), 3.37, 3.23 (2 × d, $^2J_{HH}$ = 8.3 Hz, 1H, O–CH_2), 2.82, 2.75 (2 × d, 1H, $^2J_{HH}$ = 11.3 Hz, CH_2Ph), 1.89, 1.43 (2 × s, 9H, C(CH_3)$_3$), 1.14, 0.85 (2 × s, 3H, N–C(CH_3)$_2$)

$^{13}C\{^1H\}$ NMR 75 MHz (C_6D_6): δ ppm 168.9 (N=*C*), 161.6, 151.3, 141.4, 140.2 (Ar), 131.3, 127.9, 127.2, 125.0, 120.6 (Ar *C*-H), 78.5 (O-*C*-C(CH_3)$_2$), 75.8 (C-*C*(CH_3)$_2$-N), 69.6 (CH_2Ph), 36.1, 34.9 (*C*(CH_3)$_3$), 32.0, 31.1 (C(*C*H_3)$_3$),28.2, 26.7 (C(*C*H_3)$_2$)

EA: found (calc for $C_{52}H_{70}N_2O_4Hf$) C: 62.91 (64.68), H: 7.18 (7.31), N: 3.16 (2.90)

MS (EI^+): m/z 875 ([M–(CH_2Ph)]$^+$)

6.6.2.5 [L$^{12}_2$Zr(CH_2Ph)$_2$]

To H**L^{12}** (0.183 g, 0.66 mmol), in a Schlenk vessel under argon was added [Zr(CH_2Ph)$_4$] (0.152 g, 0.334 mmol), and the mixture made up with toluene (~20 ml), with stirring and the exclusion of light. The mixture was stirred for 30 min, and then the solvent was removed *in vacuo*. The product was recrystallized from pentane, yielding [L$^{12}_2$Zr(CH_2Ph)$_2$] as a deep yellow powder (0.140 g, 26%).

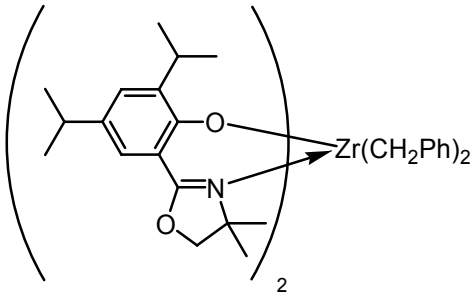

^1H NMR 400 MHz (d$_8$-toluene): δ ppm 7.85, 7.46 (2 × d, $^4J_{HH}$ = 2 Hz, 1H, Ar*H*), 7.00-7.10 (m, 4H, overlapping benzyl C_6H_5 signals), 6.70-6.86 (m, 1H, C_6H_5), 4.03 (sept., $^3J_{HH}$ = 7 Hz, 1H, C*H*(CH_3)$_2$), 3.38, 3.30 (2 × d, $^2J_{HH}$ = 8 Hz, 1H, O–CH_2), 2.82 (sept., $^3J_{HH}$ = 7 Hz, 1H, C*H*(CH_3)$_2$) 2.74, 2.69 (2 × d, 1H, $^2J_{HH}$ = 11 Hz, CH_2Ph), 1.54, 1.46 (2 × d, $^3J_{HH}$ = 7 Hz, 3H, CH(CH_3)$_2$), 1.28 (s, 3H, N–C(CH_3)$_2$), 1.27, 1.25 (2 × d, $^3J_{HH}$ = 7 Hz, 3H, CH(CH_3)$_2$), 0.70 (s, 3H, N–C(CH_3)$_2$)

$^{13}C\{^{1}H\}$ NMR 100 MHz (C_6D_6): δ ppm 167.5 (N=*C*), 159.1, 149.6, 139.4, 138.9 (Ar), 130.1, 126.3, 124.6, 120.1 (Ar *C*-H), 114.8 (Ar), 78.3 (O-*C*-C(CH_3)$_2$), 70.4 (*C*H_2Ph), 68.8 (C-*C*(CH_3)$_2$-N), 34.0, 26.7 (*C*H(CH_3)$_2$), 27.8, 27.7, 24.4, 24.4 (CH(*C*H_3)$_2$), 23.9, 23.5 (C(*C*H_3)$_2$)

EA: found (calc for $C_{48}H_{62}N_2O_4Zr$) C: 69.21 (70.11), H: 7.48 (7.60), N: 3.52 (3.41)

MS (EI^+): m/z 729 ([M–(CH_2Ph)]$^+$)

6.6.2.6 [L$^{12}_2$Hf(CH_2Ph)$_2$]

To H**L^{12}** (0.192 g, 0.69 mmol), in a Schlenk vessel under argon was added [Hf(CH_2Ph)$_4$] (0.189 g, 0.34 mmol), and the mixture made up with toluene, with stirring and the exclusion of light. The mixture was stirred for 1 h, then the solvent was removed *in vacuo*. The product was recrystallized from toluene/pet. ether (40-60°), yielding [L$^{12}_2$Hf(CH_2Ph)$_2$] as a deep yellow powder (0.101 g, 32%).

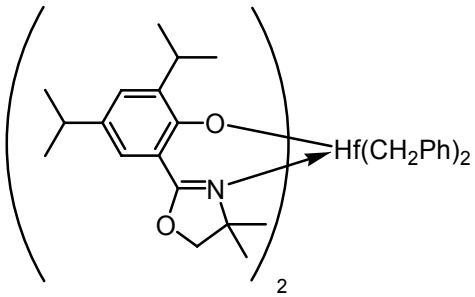

^{1}H NMR 400 MHz (C_6D_6): δ ppm7.78, 7.37 (2 × d, $^{4}J_{HH}$ = 2.4 Hz, 1H, Ar*H*), 6.9-7.1 (m, 4H, overlapping benzyl C_6H_5 signals), 6.66 (tt, $^{3}J_{HH}$ = 7.2 Hz, $^{4}J_{HH}$ = 1.2 Hz, 1H, C_6H_5), 3.90 (sept., $^{3}J_{HH}$ = 6.8 Hz, 1H, C*H*(CH_3)$_2$), 3.35, 3.24 (2 × d, $^{2}J_{HH}$ = 8.3 Hz, 1H, O–CH_2), 2.76 (sept., $^{3}J_{HH}$ = 6.8 Hz, 1H, C*H*(CH_3)$_2$) 2.51, 2.43 (2 × d, 1H, $^{2}J_{HH}$ = 11.4 Hz, CH_2Ph), 1.44, 1.38, (2 × d, $^{3}J_{HH}$ = 7.0 Hz, 3H, CH(CH_3)$_2$), 1.28 (s, 3H, N–C(CH_3)$_2$), 1.22, 1.20 (2 × d, $^{3}J_{HH}$ = 4.4 Hz, 3H, CH(CH_3)$_2$), 0.66 (s, 3H, N–C(CH_3)$_2$)

$^{13}C\{^1H\}$ NMR 100 MHz (C_6D_6): δ ppm 168.0 (N=*C*), 159.4, 150.8, 139.5, 139.2 (Ar), 131.0, 127.6, 126.4, 124.3, 120.0 (Ar *C*-H), 114.5 (Ar), 78.6 (O-*C*-C(CH_3)$_2$), 74.5 (*C*H_2Ph), 68.8 (C-*C*(CH_3)$_2$-N), 34.0, 26.6 (*C*H(CH_3)$_2$), 27.8, 27.8, 24.4, 24.4 (CH(*C*H_3)$_2$),23.8, 24.6 (C(*C*H_3)$_2$)

EA: found (calc for $C_{48}H_{62}N_2O_4Hf$) C: 62.93 (63.39), H: 6.78 (6.87), N: 3.12 (3.08)

MS (EI^+): m/z 819 ($[M–(CH_2Ph)]^+$)

6.6.2.7 [L$^{13}_2$Zr(CH$_2$Ph)$_2$]

To H**L^{13}** (0.013 g, 0.04 mmol), in a Young's-tap NMR tube under argon was added [Zr(CH_2Ph)$_4$] (0.030 g, 0.02 mmol), and the mixture made up with C_6D_6, sealed and briefly shaken. The ^1H NMR spectrum was recorded immediately.

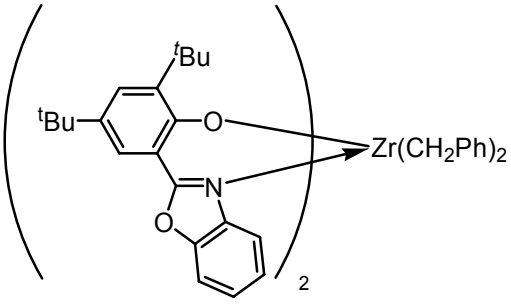

6.9-7.2 (m, 4H, overlapping benzyl C_6H_5 signals), 6.75 (m, 1H, C_6H_5), 3-4 (br. m, 4H, CH_2–CH_2), 2.92 (br. s, 2H, CH_2Ph), 1.87 (br. s, 9H, C(CH_3)$_3$), 1.43 (s, 9H, C(CH_3)$_3$)

6.6.2.8 [L$^{15}_2$Zr(CH$_2$Ph)$_2$]

To H**L^{15}** (0.265 g, 0.98 mmol), in a Schlenk vessel under argon was added Zr(CH_2Ph)$_2$ (0.225 g, 0.49 mmol), and the mixture made up with Et_2O (~20 ml), with stirring at -78 °C and the exclusion of light. The mixture was stirred for 15 min, and then allowed to warm to room temperature, yielding an orange precipitate which was recovered by cannula filtration, and was washed with Et_2O, yielding [L$^{15}_2$Zr(CH_2Ph)$_2$] as a yellow powder (0.255 g, 31%).

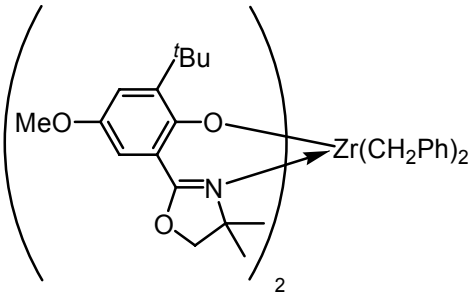

^{1}H NMR 400 MHz (C_6D_6): δ ppm 7.61, 7.56 (2 × d, $^{4}J_{HH}$ = 3.2 Hz, 1H, Ar*H*), 7.14 (m, 4H, overlapping benzyl C_6H_5 signals), 6.84 (m, 1H, C_6H_5), 3.56 (s, 3H, OCH_3), 3.34, 3.26 (2 × d, $^{2}J_{HH}$ = 8 Hz, 1H, O–CH_2), 3.12, 3.04 (2 × d, 1H, $^{2}J_{HH}$ = 11 Hz, CH_2Ph), 1.83 (s, 9H, C(CH_3), 1.07, 0.85 (2 × s, 3H, N–C(CH_3)$_2$)

^{13}C{^{1}H} NMR 100 MHz (C_6D_6): δ ppm 167.7 (N=*C*), 157.8, 152.3, 150.4, 141.5 (Ar), 126 (overlapping Ar *C*-H), 122.7, 122.5, 120.2 (Ar *C*-H), 116.6 (Ar), 109.8, 109.6 (Ar *C*-H) 77.8 (O-*C*-C(CH$_3$)$_2$), 71.8 (*C*H$_2$Ph), 69.2 (C-*C*(CH$_3$)$_2$-N), 55.1 (OCH$_3$) 35.7 (*C*(CH$_3$)$_3$), 30.5 (C(*C*H$_3$)$_3$), 26.5, 26.4 (C(*C*H$_3$)$_2$)

EA: found (calc for $C_{46}H_{58}N_2O_6Zr$) C: 66.29 (66.87), H: 7.06 (7.08), N: 2.97 (3.39)

MS (EI$^+$): m/z 732 ([M–(CH$_2$Ph)]$^+$)

6.6.2.9 [L$^{15}_2$Hf(CH$_2$Ph)$_2$]

To H**L^{15}** (0.245 g, 0.90 mmol), in a Schlenk vessel under argon was added [Hf(CH$_2$Ph)$_4$] (0.250 g, 0.46 mmol). Et$_2$O (~20 ml) was added with stirring at -78 °C and the exclusion of light. The mixture was stirred for 15 min, and then allowed to warm to room temperature (1 h) with stirring, yielding an orange precipitate. The solution was cooled to -18 °C for 15 h, and then to -78 °C, and the product was then recovered by cannula filtration, washed with Et$_2$O, and dried *in vacuo* yielding [L$^{15}_2$Hf(CH$_2$Ph)$_2$] as a yellow powder (0.155 g, 37%).

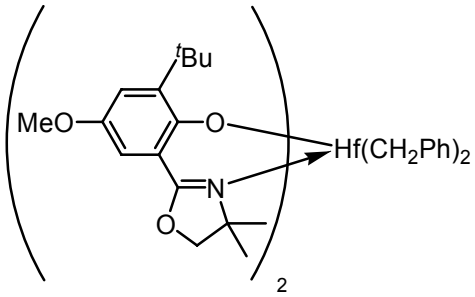

^{1}H NMR 400 MHz (C_6D_6): δ ppm 7.59, 7.56 (2 × d, $^{4}J_{HH}$ = 3.2 Hz, 1H, Ar*H*), 7.19-7.07 (m, 4H, overlapping benzyl C_6H_5 signals), 6.84 (m, 1H, C_6H_5), 3.56 (s, 3H, OCH_3), 3.35, 3.26 (2 × d, $^{2}J_{HH}$ = 8 Hz, 1H, O–CH_2), 2.80, 2.74 (2 × d, 1H, $^{2}J_{HH}$ = 11 Hz, CH_2Ph), 1.79 (s, 9H, C(CH_3), 1.79, 0.87 (2 × s, 3H, N–C(CH_3)$_2$)

^{13}C{^{1}H} NMR 100 MHz (C_6D_6): δ ppm 168.1 (N=*C*), 158.2, 152.2, 151.0, 142.1 (Ar), 126.8, 123.0, 122.9, 120.3, (Ar *C*-H), 116.2 (Ar), 109.5, 109.4 (Ar *C*-H) 78.0 (O-*C*-C(CH_3)$_2$), 75.4 (CH_2Ph), 69.3 (C-*C*(CH_3)$_2$-N), 55.1 (OCH_3) 35.6 (*C*(CH_3)$_3$), 30.4 (C(CH_3)$_3$), 26.4 (overlapping C(CH_3)$_2$)

EA: found (calc for $C_{46}H_{58}N_2O_6Hf$) C: 59.54 (60.48), H: 6.36 (6.40), N: 2.89 (3.07)

MS (EI$^+$): m/z 822 ([M–(CH_2Ph)]$^+$)

6.7 Alkyl Cations

6.7.1 General Procedure for Formation of Alkyl Cations

To the appropriate precursor (L_2MCl_2 or $L_2M(CH_2Ph)$) (~15 mg) in a sample vial was added MAO (20 eq.) or [$B(C_6F_5)_3$] or [$PhNHMe_2$][$B(C_6F_5)_4$] (1.1 eq.) as appropriate, in a glovebox under argon. d_5-bromobenzene (~3 ml) was added, and the mixture was transferred to a Young's-tap NMR tube and sealed. The samples were handled with exclusion of light as far as possible.

6.7.2 $[L^{11}{}_2Zr(CH_2Ph)]^+$

Following the general procedure, $[L^{11}{}_2Zr(CH_2Ph)_2]$ (15.0 mg, 27.1 µmol) and $[PhNHMe_2][B(C_6F_5)_4]$ (23.5 mg 29.8 µmol) were used. NMR shows the presence of two compounds (*q.v.* Chapter 5), the major one is reported here.

^{1}H NMR 400 MHz (C_6D_5Br): δ ppm 7.94, 7.89 (2 × d, $^4J_{HH}$ = 2.5 Hz, 2H, Ar*H*), 6.5-7.2 (m, overlapping Ar and solvent signals), 3.66 (m, 4H, C*H*$_2$), 3.22, 2.99 (2 × d, $^3J_{HH}$ = 8.6 Hz, 1H, C*H*$_2$Ph), 2.61 (s, 12H, PhNMe$_2$), 2.17 (s, 6H, C*H*$_3$Ph), 1.58, 1.31 (2 × s, 18H, C(C*H*$_3$)$_3$), 1.05, 0.76 (2 × s, 6H, C(CH$_3$)$_2$)

6.7.3 $[L^{15}{}_2Zr(CH_2Ph)]^+$

Following the general procedure, $[L^{15}{}_2Zr(CH_2Ph)_2]$ (15.0 mg, 18.2 µmol) and $[PhNHMe_2][B(C_6F_5)_4]$ (16.0 mg 19.9 µmol) were used.

^{1}H NMR 400 MHz (C_6D_5Br): δ ppm 6.5-7.3 (m, overlapping Ar and solvent signals), 3.50 (m, 4H, C*H*$_2$), 3.55 (s, 6H, OMe), 3.10, 2.88 (2 × d, $^3J_{HH}$ = 8.8 Hz, 1H, C*H*$_2$Ph), 2.58 (s, 9H, PhNMe$_2$), 2.09 (s, 3H, tol), 1.42 (s, 18H, C(C*H*$_3$)$_3$), 0.97, 0.72 (2 × s, 6H, C(CH$_3$)$_2$)

6.7.4 $[L^{15}{}_2TiMe]^+$

Following the general procedure, $[L^{15}{}_2TiCl_2]$ (12.1 mg, 18.1 µmol) and MAO (19.4 mg 0.35 mmol) were used.

^{1}H NMR 400 MHz (C_6D_5Br): δ ppm 7.34, 7.18 (2 × br. s, 1H, Ar), 3.92 (br. d, 1H, C*H*$_2$), 3.62-3.70 (overlapping signals from OMe and CH$_2$, 4H), 1.54 (br. s, 9H, C(C*H*$_3$)$_3$), 1.40, 0.95 (2 × br. s, 3H, C(CH$_3$)$_2$)

6.7.5 $[L^{15}{}_2ZrMe]^+$

Following the general procedure, $[L^{15}{}_2ZrCl_2]$ (15.0 mg, 21 µmol) and MAO (23.0 mg 0.41 mmol) were used.

^{1}H NMR 400 MHz (C_6D_5Br): δ ppm 7.46, 7.38 (2 × br. s, 1H, Ar), 3.82 (br. d, 1H, CH_2), 3.66-3.71 (overlapping signals from OMe and CH_2, 4H), 1.61 (br. s, 9H, C(CH_3)$_3$), 1.47, 0.96 (2 × br. s, 3H, C(CH_3)$_2$)

6.8 References for Chapter 6

1 P. Scott, *Syntheticpages*, 2001, http://www.syntheticpages.org/pages/1; I. Westmoreland, *Syntheticpages*, 2003, http://www.syntheticpages.org/pages/211; C. Morton, S*yntheticpages*, 2001, http://www.syntheticpages.org/pages/180.

2 B. Delley, *J. Chem. Phys.*, 1990, **92**, 508; B. Delley, *J. Chem. Phys.*, 1996, **100**, 6107; B. Delley, *J. Chem. Phys.*, 2000, **113**, 7756.

3 Accelrys, 'MaterialsStudio 3.1, 3.2' - http://www.accelrys.com

4 J. Andzelm, R. King-Smith and G. Fitzgerald, *Chem. Phys. Lett.*, 2001, **335**, 321.

5 A. Becke, *Phys. Rev. B*, 1988, **38**, 3098.

6 J. P. Perdew, K. Burke and Y. Wang, *Phys. Rev. B*, 1996, **54**, 16533-39.

7 N. Govind, M. Petersen, G. Fitzgerald, R. King-Smith and J. Andzelm, *Comput. Mater. Sci.*, 2003, **28**, 250.

8 L. E. Manzer, *Inorg. Synth.*, 1982, **21**, 135-40.

9 T. Fujita, Y. Tohi, M. Mitani, S. Matsui, J. Saito, M. Nitabaru, K. Sugi, H. Makio and T. Tsutsui, EP874005 (Mitsui Chemicals, Inc., Japan), 1998.

10 P. D. Knight, 'Chiral at Metal Catalyst Designs for Alkene Polymerisation and Hydroamination', Ph.D. Thesis, University of Warwick, Coventry, 2003; P. D. Knight, A. J. Clarke, B. S. Kimberley, R. A. Jackson and P. Scott, *Chem. Commun.*, 2002, 352-53.

11 C. A. Bischoff, *Chem. Ber.*, 1888, **21**, 2071-78; A. Blanc and C. G. Bochet, *J. Org. Chem.*, 2003, **68**, 1138-41.

12 J. Thiele and O. Dimroth, *Chem. Ber.*, 1895, **28**, 1411-14.

Appendix A Design of Gas Pressure Burette

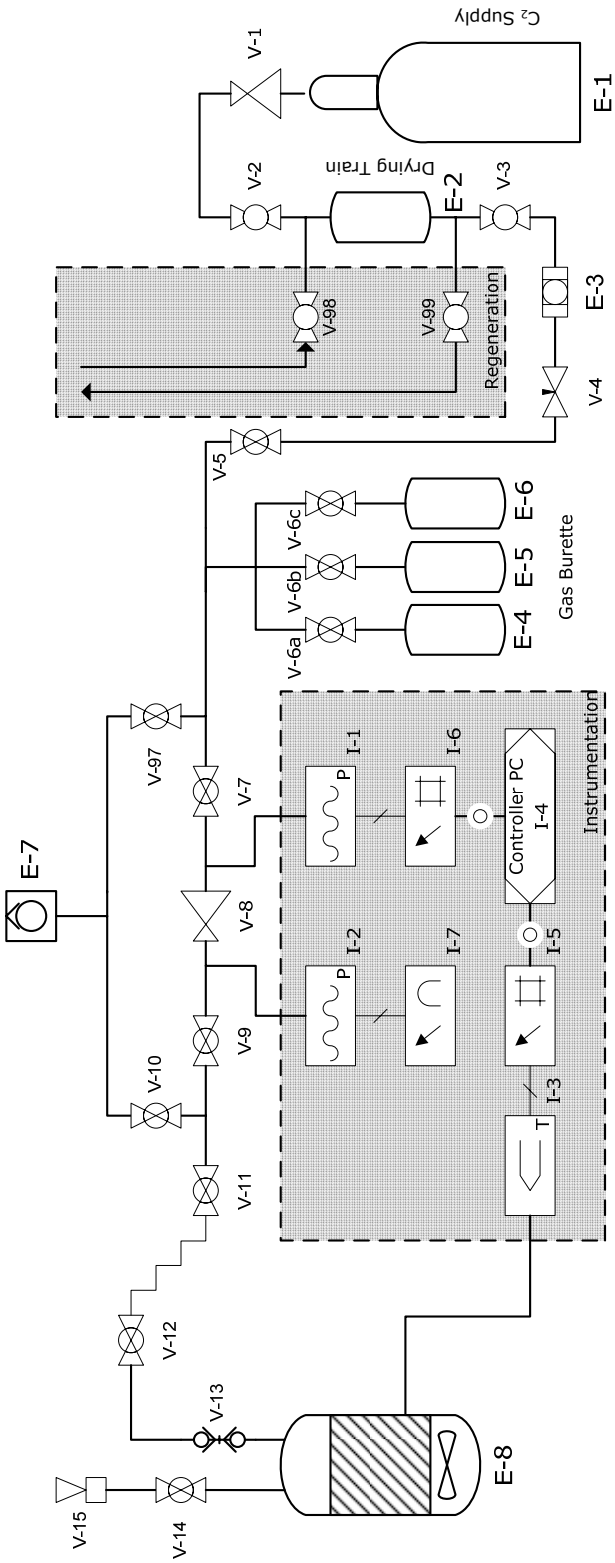

Figure A.1 - Gas Burette Schematic

Component	Description	Manufacturer	Model
E-1	Ethylene supply cylinder		
E-2	R3-11G/3A molecular sieves drying train	Swagelok	304L-HDF4-300
E-3	2 micron filter	Swagelok	SS-4FW-2
E-4	300CC sample cylinder	Swagelok	304L-HDF4-300
E-5	1000CC sample cylinder	Swagelok	304L-HDF4-1000
E-6	2250CC sample cylinder	Swagelok	304L-HDF4-2250
E-7	Connection to Schlenk line		
E-8	Reaction Vessel		
I-1	Input Gauge	Druck	PDCR 4010 (20 bar)
I-2	Output gauge	Tescom	4802-V200N
I-3	Thermocouple in reaction media		
I-4	Control		
I-5	Meter with RS232 interface	Druck	DPI282 with RS232 interface
I-6	ADC with RS232 Interface	Druck	DPI280 with RS232 interface
I-7	Pressure Dial	Tescom	4802-V200N
V-1	20 bar cylinder regulator	BOC	HP1502B-GL-BS4
V-2	C2 Isolation	Swagelok	SS-4P4T-BK
V-3	Rig isolation	Swagelok	SS-4P4T-BK
V-4	Meter Valve	Swagelok	SS-4L2
V-5, V-6, V-7		Swagelok	SS-42S4
V-8	Reactor Regulator	Tescom	44-2262-241
V-9, V-10, V-11, V-12		Swagelok	SS-42S4
V-13	Quick Connect	Swagelok	SS-QC4-D-400/SS-QC4-B-400
V-14	Catalyst Injection Valve	Swagelok	SS-43S4
V-15	Catalyst Injection Port	Swagelok	
V-97	Commissioning purge	Swagelok	SS-42S4
V-98	Regeneration Gas Connection	Swagelok	SS-4P4T-RD
V-99	Regeneration Purge Connection	Swagelok	SS-4P4T-RD

Table A.5 - Gas Burette Components

Appendix B Derivation from Eyring Equation

Energies of activation $\Delta G^{\ddagger}$ may be calculated using the Eyring equation (Equation 3)[1]

$$k = \kappa \frac{k_B T}{h} e^{\left(-\Delta G^{\ddagger}/RT\right)}$$

Equation 3

k = rate constant

κ = transmission coefficient*

k_B = Boltzmann constant

h = Planck Constant

T = Temperature

Now, at the coalescence temperature,

$$k = \frac{\pi \delta \upsilon}{\sqrt{2}}$$

Equation 4

$\delta\nu$ = Frequency difference between exchanging signals

* The transmission coefficient κ is the fraction of all reacting molecules reaching the transition state that proceed to deactivated product molecules, which can generally be assumed to be unity for polyatomic molecules in adiabatic reactions

Incorporating this into the Eyring equation, and assuming $\kappa = 1$, that equation may be rearranged to the form shown in Equation 5, and it is this equation which has been used to calculate $\Delta G^{\ddagger}$ values.*

$$\Delta G^{\ddagger} = aT_c\left[9.972 + \log\left(\frac{T_c}{\delta\upsilon}\right)\right]$$

Equation 5

a = 1.914×10^{-2} kJ mol^{-1} K^{-1}

T_c = Coalescence Temperature

It is also possible to rewrite Equation 3 by substitution with $\Delta G^{\ddagger} = \Delta H^{\ddagger} - T\Delta S^{\ddagger}$

$$k = \kappa\frac{k_B T}{h}e^{\left(\frac{\Delta S^{\ddagger}}{R}\right)}e^{\left(\frac{-\Delta H^{\ddagger}}{RT}\right)}$$

Equation 6

Inserting the physical constants, and again assuming that κ=1, the equation may be rearranged to:

$$a\left[\log\frac{k}{T} - 10.319\right] = \frac{-\Delta H^{\ddagger}}{T} + \Delta S^{\ddagger}$$

Equation 7

Thus, if it is possible to determine the rate of exchange across a range of temperatures, a plot of $a\left[\log\frac{k}{T} - 10.319\right]$ *vs.* $\frac{1}{-T}$ should be a straight line with intercept $\Delta S^{\ddagger}$ and gradient $\Delta H^{\ddagger}$.

* There is also a contribution from the coupling energy, as this is a coalescing AB system. However, this contribution is 2 orders of magnitude lower than the uncertainty in the measurement for these systems and is ignored here.

Appendix C Crystallographic Details

	$[L^2TiCl_2]$	"L^8Ti" dimer	$[L^{11}TiCl_2]$[a]	$[L^{10}{}_2Hf(CH_2Ph)_2]$	$[L^{12}{}_2Hf(CH_2Ph)_2]$
Molecular Formula	$C_{38}H_{42}Cl_2N_2O_2Ti$	$C_{78}H_{80}Cl_6N_4O_5Ti_2$	$C_{46.75}H_{66}Cl_2N_2O_4Ti$	$C_{48}H_{62}HfN_2O_4$	$C_{48}H_{62}HfN_2O_4$
Formula Weight	677.54	1461.96	838.82	909.49	909.49
Crystal System	Monoclinic	Triclinic	Monoclinic	Orthorhombic	Orthorhombic
Space group	P2(1)/c	P-1	P2(1)/c	Pna2(1)	Pbcn
a (Å)	10.0069(10)	10.1255(5)	9.7104(14)	11.767(4)	11.5979(13)
b (Å)	24.991(3)	13.3124(6)	34.437(5)	13.767(4)	14.6219(16)
c (Å)	14.2392(14)	15.5812(8)	15.283(2)	27.252(9)	26.033(3)
α (°)	90	111.086(2)	90	90	90
β (°)	103.530(2)	105.789(2)	97.594(3)	90	90
γ (°)	90	91.592(2)	90	90	90
Cell Volume (Å³)	3462.2(6)	1867.13(16)	5065.7(12)	4415(2)	4414.7(8)
Z	4	1	4	4	4
μ (mm^{-1})	0.437	0.481	0.313	2.406	2.407
Total Reflections	18169	9875	27654	26348	26180
Unique Reflections	4516	6473	9885	9175	5466
R_1, wR_2 [I>2σ(I)]	0.0348, 0.0942	0.0787, 0.1858	0.0761, 0.2520	0.0357, 0.0697	0.0393, 0.0794

[a] The asymmetric unit contains the Ti, two ligands, two chlorines and one and a quarter toluenes. One of the toluenes (C301-C307/C31A-C37A) was highly disordered. The disordered toluene was modelled at a half occupancy over two positions (roughly 3:2, C301-C307:C31A-C37A) with the minor component being refined isotropically. The other toluene C401-C407 was refined at 3/4 occupancy and hence 1.25 molecules of toluene in the asymmetric unit. This explains the fractional empirical formula.

References for Appendices

1 J. Sandström, 'Dynamic NMR spectroscopy', Academic Press, 1982.